



ISSN 1343-2230

CNS-REP-86
February, 2011

Annual Report 2009

Center for Nuclear Study,
Graduate School of Science, the University of Tokyo

Editors

Taku Gunji

Center for Nuclear Study

CNS Reports are available from:

Wako-Branch at RIKEN

Center for Nuclear Study,

Graduate School of Science, the University of Tokyo

2-1 Hirosawa, Wako

351-0198, Japan

Tel: +81-48-464-4191

Fax: +81-48-464-4554

Annual Report 2009

Center for Nuclear Study,
Graduate School of Science, the University of Tokyo

Preface

This is the annual report of the Center for Nuclear Study (CNS), Graduate School of Science, the University of Tokyo, for the fiscal year 2009 (April 2009 through March 2010). During this period, a lot of research activities in various fields of nuclear physics have been carried out and a wide variety of fruitful results have been obtained at CNS. This report summarizes research such activities. I hereby mention some highlights of the report.

The NUSPEQ (NUclear SPectroscopy for Extreme Quantum system) group studies exotic structures in high-isospin and/or high-spin states in nuclei. The CNS GRAPE (Gamma-Ray detector Array with Position and Energy sensitivity) is a major apparatus for high-resolution in-beam gamma-ray spectroscopy. In 2009, the following progress has been made. Neutron-rich nuclei around island-of-inversion have been studied by using nucleon transfer and inelastic scattering where the final states are identified by measuring de-excited gamma-rays. Several candidates of cluster states in ^{12}Be was found especially for odd-spin states suggesting asymmetric cluster configuration. New high-spin states in $^{49-51}\text{Ti}$ populated by fusion reactions of an RI beam have been found, which gives information on the $N=28$ shell gap and the single particle energies in the fp-shell. High-spin states in $A \sim 40$ mass region were studied via $^{18}\text{O}+^{26}\text{Mg}$ fusion evaporation reactions. A superdeformed rotational band up to $12+$ state was observed in ^{40}Ar . This finding indicates the presences of the $N=22$ and $Z=18$ superdeformed shell structure in this region. High-spin states of ^{107}In was studied via $^{58}\text{Ni}(^{52}\text{Cr},3p)$ reaction. A rotational cascade consisting ten gamma-ray transitions was observed. The band exhibits the features typical for smooth terminating bands in $A \sim 100$ mass region. Upgrade of the readout system of the CNS GRAPE has started, where digital pulse data taken by sampling ADCs are analyzed by FPGAs on boards.

Major activity of the nuclear astrophysics group of the year is to study explosive mechanism of Hydrogen burning at extremely high temperatures, which may take place typically in type II supernovae. The α -induced reactions such as (α, γ) and (α, p) would play a crucial role there, but is little investigated so far. Several experiments were performed with the direct method as well as indirect methods for the problem, using the RI beams obtained from the CNS low-energy RI beam separator CRIB. The programs include investigations of key reactions in the αp -process such as $^{11}\text{C}(\alpha, p)$. The activity also includes a study of influence of the environments to the half-life of ^7Be nucleus, by implanting ^7Be into materials. In addition, a sensitive non-destructive beam monitor for the primary beams was developed for the CRIB system, which is sensitive to a few nano amperes for light heavy ions at around 10 MeV/u.

The spin physics group is pursuing research project with spin polarized targets. Performance of the polarized proton solid target was significantly improved in 2009. It was found that the proton polarization can be enhanced by a factor of four by introducing a new pulse structure with a duty factor of 50% and a repetition rate of 9 kHz.

The first physics program with the newly-constructed SHARAQ spectrometer was performed in November 2009. The β^+ -type isovector spin monopole resonances (IVSMR) in ^{90}Zr and ^{208}Pb were identified via the $(t, ^3\text{He})$ reaction at 300 MeV/u. They are the first observations of the β^+ -IVSMR. Ion-optical studies of the SHARAQ spectrometer and the high-resolution beam-line were continued. In the second commissioning run conducted in May 2009, it was demonstrated for a primary beam of ^{14}N beam at 250 MeV/u that the lateral and angular dispersion matching conditions can be achieved simultaneously.

Main goal of the quark physics group is to understand the properties of hot and dense nuclear matter created by colliding heavy nuclei at relativistic energies. The group has been involved in the PHENIX experiment at Relativistic Heavy Ion Collider (RHIC) at Brookhaven National Laboratory, and in the ALICE experiment at Large Hadron Collider (LHC) at CERN. In 2009, LHC finally started making collisions. As for PHENIX, the group has been concentrating on the physics analysis with

leptons and photons, which include direct photon yield at low transverse momentum using the virtual-gamma method, neutral pion yield at high transverse momentum as a function of azimuthal angle from the reaction plane in Au+Au collisions, J/ψ production in ultra-peripheral Au+Au collisions. As for ALICE, the group has been committing the commissioning of the Transition Radiation Detector (TRD), and calibration and performance study of Time Projection Chamber (TPC). The group has been leading development of forward calorimeter for a possible future upgrade. R&D of gas electron multiplier (GEM) and related techniques has been continuing. Time projection chamber, to be used as an active target at RIBF experiments, was developed. Resistive GEM, which utilizes resistive anodes, has been developed.

The nuclear theory group has been promoting the RIKEN-CNS joint research project on large-scale nuclear-structure calculations since 2001 under mutual agreement with RIKEN and maintaining its parallel computing cluster. In 2008, we have added 32 cores to this cluster. Among major developments of the academic year 2009, we would like to mention two. One was the clarification of “shell evolution” mechanism with a comprehensive picture of the central and tensor forces, particularly between proton and neutron, acting over almost all nuclei. This work has been published in Physical Review Letters and was selected as a Viewpoint paper in January 2010. Another important development is the creation of the effective interaction JUN45, which will play significant roles in future studies on nuclei with $A=60-100$. Besides these studies, we mention an interesting development by a postdoc in CNS, and also many intriguing works by our guest professor on astrophysical application of nuclear structure physics.

The 8th CNS International Summer School (CISS09) has been organized in August 2009 with many invited lecturers including four foreign distinguished physicists.

Finally, I thank Ms. M. Hirano and other administrative staff members for their heartfelt contributions throughout the year.

Takaharu Otsuka
Director of CNS



Table of Contents

1a. Experimental Nuclear Physics: Low and Intermediate Energies

Measurement of alpha resonance scattering on ${}^7\text{Be}$	1
<i>H. Yamaguchi, T. Hashimoto, S. Hayakawa, D.N. Binh, D. Kahl, S. Kubono, T. Kawabata, Y. Wakabayashi, N. Iwasa, Y. Miura, Y.K. Kwon, L.H. Khiem, N.N. Duy, and T. Teranishi</i>	
R-matrix analysis on the excitation function of ${}^7\text{Li}+\alpha$ elastic scattering	3
<i>H. Yamaguchi, T. Hashimoto, S. Hayakawa, D.N. Binh, D. Kahl, S. Kubono, Y. Wakabayashi, T. Kawabata, and T. Teranishi</i>	
Multichannel R-matrix analysis for an alpha scattering in inverse kinematics using a ${}^{21}\text{Na}$ radioisotope beam	5
<i>D. N. Binh, L. H. Khiem, N. T. Tho, S. Kubono, H. Yamaguchi, Y. Wakabayashi, S. Hayakawa, D. Kahl, T. Hashimoto, T. Teranishi, S. Kato, K. Iwasa</i>	
First direct measurement of the ${}^{11}\text{C}(\alpha, p){}^{14}\text{N}$ stellar reaction	7
<i>S. Hayakawa, S. Kubono, T. Hashimoto, H. Yamaguchi, D.N. Binh, D. Kahl, Y. Wakabayashi, N. Iwasa, N. Kume, Y. Miura, T. Teranishi, J.J. He, Y.K. Kwon, T. Komatsubara, S. Kato, S. Wanajo</i>	
Present status of the direct measurement of the ${}^{18}\text{Ne}(\alpha, p){}^{21}\text{Na}$ reaction cross sections using the GEM – MSTPC	9
<i>T. Hashimoto, S. Kubono, H. Yamaguchi, S. Hayakawa, D. Kahl, S. Ota, S. Michimasa, H. Tokieda, K. Yamaguchi, I. Arai, T. Komatsubara, H. Ishiyama, Y.X. Watanabe, H. Miyatake, Y. Hirayama, N. Imai, S. C. Jeong, Y. Mizoi, S. K. Das, T. Fukuda, H. Makii, Y. Wakabayashi, N. Iwasa, T. Yamada, A. A. Chen, J. J. He</i>	
${}^{30}\text{S}$ Beam Production and RI Beam Modeling at CRIB	11
<i>D. Kahl, A. A. Chen, S. Kubono, D. N. Binh, J. Chen, T. Hashimoto, S. Hayakawa, N. Iwasa, D. Kaji, A. Kim, Y. Kurihara, N. H. Lee, M. Mazzocco, S. Nishimura, Y. Ohshiro, K. Setoodehnia, Y. Wakabayashi, H. Yamaguchi</i>	
Beta-decay measurement of ${}^{46}\text{Cr}$	13
<i>Y. Wakabayashi, H. Yamaguchi, T. Hashimoto, S. Hayakawa, Y. Kurihara, D. N. Binh, D. Kahl, S. Nishimura, Y. Gono, Y. Fujita, S. Kubono</i>	
Indirect measurement of astrophysical ${}^{12}\text{N}(p, \gamma){}^{13}\text{O}$ reaction rate	15
<i>W.P. Liu, B. Guo, J. Su, Zhi-Hong Li, D.N. Binh, Y.L. Han, H. Hashimoto, S. Hayakawa, J.J. He, J. Hu, N. Iwasa, D.M. Kahl, S. Kubono, N. Kume, Y.J. Li, Zhi-Huan Li, Y.B. Wang, S.W. Xu, H. Yamaguchi, S.Q. Yan, X.X. Bai, G. Lian, B.X. Wang, S. Zeng</i>	
Test measurement of ${}^{17}\text{Ne}+p$ resonance elastic scattering	17
<i>T. Teranishi, S. Kubono, H. Yamaguchi, T. Hashimoto, S. Hayakawa, Y. Kurihara, D.N. Binh, D. Kahl, Y. Wakabayashi, L.H. Khiem, P.V. Cuong, S. Watanabe, A. Goto</i>	
Spectroscopy of ${}^6\text{Be}$ by the ${}^3\text{He}({}^7\text{Be}, \alpha){}^6\text{Be}$ reaction	19
<i>R. P. Condori, R. Lichtenthaler, V. Guimarães, S. Kubono, H. Yamaguchi, A. Lépine-Szily, Y. Wakabayashi, S. Hayakawa, Y. Kurihara, J.S. Yoo, N. Iwasa, S. Kato</i>	
Elastic scattering for 60MeV ${}^{17}\text{F}$ on ${}^{12}\text{C}$ target	21
<i>G. L. Zhang, H. Q. Zhang, C. J. Lin, C. L. Zhang, G. P. An, Z. D. Wu, H. M. Jia, X. X. Xu, F. Yang, Z. H. Liu, S. Kubono, H. Yamaguchi, S. Hayakawa, D. N. Binh, Y. K. Kwon, N. Iwasa</i>	
Study of High-Spin States in ${}^{35}\text{S}$	23
<i>E. Ideguchi, S. Ota, T. Morikawa, M. Oshima, M. Koizumi, Y. Toh, A. Kimura, H. Harada, K. Furutaka, S. Nakamura, F. Kitatani, Y. Hatsukawa, T. Shizuma, M. Sugawara, Y.X. Watanabe, Y. Hirayama, M. Oi</i>	
Measurement of the isovector spin monopole resonance via the $(t, {}^3\text{He})$ reaction at 300 MeV/nucleon	25

K. Miki, H. Sakai, T. Uesaka, H. Baba, G.P.A. Berg, N. Fukuda, D. Kameda, T. Kawabata, S. Kawase, T. Kubo, K. Kusaka, S. Michimasa, H. Miya, S. Noji, T. Ohnishi, S. Ota, A. Saito, Y. Sasamoto, M. Sasano, S. Shimoura, H. Takeda, H. Tokieda, K. Yako, Y. Yanagisawa, A. Yoshida, K. Yoshida, R.G.T. Zegers

The super-allowed Fermi type charge exchange reaction for studies of isovector non-spin-flip monopole resonance .. 27
Y. Sasamoto, T. Uesaka

1b. Experimental Nuclear Physics: PHENIX Experiment at BNL-RHIC and ALICE Experiment at CERN-LHC

Activities on the RHIC-PHENIX and LHC-ALICE experiments in the Year 2009 29
H. Hamagaki, T. Gunji, Y. Tsuchimoto, Y. Aramaki, Y.L. Yamaguchi, S. Sano, A. Takahara, R. Akimoto, Y. Hori, and T. Tsuji

Performance Report of the ALICE for the first $p + p$ collisions at $\sqrt{s}=0.9$ and 7 TeV 31
T. Gunji, H. Hamagaki, S. Sano, Y. Hori, for the ALICE Collaboration

Measurement for charged particle multiplicity in $\sqrt{s}=0.9, 2.36,$ and 7 TeV $p+p$ collisions at LHC-ALICE 33
S. Sano, H. Hamagaki, T. Gunji, for the ALICE collaboration

Measurement of Low-Mass Vector Mesons in RHIC-PHENIX 35
Y. Tsuchimoto, D. Sharma, K. Kijima, Y. Nakamiya, K. Shigaki

Direct virtual photon measurement in $\sqrt{s_{NN}} = 200$ GeV $d+Au$ collisions at RHIC-PHENIX 37
Y.L. Yamaguchi, H. Hamagaki, Y. Akiba, T. Gunji for the PHENIX collaboration

Azimuthal angular dependence of neutral pion production in $\sqrt{s_{NN}} = 200$ GeV Au+Au collisions at PHENIX 39
Y. Aramaki, T. Sakaguchi, G. David, H. Hamagaki, for the PHENIX Collaboration

Measurement of J/ψ and high-mass e^+e^- pairs in Ultra-Peripheral $\sqrt{s_{NN}} = 200$ GeV Au+Au Collisions at RHIC-PHENIX 41
A. Takahara, H. Hamagaki, T. Gunji, Z. C. Valle, Y. Akiba, M. Chiu, J. Nystrand, S. White, K. Skjerdal, E. T. Atomssa, for the PHENIX Collaboration

2. Accelerator and Instrumentation

SHARAQ Project – Progress in FY2009 – 43
T. Uesaka, S. Michimasa, K. Nakanishi, A. Saito, S. Ota, Y. Sasamoto, K. Miki, S. Noji, H. Miya, H. Tokieda, S. Kawase, M. Sasano, S. Itoh, H. Kurei, T. Kawabata, N. Yamazaki, A. Yoshino, S. Shimoura, H. Sakai, T. Kubo, Y. Yanagisawa, K. Itahashi, H. Baba, G. P. Berg, P. Roussel-Chomaz, D. Bazin, for the SHARAQ collaboration.

Focal-Plane Detector System of SHARAQ Spectrometer 45
S. Michimasa, H. Tokieda, S. Noji, S. Ota, S. Shimoura, T. Uesaka, H. Sakai, P. Roussel-Chomaz, J-F. Libin, P. Gangnant, C. Spitaels

Focus tuning method of the high-resolution beam line for the SHARAQ spectrometer 47
Y. Sasamoto, T. Uesaka, S. Shimoura, H. Sakai, T. Kubo, Y. Yanagisawa, H. Takeda, S. Michimasa, A.Saito, S. Ota, S. Noji, K. Miki, H. Tokieda, H. Miya, S. Kawase, T. Kawabata, G.P.A. Berg, for the SHARAQ collaboration

Performance of Focal-Plane Tracking Detector CRDC in SHARAQ 49
H. Tokieda, S. Michimasa, S. Noji, S. Ota, S. Shimoura, T. Uesaka, H. Sakai, P. Roussel-Chomaz, J-F. Libin, P. Gangnant, C. Spitaels

PACIFIC data processing system for high-rate RI-beam experiments 51

S. Ota, S. Shimoura, H. Baba, E. Ideguchi, M. Kurokawa, A. Saito, H. Tokieda, T. Otsuka

Performance evaluation of Low-Pressure Multi-Wire Drift Chamber for RI Beam	53
<i>H. Miya, S. Shimoura, A. Saito, K. Miki, T. Kawabata, K. Itahashi, S. Itoh, S. Ota, M. Sasano, Y. Shimizu, H. Baba, H. Kurei, S. Michimasa, S. Noji, K. Nakanishi, Y. Sasamoto, Y. Shimbara, H. Tokieda, T. Uesaka, H. Sakai</i>	
Evaluation of basic performance of Charge-to-Time Converter Module (QTM)	55
<i>S. Kawase, S. Ota, H. Baba, S. Shimoura, T. Uesaka</i>	
New Intergroup Collaboration for Development of GEM-TPC Active Target	57
<i>S. Ota, S. Michimasa, T. Gunji, H. Yamaguchi, R. Akimoro, T. Hashimoto, K. Devid, S. Hayakawa, H. Tokieda, S. Kawase, T. Tsuji, S. Kubono, H. Hamagaki, T. Uesaka</i>	
Development and performance evaluation of a GEM-TPC for the experiment of highly excited state of nuclei with high rate and high energy unstable nuclear beam	59
<i>R. Akimoto, S. Ota, S. Michimasa, T. Gunji, H. Yamaguchi, T. Hashimoto, H. Tokieda, T. Tsuji, S. Kawase, H. Hamagaki, T. Uesaka, S. Kubono, T. Isobe, T. Kawabata, A. Ozawa, H. Suzuki, D. Nagae, T. Moriguchi, Y. Ito, Y. Ishibashi, H. Ooishi, Y. Abe</i>	
Simulation Study for Forward Calorimeter in LHC-ALICE experiment	61
<i>Y. Hori, H. Hamagaki, T. Gunji</i>	
Simulation Study of the Forward Calorimeter for the upgrade of the LHC-ALICE experiment	63
<i>T. Gunji, H. Hamagaki, Y. Hori</i>	
Performance evaluation of the Forward Calorimeter for PHENIX upgrade	65
<i>T. Tsuji, H. Hamagaki, T. Gunji, Y. Hori, E. Kistenev, M. Chiu, A. Sukhanov, R. Seto, for the PHENIX FO-CAL group</i>	
Pulse structure dependence of the proton polarization rate	67
<i>T. Kawahara, T. Uesaka, Y. Shimizu, S. Sakaguchi, A. Shibusawa, T. Wakui</i>	
Method of pulse shape analysis for segmented Ge detectors	69
<i>S. Go, S. Shimoura, E. Ideguchi, S. Ota, H. Miya, H. Baba</i>	

3. Theoretical Nuclear Physics

Algebraic $N\alpha$ model (Applications for ^{12}C)	71
<i>T. Yoshida, N. Itagaki, K. Katō</i>	
Activities of Nuclear Shell-Model Studies in CNS	73
<i>N. Shimizu, T. Otsuka, and Y. Utsuno</i>	

4. Other Activities

Laboratory Exercise for Undergraduate Students	76
<i>S. Ota, K. Yako, H. Tokieda, K. Ozawa, S. Shimoura</i>	

Appendices

Symposium, Workshop, Seminar, PAC and External Review	79
CNS Reports	81
Publication List	82
Talks and Presentations	88
Personnel	94

Experimental Nuclear Physics: Low and Intermediate Energies

Measurement of alpha resonance scattering on ${}^7\text{Be}$

H. Yamaguchi, T. Hashimoto, S. Hayakawa, D.N. Binh, D. Kahl, S. Kubono, T. Kawabata^a, Y. Wakabayashi^b, N. Iwasa^c, Y. Miura^c, Y.K. Kwon^d, L.H. Khiem^e, N.N. Duy^e, and T. Teranishi^f

Center for Nuclear Study, Graduate School of Science, University of Tokyo

^a*Department of Physics, Kyoto University*

^b*Advanced Science Research Center, JAEA*

^c*Department of Physics, Tohoku University*

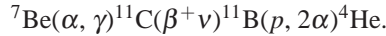
^d*Department of Physics, Chung-Ang University*

^e*Institute of Physics and Electronics, Vietnam Academy of Science and Technology*

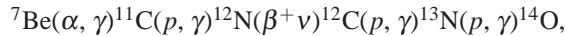
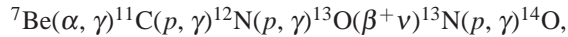
^f*Department of Physics, Kyushu University*

A measurement of the ${}^7\text{Be}+\alpha$ elastic scattering was performed at CRIB [1, 2], to study the resonance structure of ${}^{11}\text{C}$. The excited states of ${}^{11}\text{C}$ above the threshold for the α -particle decay are particularly of interest from the following points of view.

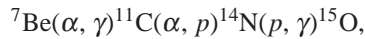
The first is on the astrophysical interest. The ${}^7\text{Be}(\alpha, \gamma){}^{11}\text{C}$ reaction is considered to play an important role in the hot p - p chain and related reaction sequences [3]. Several reaction sequences including the ${}^7\text{Be}(\alpha, \gamma){}^{11}\text{C}$ reaction should take place in some high-temperature environments ($T_9 > 0.2$). One of those sequences is called pp-V,



Others are rap (II, III and IV) sequences,



and



which are reaction chains to synthesize CNO nuclei without the triple- α process. The ${}^7\text{Be}(\alpha, \gamma){}^{11}\text{C}$ reaction and these sequences are considered to be important in the explosion of supermassive objects with lower metallicity [4], novae [5] and big-bang nucleosynthesis. The ${}^7\text{Be}(\alpha, \gamma){}^{11}\text{C}$ reaction rate is greatly affected by the resonances. At the lowest temperature, the reaction rate is determined by the subthreshold resonance at the excitation energy $E_{\text{ex}}=7.50$ MeV and the direct capture rate. The two resonances located at $E_{\text{ex}}=8.11$ MeV and $E_{\text{ex}}=8.42$ MeV determine the rate at high temperature around $T_9 = 0.5$ – 1 . Higher excited states may contribute to the reaction rates at very high temperature ($T_9 > 1$).

Resonance states above 9 MeV were previously studied via ${}^{10}\text{B}(p, \alpha)$ and single-nucleon transfer reactions such as ${}^{12}\text{C}(p, d){}^{11}\text{C}$ [6, 8, 7, 9]. The resonances have typically widths of the order of 100 keV, but their α -decay widths are still not known with a good precision, and the spin and parity have not been clearly determined yet. The excited states at lower energies ($E_{\text{ex}}=8$ – 9 MeV) have narrower particle widths, and the α widths are unknown, except for the two

resonances located at $E_{\text{ex}}=8.11$ MeV and $E_{\text{ex}}=8.42$ MeV. The ${}^7\text{Be}(\alpha, \gamma){}^{11}\text{C}$ reaction rate was directly measured only at the energies of these two resonances [10], where the resonance parameters including α widths were determined.

The $3/2_3^-$ state in ${}^{11}\text{C}$ at $E_{\text{ex}}=8.11$ MeV is regarded as a dilute cluster state [11], where two α particles and ${}^3\text{He}$ are weakly interacting and spatially much developed. Its exotic structure is attracting much attention [12]. The cluster structure in ${}^{11}\text{B}$, the mirror nucleus of ${}^{11}\text{C}$, was studied by measuring its isoscalar monopole and quadrupole strengths in the ${}^{11}\text{B}(d, d')$ reaction [13, 14]. As a result, they indicated that the mirror state of the 8.11-MeV state is considered to have a dilute cluster structure. It is also claimed that the large monopole strength for the $3/2_3^-$ state at $E_{\text{ex}}=8.56$ MeV in ${}^{11}\text{B}$ is an evidence of the $2\alpha + t$ cluster structure. If the $3/2_3^-$ state has a large deformation that arises from the developed cluster structure, a characteristic rotational band is expected to be formed. It is interesting to search for the rotational band built on the $3/2_3^-$ state in the present measurement.

In the present study, we used the ${}^7\text{Be}+\alpha$ resonant elastic scattering to observe α resonances. The strength of the resonances are expected to provide information on the α -cluster structure of ${}^{11}\text{C}$, and on the astrophysical ${}^7\text{Be}(\alpha, \gamma)$ reaction rate. The measurement was performed using the thick target method in inverse kinematics [15] to obtain the excitation function for E_{ex} at 8.5–13.0 MeV in ${}^{11}\text{C}$. The experimental setup is almost identical to the one used in the ${}^7\text{Li}+\alpha$ measurement [17]. A pure and intense ${}^7\text{Be}$ beam can be produced at CRIB using a cryogenic target [16]. In the present measurement, a low energy ${}^7\text{Be}$ beam at 14.7 MeV was produced using a 2.3-mg/cm²-thick hydrogen gas target and a ${}^7\text{Li}$ beam at 5.0 MeV/u. The purity of the ${}^7\text{Be}$ beam was almost 100% after the Wien filter. The typical ${}^7\text{Be}$ beam intensity used in the measurement was 2×10^5 per second at the secondary target, and the main measurement using a helium-gas target was performed for 4 days.

A Micro-Channel Plate (MCP) was used for the detection of the beam position and timing. A CsI-evaporated 0.7- μm -thick aluminum foil was placed on the beam axis for the secondary electron emission. The secondary electrons were reflected by 90 deg at a biased thin-wire reflector and detected at the MCP with a delay-line readout.

The gas target consisted of a 50-mm-diameter duct and

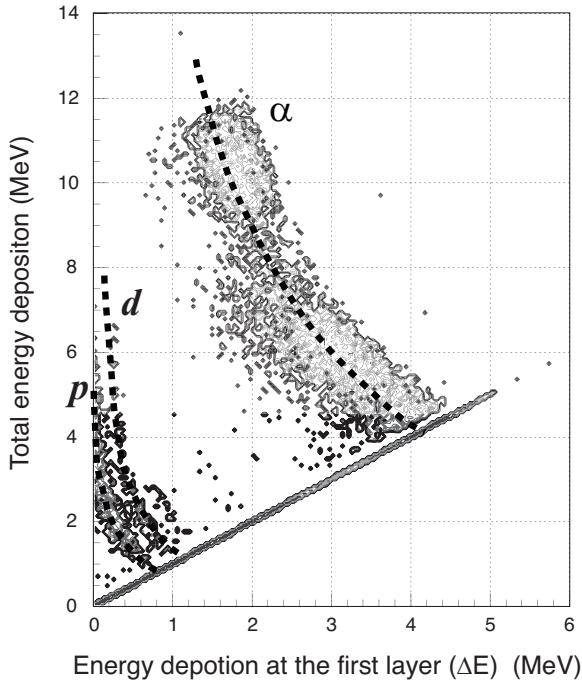


Figure 1. ΔE - E plot for the particle identification.

a small chamber. Helium gas at 800 Torr was filled and sealed with a 2.5- μm -thick Havar foil as the beam entrance window. The helium gas was sufficiently thick to stop the ^7Be beam in it. α particles recoiling to the forward angles were detected by the “ ΔE - E detector”. The detector, consisting of 20- μm - and 490- μm -thick silicon detectors, was placed in the gas chamber. The distance from the beam entrance window to the detector was 250 mm. To measure 429-keV gamma rays from inelastic scattering to the first excited state of ^7Be , NaI detectors were placed around the duct. We used ten NaI crystals, each with a geometry of $50 \times 50 \times 100$ mm. They covered 20–60% of the total solid angle, depending on the reaction position.

Figure 1 shows the energies of particles detected at the ΔE - E detector, in coincidence with the ^7Be beam at the MCP. Most of the particles measured was α from the elastic scattering, and a small number of protons and deuterons were observed in the measurement. A measurement using an argon-gas target of the equivalent thickness was also performed to evaluate the background α particles as the contamination in the beam.

The calculation of the kinematics by taking into account the energy loss in the gas target provided the excitation energy of ^{11}C from the measured energy of the α particle. The obtained energy spectrum of alpha particles is shown in Fig. 2. A structure with peaks, considered to be due to alpha resonances, was observed. An excitation function for the $^7\text{Be}+\alpha$ elastic scattering will be obtained in the future analysis. The resonance parameters to be determined in this study, such as the spin, parity and α width (related with the spectroscopic factor of the α -cluster configuration) would provide valuable information for the α -cluster structure in

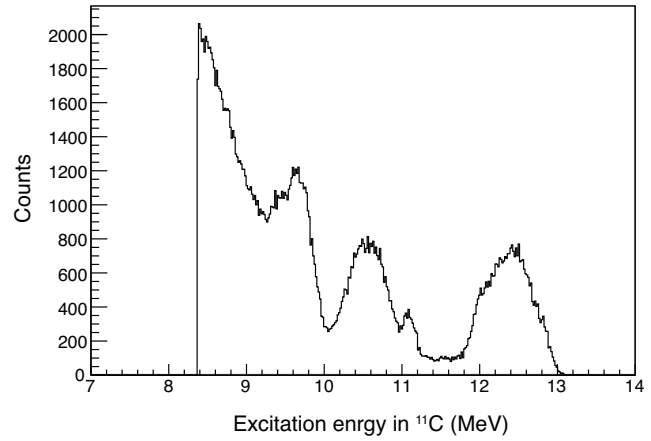


Figure 2. Energy spectrum of the α particles in the measurement. The α particles were mostly from $^7\text{Be}+\alpha$ elastic scattering.

the high excited states, and astrophysical reaction rates in high-temperature phenomena.

References

- [1] S. Kubono *et al.*, *Eur. Phys. J. A* **13** (2002) 217.
- [2] Y. Yanagisawa *et al.*, *Nucl. Instrum. Methods Phys. Res., Sect. A* **539** (2005) 74.
- [3] M. Wiescher *et al.*, *Astrophys. J.* **343** (1989) 352.
- [4] G. Fuller *et al.*, *Astrophys. J.* **307** (1986) 675.
- [5] M. Hernanz *et al.*, *Astrophys. J.* **465** (1996) L27.
- [6] S. Hunt *et al.*, *Phys. Rev.* **106** (1957) 1012.
- [7] J. Olness *et al.*, *Phys. Rev.* **139** (1965) B512.
- [8] J. Overley and W. Whaling, *Phys. Rev.* **128**, (1962) 315.
- [9] H. Hauser *et al.*, *Nucl. Phys. A* **456** (1986) 253.
- [10] G. Hardie *et al.*, *Phys. Rev. C* **29** (1984) 1199.
- [11] A. Tohsaki *et al.*, *Phys. Rev. Lett.* **87** 192501 (2001).
- [12] Y. Kanada-En'yo, *Phys. Rev. C* **75** 024302 (2007).
- [13] T. Kawabata *et al.*, *Phys. Rev. C* **70** 034318 (2004).
- [14] T. Kawabata *et al.*, *Phys. Lett. B* **646** 6 (2007).
- [15] K. Artemov *et al.*, *Sov. J. Nucl. Phys* **52** (1990) 408.
- [16] H. Yamaguchi *et al.*, *Nucl. Instrum. Meth. Phys. Res., Sect. A* **589**, (2008) 150–156.
- [17] H. Yamaguchi *et al.*, *CNS Annual Report 2008* (2009).

R-matrix analysis on the excitation function of ${}^7\text{Li}+\alpha$ elastic scattering

H. Yamaguchi, T. Hashimoto, S. Hayakawa, D.N. Binh, D. Kahl, S. Kubono, Y. Wakabayashi^a,
T. Kawabata^b, and T. Teranishi^c

Center for Nuclear Study, Graduate School of Science, University of Tokyo

^aAdvanced Science Research Center, JAEA

^bDepartment of Physics, Kyoto University

^cDepartment of Physics, Kyushu University

A measurement of ${}^7\text{Li}+\alpha$ was performed at CRIB [1, 2], as previously reported in ref. [3]. An excitation function of ${}^7\text{Li}+\alpha$ elastic scattering was obtained as shown in Fig. 1, and a structure with several peaks were clearly observed. We performed an analysis using an R-matrix cal-

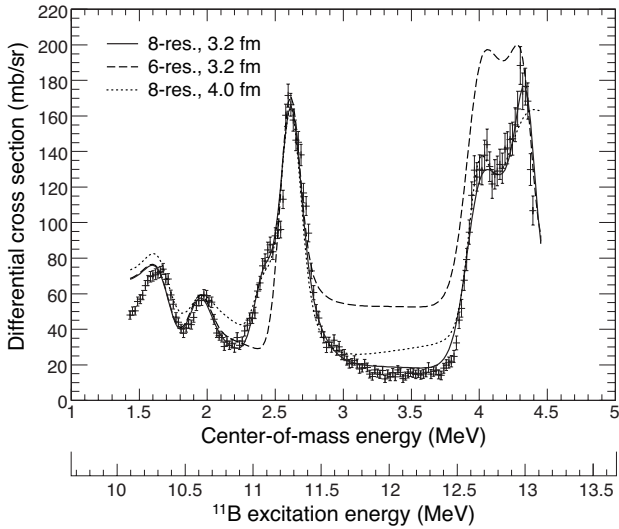


Figure 1. Excitation function of ${}^7\text{Li}+\alpha$ elastic scattering fitted by R-matrix calculation curves. The solid curve is the best fit with $R_c=3.2$ fm, and the dashed curve shows the same calculation without 2 newly introduced resonances. The dotted curve is the best fit for $R_c=4.0$ fm.

ulation code (SAMMY-M6) to deduce resonance parameters. Initially we calculated the excitation function assuming 6 known alpha resonances shown in Table. 1. The energy, spin and parity (J^π) of each resonance were fixed to the known values [4], and the α width (Γ_α) was adjusted to fit the experimental data. For the excitation energies, the values by ${}^7\text{Li}+\alpha$ measurement, among the value by other reactions, were used. For some states the energies were determined more precisely by other reactions, but basically consistent with the values by ${}^7\text{Li}+\alpha$ measurement. There are major two discrepancies which could not be explained by the 6-resonance calculation. The first one is a small bump seen around the excitation energy $E_{\text{ex}}=11.1$ MeV, on the shoulder of the peak at 11.29 MeV. The second one is at 11.5–12.5 MeV, where the measured cross section was much depleted compared to the calculation. By introducing two resonances corresponding to the discrepancies, a best fit was obtained as shown by a solid curve in Fig. 1. For the

first discrepancy, an f-wave resonance was introduced. The best fit was obtained for $J^\pi=5/2^+$, but other J^π ($3/2^+$, $7/2^+$, $9/2^+$) could not be excluded. For the latter one, a broad resonance at $E_{\text{ex}}=11.6$ MeV having a large neutron width, which is not known from previous measurements, was introduced. This assumption is quite artificial, and may not suggesting the existence of a true single resonance having a large width, which far exceeds the Wigner limit. Similarly, a broad neutron resonance at $E_{\text{ex}}=11.79$ MeV was assumed in a previous work [5] to explain their data of ${}^{10}\text{B}(n, \alpha)$ reaction measurement. A calculation with the same parameters but without the two resonances is also shown in the figure for comparison.

The calculation was best performed with a channel radius $R_c=3.2$ fm, which might be rather small for this system. A similar radius was used for an optical model calculation [6]. Larger channel radii resulted in less satisfactory fit results, as shown in the figure for the case of $R_c=4.0$ fm. The best-fit parameters are summarized in Table. 1. Here the Wigner limit Γ_w was calculated for an interaction radius $R=3.2$ fm, and the reduced width γ_α^2 was calculated by $\Gamma_\alpha/2P$, where P is the penetration factor. Γ_α was only partly known in previous measurements. Here we compared Γ_α with the R-matrix analysis parameters in ref. [7], and γ_α^2 with refs. [8] and [9], in which Γ_α was not presented explicitly. As for γ_α^2 , the agreement is not very good between the present work ($R=3.2$ fm), and previous results ($R=4.9$ fm [8] and $R=6.0$ fm [9]), partly because they use different R to explain their data. Our measurement is considered to be quite insensitive to the total width, since the spectral widths of all the resonances are mostly determined by the experimental resolution and Γ_α . Below we discuss the highest two resonances in detail.

Resonance at 12.63 MeV

We started the calculation with a known resonance energy of 12.55 MeV, but the measured peak appeared at a higher energy of 12.63 MeV. The state at 12.55 MeV is considered to have $J^\pi=1/2^+$ and an isospin $T=3/2$, being analogue of the ${}^{11}\text{Be}$ ground state. It was observed via ${}^9\text{Be}({}^3\text{He}, p)$ [10], ${}^{11}\text{B}({}^3\text{He}, {}^3\text{He})$ [11], and other reactions [4]. The assignment $J^\pi=1/2^+(3/2^+)$ was proposed by a measurement of ${}^{10}\text{Be}(p, \gamma){}^{11}\text{B}$ reaction [12]. They measured the angular distribution of γ rays, and concluded the distribution is consistent only with $J^\pi=1/2^+$ or $3/2^+$, and the former is more likely. However, a $T=3/2$ state is unexpected to be observed as a strong resonance via ${}^7\text{Li}+\alpha$ scattering, as in the present work and in ref. [9]. The dual

Table 1. Best-fit resonance parameters of ^{11}B in the present work. The Wigner limit Γ_w and the reduced width γ_α^2 are also shown. The values shown by italic letters are from ref. [4]. *1) We do not regard this as a single-state resonance. *2) An alternative spin assignment beyond the values in ref. [4] (see text).

E_{ex} (MeV)	J^π	l	Γ_α (keV)		Γ_w (keV)	γ_α^2 (MeV)		
			present	[7]		present	[8]	[9]
<i>10.24</i>	<i>3/2⁻</i>	2	4 (< 9)		72	0.089	0.227	0.05
<i>10.34</i>	<i>5/2⁻</i>	2	19 ± 4		94	0.32		0.09
<i>10.60</i>	<i>7/2⁺</i>	3	10 ± 3	30	15	1.1	0.640	0.084
11.06 ± 0.04	$5/2^+$ ($3/2^+$, $7/2^+$, $9/2^+$)	3	32 ± 20		41	1.25		
<i>11.29</i>	<i>9/2⁺</i>	3	35 ± 4		63	0.89		
(11.59)*1	($7/2^-$)	4	270 ($\Gamma_n=580$)		(7)			
12.63 ± 0.04	$3/2^+$	3	270^{+100}_{-70}	275	330	1.3		
	$9/2^{+*2}$	3	42^{+11}_{-9}	275	330	0.20		
<i>13.03</i>	<i>9/2⁻</i>	4	140^{+80}_{+110}		58	2.5		

character ($T = 3/2$ and $1/2$) of this state, possibly suggesting a large isospin mixing, is a long standing problem and remained unsolved for a long time [12, 13, 14, 15]. A complete understanding, including theoretical prediction for the width, is still not obtained yet. Recently Fortune [16] made a reanalysis of the data in ref. [12] and pointed out the $1/2^+$ resonance could be much broader than considered before. To form a $1/2^+$ resonance, the α particle must be coupled by $l=1$ (p-wave). Our R-matrix calculation indicates that the sharp resonance could not be formed with a p-wave, but an f-wave resonance fits the experimental result perfectly.

Considering above, the present result suggests a different point of view: The resonance observed in this work may not be the known one at 12.55 MeV, but another one located at 12.63 MeV having a different J^π . They might have been considered as the same resonance in some previous measurements such as in ref. [9]. The J^π of the state can be $3/2^+$, which was listed as a possible assignment in ref. [12]. Another suggestion made by Soić and co-workers [17] was this state can have a $J^\pi=9/2^+$ from schematics of the rotational band of an alpha cluster state. Therefore, we performed the R-matrix analysis for both cases, $J^\pi=3/2^+$, and $9/2^+$.

Resonance at 13.03 MeV

This resonance was observed initially via the $^{10}\text{B}(n, \alpha)^7\text{Li}$ reaction [18], and then via $^7\text{Li}+\alpha$ inelastic scattering at 13.03 MeV [9]. Later two states at 13.12 MeV ($J^\pi=9/2^-$) and 13.17 MeV ($5/2^+$, $7/2^+$) were introduced in the analysis of ref. [7], and the 13.03 MeV resonance was regarded as the former one [4]. Zwiegliniski and co-workers [19] observed a state by the $^9\text{Be}(^3\text{He}, p)^{11}\text{B}$ reaction at 13.137 MeV, which is the value in the compilation [4] for the $J^\pi=9/2^-$ state. However, obviously there is a confusion on the energy and J^π of this level, because they also mention a state with $J^\pi=9/2^-$ was not expected to be strongly excited by that reaction. After all the assignment of $J^\pi=9/2^-$ is not so evident, since no measurement is known that observed this resonance separately from other ones and determined its J^π as $9/2^-$.

In the present analysis, we considered three possible J^π for the levels previously observed at 13.03, 13.137 and

13.16 MeV, $9/2^-$, $5/2^+$, and $7/2^+$, and only the calculation with $J^\pi=9/2^-$ resulted in a reasonable fit. A sudden fall in the spectrum at 4.4 MeV corresponds to the the highest limit of the energy acceptance of our measurement. The two highest energy points shown in the figure were excluded in the R-matrix fitting. The rest points, covering the peak cross section, were within the energy acceptance.

References

- [1] S. Kubono *et al.*, Eur. Phys. J. A **13** (2002) 217.
- [2] Y. Yanagisawa *et al.*, Nucl. Instrum. Meth. A **539** (2005) 74.
- [3] H. Yamaguchi *et al.*, CNS Annual Report 2008 (2009).
- [4] F. Ajzenberg-Selove, Nucl. Phys. A **506**, (1990) 1.
- [5] R. Lane *et al.*, Phys. Rev. C **4**, (1971) 380.
- [6] H. Bingham *et al.*, Nucl. Phys. A **175**, (1971) 374.
- [7] S.L. Hausladen *et al.*, Nucl. Phys. A **217** (1973) 563.
- [8] P. Paul *et al.*, Phys. Rev. **164** (1967) 1332–1342.
- [9] R.Y. Cusson *et al.*, Nucl. Phys. **86** (1966) 481–508.
- [10] D. Groce, J. McNally, and W. Whaling, Bull. Am. Phys. Soc. **8**, (1963) 486.
- [11] B. Watson, C. Chang, and M. Hasinoff, Nucl. Phys. A **173**, (1971) 634.
- [12] D. Goosman, E. Adelberger, and K. Snover, Phys. Rev. C **1**, (1970) 123.
- [13] R. Sherr and G. Bertsch, Phys. Rev. C **32**, (1985) 1809.
- [14] R. Sherr and H. Fortune, Phys. Rev. C **64**, (2001) 064307.
- [15] F. Barker, Phys. Rev. C **69**, (2004) 024310.
- [16] H. Fortune, Phys. Rev. C **74**, (2006) 034328.
- [17] N. Soić *et al.*, Nucl. Phys. A **742** (2004) 271–290.
- [18] B. Petree *et al.*, Phys. Rev. **83**, (1951) 1148.
- [19] B. Zwiegliniski *et al.*, Nucl. Phys. A **389** (1982) 301.

Multichannel R-matrix analysis for an alpha scattering in inverse kinematics using a ^{21}Na radioisotope beam

D. N. Binh^a, L. H. Khiem^b, N. T. Tho^b, S. Kubono^a, H. Yamaguchi^a, Y. Wakabayashi^a, S. Hayakawa^a, D. Kahl^a, T. Hashimoto^a, T. Teranishi^c, S. Kato^d, K. Iwasa^e

^aCenter for Nuclear Study, Graduate School of Science, University of Tokyo

^bInstitute of Physics and Electronics, Vietnamese Academy for Science and Technology

^cDepartment of Physics, Kyushu University

^dPhysics Department, Yamagata University

^eDepartment of Physics, Tohoku University

1. Introduction

Nucleosynthesis of ^{22}Na is an astronomically interesting subject because of potential Galactic γ -ray observation [1, 2, 3], and isotopic abundance anomalies of ^{22}Ne in presolar grains [4]. In the stellar environment, ^{22}Na would be mainly produced through the hot NeNa cycle from the seed nucleus ^{20}Ne , and the β -decay ($T_{1/2}=2.6$ yr) leads to the first excited state in ^{22}Ne , which de-excites to its ground state by emitting a characteristic 1275 keV γ -ray [1]. A few observational searches for this γ -ray signal have been performed utilizing satellite observatories, but this γ -ray has not been observed yet [5]. It is pointed out that the Ne-E problem, which is very high enrichment of ^{22}Ne in certain meteorites, would originate from ^{22}Na [4]. The $^{21}\text{Na}(\alpha, p)^{24}\text{Mg}$ stellar reaction is a break-out process from the NeNa cycle to the MgAl cycle. It could bypass ^{22}Na , resulting in reduction of ^{22}Na production. In order to understand these processes, we performed for the first time the measurement of the $^{21}\text{Na} + \alpha$ scattering and a direct measurement of the $^{21}\text{Na}(\alpha, p)$ reaction in inverse kinematics with the thick target method [7, 6] using a ^{21}Na RI beam. In this report, we discuss only the alpha scattering experiment result and an application of a multichannel R-matrix method to extract resonance parameters.

2. Experiment and Data Analysis

The ^{21}Na beam used in the experiment was produced by the CNS low-energy in-flight separator (CRIB) [8] which consists of a cryogenic gas production target, a double-achromatic magnetic separator, a Wien filter, and a scattering chamber [9]. The experimental setup was set in the scattering chamber. There are two parallel-plate avalanche counters (PPACs) [10] to track the beam direction and to deduce fast timing information. They were followed by a semi-cylinder gas target with a length of 15 cm which contained helium gas at a pressure of 580 Torr. $\Delta E - E$ telescopes were mounted downstream of the gas target at three different scattering angles (6° , 16° and 26°) with respect to the beam line. The reaction products, which were mainly alphas and protons, were measured by three $\Delta E - E$ telescopes. The alpha and proton particles were clearly identified by the $\Delta E - E$ method and the E - TOF method, where, the TOF is a flight time of particles measured from the first PPAC to the Si telescope.

The energy region in the center of mass system covered

by the experimental setup was from 1.6 MeV to 6.2 MeV. The data were analyzed event-by-event. The incident energy of ^{21}Na at the interaction and the scattering angle were determined by solving the kinematics equation with energy loss correction. The excitation functions were deduced for three different scattering angular regions, $0^\circ - 5^\circ$, $5^\circ - 10^\circ$ and $10^\circ - 15^\circ$. The data were separated into low and high energy parts by an energy gap (from 3.48 MeV to 3.79 MeV) due to the dead layer of the ΔE detector. The low energy part mainly contained Coulomb scattering, and there could be a resonance at about 3.3 MeV. Five resonances have been observed for the first time as presented in Fig. 1. In the high energy part, four resonances have been observed clearly. The uncertainties in the resonance energies mainly resulted from the energy resolution of the detectors themselves, the angular resolution due to the finite size of strip (3 mm) of detectors, and the energy straggling of the alpha particles through the gas target and the exit window foil. In total, the energy resolution obtained was 50 – 80 keV depending on the scattering angles and the resonance energies.

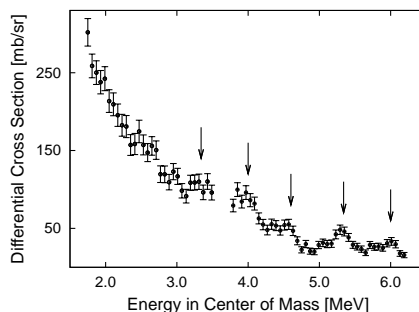


Figure 1. The excitation function of the alpha scattering cross sections (Observed resonances are indicated by arrows).

3. Multichannel R-matrix Analysis and Results

Resonance parameters were assigned using the multichannel R-matrix analysis method [11] with the SAMMY code [12]. The effect of other decay channels than the alpha channel were considered. According to a Q-value consideration, proton and γ channels are opened with high positive Q-values. Since the decay width of the γ channel (Γ_γ) is much smaller than those of the alpha (Γ_α) and proton (Γ_p) channels, $\Gamma_{tot} \approx \Gamma_\alpha + \Gamma_p$ and the proton decay channel

could mainly affect the alpha scattering cross section. The energies and total widths of resonances were derived by fitting the experimental data with a Lozentzian function. In order to vary the alpha and proton widths within the total width, we proposed to vary a ratio between proton reduced width and alpha reduced width ($\theta_p^2/\theta_\alpha^2$) in steps of 0.1 %. The R-matrix fitting has been applied for the low and high energy parts separately. For each energy part, all possible combinations of the alpha and proton widths as well as spin-parities were considered. We found that there are only four configurations in the high energy part and one resonance in the low energy part that the R-matrix fitting has a χ^2 value within a standard deviation, corresponding to certain range of $\theta_p^2/\theta_\alpha^2$ value, as shown in Fig. 2.

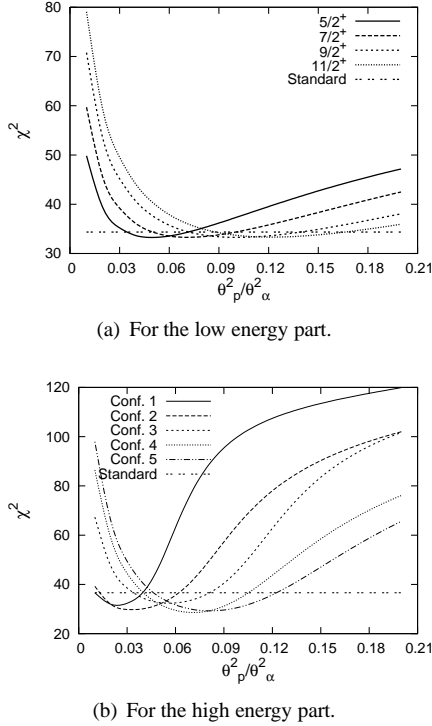


Figure 2. The χ^2 of the R-matrix fitting.

The experimental data of the $^{24}\text{Mg}(p,\alpha)^{21}\text{Na}$ reaction, measured with the activation method [13], were used to deduce the $^{21}\text{Na}(\alpha,p_0)^{24}\text{Mg}$ cross section by the detailed-balance theorem. The proton width obtained above by the R-matrix could include several transitions, not only transition to the ground state of ^{24}Mg . Therefore, if they are used to calculate the $^{21}\text{Na}(\alpha,p)^{24}\text{Mg}$ cross section, this cross section should be larger than that of the $^{21}\text{Na}(\alpha,p_0)$ reaction cross section from the time-reversed reaction study. Under this condition, two configurations in the high energy region were eliminated, since their calculated cross sections were smaller than that of the time-reversed cross section around the resonance at 5.97 MeV.

Figure 3 shows the best case by combining the best fittings of the separate low and high energy parts which had the smallest χ^2 values. The result of the R-matrix analysis is summarized in Table 1. The obtained resonance parameters can be used to calculate a rate of the $^{21}\text{Na}(\alpha,p)^{24}\text{Mg}$

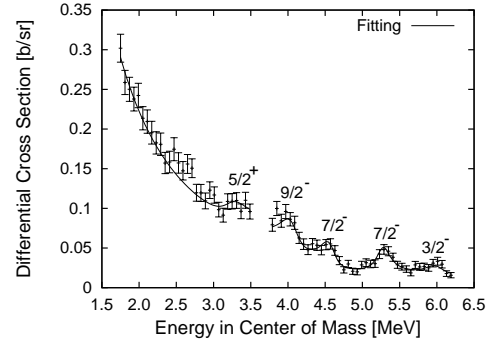


Figure 3. The best fitting lines by the R-matrix analysis (See text for detail).

reaction. It is important to understand experimentally a contribution of this reaction to the production of ^{22}Na . A detail of this discussion is not represented in this report.

Table 1. Resonant states in ^{25}Al observed in the present work.

E_r (MeV)	Γ_α (MeV)	Γ_p (MeV)	J^π
3.32 ± 0.07	$0.05 - 0.12$	$0.15 - 0.23$	$(5/2^+, 7/2^+, 9/2^+, 11/2^+)$
4.10 ± 0.08	$0.15 - 0.19$	$0.10 - 0.22$	$9/2^-$
$4.57^{+0.09}_{-0.06}$	$0.12 - 0.19$	$0.05 - 0.13$	$5/2^-$ $7/2^-$
$5.33^{+0.07}_{-0.06}$	$0.17 - 0.19$	$0.05 - 0.13$	$7/2^-$
$5.97^{+0.07}_{-0.09}$	$0.22 - 0.24$	$0.05 - 0.12$	$3/2^-$ $(3/2^-, 5/2^-)$

References

- [1] D. D. Clayton and F. Hoyle, *Astro. Journa.* **187** (1974) 101.
- [2] P. Jean and *et al.*, *Proc. of the 5th INTEGRAL Workshop ESA-SP 552* (2004) 119.
- [3] M. Aliotta, *Eur. Phys. J. Special Topics* **150** (2007) 201.
- [4] M. Arnould and H. Norgaard, *Astro. Astrophys.* **64** (1978) 195.
- [5] A. F. Iyudin *et al.*, *Astro. Astrophys.* **443** (2005) 447.
- [6] Artemov, K. P. and *et al.*, *Sov. J. Nucl. Phys.* **52** 408.
- [7] S. Kubono, *Nucl. Phys. A* **693** (2001) 221.
- [8] Y. Yanagisawa *et al.*, *Nucl. Instru. Meth. A* **539** (2005) 1.
- [9] Kubono, S., *Eur. Phys. J. A*, **13** (2002) 217.
- [10] H. Kumagai *et al.*, *Nucl. Instru. Meth. A* **470** (2001) 562.
- [11] A. M. Lane and R. G. Thomas, *Rev. Mod. Phys.* **30** (1958) 257.
- [12] N. M. Larson, *A code system for multilevel R-matrix fits to neutron data using Bayes' equations*, ORNL/TM-9179/R5 (2000).
- [13] W. Gruhle and B. Kober, *Nucl. Phys. A* **286** (1977) 523.

First direct measurement of the $^{11}\text{C}(\alpha, p)^{14}\text{N}$ stellar reaction

S. Hayakawa, S. Kubono, T. Hashimoto, H. Yamaguchi, D.N. Binh, D. Kahl, Y. Wakabayashi^a,
N. Iwasa^b, N. Kume^b, Y. Miura^b, T. Teranishi^c, J.J. He^d, Y.K. Kwon^e, T. Komatsubara^f, S. Kato^g
and S. Wanajo^h

Center for Nuclear Study, Graduate School of Science, University of Tokyo

^aAdvanced Science Research Center, Japan Atomic Energy Agency

^bDepartment of Physics, Tohoku University

^cDepartment of Physics, Kyushu University

^dInstitute of Modern Physics, Chinese Academy of Science

^eDepartment of Physics, Chung Ang University

^fDepartment of Physics, University of Tsukuba

^gDepartment of Physics, Yamagata University

^hDepartment of Physics, Munich University of Technology

1. Introduction

The $^{11}\text{C}(\alpha, p)^{14}\text{N}$ reaction is considered to be a pathway responsible for the nucleosynthesis from the pp-chain region to the CNO region, in addition to the well-known triple-alpha process. This reaction path is likely to be effective in high-temperature hydrogen burning processes, such as the breakout process from the hot pp-chains [1] in low-metallicity stars, or the vp-process [2, 3, 4] in core-collapse supernovae. Recent simulations of the vp-process [5] suggest that this reaction path considerably contributes at 1.5–3 GK and eventually affects the abundance pattern of the p-nuclei around $A = 90$ –110.

There are reaction rate data sets of this reaction available from the time-reversal reaction measurements with the activation method [6] or the Hauser-Feshbach statistical model calculations by the code NON-SMOKER^{WEB} [7]. But the former provides only the $^{11}\text{C}(\alpha, p_0)^{14}\text{N}$ reaction rate, and the latter is not always properly applicable for such resonance-dominant light nuclei, thus both of them could provide incorrect reaction rates. In order to resolve this issue, we have performed the first-ever direct measurement of the $^{11}\text{C}(\alpha, p)^{14}\text{N}$ reaction cross sections aiming at distinguishing among the $^{11}\text{C}(\alpha, p_0)^{14}\text{N}$, $^{11}\text{C}(\alpha, p_1)^{14}\text{N}^*$, $^{11}\text{C}(\alpha, p_2)^{14}\text{N}^*$, etc. in the center-of-mass energy range from 1 to 4.5 MeV, including the Gamow windows from 1.5 to 3 GK of astrophysical interest.

2. Experiment

The measurements were performed by means of the thick-target method [8] in inverse kinematics using secondary beams produced by CRIB (CNS Radioactive Ion Beam separator) at the Center for Nuclear Study (CNS), the University of Tokyo [9].

We used two ^{11}C beams at different kinetic energies to cover a wide excitation energy range in the compound nucleus ^{15}O , and a ^{11}B beam to compare with the known $^{11}\text{B}(\alpha, p)^{14}\text{C}$ reaction cross section [10, 11]. The $^{11}\text{B}^{3+}$ primary beam was provided by the RIKEN AVF cyclotron at 4.6 MeV/u with a maximum intensity of 1 μA . The secondary beam particles ^{11}C were produced via the $^1\text{H}(^{11}\text{B}, ^{11}\text{C})n$ reaction with a 1.2–1.7-mg/cm²-thick cryo-

Table 1. Secondary beam conditions used for the experiment

Beam particle	E_{cm} range [MeV]	Beam rate [pps]
$^{11}\text{C}^{6+}$	2.3–4.5	1.0×10^5
$^{11}\text{C}^{6+}$	0.0–2.7	3.1×10^5
$^{11}\text{B}^{5+}$	2.9–4.5	2.6×10^5

genic hydrogen gas target. The same target condition was also utilized for energy degrading of the ^{11}B beam used for the reference purpose. The energy losses of the secondary beams in the secondary ^4He gas target were directly measured independently from the reaction measurement runs with a Si detector at 5 different gas thicknesses from 0 to 1.24 mg/cm². The resultant beam purities were almost 100%. Other beam conditions used for the experiment are summarized in Table 1.

A schematic plane view of the experimental setup is illustrated in Fig. 1. We used two types of beam detectors (*i.e.* Parallel Plate Avalanche Counters (PPAC1, PPAC2) and/or a Microchannel Plate (MCP) detector) for beam trajectory and timing measurement. By switching between PPAC2 and the MCP detector, we produced different incident ^{11}C energies as shown in Table 1 without changing the condition of the achromatic system of CRIB. The target has a semi-cylindrical shape whose length from entrance to exit on the beam axis was 140 mm. The 400-Torr ^4He gas was confined by a 2.5- μm -thick Havar foil at the entrance and a 25- μm -thick Mylar foil at the exit. The incident ^{11}C beam energy of 10.1 MeV and 16.9 MeV covered the center-of-mass en-

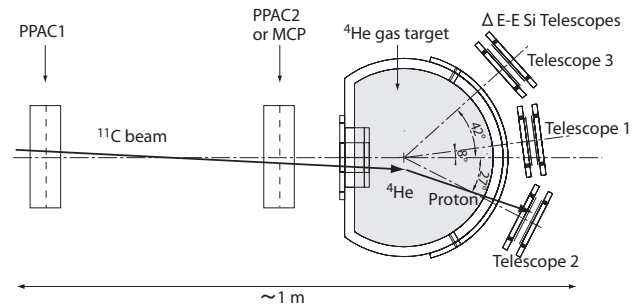


Figure 1. Schematic plane view of the experimental setup

ergy range of 0–4.5 MeV in the ^4He gas target. Recoil protons and α particles, as well as small numbers of deuterons and ^3He particles, were clearly identified with ΔE -E silicon telescopes. Each ΔE counter was a double-sided stripped silicon detector and the E counter was a single-pad silicon detector.

3. Analysis and Results

We successfully identified the final states in the time-versus-energy spectra of the recoil protons in which several separable groups corresponds to the (α, p_0) , (α, p_1) and (α, p_2) , as each transition for a given recoil proton energy has a different time information.

The center-of-mass energy, as well as the scattering angle, can be uniquely reconstructed with the kinematic quantities, such as the beam energy loss distribution in the target, the beam track, the proton energy, and the proton detection position. At present, the cross section was determined assuming isotropic decay, with the error bars including the statistical error and the isotropic fitting error. In Fig. 2, the newly determined excitation functions for the (α, p_0) , (α, p_1) and (α, p_2) are plotted. The resonant shapes of the (α, p_0) of this work were found to be consistent with the excitation function deduced from the time-reversal reaction data [12] via the principle of detailed balance. The (α, p_0) values for the high-energy run and the low-energy run show good consistency in their overlap region. The (α, p_1) and (α, p_2) excited functions are plotted only in limited ranges, but still cover most of the stellar energies up to 2.7 MeV.

Figure 3 shows the comparison of the relative reaction rates among the NON-SMOKER^{WEB} calculation [7], the $(\alpha, p_{0,1,2})$ reaction of this work and the (α, p_0) reaction of this work to the time-reversal reaction data labeled “CF88” [6], which is the one posted in the currently available data bases. The newly obtained reaction rate for the $(\alpha, p_{0,1,2})$ differs from either CF88 or NON-SMOKER^{WEB}.

More detailed discussions requires further works; the an-

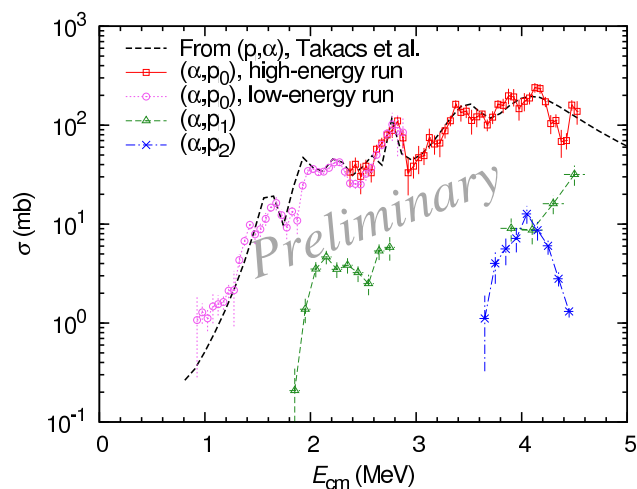


Figure 2. Excitation functions of the $^{11}\text{C}(\alpha, p_0)^{14}\text{N}$ (high-energy run: square, low-energy run: circle), $^{11}\text{C}(\alpha, p_1)^{14}\text{N}^*$ (triangle), and $^{11}\text{C}(\alpha, p_2)^{14}\text{N}^*$ (cross) reactions. The dashed line is obtained from the past time-reversal reaction studies [12].

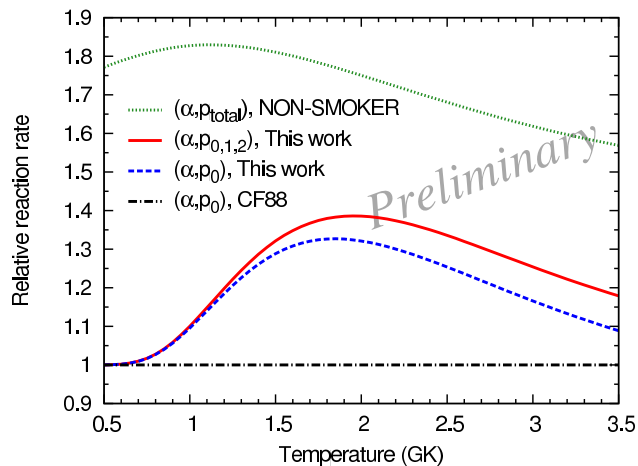


Figure 3. Comparison of the relative reaction rates among the NON-SMOKER^{WEB} calculation [7] (dotted line), the $(\alpha, p_{0,1,2})$ reaction of this work (solid line), and the (α, p_0) reaction of this work (dashed line) to the time-reversal reaction data (dashed-dotted line).

gular distributions of the differential cross sections are being analyzed for more proper integrations instead of assuming isotropy.

4. Conclusions

We successfully identified the (α, p_0) , (α, p_1) and (α, p_2) transitions and determined their preliminary excitation functions. The resonant shapes and absolute values of the (α, p_0) excitation function substantially agree well with the ones from the time-reversal reaction data over the energy range of measurement. Although the (α, p_1) , (α, p_2) excitation functions can be deduced only at limited energy ranges, we can reasonably estimate their contribution to the reaction rates at the stellar temperatures 1.5–3 GK. The preliminary reaction rate including measured $(\alpha, p_{0,1,2})$ is determined to be between the one in the current data base (CF88) and the Hauser-Feshbach calculation.

References

- [1] M. Wiescher *et al.*, *Astrophys. J.* **343** (1989) 352.
- [2] C. Fröhlich *et al.*, *Phys. Rev. Lett.* **96** (2006) 142502.
- [3] J. Pruet *et al.*, *Astrophys. J.* **644** (2006) 1028.
- [4] S. Wanajo, *Astrophys. J.* **647** (2006) 1323.
- [5] S. Wanajo *et al.*, arXiv:1004.4487 (2010).
- [6] G. Caughlan and W. Fowler, *Atomic data and nuclear data tables* **40**, (1988), 283.
- [7] T. Rauscher, http://nucastro.org/reaclib.html#ns_web.
- [8] K.P. Artemov *et al.*, *Sov. J. Nucl. Phys.* **52** (1990) 480.
- [9] Y. Yanagisawa *et al.*, *Nucl. Instrum. Meth. A* **539** (2005) 74.
- [10] W.S. Hou *et al.*, *Nucl. Sci. and Engin.* **66** (1978) 188.
- [11] L.L. Lee, Jr., J.P. Schiffer, *Phys. Rev.* **115** (1959) 160.
- [12] Takács *et al.*, *Nucl. Instrum. Meth. B* **240** (2005) 790.

Present status of the direct measurement of the $^{18}\text{Ne}(\alpha, p)^{21}\text{Na}$ reaction cross sections using the GEM – MSTPC

T. Hashimoto, S. Kubono, H. Yamaguchi, S. Hayakawa, D. Kahl, S. Ota, S. Michimasa, H. Tokieda, K. Yamaguchi^a, I. Arai^a, T. Komatsubara^a, H. Ishiyama^b, Y.X. Watanabe^b, H. Miyatake^b, Y. Hirayama^b, N. Imai^b, S. C. Jeong^b, Y. Mizoi^c, S. K. Das^c, T. Fukuda^c, H. Makii^d, Y. Wakabayashi^d, N. Iwasa^e, T. Yamada^e, A. A. Chen^e, J. J. He^g,

Center for Nuclear Study, Graduate School of Science, University of Tokyo

^a*Graduate School of Pure and Applied Sciences, University of Tsukuba*

^b*Institute of Particle and Nuclear Studies (IPNS), High Energy Accelerator Research Organization (KEK)*

^c*Research Center for Physics and Mathematics, Faculty of Engineering, Osaka Electro-Communication University*

^d*Advanced Science Research Center, Japan Atomic Energy Agency (JAEA)*

^e*Department of Physics, Tohoku University*

^f*Department of Physics and Astronomy, McMaster University*

^g*Institute of Madam Physics*

1. Introduction

The $^{18}\text{Ne}(\alpha, p)^{21}\text{Na}$ reaction is considered as one of the main possible breakout routes from the hot-CNO cycle to the rp-process. This reaction is considered to be dominant at around $T = 0.6 - 1.0$ GK which corresponds to the Gamow energy of $0.5 - 1.5$ MeV.

Although several experimental efforts on the $^{18}\text{Ne}(\alpha, p)^{21}\text{Na}$ reaction have been made in this energy region [1], the information is very limited yet. In order to determine the absolute reaction rate, the absolute cross sections in the energy region are needed. However no direct cross-section measurement of the reaction have been successfully performed yet in this energy region.

We plan to directly measure the excitation function of the $^{18}\text{Ne}(\alpha, p)^{21}\text{Na}$ reaction in the low energy region using a sophisticated active target type detector system, Multiple Sampling and Tracking Proportional Chamber with Gas Electron Multiplier (GEM–MSTPC). Figure 1 shows the experimental setup, which consists of a beam monitor, the GEM – MSTPC, and a Si detector array.

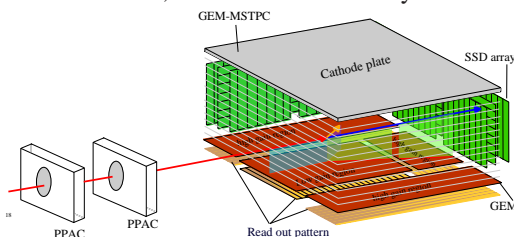


Figure 1. Experimental setup for the $^{18}\text{Ne}(\alpha, p)^{21}\text{Na}$ reaction.

The beam monitor consists of two PPACs. It can measure the time-of-flight of secondary beam and the position at each counter. Absolute beam energy and injected angle can be obtained by these values on event by event.

The Si detector array is set just outside of the gas sensitive area of the GEM –MSTPC in order to measure the energies and directions of protons. The telescope consists of 18 Si detectors. The Si detector is 90×90 mm² in size and consists of $450 \mu\text{m}$ thick with 9 strips. The solid angle and the angular range are 15% and $0 - 115$ degrees,

respectively.

The main chamber GEM – MSTPC has a structure based on the MSTPC [5, 6], It can measure the three dimensional trajectories and the energy loss of all relevant charged particle of reaction, which makes it possible to identify the true reaction events. In order to avoid a limitation of beam injection rate, we adopted a Gas Electron Multiplier (GEM) [7] foil in substitution for a multi-wire proportional counter of the MSTPC.

The GEM – MSTPC consists of a drift space region and GEMs and read – out pads. The drift space region has an active volume of 295 mm long, 278 mm wide 100 mm high. The proportional counter region consists of a low – gain regions for measurement of beam and/or recoil particles, and three high – gain region for measurement of emitted protons. Each region consists of one or more GEM foils and a position sensitive read – out pads. A Operating gas and its pressure are 90% ^4He and 10% CO_2 and 0.2 atm.

The feasibility of the experiment was discussed in Ref. [2]. In this report, the result of ^{18}Ne beam production and the development status of the GEM – MSTPC are described.

2. Low–energy ^{18}Ne beam production

We have performed a low–energy ^{18}Ne beam production at CNS Radioactive Ion Beam Separator (CRIB) [3]. The required conditions of ^{18}Ne beam are listed in Table 1. These conditions were achieved as described in the

Table 1. The required conditions of ^{18}Ne beam.

Intensity	$\geq 2 \times 10^5$ pps
Energy	≤ 4 MeV/u
Purity	$\geq 70\%$

following. The production reaction of ^{18}Ne particles is $^3\text{He}(^{16}\text{O}, n)^{18}\text{Ne}$ reaction. The ^{16}O beam, with energy of 6.8 MeV/u and the intensity of 560 particle nA, was irradiated on a cryogenic gas target [4] of ^3He at 90 K. Optimum gas pressure needs to be determined as a trade–off between the production rate and beam transition rate. The production rate increase with the production gas pressure, while

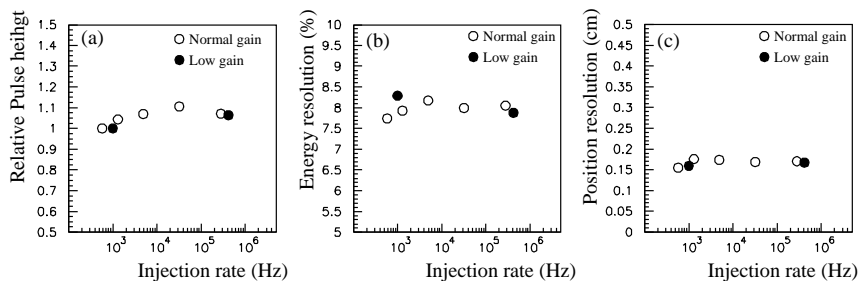


Figure 2. The results of the test experiment of the high beam injection capability. (a) indicates the relative pulse height, (b) is the energy resolution, and (c) is the position resolution of the pad direction.

a beam transmission decrease with it due to a beam emittance. We have measured beam purity and intensity of ^{18}Ne beam in several gas pressure conditions. Table 2 shows the measured results. ^{11}C is the competing background source with almost the same velocity, and the purity is the worst at 400 torr. At 760 torr, although the beam purity is good, the

Table 2. The production conditions of ^{18}Ne beam.

Gas pressure (torr)	Purity (%)	Intensity (pps)
760	70.3	3.3×10^4
560	81.2	5.1×10^5
400	15.3	1.8×10^4

beam intensity is lower compared the case at 560 torr. We consider that it is due to the beam transmission. From these results, the best condition of the production gas pressure is 560 torr. The energy and energy spread of ^{18}Ne beam were 3.7 MeV/u and 0.8 MeV in σ . At the required conditions were fulfilled in the case.

3. Status of the GEM–MSTPC

The required performances of the GEM – MSTPC are listed in Table 3. At first, we studied some proper-

Table 3. The required conditions of GEM – MSTPC.

Gas gain of low gain region	$\geq 10^3$
Gas gain of high gain region	$\geq 10^5$
Long time gain stability	≥ 120 min
High rate beam injection capability	$\geq 2 \times 10^5$ pps
Energy resolution	$\leq 10\%$
Position resolution	≤ 2 mm

ties of a 400 μm thick GEM foils in the low-pressure He +CO₂ (10%) gas. The detail of the results of 400 μm GEM are shown in Ref. [8, 9]. 400 μm GEM could be stable operation in Ref [8, 9]. However, the gas gain under the 10^4 pps injection condition is about 5 times lower than one of the result of offline test. The reason is continuous discharge around the GEM hole. When the discharge occurs, electric current flows into the circuit. In order to avoid this, the hole size of the GEM was modified from 500 μm to 300 μm which made it possible to operate at lower voltage. Although the discharge phenomena disappeared, the gas gain shifted about 5% during 100 min. This shift may be ascribed to the charge up effect of the insulator in GEM hole. We started the study of the properties of 200 μm thick GEM to avoid the charge up. The gas gain of 200 μm GEM also could be higher than 10^3 . It means that 10^5 gas gain can be reached by using the multi GEM configuration. In addition, the gas gain shift is less than 1% during 150 min. Therefore, we adopted 200 μm GEM as a

proportional counter of GEM – MSTPC.

The high beam injection rate capability of the GEM – MSTPC was tested at the pelletron accelerator facility of RIKEN. The injected beam was ^{11}B with energy of 6 MeV and the beam spot size is 1 mm in diameter. Gas gain was tested by varying the beam intensity from 500 pps to 420 kpps.

The experimental results are shown in Fig 2, where (a), (b), (c) indicate the relative pulse height, the energy resolution and the position resolution of the pad direction as a function of the beam injection rate, respectively. The open circles are for so called normal gain which correspond to the same pulse height expected for ^{18}Ne beams and the closed circles are for low gain which corresponds to the half of the normal gain. The results indicate that the gas gain does not depend the beam rate. In addition, the energy and the position resolution are 8% and 1.7 mm, respectively. These results satisfy our requirement.

The remaining problem is the ion feed back from GEM foil. It was possible to make ion feed back ratio less than 2% using 200 μm GEM under the same field condition of Ref [9]. In order to judge whether this ratio is acceptable or not, measurement of the position distortion along the drift direction will be performed at the pelletron accelerator facility.

After finishing all development, we will perform the excitation function measurement of the $^{18}\text{Ne}(\alpha, p)^{21}\text{Na}$ reaction.

References

- [1] J. J. He *et al.*, Eur. Phys. J. A **36** (2008) 1, and references therein.
- [2] T. Hashimoto *et al.*, CNS Annual Rep. 2008 17.
- [3] S. Kubono, *et al.*, Nucl. Phys. A **558** (1995) 305.
- [4] H. Yamaguchi, *et al.*, Nucl. Instrum. Meth. A **589** (2008) 150.
- [5] Y. Mizoi *et al.*, Nucl. Instrum. Meth. A **431** (1999) 112.
- [6] T. Hashimoto *et al.*, Nucl. Instrum. Meth. A **556** (2006) 339.
- [7] F. Sauli Nucl. Instrum. Meth. A **386** (1997) 531.
- [8] S. K. Das *et al.*, Nucl. Instrum. Meth. A **625** (2011) 39.
- [9] K. Yamaguchi *et al.*, Nucl. Instrum. Meth. A **623** (2010) 135.

^{30}S Beam Production and RI Beam Modeling at CRIB

D. Kahl, A. A. Chen^a, S. Kubono, D. N. Binh, J. Chen^a, T. Hashimoto, S. Hayakawa, N. Iwasa^b, D. Kaji^c, A. Kim^d, Y. Kurihara, N. H. Lee^d, M. Mazzocco^e, S. Nishimura^c, Y. Ohshiro, K. Setoodehnia^a, Y. Wakabayashi^f, and H. Yamaguchi^a

Center for Nuclear Study, Graduate School of Science, the University of Tokyo

^a*Department of Physics & Astronomy, McMaster University*

^b*Department of Physics, Tohoku University*

^c*RIKEN (The Institute of Physical and Chemical Research)*

^d*Department of Physics, Ewha Womans University*

^e*Department of Physics, University of Padova and Istituto Nazionale di Fisica Nucleare (INFN)*

^f*Advanced Science Research Center, Japan Atomic Energy Agency (JAEA)*

We performed a third and final low-energy ^{30}S RI beam development test in preparation for a future measurement of the $^4\text{He}(^{30}\text{S},\text{p})$ cross section. Our July 2009 experiment [1], reported here, was a follow-up to our previous beam tests in December 2006 [2] and May 2008 [3]. This work is performed at the low-energy Center for Nuclear Study (CNS) radioactive ion beam (CRIB) separator facility [4, 5] of the University of Tokyo and located at the RI Beam Factory, RIKEN. In 2010, we will perform the first-ever direct measurement of the $^4\text{He}(^{30}\text{S},\text{p})$ cross-section at astrophysical energies relevant to type I X-ray bursts. The $^{30}\text{S}(\alpha,\text{p})$ reaction rate is important to the overall energy generation of X-ray bursts [6], influences the neutron star crustal composition [7], and may explain the bolometric double-peaked nature of some rare X-ray bursts [8].

We produce ^{30}S via the $^3\text{He}(^{28}\text{Si},^{30}\text{S})\text{n}$ reaction by bombarding a Havar-windowed (2.5 μm), cryogenic gas target [9] of ^3He at 90 K with beams of ^{28}Si . In 2008, we tested ^3He gas pressures of 200, 300 and 400 Torr, finding ^{30}S RI beam intensity was maximized at the highest pressure tested; all other tests were conducted only at 400 Torr. Although the $^{30}\text{S}^{14+},^{15+}$ species are more preferentially populated at the achromatic focal plane F2, as shown in Fig. 1, they are difficult to separate and purify. The beam purity at the target focal plane F3 is improved compared to Fig. 1 by passing the beam through a Wien (velocity) filter after F2. All our results quoted in Table 1 are for $^{30}\text{S}^{16+}$, which we can successfully separate and purify. For each primary beam species, we took the highest beam current and corresponding cyclotron energy available at that time; the improvements in the primary beam energy are a result of recent upgrades to the practical K value of the Nishina Center AVF cyclotron [10]. The primary beam intensity is ultimately limited to ~ 150 pA by the maximum heat deposit of 2 W in the production target Havar exit window, but practically considering the output of the CNS HyperECR ion source and the cyclotron transport efficiency, we have not yet needed to limit the ^{28}Si beam intensity delivered to CRIB.

As we are interested only in the fully-stripped charge-state of ^{30}S , which is not preferentially populated at CRIB energies in the production target Havar exit window, we

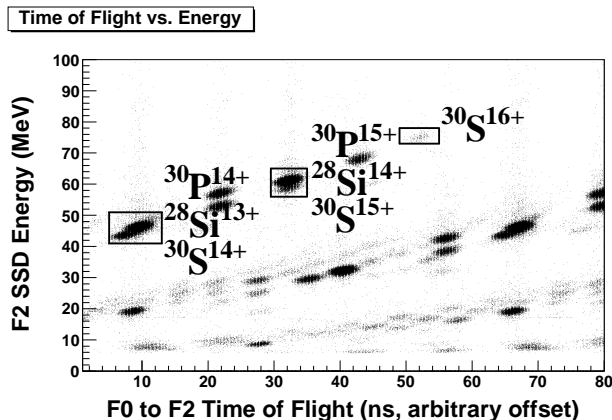


Figure 1. ToF-E spectrum using a delay-line PPAC and SSD at F2. $^{30}\text{S}^{16+}$ is clearly separated.

Year	Beam	E_{beam} (MeV/u)	I_{beam} (pA)	RI Purity (%)	I_{RI} (kpps)
2006	$^{28}\text{Si}^{9+}$	6.9	100	13	1.8
2008	$^{28}\text{Si}^{10+}$	7.54	10	30	0.5
2009	$^{28}\text{Si}^{9+}$	7.4	144	24	8.6

Table 1. Variation of $^{30}\text{S}^{16+}$ results with different primary beam conditions; production target is ^3He at 400 Torr and 90 K.

considered the positive effects of adding a charge-stripper foil immediately following the production target. In July 2008, we experimentally tested the charge-state distribution of ^{28}Si at 3.4 MeV/u ($\sim E_{\text{beam}}$ of ^{30}S) in thick carbon foil (550 $\mu\text{g}/\text{cm}^2$) compared to Havar foil (2.2 μm) (see Table 2). We found that the transmission of high charge states improved in carbon, with a ratio consistent with the predictions in [11]. Thus, by placing a Be foil (2.5 μm) after the production target in 2009, we are able to increase the population of the $^{30}\text{S}^{16+}$ species (compared to the charge-state distribution of the gas-cell Havar exit window and RI beam intensities of previous tests). However, the improvement was a factor of two to five, whereas Leon's model predicts a factor of 10–20 improvement in the abundance of $^{30}\text{S}^{16+}$ after traversing Be compared to Havar. The discrepancy between predictions and experimental results can possibly be explained by the partially broken state of the Be foil we

used, as well as our difficulty to normalize the results for direct comparison under different CRIB operational conditions.

Target	Species	Normalized pps @ 10 enA
Havar	$^{28}\text{Si}^{12+}$	1.075×10^8
Havar	$^{28}\text{Si}^{13+}$	6.013×10^7
Havar	$^{28}\text{Si}^{14+}$	3.901×10^6
Carbon	$^{28}\text{Si}^{12+}$	1.758×10^8
Carbon	$^{28}\text{Si}^{13+}$	1.300×10^8
Carbon	$^{28}\text{Si}^{14+}$	4.365×10^7

Table 2. Intensity of selected charge states of ^{28}Si after passing through Havar foil or carbon foil.

Clearly from this work, a sophisticated and realistic beam production and ion-optical transport model would be useful for CRIB. No known existing code is capable of properly treating low-energy radioactive beam production. We have recently developed such a model, called `cribbon`, due to its manner of weaving together many different pieces of code; here its properties and development status are over-viewed.

Such a model of CRIB was initiated based on the design of `MOCADI_FUSION` [12]. The beam production code has been entirely re-written for the needs of CRIB. It performs a Monte Carlo simulation, producing the nuclear species and charge state of interest at a random point in the target. The user can select either an isotropic or a forward-angle-weighted angular distribution in the center of mass. Fully relativistic kinematics are computed using the `ROOT` library `KaliVeda`, and the primary beam energy loss is calculated strictly along the beam axis using the `Fortran` code `enewz` as a subroutine, originally written by Yutaka Watanabe and based on Ziegler’s method. As the code is only capable to deal with one nuclear and ion species for each execution, one must rely on existing experimental data with regards to the nuclear cross section and charge-state distribution; `cribbon` gives the kinematic production and ion-optical transport efficiency of CRIB only. Charge-state distributions are well-documented near CRIB energies [11]. However, the heavy RIs with the highest transport yield correspond to the light ejectiles with $\theta_{cm} \approx 180^\circ$, where the cross sections are smaller and difficult to measure under normal kinematic conditions; this point is often overlooked in CRIB yield estimations.

It is important to note that such an implementation of the code is absolutely universal for CRIB beams, independent of the primary beam or production target, as long as the production mechanism is predominately either direct or compound. After the RI beam is produced, its energy loss through the remainder of the target, and any subsequent charge stripper foil, is calculated three dimensionally using `SRIM` [13].

After the RI beam is produced and has exited the target, it is merely a matter of the ion-optical transmission efficiency of CRIB we are interested to know under a given set of initial conditions. We use the code `TRANSPORT`, which is

the same actually used to set the magnet currents of CRIB, in order to predict the initial magnet settings. These are fed into `GICOSY` [14], which produces third-order transfer matrices, including the effects of magnetic field fringing. One remaining point of work for the ion-optics is to add in the higher order terms for the magnetic dipoles, which are known from the `DUMAS` [15] specifications.

Given the transfer matrices and the individual beam ion momentum vectors, these are processed by `MOCADI` [16], where phase space parameters of the beam can be plotted at any region of interest (typically those corresponding to CRIB focal planes). The interfacing of these various programs is automated by a shell script. In the future, the available free parameters in the Monte Carlo beam production will be optimized to best reproduce past RI beam data at CRIB. The ultimate goal of this model is to optimize the primary beam energy and production target thickness for future CRIB experiments, not only for the case of ^{30}S detailed here.

In September 2010, we will measure the $^4\text{He}(^{30}\text{S},p)$ cross section on an event-by-event basis using an active target method using the thick-target method in inverse-kinematics [17]. It is critical that we may get a $^{28}\text{Si}^{9+}$ beam at 1.3 μA with long-term current-stability delivered to the primary beam focal point of CRIB for the future experiment using the ^{30}S beam developed and detailed in this report.

These experiments were made possible through the CNS and RIKEN collaboration. The McMaster University group is appreciative of funding from the Natural Science and Engineering Research Council of Canada.

References

- [1] D. Kahl *et al.*, *AIPC* **1213** (2010) 208.
- [2] D. Kahl *et al.*, *ASPC* **393** (2008) 219.
- [3] D. Kahl *et al.*, *PoS NIC X* (2008) 171.
- [4] S. Kubono *et al.*, *Eur. Phys. J. A* **13** (2002) 217.
- [5] Y. Yanagisawa *et al.*, *Nucl. Instrum. Meth. A* **539** (2005) 74.
- [6] A. Parikh *et al.*, *ApJS* **178** (2008) 110.
- [7] H. Schatz and K. E. Rehm, *Nucl. Instrum. Meth. A* **777** (2006) 601.
- [8] J. L. Fisker, F.-K. Thielemann and M. Wiescher, *ApJ* **608** (2004) L61.
- [9] H. Yamaguchi *et al.*, *Nucl. Instrum. Meth. A* **589** (2008) 150.
- [10] A. S. Vorozhtsov *et al.*, *CNS Report* **82** (2009).
- [11] A. Leon *et al.*, *ADNDT* **69** (1998) 217.
- [12] M. Mazzocco *et al.*, *Nucl. Instrum. Meth. B* **266** (2008) 3467.
- [13] J. F. Ziegler, M. D. Ziegler, and J. P. Biersack, *NIMP B* **268** (2010) 1818.
- [14] M. Berz, H. C. Hoffmann and H. Wollnik, *Nucl. Instrum. Meth. A* **258** (1987) 402.
- [15] T. Noro *et al.*, *RCNP Annual Report* (1983) 173.
- [16] N. Iwasa *et al.*, *Nucl. Instrum. Meth. B* **126** (1997) 284.
- [17] K. P. Artemov *et al.*: *Soviet JNP* **52** (1990) 408.

Beta-decay measurement of ^{46}Cr

Y. Wakabayashi^a H. Yamaguchi^b T. Hashimoto^b S. Hayakawa^b Y. Kurihara^b D. N. Binh^{b,c},
D. Kahl^b, S. Nishimura^d, Y. Gono^d, Y. Fujita^e, and S. Kubono^b

^aAdvanced Science Research Center, Japan Atomic Energy Agency

^bCenter for Nuclear Study, Graduate School of Science, University of Tokyo

^cInstitute of Physics and Electronic, Vietnam Academy of Science and Technology

^dRIKEN (The Institute of Physical and Chemical Research)

^eDepartment of Physics, Osaka University

1. Introduction

For the rapid proton capture process (*rp*-process) in X-ray burst and the core-collapse stage of supernova, weak interaction processes of proton-rich *pf*-shell nuclei far from stability play important roles [1]. Studies of the β decay and electron capture of these proton-rich *pf*-shell nuclei are of great astrophysical interest. These decays which involve the charged-current processes, e.g., $p \rightarrow n + e^+ + \nu$, are predominated by the Fermi and Gamow-Teller (GT) transitions.

Information on the GT transitions are derived directly from β -decay measurements. Pioneering works were done for several proton-rich *pf*-shell nuclei [2, 3, 4, 5]. However, the GT transition strengths (B(GT)'s) of these proton-rich nuclei were measured for only at most one or two low-lying states with large errors due to the small production cross sections and short half lives. To determine the B(GT) accurately, it is important to measure the feeding ratio and the half life of the β decay accurately.

As for the β decay of ^{46}Cr , one of proton-rich *pf*-shell nuclei, half life has been reported with a large uncertainty; 240(140) [2] ms and 260(60) [6] ms, and only a gamma line of 993 keV was measured in coincidence with the β decay [2].

In this study, the final goal is to measure i) the half life of the β decay with an accuracy better than 10 %, and ii) the decay branching ratios to the ground state (Fermi transition) and GT states accurately.

2. Experimental procedure

The experiment to measure the half life of ^{46}Cr was performed using the low-energy RI beam separator (CRIB) [7, 8] of Center for Nuclear Study (CNS), the University of Tokyo. The ^{46}Cr nuclei were produced using the $^{36}\text{Ar} + ^{12}\text{C}$ fusion reaction. A natural C foil of 0.56 mg/cm² was used as the primary target. The ^{36}Ar primary beam was accelerated to 3.6 MeV/nucleon by the RIKEN AVF cyclotron, and degraded to 3.0 MeV/nucleon by a 2.2- μm -thick Havar foil placed in front of the primary target to maximize production of ^{46}Cr . To separate ^{46}Cr from other nuclei produced in the fusion reaction, a Wien filter (W.F.) was used at high voltages of ± 85 kV. A microchannel plate (MCP) [9, 10] was placed at the final focal plane (F3) to monitor the beam position. An ionization chamber (IC) with a 56-mm length was placed behind the MCP as a ΔE detector. The IC was operated using isobutane gas at 25 Torr. A double-sided Si strip

detector (DSSD) with a thickness of 500- μm was placed in the IC so as to measure E of nuclei and β -rays. A Si detector of 1.5-mm thickness was placed behind the DSSD to detect β -rays. To measure β -delayed γ rays, 3 clover and 1 coaxial Ge detectors were set around the I.C. The primary beam was pulsed to measure the half life of ^{46}Cr . The durations of the beam-on and beam-off periods were 500 and 700 ms, respectively. Non-stop TDC (NSTDC) was used to record absolute time of delayed β -ray in a pulsed-beam cycle.

3. Experimental results

Figure 1 shows a scatter plot between the ΔE and the time-of-flight (TOF) between the MCP and the RF signals, where good particle identification capability is demonstrated. In this experiment, the purity and the intensity of ^{46}Cr were 2.2 % and 9 particle per second (pps), respectively, with the primary beam of 80 particle nA. The purities and intensities of ^{46}Cr and other nuclides in the secondary beam are summarized in Table 1.

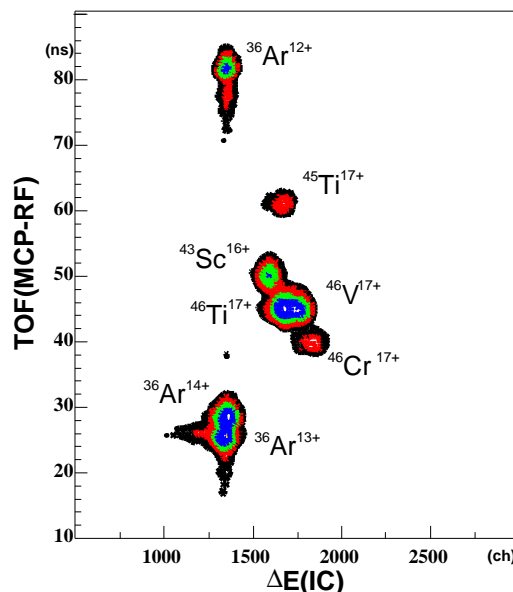


Figure 1. TOF- ΔE spectrum obtained by the I.C and MCP placed at F3.

Figure 2 shows a decay spectrum of fusion products during beam off. The spectrum have only two-decay components from ^{46}V and ^{46}Cr , because ^{46}Ti and ^{36}Ar are sta-

Table 1. Purities and intensities of nuclides with the primary beam of 80 particle nA, where the purities and intensities are in the unit of % and pps, respectively. Branching ratio indicates the fraction decayed to the excited states. Half lives are shown by each unit.

Nuclide	$^{46}\text{Cr}^{17+}$	$^{46}\text{V}^{17+}$	$^{45}\text{Ti}^{17+}$	$^{46}\text{Ti}^{17+}$	$^{43}\text{Sc}^{16+}$	^{36}Ar
Purity (%)	1.8	8.8	2.2	15.6	4.5	50.7
Intensity (pps)	5.6	27.2	6.5	48.6	14.0	157.2
Half life	257 ms	422.4 ms	184.8 m	Stable	3.891 h	Stable
Branching ratio (%)	21.6 [2]	0.019	0.315		22.5	

ble nuclei and ^{45}Ti and ^{43}Sc have much longer half lives than the duration of beam-off period. The half life of ^{46}Cr was determined as $T_{1/2} = 235 \pm 12$ ms by fitting this spectrum with a function having two-decay components, one of which was fixed to half life of ^{46}V of 422.5(11) ms [11]. This value is consistent with the previous results [2, 6].

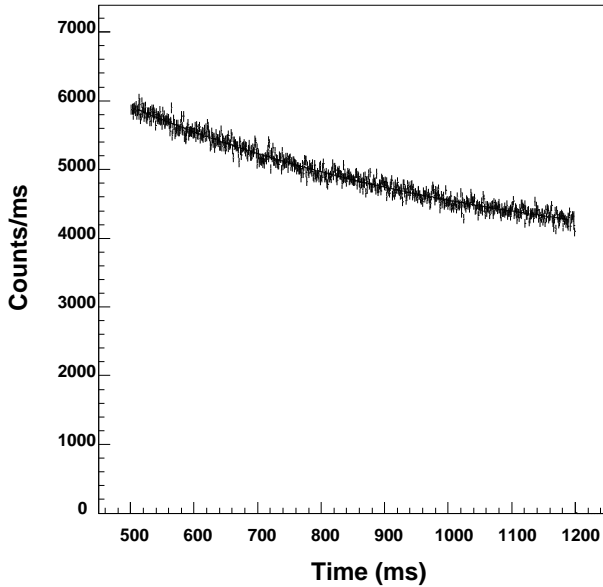


Figure 2. Decay spectrum of fusion products at beam off.

Figure 3(a) and (b) show the γ -ray energy spectrum in the energy range between 300 keV and 540 keV, and between 540 keV and 1040 keV obtained by the β - γ coincidence method during beam off. A 511 keV γ ray in Fig. 3(a) is due to annihilation of positrons emitted from β^+ decay. In Fig. 3(a), a 373 keV β -delayed γ ray of ^{43}Sc is seen. A 993 keV γ ray from β decay of ^{46}Cr [2] is seen in Fig. 3(b). The branching ratio $b_{993\text{keV}}$ of 3.8(1.5)% was calculated using the following relation,

$$b_{\gamma} = \frac{N_{\gamma}}{N_i \times d \times \epsilon_{\beta} \times \epsilon_{\gamma}}, \quad (1)$$

where N_{γ} is peak area of the γ ray, N_i is the number of implanted nuclide into the DSSD, d is the dead time correction, ϵ_{β} and ϵ_{γ} are the efficiencies of β and γ rays, respectively.

More detailed analysis is in progress, which includes the simulation efforts of β -ray efficiency.

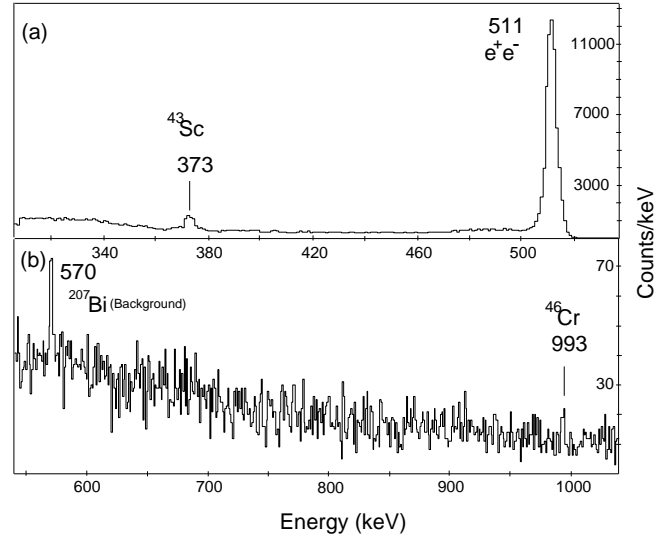


Figure 3. γ -ray energy spectrum at beam off. Figure 3(a) and (b) show spectra for different energy ranges; (a) 300 keV to 540 keV, (b) 540 keV to 1040 keV.

References

- [1] K. Langanke and G. Martinez-Pinedo, *Rev. Mod. Phys.* **75**, 819 (2003).
- [2] T.K. Onishi *et al.*, *Phys. Rev. C* **72**, 024308 (2005).
- [3] V.T. Koslowsky *et al.*, *Nucl. Phys. A* **624**, 293 (1997).
- [4] I. Reusen *et al.*, *Phys. Rev. C* **59**, 2416 (1999).
- [5] A. Jokinen *et al.*, *Eur. Phys. J. A* **3**, 271 (1998).
- [6] J. Zioni *et al.*, *Nucl. Phys. A* **181**, 465 (1972).
- [7] S. Kubono *et al.*, *Eur. Phys. J. A* **13**, 217 (2002).
- [8] Y. Yanagisawa *et al.*, *Nucl. Instrum. Meth. A* **539**, 73 (2005).
- [9] J.L. Wiza, *Nucl. Instrum. Meth.* **162**, 587 (1979).
- [10] D. Shapira *et al.*, *Nucl. Instrum. Meth. A* **454**, 409 (2000).
- [11] Nuclear Data Sheets **91**, 64 (2000).

Indirect measurement of astrophysical $^{12}\text{N}(p, \gamma)^{13}\text{O}$ reaction rate

W.P. Liu, B. Guo, J. Su, Zhi-Hong Li, D.N. Binh^a, Y.L. Han, H. Hashimoto^a, S. Hayakawa^a, J.J. He^b, J. Hu^b, N. Iwasa^c, D.M. Kahl^a, S. Kubono^a, N. Kume^c, Y.J. Li, Zhi-Huan Li^d, Y.B. Wang, S.W. Xu^b, H. Yamaguchi^a, S.Q. Yan, X.X. Bai, G. Lian, B.X. Wang and S. Zeng

China Institute of Atomic Energy, Beijing, China

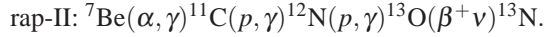
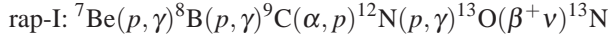
^a*Center for Nuclear Study, University of Tokyo, Wako, Japan*

^b*Institute of Modern Physics, Chinese Academy of Sciences, Lanzhou, China*

^c*Department of Physics, Tohoku university, Sendai, Japan*

^d*Peking university, Beijing, China*

Nuclear capture reactions, such as (p, γ) and (α, γ) , play a crucial role in the evolution of stars. The reactions on proton-rich unstable nuclei of $A \leq 13$ are thought to be a possible way alternative to 3α process for transforming nuclei from the pp chains to the CNO cycle in the peculiar astrophysical sites where the temperature and density are so high that the capture reaction becomes faster than the competing β decay [1]. The reaction chains which link the pp chains, the CNO nuclei and rp-process are so-called Rapid Alpha-Proton (rap) process. The $^{12}\text{N}(p, \gamma)^{13}\text{O}$ reaction is one of the key reactions in rap-I and rap-II chains [1]:



Due to the low Q-value (1.516 MeV), the $^{12}\text{N}(p, \gamma)^{13}\text{O}$ cross sections at low energies of astrophysical interest are dominated by the direct capture into the ground state and the resonant capture via the first excited state of ^{13}O . In 1989, Wiescher et al. derived the astrophysical S-factor $S(0)$ at zero energy to be about 40 keV b based on shell model calculation [1]. In 2006, Warner et al. extracted the SF to be 0.623 (0.537 for $1p_{1/2}$ orbit, 0.086 for $1p_{3/2}$ orbit) using shell model calculation, by which the proton-removal cross section of ^{13}O on Si target was reproduced using an extended Glauber model [2]. Z.H. Li extracted the $S(0)$ factor to be 0.31 keV b [3] by using the SF from Ref. [2]. In 2009, Banu et al. derived the asymptotic normalization coefficient (ANC) for virtual decay of $^{13}\text{O} \rightarrow ^{12}\text{N} + p$ from the measurement of the $^{14}\text{N}(^{12}\text{N}, ^{13}\text{O})^{13}\text{C}$ angular distribution and then calculated the direct $S(0)$ factor to be 0.33 ± 0.04 keV b for $^{12}\text{N}(p, \gamma)^{13}\text{O}$ [4]. Therefore, it seems that a new measurement of $S(0)$ factor through different reaction is desirable as an independent examination to the preexisting results. As for resonant capture component, the resonant parameters of low excited states in ^{13}O have been studied through a thick target technique [5, 6, 7].

In the present work, the $^{12}\text{N}(d, n)^{13}\text{O}$ angular distribution was measured in inverse kinematics, and then the SF of ^{13}O was extracted through Johnson-Soper approach [8].

The experiment was performed with the CNS Radioactive Ion Beam (CRIB) facility [9] at CNS/RIKEN. A primary ^{10}B beam with the energy of 82 MeV was yielded from AVF cyclotron with $K = 70$. The primary beam impinged on the ^3He gas cell with the pressure of 360 Torr

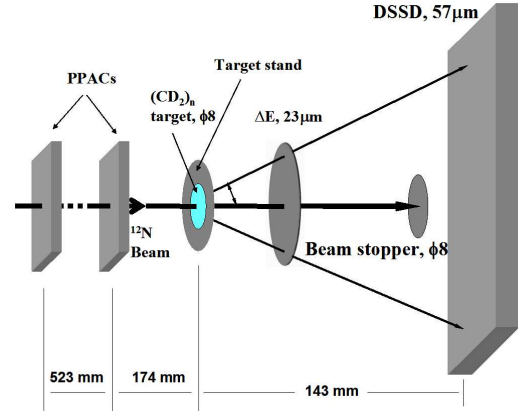


Figure 1. Schematic layout of the experimental setup at F3 chamber of CRIB for the $^2\text{H}(^{12}\text{N}, ^{13}\text{O}_{g.s.})n$ reaction.

and the temperature of 80 K. The front and rear windows of gas cell are Havar foils with the thickness of $2.2 \mu\text{m}$. The secondary ^{12}N ions with the energy of 70 MeV were produced through the $^3\text{He}(^{10}\text{B}, ^{12}\text{N})n$ reaction and then separated by CRIB facility. Two parallel plate avalanche counters (PPACs) were used to trace incident ^{12}N particle and determine its incident angle and position on secondary target. After two PPACs, the secondary ^{12}N beam bombarded a $(\text{CD}_2)_n$ film with the thickness of 1.5 mg/cm^2 and the diameter of 8 mm to study the $^2\text{H}(^{12}\text{N}, ^{13}\text{O})n$ reaction. A carbon foil with the thickness of 1.5 mg/cm^2 was utilized to evaluate the background from the carbon atoms in $(\text{CD}_2)_n$ target. The typical purity and intensity of ^{12}N beam on target were approximately 30% and 200-600 pps, respectively. The ^{12}N beam energy at the center of $(\text{CD}_2)_n$ target is 59 MeV. The reaction products ^{13}O were detected and identified with a telescope consisting of a $23 \mu\text{m}$ silicon detector (ΔE) and a $57 \mu\text{m}$ double-sided silicon strip detector (DSSD). A beam stopper (close to DSSD) with the diameter of 8 mm was used to block unreacted beam particles in order to reduce radiation damage to DSSD. A schematic layout of the experimental setup at F3 chamber of CRIB separator is shown in Fig. 1.

The emitted angle of reaction products was determined by combining the information from DSSD and two PPACs. As an example, Fig. 2 shows the scatter plot of energy loss (ΔE) vs. total energy (E_{tot}) for the events in the angular range of $3^\circ < \theta_{\text{c.m.}} < 4^\circ$. The two dimension cuts of ^{13}O events from $^2\text{H}(^{12}\text{N}, ^{13}\text{O})n$ were determined with a Monte

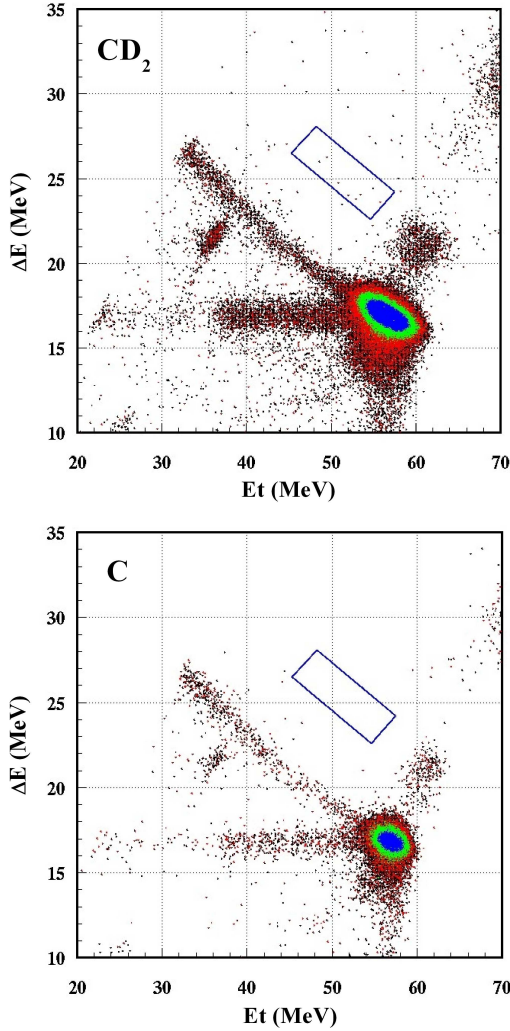


Figure 2. Scatter plot of ΔE vs. E_t for the events in the angular range of $3^\circ < \theta_{c.m.} < 4^\circ$, $(CD_2)_n$ target (top) for the measurement of ${}^2\text{H}({}^{12}\text{N}, {}^{13}\text{O})n$, while C target (bottom) for background evaluation. The two dimension cuts for ${}^{13}\text{O}$ events from ${}^2\text{H}({}^{12}\text{N}, {}^{13}\text{O})n$ were determined with a MC simulation.

Carlo (MC) simulation, which took into account the kinematics, geometrical factor, angular and energy straggling effects in two PPACs, secondary target and ΔE detector, and were calibrated with the ${}^{12}\text{N}$ beam. The detection efficiency correction from beam stopper was also computed via MC simulation. After beam normalization and background subtraction, the ${}^2\text{H}({}^{12}\text{N}, {}^{13}\text{O})n$ angular distribution in center of mass frame was obtained and shown in Fig. 3.

In this work, the code FRESKO [10] was used to analyze the experimental angular distribution. In order to include the breakup effects of deuteron in the entrance channel, the angular distribution was calculated within the Johnson-Soper adiabatic approximation to the neutron, proton, and target three-body system [8]. In the present calculation, the optical potentials of nucleon-target were taken from Ref. [11, 12] respectively, which have been successfully used in the DWBA calculations for the reaction on light nuclei [13, 14, 15]. The theoretical calculations on direct process with two sets of optical potential were displayed in

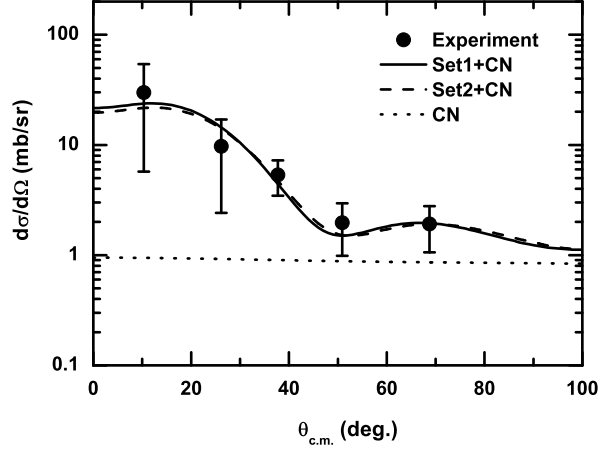


Figure 3. Measured angular distribution of ${}^2\text{H}({}^{12}\text{N}, {}^{13}\text{O}_{g.s.})n$ at $E_{c.m.} = 8.4$ MeV, together with the theoretical calculations on direct process using two sets of optical potential (Set1 and Set2) and compound nucleus contribution (CN).

Fig. 3, together with compound nucleus (CN) contribution obtained by UNF code [16]. After subtract CN contribution, the first three data points were used to derive the SF of ${}^{13}\text{O}$ by the normalization of experimental data to theoretical calculations. For one set of optical potential, three SFs can be obtained by using three data points, their weighted value was then taken as SF for this set of optical potential. The ratio of $1p_{3/2}:1p_{1/2}$ was derived to be 0.16 based on shell model calculation [2].

The SF was extracted to be 0.80 ± 0.30 (0.69 ± 0.26 for $1p_{1/2}$ orbit, 0.11 ± 0.04 for $1p_{3/2}$ orbit). The error results from the measurement (36%) and the uncertainty of optical potential (11%). Our result is in agreement with that from the ${}^{14}\text{N}({}^{12}\text{N}, {}^{13}\text{O}){}^{13}\text{C}$ reaction [4] and two shell model calculations [1, 2]. The calculation on astrophysical S-factors and reaction rates for ${}^{12}\text{N}(p, \gamma){}^{13}\text{O}$ is in progress now.

The authors would like to thank the staff of AVF accelerator for the smooth operation of the machine. This work was supported by the National Natural Science Foundation of China under Grants 10875175 and 10720101076.

References

- [1] M. Wiescher *et al.*, *Astrophys. J.* **343** (1989) 352.
- [2] R.E. Warner *et al.*, *Phys. Rev. C* **74** (2006) 014605.
- [3] Z.H. Li, *Chin. Phys. Lett.* **23** (2006) 3219.
- [4] A. Banu *et al.*, *Phys. Rev. C* **79** (2009) 025805.
- [5] T. Teranishi *et al.*, *Nucl. Phys. A* **718** (2003) 207c.
- [6] T. Teranishi *et al.*, *Nucl. Phys. A* **719** (2003) 253c.
- [7] B. Skorodumov *et al.*, *Phys. Rev. C* **75** (2007) 024607.
- [8] G.L. Wales *et al.*, *Nucl. Phys. A* **274** (1976) 168.
- [9] S. Kubono *et al.*, *Eur. Phys. J. A* **13** (2002) 217.
- [10] I.J. Thompson, *Comput. Phys. Rep.* **7** (1988) 167.
- [11] R.L. Varner *et al.*, *Phys. Rep.* **201** (1991) 57.
- [12] A.J. Koning *et al.*, *Nucl. Phys. A* **713** (2003) 231.
- [13] M.B. Tsang *et al.*, *Phys. Rev. Lett.* **95** (2005) 222501.
- [14] X.D. Liu *et al.*, *Phys. Rev. C* **69** (2004) 064313.
- [15] B. Guo *et al.*, *J. Phys. G: Nucl. Part. Phys.* **34** (2007) 103.
- [16] J. Zhang, *Nucl. Sci. Eng.* **142** (2002) 207.

Test measurement of $^{17}\text{Ne}+p$ resonance elastic scattering

T. Teranishi^a, S. Kubono, H. Yamaguchi, T. Hashimoto, S. Hayakawa, Y. Kurihara, D.N. Bihn, D. Kahl, Y. Wakabayashi^b, L.H. Khiem^c, P.V. Cuong^c, S. Watanabe, and A. Goto^d

Center for Nuclear Study, Graduate School of Science, University of Tokyo

^aDepartment of Physics, Kyushu University

^bJapan Atomic Energy Agency (JAEA)

^cInstitute of Physics, Vietnam

^dRIKEN Nishina Center

We performed a test measurement of $^{17}\text{Ne}+p$ for observing proton-rich unbound ^{18}Na nucleus. Information of ^{18}Na resonances is useful for studying direct two proton decay of ^{19}Mg [1] and also a possible two-proton halo structure of ^{17}Ne [1] [2] [3] [4] [5]. There is few experimental data on ^{18}Na : an invariant mass spectrum of $^{17}\text{Ne}+p$ was measured at GANIL using a projectile fragmentation reaction of ^{20}Mg at 43 MeV/u [6]. Two large peaks were observed in the spectrum at $\Delta = 24.19$ and 25.04 MeV (peak 1 and 2, respectively), where Δ denotes the ^{18}Na mass excess. The peak 1 and 2 may be assigned to the ground and the first excited states, respectively. However, $\Delta = 24.19$ MeV for the ground state is significantly lower than theoretical predictions of around 25.3 MeV [6] [7]. There is a possibility that the peak 1 is due to the decay $^{18}\text{Na}_{1st}^* \rightarrow ^{17}\text{Ne}_{1st}^*+p$ and the peak 2 is due to the decay $^{18}\text{Na}_{g.s.} \rightarrow ^{17}\text{Ne}_{g.s.}+p$. It is also pointed out that the experimental resolution is about 250 keV and each of the peaks might contain two levels [7]. To observe the ^{18}Na resonance levels more directly, we planned measuring $^{17}\text{Ne}+p$ resonance elastic scattering at the CRIB beam line in the RI Beam Factory. We performed a beam production test and a test measurement of $^{17}\text{Ne}+p$ scattering as the first step.

The secondary ^{17}Ne particles were produced using the $^3\text{He}(^{16}\text{O}, ^{17}\text{Ne})2n$ reaction at $E_{^{16}\text{O}} = 11.0$ MeV/u and separated by the CRIB separator, which has three focal planes (F1, F2, and F3). The secondary particles were selected at the dispersive focal plane F1 with a momentum width of $\pm 1.6\%$. The Wien filter section between F2 and F3 was used to select particles by velocity. Two parallel plate avalanche counters (PPACs) were mounted in a chamber at F3 to monitor the beam position and direction and time-of-flight (TOF) between the two PPACs. The beam spot size at F3 was approximately 15 mm diameter (FWHM). The ^{17}Ne purity in the secondary beam was 2 %, which was not a problem in measuring the $^{17}\text{Ne}+p$ scattering because identification of the beam particles was possible on an event-by-event basis using the TOF information. Major contaminants in the secondary beam were ^{14}O and ^{18}Ne . The ^{17}Ne beam energy was 4.9 MeV / nucleon after the second PPAC. During the present experiment, we had a primary ^{16}O (7+) beam with an intensity of 150 pA, resulting in the secondary ^{17}Ne beam intensity of approximately 500 particles/sec. The primary beam intensity was limited due to a trouble in the cyclotron RF resonator in the present experiment and will be double in future.

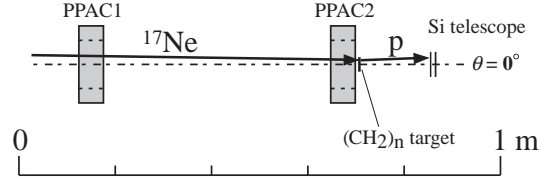


Figure 1. Experimental setup for $^{17}\text{Ne}+p$ scattering.

Using the produced ^{17}Ne beam we performed a test $^{17}\text{Ne}+p$ measurement for 20 hours. Figure 1 shows the experimental setup at F3. A $(\text{CH}_2)_n$ target of 10 mg/cm^2 was mounted at the downstream side of the second PPAC and used as a proton target. We utilized a thick-target method in inverse kinematics (TTIK) [8] [9] for deducing the $^{17}\text{Ne}+p$ excitation function. The beam particles were completely stopped in the target, while recoil protons were detected by a Si detector telescope at 0° (LAB). The Si detector telescope consisted of a double-sided strip detector (DSSD) with $16 + 16$ strips for ΔE information and a single pad detector for E information. The ΔE and E detectors were 70 and 1500 μm thick, respectively, and had the identical sensitive area of $50 \times 50 \text{ mm}^2$. The distance between the telescope and the target was 15 cm. Identification of proton was made using the ΔE and E information. The proton scattering angle was determined using the PPAC and DSSD information. The proton energy was deduced from the sum of ΔE and E . We performed proton energy calibration using secondary proton beams of known energies. In order to deduce the $^{17}\text{Ne}+p$ excitation function, we reconstructed the center-of-mass energy on an event by event basis from the proton energy and angle by taking into account the elastic scattering kinematics and also energy losses of ^{17}Ne and proton in the target.

Figure 2 shows a preliminary result of the $^{17}\text{Ne}+p$ excitation function. We found a narrow peak at $E_{\text{CM}} \sim 2.05$ MeV, which may be attributed to a ^{18}Na level. The intrinsic peak width was roughly estimated to be $\Gamma \sim 100$ keV from the spectrum by taking into account the energy resolution. Because the peak width is sufficiently narrow, we may neglect interference effects and assume that the peak energy and the width are roughly the same as the level energy and width, respectively. The level energy of $E_{\text{CM}} \sim 2.05$ MeV corresponds to a mass excess of $\Delta \sim 25.80$ MeV, which is a little higher than the prediction of 25.3 MeV for the ground state [6] [7]. One possible interpretation is therefore that the observed level is one of low-lying excited levels. The narrow width for the $^{17}\text{Ne}+p$ resonance is probably due to the

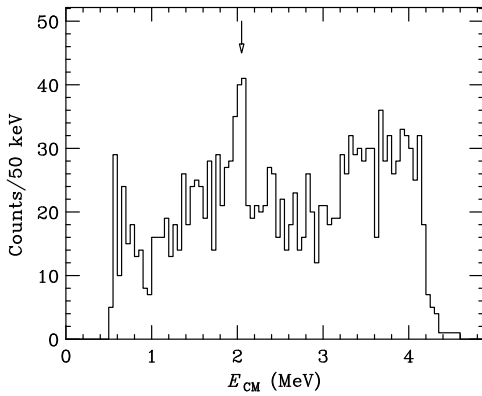


Figure 2. Preliminary $^{17}\text{Ne}+p$ spectrum. The arrow indicates the observed peak energy.

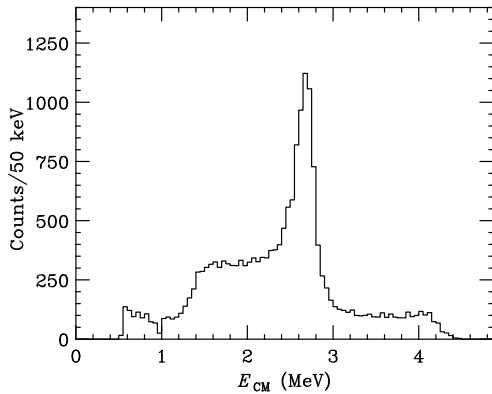


Figure 3. Preliminary $^{14}\text{O}+p$ spectrum.

$l = 2$ orbital angular momentum, which is consistent with the $d_{5/2}$ or $d_{3/2}$ orbital predicted for the last proton in the low-lying ^{18}Na levels.

Using ^{14}O contaminant in the secondary beam, we also simultaneously measured an $^{14}\text{O}+p$ spectrum to check the energy calibration. A sharp peak in Fig. 3 at $E_{\text{CM}} \sim 2.7$ MeV is attributed to the first excited ^{15}F level with a resonance energy of $E_R \sim 2.8$ MeV. Note that the energy at which cross section is maximum is a little lower than E_R in the present case due to interference effects. The peak position agrees with previous results of $^{14}\text{O}+p$ experiments [10] [11] within 50 keV. Since the present test measurement was performed in a limited time, we did not measure a spectrum with a C target for estimating a background contribution from C atoms in the $(\text{CH}_2)_n$ target. The observed peak probably is not due to $^{17}\text{Ne}(p,p')$ inelastic scattering because the peak has a relatively large yield in the spectrum. We, however, did not measure angular dependence of the peak energy in a wide angular range, and therefore could not completely exclude possibility of the inelastic scattering. The present test experiment confirmed the feasibility of the experimental method for the $^{17}\text{Ne}+p$ resonance scattering. A future measurement with high statistics, with angular information, and with background subtraction may clarify the ambiguity in ^{18}Na level assignments.

References

- [1] L.V. Grigorenko, I.G. Mukha, M.V. Zhukov, Nucl. Phys. A **713** (2003) 372.
- [2] A. Ozawa et al., Phys. Lett. B **334** (1994) 18.
- [3] N.K. Timofeyuk, P. Descouvemont, D. Baye, Nucl. Phys. A **600** (1996) 1.
- [4] V. Guimarães, S. Kubono et al., Phys. Rev. C **58** (1998) 116.;
S. Nakamura, V. Guimarães, S. Kubono, Phys. Lett. B **416** (1998) 1.
- [5] H.T. Fortune, R. Sherr, Phys. Lett. B **503** (2001) 70.
- [6] T. Zerguerras et al., Eur. Phys. J. A **20** (2004) 389.
- [7] H.T. Fortune, R. Sherr, Phys. Rev. C **72** (2005) 034304.;
H.T. Fortune, R. Sherr, B.A. Brown, Phys. Rev. C **73** (2006) 064310.
- [8] K.P. Artemov et al., Sov. J. Nucl. Phys. **52** (1990) 408.
- [9] S. Kubono, Nucl. Phys. A **693** (2001) 221.
- [10] F.Q. Guo et al., Phys. Rev. C **72** (2005) 034312.
- [11] V.Z. Goldberg et al., Phys. Rev. C **69** (2004) 031302(R).

Spectroscopy of ${}^6\text{Be}$ by the ${}^3\text{He}({}^7\text{Be},\alpha){}^6\text{Be}$ reaction

R. P. Condori^a, R. Lichtenthaler^a, V. Guimaraes^a, S. Kubono^b, H. Yamaguchi^b, A. Lepine-Szily^a,
Y. Wakabayashi^b, S. Hayakawa^b, Y. Kurihara^b, J.S. Yoo^c, N. Iwasa^d, S. Kato^e

^aInstituto de Fısica da Universidade de Sao Paulo, 05315-970, Sao Paulo, SP, Brazil

^bCenter for Nuclear Study (CNS), University of Tokyo, RIKEN campus, 2-1 Hirosawa, Wako, Saitama 351-0198, Japan

^cDepartment of Physics, Ewha Womans University, 11-1, Daehyun-dong, Seodaemun-gu, Seoul, 120-750, Korea

^dDepartment of Physics, Tohoku University, Aoba, Sendai, Miyagi 980-8578, Japan ^eDepartment of Physics, Yamagata University, Yamagata 990-8560, Japan

1. Introduction

The structure of the energy levels of light nuclei still has several unknown states. In particular in the $A=6$ triplet ${}^6\text{Li}$, ${}^6\text{He}$ and ${}^6\text{Be}$ several excited states have been identified in ${}^6\text{Li}$ and ${}^6\text{He}$ which are not present in the ${}^6\text{Be}$ isobar. Only the ${}^6\text{Be}$ ground state $J^\pi = 0^+(\Gamma = 92\text{KeV})$, an excited state at $E = 1.67\text{MeV}$ with $J^\pi = 2^+(\Gamma = 1.16\text{MeV})$, and three broad structures at high excitation energies at 23, 26, and 27MeV have been observed [1].

In addition to the interest in its nuclear structure, the importance of the existence of excited states in the ${}^6\text{Be}$ near to the ${}^3\text{He}-{}^3\text{He}$ threshold at 11.48MeV resides mainly in the astrophysics. The possible existence of resonances near to this threshold could have strong implications in the p-p burning, since the ${}^3\text{He}+{}^3\text{He}$ capture is one the most important captures in the p-p chain. In addition, possible resonances in this capture reaction at low energies would have consequences in the ${}^3\text{He}$ destruction and, as a consequence, in the ${}^7\text{Be}$ synthesis and in the solar neutrino problem.

The explanation for not observing such excited states in ${}^6\text{Be}$ until now could be in the transfer reactions used to populate those states. In light nuclei, many excited states are expected to have a pronounced cluster structure and a poor overlap between the wave functions in the entrance and exit channels could prevent the formation of those states. In ref. [2] we have successfully used the ${}^3\text{He}({}^7\text{Li},\alpha){}^6\text{Li}$ reaction to populate all the known excited states of ${}^6\text{Li}$ and, in addition, two new broad states at 12.45 and 15.31MeV excitation energies. The idea here is to use a similar reaction ${}^3\text{He}({}^7\text{Be},\alpha){}^6\text{Be}$ to populate the ${}^6\text{Be}$. This reaction in fact involves two different mechanisms, a ${}^3\text{He}$ transfer or a neutron transfer from the projectile to the target, both leading to the same outgoing channel. By detecting the α particles emitted at forward angles, we would in principle select the ${}^3\text{He}$ transfer mechanism favoring the formation of an ${}^3\text{He}-{}^3\text{He}$ 'molecule' in the exit channel.

2. Experimental Procedure

The experiment was performed at CRIB-RIKEN using a pure ${}^7\text{Be}$ beam and a ${}^3\text{He}$ gas target. The ${}^7\text{Be}$ beam of intensity of about $3 - 5 \times 10^5\text{pps}$ and $E_l = 53.4\text{MeV}$ was produced by the primary reaction ${}^7\text{Li}(p,n){}^7\text{Be}$ using the cryogenic H_2 target at CRIB. The system of two dipoles and a Wien Filter of CRIB makes the energy and mass selection of the particles produced in the primary target. Two X-Y PPACs placed before the secondary target allows the mea-

surement of the X-Y position of the beam particles and the reconstruction of their trajectory. The secondary gas cell target was made in Sao Paulo and has 1 inch diameter and 1.8cm length. Two ($6\mu\text{m}$) Havar foils were used as windows. The pressure inside the gas target was about 0.5atm of ${}^3\text{He}$ at room temperature. A system of two E- ΔE telescopes (telescopes 1 and 2) was used to detect the particles scattered in the gas cell and a third E- ΔE telescope (telescope 3) was mounted in the other sector to detect the recoil products in coincidence with the scattered particles as we can see in the Fig. 1. The Double Sided Silicon Detectors (DSSD) ΔE had thickness of $65\mu\text{m}$ (telescopes 1 and 2) and $20\mu\text{m}$ (telescope 3). The coincidence was required due to the enormous background of alpha particles produced by the breakup of the ${}^7\text{Be}$ in the Havar foils, that would completely mask the existence of any peak from the transfer reaction mainly in the high excitation energy range. By imposing the coincidence with light particles (protons, alphas or ${}^3\text{He}$ on telescope 3) coming from the decay of the recoil ${}^6\text{Be}$, one is in principle able to select the alphas coming from the transfer reaction. The telescopes covered an angular range from 10 – 30deg for telescope 1 and 34 – 48deg for telescope 2 in the laboratory system. The coincidence telescope 3 was in the range from –12 to –38deg.

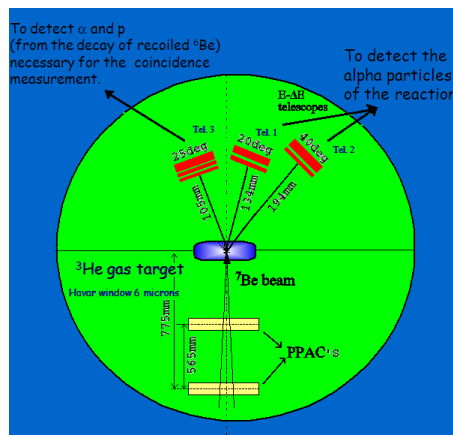


Figure 1. Schematic drawing of the setup for the elastic and transfer reaction.

3. Preliminary Analysis

A E- ΔE spectrum for telescope 1 is shown in Fig. 2 where one can see the well separated lines corresponding to the ${}^3\text{He}$ and ${}^4\text{He}$ particles coming from the target. From the

X-Y position of each scattered particle in the telescope 1, the beam hit position and its incident angle in the target, the later obtained from the PPAC's, we can calculate the scattering angle Θ in the laboratory frame for each event.

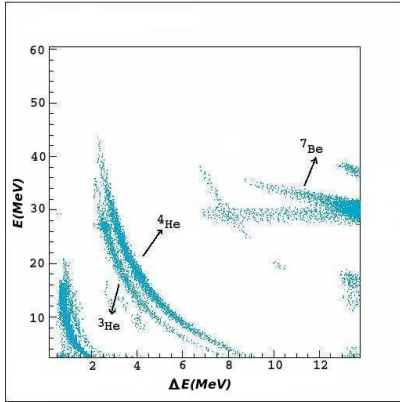


Figure 2. ΔE -E spectrum for telescope 1. The lines correspond to ^3He and α particles.

From the information of the total alpha particle energy and the scattering angle we are able to calculate the excitation energy of the recoil particle ^6Be and to build the ^6Be excitation energy versus the scattering angle spectrum. As the excitation energy of the recoil ^6Be does not depend on the scattering angle we can project the spectrum $E_{\text{exc}} \times \Theta$ on the E_{exc} axis. The results are still preliminary but one can see in the upper part of Fig. 3 that there is a broad structure at ≈ 21 MeV and, apparently, superimposed peaks in the energy range from 10 – 22.5 MeV excitation energy which could correspond to states of the ^6Be nucleus. The maximum excitation energy of the experiment was at about 24 MeV, limited by the detection threshold of telescope 1 for α -particles (10 MeV) which is determined by the maximum energy of the alpha particles which stop in the $65\mu\text{m}$ ΔE detector. Due to the fact that the kinetic energy of the protons and alphas coming from the decay of the recoil become smaller as the excitation energy of ^6Be decreases, the Havar exit window of the target imposes a lower limit in the energy of the decay particles that will punch through the foil and reach the telescope 3. This limit is around $E_{\text{exc}} = 10$ MeV so we don't expect to see states below this limit.

During the experiment we performed runs with and without ^3He gas in the target in order to subtract the background. In Fig. 3 at the bottom we show the spectrum obtained by subtracting the background runs. The background runs were obtained by summing all runs without gas and properly normalized by the integrated ^7Be beam. We observe that the peaks become more visible as the vertical lines show. This is in part due to the presence of peaks in the background spectrum as can be seen in Fig. 3 middle.

We also performed runs using a gold target. As the scattering $^7\text{Be}+^{197}\text{Au}$ is pure Rutherford at the angles of this experiment (see Fig. 4) it will be used to obtain an angular distribution and the solid angles. We build biparametric spectra of the energy of the scattered ^7Be particles versus the scattering angle $E_{7\text{Be}}^{(1,2)} \times \Theta$ for telescopes 1 and 2. The scattering angle axis was sliced in intervals $\Theta \pm 1$ deg and

projected on the $E_{7\text{Be}}$ axis to obtain an angular distribution of the elastic peak. The angular distribution $\sigma/\sigma_{\text{Ruth}}$ for telescope 1 is shown in Fig. 4 using a constant solid angle of 9.5msr for each slice. This procedure allows to obtain the solid angle of every slice in order to have $\sigma/\sigma_{\text{Ruth}} = 1$. Those solid angles will be used later to obtain the angular distribution of the peaks of the ^6Be states seen in figure 3.

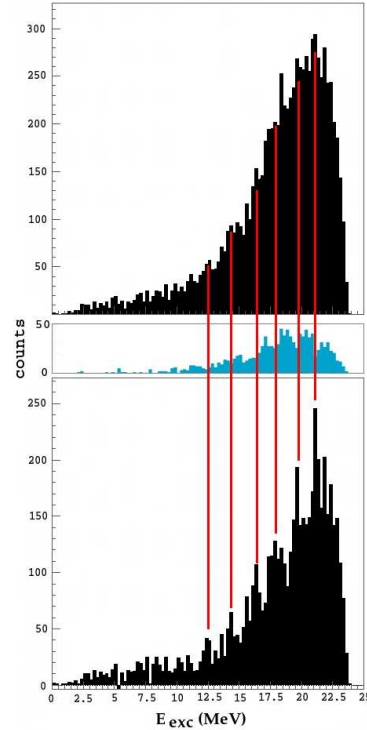


Figure 3. Comparison between the spectrum obtained with ^3He gas (top), no-gas background (middle) and the subtraction spectrum (bottom).

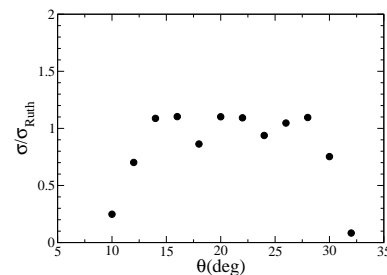


Figure 4. Angular distribution for $^7\text{Be}+^{197}\text{Au}$ using a constant solid angle of 9.5msr for each slice.

References

- [1] D.R. Tilley, C.M. Cheves, J.L. Goodwin, G.M. Hale H.M. Hofmann, J.H. Kelley, C.G.Sheu, H.R. Weller Nucl. Phys. **A708**(2002) 3 .
- [2] R. Kuramoto, R. Lichtenthaler, A. Lepine-Szily, V. Guimaraes, G.F. Lima, E. Benjamim, P.N. de Faria Braz. Journ. of Physics **34** (2004) 933.

Elastic scattering for 60MeV ^{17}F on ^{12}C target

G. L. Zhang^{a,b}, H. Q. Zhang^a, C. J. Lin^a, C. L. Zhang^a, G. P. An^a, Z. D. Wu^a, H. M. Jia^a, X. X. Xu^a, F. Yang^a, Z. H. Liu^a, S. Kubono^c, H. Yamaguchi^c, S. Hayakawa^c, D. N. Binh^c, Y. K. Kwon^d, N. Iwasa^e,

^aChina Institute of Atomic Energy, Beijing 102413, China

^bSchool of Physics and Nuclear Energy Engineering, Beihang University, Beijing 100191, China

^cCenter of Nuclear Study, University of Tokyo, Japan

^dDepartment of Physics, Chung-Ang University, Seoul 156-756, South Korea

^eDepartment of Physics, Tohoku University, Aoba, Sendai, Miyagi 980-8578, Japan

Our knowledge of nuclei comes mainly from the experiments with nuclei in the valley of the stability. Experiments with nuclei far from the stability-line are expected to provide tests of current nuclear structure models. In particular, light nuclei locating near the drip line may exhibit exotic phenomena, such as manifestations of halo/skin structure. Information on the nuclear structure can be extracted from the reaction data. Among many nuclear reactions, the elastic scattering is a major channel and will provide rich information on reaction mechanism and structures of the nuclei. It is also used to determine optical potentials which are important inputs for any reaction studies. However, elastic scattering data for light exotic nuclei are extremely scarce, which raises questions about accuracy and reliability of nuclear structure information extracted from the reaction studies. Because of halo/skin structures and the small binding energy of the last nucleon(s), the light exotic nuclei may behave differently from stable, well-bound nuclei in reactions and reliability of simple-minded extrapolation from the systematics in stable nuclei is open to doubt. Thus, studies of elastic scattering induced by light exotic nuclei are of particular interest.

Study of the ^{17}F elastic scattering is motivated by our interest described above. The study of this nucleus is quite interesting for three reasons: (i) Because of its small binding energy of 601keV, the rms radius could be significantly larger than that of ^{16}O core. (ii) It has only one bound state below the breakup threshold, (iii) its first excited state has a halo structure [1, 2]. Many experiments have been performed to explore its structure and reaction mechanisms in recent years. Elastic scattering of $^{17}\text{F}+^{208}\text{Pb}$ was measured at 10MeV/nucleon, [3] 98MeV and 120 MeV, [4] 90.4MeV, [5] respectively. Precise data have been obtained for the elastic scattering of ^{17}F on ^{12}C and ^{14}N at 10MeV/nucleon [6].

In most of the above cases, the data are taken for the ^{208}Pb target. The experimental data on light targets are hardly found, except for the data on ^{12}C and ^{14}N at the energy of 10MeV/nucleon [6]. Therefore the experiment was planned to extract the optical potential of the elastic scattering for ^{17}F on ^{12}C target at 60MeV.

In order to obtain the elastic scattering data at energy near Coulomb barrier, 60MeV $^{17}\text{F}+^{12}\text{C}$ reaction was studied at CNS Radioactive Ion Beam separator (CRIB). The beam intensity on the target was about 4×10^5 pps. A

$435\mu\text{g}/\text{cm}^2$ -thick ^{12}C target was used. Projectile ^{17}F was identified by the time of flight (TOF) method. The Position of ^{17}F on ^{12}C target was determined by using information from two position-sensitive PPACs (Parallel Plate Avalanche Counters) set in the beam line. Six sets of $\Delta\text{E-E}$ detector telescopes were composed of double sided Silicon strip detectors(50mm \times 50mm in area)(DSSD) and silicon detectors without strips (SSD), and covered angle range $\theta_{lab} = 5^\circ - 80^\circ$. They were symmetrically positioned around the beam axis in order to measure efficiently the events of ^{17}F elastic scattering. The distance from the target center to the strip detectors are 145 mm, 115 mm and 85 mm depending on the three angle settings, which correspond to 13.6° , 35.4° and 63.4° , respectively. Thin ΔE detectors (DSSD, $65\mu\text{m}$ thickness) were placed in front of 300 μm -thick E detectors (SSD). Such detector configuration allowed identification of the atomic number Z of the scattered charged particles. The emission angle of ^{17}F can be determined precisely by the silicon strip detectors. We will be able to extract precisely the angular distribution of elastic scattering for $^{17}\text{F}+^{12}\text{C}$.

Fig. 1 shows the particle identification before target. RF1

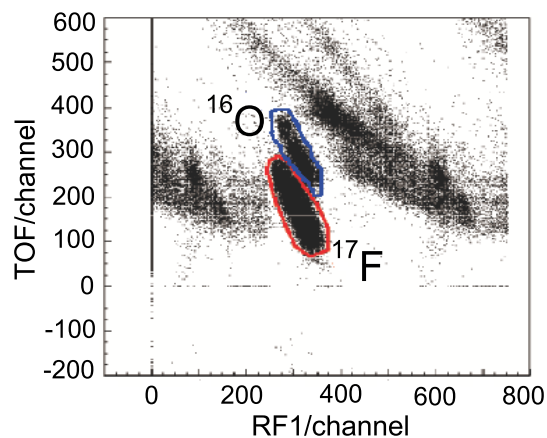


Figure 1. The particle identification before target.

is the time when the beam particle arrives at a PPAC relative to the radiofrequency signal from the cyclotron resonator. TOF is obtained by using the time signals of two PPACs before target. It is shown that ^{17}F particles can be identified

clearly from the primary ^{16}O beam with a high intensity.

Fig. 2 shows the energy spectrum of ^{17}F measured by a strip detectors. The elastic peak of ^{17}F is shown clearly. The excited state at 495keV in ^{17}F can not be resolved because of the limited resolution. The other continuous distribution could be from inelastic excitation of the target ^{12}C and some instrumental background. The scattering angle

- [2] M. J. Borge *et al.*, Phys. Lett. B. **217** (1993) 25.
- [3] J. F. Liang *et al.*, Phys. Rev. C **65**, (2002) 051603.
- [4] J. F. Liang *et al.*, Phys. Rev. C **67**, (2003) 044603.
- [5] M. Romoli *et al.*, Phys. Rev. C **69**, (2004) 064614.
- [6] J. C. Blackmon *et al.*, Phys. Rev. C **72**, (2005) 034606.

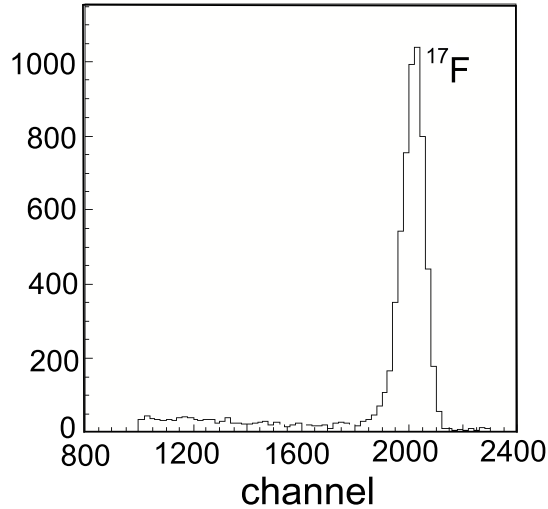


Figure 2. ^{17}F elastic scattering on silicon strip detector.

can be obtained by the position information given by the two PPACs in the beam line and the double sided silicon detectors. The experimental angular distribution of elastic scattering for ^{17}F on ^{12}C target is shown in Fig.3. More detailed theoretical analyses are in progress.

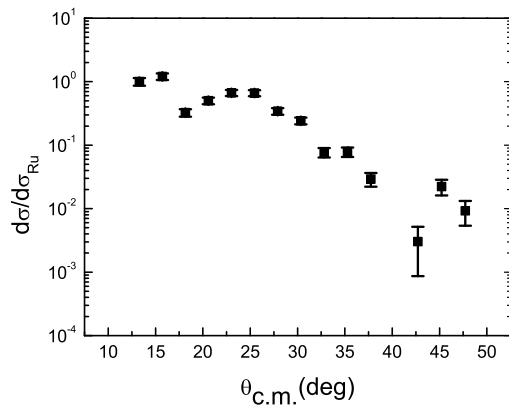


Figure 3. The experimental angular distribution of elastic scattering for 60MeV ^{17}F on ^{12}C target. $\frac{d\sigma}{d\sigma_{Ru}}$ is the ratio of the experimental cross section to Rutherford cross section.

References

- [1] R. Morlock *et al.*, Phys. Rev. Lett. **79** (1997) 3837.

Study of High-Spin States in ^{35}S

E. Ideguchi, S. Ota, T. Morikawa^a, M. Oshima^b, M. Koizumi^b, Y. Toh^b, A. Kimura^b, H. Harada^b,
K. Furutaka^b, S. Nakamura^b, F. Kitatani^b, Y. Hatsukawa^b, T. Shizuma^b, M. Sugawara^c,
Y.X. Watanabe^d, Y. Hirayama^d, and M. Oi^e

Center for Nuclear Study, Graduate School of Science, University of Tokyo

^a*Department of Physics, Kyushu University*

^b*Japan Atomic Energy Agency*

^c*Chiba Institute of Technology*

^d*Institute of Particle and Nuclear Studies, High Energy Accelerator Research Organization (KEK)*

^e*Institute of Natural Sciences, Senshu University*

We have been systematically studying high-spin states in $A=30\sim 40$ nuclei to clarify the superdeformed (SD) shell structure and to investigate the spherical and SD shape co-existences in this mass region. Recently, we have found a SD rotational band in ^{40}Ar [1] and the SD region in $A=30\sim 40$ nuclei is extended from $N=Z$ (i.e., ^{36}Ar [2], ^{40}Ca [3, 4], and ^{44}Ti [5]) to neutron-rich side. Another SD shell structure is predicted in $Z=16$ and the onset of SD bands in sulfur isotopes is expected. Cranked Skyrme-Hartree-Fock calculations predict the SD structure in ^{32}S and ^{36}S isotopes [6]. However, spectroscopic studies of sulfur isotopes are not well explored and only low-lying levels near the ground state are studied. In order to clarify high-spin levels and to investigate collective structure in ^{35}S , we have performed an in-beam γ -ray spectroscopy experiment.

The experiment was performed at the tandem accelerator facility of the Japan Atomic Energy Agency. An ^{18}O beam of 70 MeV was used to irradiate a ^{26}Mg target of 0.5 mg/cm^2 thickness with Pb backing and the two stacked self-supporting ^{26}Mg target foils of 0.47 and 0.43 mg/cm^2 thickness. The Pb backed target is used to establish low-lying levels, while the thin target is used for investigating high-spin levels. A $^{26}\text{Mg}(^{18}\text{O}, 2p2n)^{40}\text{Ar}$ fusion-evaporation reaction was employed to populate high-spin states in ^{35}S . Gamma rays were detected by the GEMINI-II array [7] comprised of 16 HPGe detectors with BGO Compton suppressor shields, in coincidence with charged particles detected by the Si-Ball [8], a 4π array consisting of 11 ΔE Si detectors of $170\text{ }\mu\text{m}$ thickness. The HPGe detectors were placed at 6 different angles, namely 47° (4 Ge's), 72° (2 Ge's), 90° (2 Ge's), 105° (4 Ge's), 144° (1 Ge) and 147° (1 Ge) with respect to the beam direction, which enables us to perform angular distribution and DCO (Directional Correlations from Oriented states) analyses [9]. The most forward placed Si detector was segmented into five sections and the other Si detectors were segmented into two sections each, giving a total of 25 channels that were used to enhance the selectivity of multi-charged-particle channels.

With a trigger condition of more than two Compton suppressed Ge detectors firing in coincidence with charged particles, a total number of 6.6×10^8 events for the experiment using backed target and 1.7×10^8 events for that using thin target were collected, respectively. Figure 1 shows γ -ray

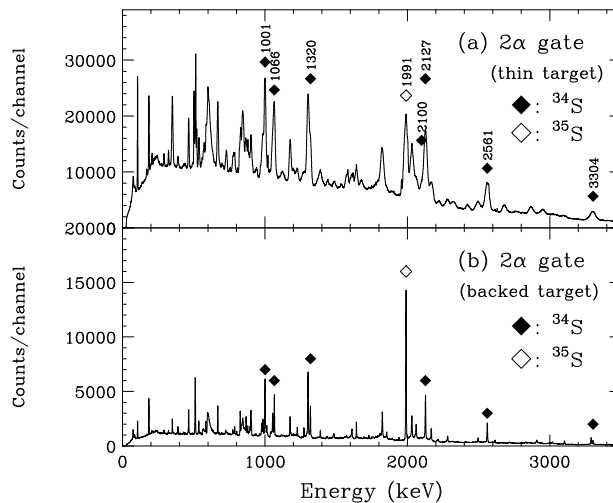


Figure 1. Gamma-ray spectra obtained by gating the events with two alpha particles detected in the experiments using the backed target (lower panel) and the thin target (upper panel).

spectra of backed target (lower panel) and thin target (upper panel) experiments with charged particle gates of two alpha particle detected simultaneously. As seen in the figure, γ -ray peaks associated with ^{34}S and ^{35}S were clearly identified.

Previously, excited levels of ^{35}S were studied via $\beta - \gamma$ spectroscopy of ^{35}P [10], $^{34}\text{S}(n, \gamma)$ [11] as well as nucleon transfer reactions, i.e. $^{34}\text{S}(d, p\gamma)$ [12], $^{160}\text{Gd}(^{34}\text{S}, ^{35}\text{S})$ and $^{160}\text{Gd}(^{37}\text{Cl}, ^{35}\text{S})$ [13]. Since ^{35}S is a nucleus with $Z=16$ and $N=19$, the spin-parity of the ground state is $3/2^+$ due to the neutron hole in $d_{3/2}$ orbital. At 1.991 MeV, the $7/2^-$ isomeric state with a half-life of 1.02(5) ns is known, but higher-spin levels have not been identified. Above the 1.991 MeV level, a 2.03 MeV γ -ray transition was identified previously, but the spin-parity of the 4.021 MeV level was not known.

In order to find higher spin levels above the $7/2^-$ state, $\gamma - \gamma$ coincidence relations were examined by gating on the 1991 keV γ -ray transition as shown in Fig. 2. As shown in the figure, previously identified γ -ray peak appears at 2032 keV. In addition, several γ -ray transitions are found in coincidence with the 1991 keV transition.

In order to assign spins and parities of the newly identified levels, DCO analysis was performed. However, due

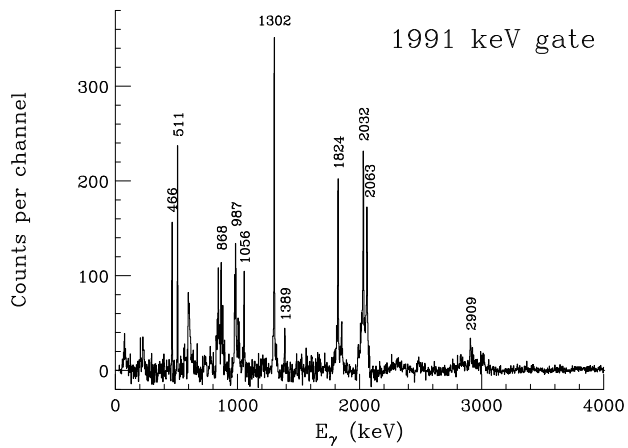


Figure 2. Gamma-ray spectrum created by gating on the 1991 keV transition in ^{35}S .

to the limited counting statistics, spin-parity of the levels could not firmly identified. In order to fix the spins and parities, linear polarization measurements of γ rays have been performed. Data analysis is in progress.

References

- [1] E. Ideguchi *et al.*, Phys. Lett. B **686**, 18-22 (2010).
- [2] C.E. Svensson *et al.*, Phys. Rev. Lett. **85**, 2693-2696 (2000).
- [3] E. Ideguchi *et al.*, Phys. Rev. Lett. **87**, 222501/1-4 (2001).
- [4] C.J. Chiara *et al.*, Phys. Rev. C **67**, 041303(R)/1-5 (2003).
- [5] C.D. OfLeary *et al.*, Phys. Rev. C **61**, 064314/1-7 (2000).
- [6] T. Inakura *et al.*, Nucl. Phys. A **728**, 52-64 (2003).
- [7] M. Oshima *et al.*, J. Radioanal. Nucl. Chem. **278**, 257-262 (2008).
- [8] T. Kuroyanagi *et al.*, Nucl. Instrum. Meth. A **316**, 289-296 (1992).
- [9] K.S. Krane, R.M. Steffen and R.M. Wheeler, Nucl. Data Tables, **11**, 351–406 (1973).
- [10] S. Raman *et al.*, Phys. Rev. C **32**, 18 (1985).
- [11] Th. W. Van del Mark *et al.*, Nucl. Phys. A **181**, 196 (1972).
- [12] E. K. Warburton *et al.*, Phys. Rev. C **34**, 1031 (1986).
- [13] B. Fornal *et al.*, Phys. Rev. C **49**, 2413 (1994).

Measurement of the isovector spin monopole resonance via the $(t, {}^3\text{He})$ reaction at 300 MeV/nucleon

K. Miki^{a,c}, H. Sakai^a, T. Uesaka^b, H. Baba^c, G.P.A. Berg^d, N. Fukuda^c, D. Kameda^c, T. Kawabata^e, S. Kawase^b, T. Kubo^c, K. Kusaka^c, S. Michimasa^b, H. Miya^b, S. Noji^a, T. Ohnishi^c, S. Ota^b, A. Saito^b, Y. Sasamoto^{b,c}, M. Sasano^a, S. Shimoura^b, H. Takeda^c, H. Tokieda^b, K. Yako^a, Y. Yanagisawa^c, A. Yoshida^c, K. Yoshida^c, and R.G.T. Zegers^f

^aDepartment of Physics, University of Tokyo

^bCenter for Nuclear Study, Graduate School of Science, University of Tokyo

^cRIKEN Nishina Center

^dJINA, Department of Physics, University of Notre Dame

^eDepartment of Physics, Kyoto University

^fNSCL, Michigan State University

The isovector spin monopole resonance (IVSMR) has been an important topic of interest in the study of spin-isospin responses in nuclei [1, 2, 3, 4]. Since the IVSMR is a breathing mode with spin and isospin flips, it can be related to a new kind of nuclear matter compressibility with spin and isospin degrees of freedom. In spite of the importance of the IVSMR, it has not been clearly identified, especially for the β^+ side. In order to identify the IVSMR(β^+), we measured the ${}^{208}\text{Pb}(t, {}^3\text{He})$ and ${}^{90}\text{Zr}(t, {}^3\text{He})$ reactions at 300 MeV/nucleon. This was the first physics experiment performed with the newly constructed SHARAQ spectrometer [5].

The experiment was performed at the RIBF facility at RIKEN. A schematic picture of the experimental setup is shown in Fig. 1. A primary α beam at 320 MeV/nucleon was bombarded onto a ${}^9\text{Be}$ production target (thickness: $d = 4$ cm) installed at F0 of BigRIPS. The produced tritons of 300 MeV/nucleon were transported along the high-resolution beam line to the secondary target installed at the pivot of the SHARAQ spectrometer. The SHARAQ facility was not operated in the high-resolution dispersive mode but in the achromatic mode because of the requirement for the large counting statistics. In order to improve the resolution, the emittance of the secondary beam was reduced by a momentum slit ($|\Delta p/p| = 0.06\%$) at F1 and an angular collimator ($|\Delta\theta| = 15$ mrad) at F2. They corresponded to an energy spread of 2 MeV (FWHM) and an angular spread of 7mrad (FWHM) at the secondary target position. The beam intensities were typically 300 particle nA for the primary beam and 1×10^7 pps for the secondary tritons. The purity of the triton beam was better than 99%. This is because no other particle has the same momentum-to-charge ratio ($p/Q = 2.4$ GeV/c) at the energy, because of kinematic restrictions.

The secondary targets used were ${}^{208}\text{Pb}$ ($d = 0.35$ mm) and ${}^{90}\text{Zr}$ ($d = 0.46$ mm) foils for the IVSMR measurements and a CH_2 ($d = 0.5$ mm) foil for calibrations. The ${}^3\text{He}$ particles in the reaction products were momentum analyzed by the SHARAQ spectrometer and counted by the cathode-readout drift chambers [6] installed in the final focal plane of the SHARAQ spectrometer. The differential

cross sections were measured at an excitation energy of $0 \leq E_x \leq 70$ MeV and scattering angles of $0^\circ \leq \theta \leq 3^\circ$.

The blank-target run was also performed for the background estimation. The distribution of the background component was uniform and the count rate was negligibly small (less than 0.1%) compared to the ${}^{208}\text{Pb}$ and ${}^{90}\text{Zr}$ runs.

Figure 2 shows the measured $\text{CH}_2(t, {}^3\text{He})$ spectra. The top panel shows the XY spectrum measured on the focal plane of the SHARAQ spectrometer. X_{FP} and Y_{FP} are proportional to the momentum and the vertical scattering angle of the ${}^3\text{He}$ particles, respectively. Two main loci can be identified in the figure; these are attributed

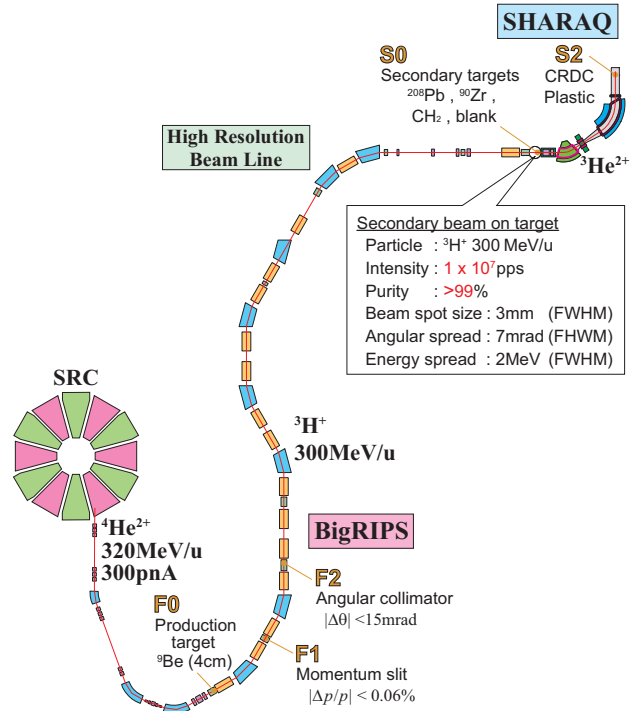


Figure 1. Experimental setup. The experiment was performed at the RIBF facility in RIKEN. See text for details.

to the ${}^1\text{H}(t, {}^3\text{He})$ and ${}^{12}\text{C}(t, {}^3\text{He})$ reactions. A

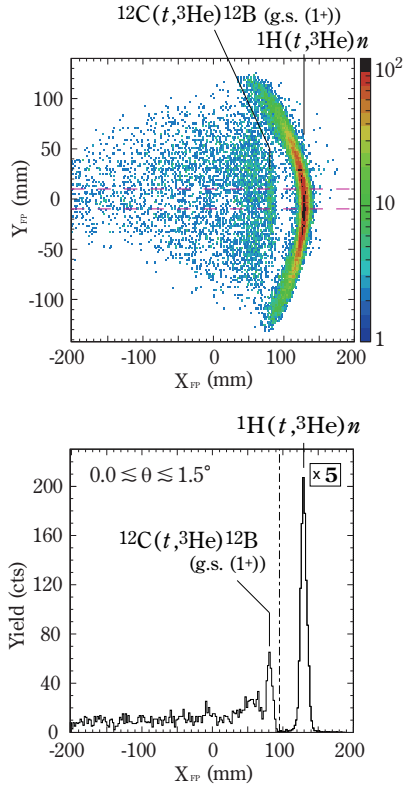


Figure 2. The obtained image at the SHARAQ focal plane for the $\text{CH}_2(t, {}^3\text{He})$ reaction [top] and its projection [bottom].

kinematic correlation due to the recoil of target protons is nicely observed for the ${}^1\text{H}(t, {}^3\text{He})n$ reaction. A projection of this picture is shown in the bottom panel. From the distance between the two observed peaks, the dispersion of the SHARAQ spectrometer is determined to be 6.10 m, which is close to the design value of 5.86 m. The energy resolution obtained from the ${}^{12}\text{C}(t, {}^3\text{He}){}^{12}\text{B}$ (g.s.) peak is about 2 MeV (FWHM).

The obtained ${}^{208}\text{Pb}(t, {}^3\text{He})$ spectra are shown in the top panel of Fig. 3. Two peaks are observed around 5 MeV and 15 MeV. Since the angular distribution for the monopole transition has its maximum at 0 degrees, monopole components can be extracted by a difference between $0.0^\circ - 0.5^\circ$ and $0.5^\circ - 1.0^\circ$ spectra as a preliminary analysis. The obtained difference spectrum is shown in the bottom panel of Fig. 3. A significant monopole component is observed at around 12 MeV, which would be attributed to the IVSMR. The broken line and the dot-broken line represent the Tamm-Dancoff approximation (TDA) calculations using the effective interaction SGII and SIII, respectively [1]. It is found that both calculations reproduces the overall shape. However, the SGII underestimates the average excitation energy and the SIII calculation gives a better description. Monopole components are discovered also for ${}^{90}\text{Zr}$ at around 20 MeV as shown in Fig. 4, and the comparison between the experimental data and the TDA calculation shows a similar characteristic as in the ${}^{208}\text{Pb}$ case.

In the future analysis, the multipole decomposition technique will be applied aiming at the more precise extraction of monopole components, and the detailed physics of the

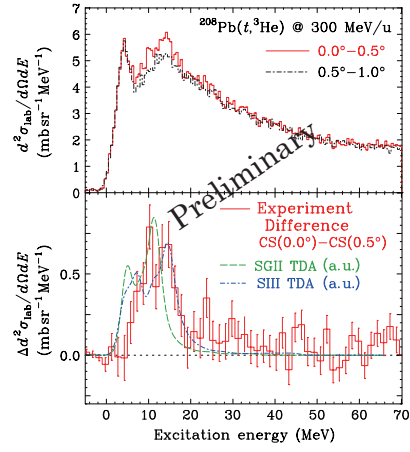


Figure 3. The double differential cross section spectra for the ${}^{208}\text{Pb}(t, {}^3\text{He})$ reaction [top] and their difference spectrum [bottom]. Monopole component is discovered at around 12 MeV.

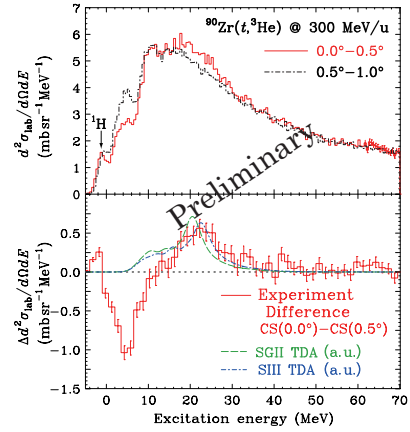


Figure 4. The double differential cross spectra for the ${}^{90}\text{Zr}(t, {}^3\text{He})$ reaction [top] (a peak at $E_x = -1.5$ MeV is due to hydrogen contaminants in the ${}^{90}\text{Zr}$ foil), and their difference spectrum [bottom]. Monopole component is discovered at around 20 MeV. (A dip around 4 MeV is due to higher multipole components.)

IVSMR will be discussed.

References

- [1] I. Hamamoto and H. Sagawa, Phys. Rev. C **62**, 024319 (2000).
- [2] N. Auerbach and A. Klein, Phys. Rev. C **30**, 1032 (1984).
- [3] D.L. Prout *et al.*, Phys. Rev. C **63**, 014603 (2000).
- [4] R.G.T. Zegers *et al.*, Phys. Rev. Lett. **90**, 202501 (2003).
- [5] T. Uesaka *et al.*, Nucl. Instrum. Meth. B **266**, 4218 (2008); RIKEN Accel. Prog. Rep. **43** (2010).
- [6] S. Michimasa *et al.*, CNS Ann. Rep. 2009 (2010).

The super-allowed Fermi type charge exchange reaction for studies of isovector non-spin-flip monopole resonance

Y. Sasamoto and T. Uesaka

Center for Nuclear Study, Graduate School of Science, University of Tokyo

1. Introduction

Isovector non-spin-flip monopole resonance (IVMR) is of particular interest, because it is an oscillation mode of isovector density $\rho_{IV} = \rho_n - \rho_p$ and its energy and width should be closely related to properties of asymmetric nuclear matter [1] and to isospin mixture in nuclei [2].

In spite of its importance, however, experimental data on IVMR are scarce so far. Pion charge exchange reactions (π^\pm, π^0) [3] and heavy-ion charge exchange (HICE) such as ($^{13}\text{C}, ^{13}\text{N}$) [4, 5] and ($^7\text{Li}, ^7\text{Be}$) [6] reactions have been used to study IVMR. These two-types of reactions provide inconsistent results of excitation energy, width, and/or multipolarity of the state [4].

Pion charge exchange reactions are selective probes to isovector non-spin-flip ($\Delta T = 1, \Delta S = 0$) transitions and are suited for IVMR studies, while difficulty in measuring $\sim 100\text{MeV}$ γ -rays in coincidence originates experimental uncertainties. On the other hand, HICE experiments can provide accurate data because magnetic analysis of forward scattered particles can be applied there. However, in those reactions, contributions from isovector spin-flip ($\Delta T = 1, \Delta S = 1$) transitions can not be ruled out and model-dependent subtraction is required to deduce isovector non-spin-flip amplitudes. It should be significant at intermediate energies, for example, at RIBF energies. The Gamow-Teller (GT) transition contaminates seriously the non-spin-flip one because the effective interaction for the isovector spin-flip transition is much stronger than the isovector non-spin-flip transitions at RIBF energies [7].

To understand nature of IVMR, a HICE probe selective to $\Delta T = 1, \Delta S = 0$ modes is essentially important.

In this report, we propose the *RI beam induced* charge exchange ($^{10}\text{C}, ^{10}\text{B}(\text{IAS})$) experiment to probe IVMR. We call this the super-allowed Fermi type charge exchange reaction. This reaction has many advantages as a probe to IVMR, over other HICE reactions used so far.

2. Super-allowed Fermi type charge exchange reaction

Suitable probe to IVMR should have the following characteristics,

- Non-spin-flip states should be selectively excited.
- Contamination due to the GT transition is reasonably small.
- Experiment can be conducted without considerable technical difficulty.

Our idea to establish a probe to isovector non-spin-flip states is based on use of a super-allowed Fermi transition

between isobaric analog states in the projectile. This necessarily leads to an RI beam induced charge exchange reaction since light stable nuclei with $J^\pi = 0^+$ have no analog states because of their isospin $T = 0$. On the other hand, some unstable nuclei with $J^\pi = 0^+$ have isobaric analog states in neighbor nuclei, as shown in Fig.1. Gamma-rays emitted from IAS are available to identify the super-allowed Fermi transition, experimentally. Among such RI beam induced charge exchange reactions, ($^{10}\text{C}, ^{10}\text{B}(\text{IAS})$) is considered to be the best one because the feedings from the highly excited GT states are expected to be negligibly small as described in the next section. This is not the case in other reactions such as ($^{14}\text{O}, ^{14}\text{N}(\text{IAS})$), ($^{18}\text{Ne}, ^{18}\text{F}(\text{IAS})$).

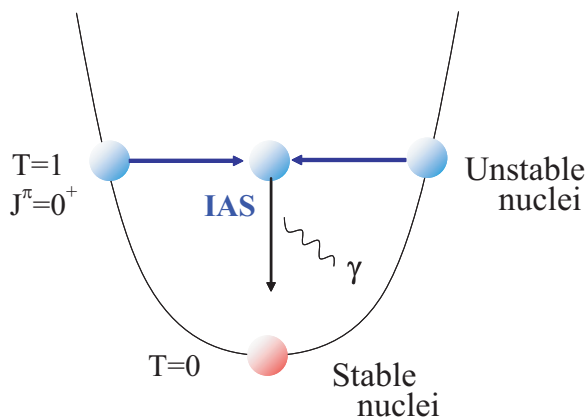


Figure 1. Schematic view of the super-allowed Fermi type charge exchange reaction. RI beams are suitable to use the a super-allowed Fermi transition between isobaric analog states for the projectile.

3. Characteristics of ($^{10}\text{C}, ^{10}\text{B}(\text{IAS})$) reaction

The analog state of the ^{10}C ground state locates at $E_x = 1.740$ MeV in ^{10}B as shown in Fig.2. The transition from the ^{10}C ground state to the 1.740-MeV state in ^{10}B can be experimentally identified by observing the emitted γ -ray of 1.022 MeV. Thus, coincident detection of ^{10}B and 1.022 MeV γ -rays in the final state can be a clear signature of $0^+ \rightarrow 0^+$ transition in the projectile, and consequently, of the non-spin-flip excitation in the target.

If the feeding from highly excited GT states is large, the tagging of $0^+ \rightarrow 0^+$ transition by detecting γ -rays is disturbed by the feedings. However, the ($^{10}\text{C}, ^{10}\text{B}(\text{IAS})$) reaction is hardly suffered from the feedings from GT contaminants, because $B(\text{GT})$ value of the GT state at $E_x = 2.154$ MeV in ^{10}B , which locates 0.414 MeV above IAS, is known to be as small as 0.01 [8]. On the other hand, the

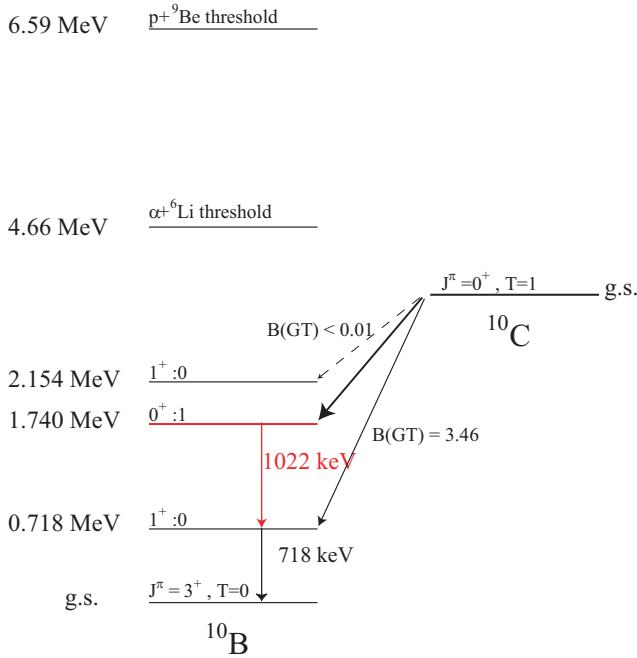


Figure 2. Levels in ^{10}B . The analog state of the ^{10}C ground state is found at $E_x = 1.740$ MeV in ^{10}B .

$B(\text{GT})$ value for the GT state at $E_x = 0.718$ MeV is known to be 3.46 (taken from Ref. [9]), which exhausts a major part of the sum-rule value of 6 when a quenching factor of 0.7 is taken into consideration. Even if the GT states exist above 1.74-MeV, those de-excite via particle decay because they are above the alpha and/or proton decay thresholds at 4.66 MeV, and 6.59 MeV, respectively.

Strong absorption nature of HICE reaction makes the reaction surface-sensitive. Since the transition density of IVMR has a radial node, a cancellation will occur if one use a transparent, volume-sensitive probe. In this respect, surface-sensitive HICE reaction is useful to avoid the cancellation and to populate IVMR with a sufficient strength. On top of that, the strong absorption produces oscillating angular distribution characteristic to the multipolarity of the state. This allows one to identify the transferred orbital angular momentum ΔL from the angular distribution.

The ($^{10}\text{C}, ^{10}\text{B}(\text{IAS})$) reaction has also advantages in terms of the reaction analysis. By use of the super allowed Fermi transition, the uncertainties of the projectile form factor is minimized since the structures of isobaric analog states are similar each other, which leads more reliable calculation.

We should also mention about experimental merit in use of the ($^{10}\text{C}, ^{10}\text{B}(\text{IAS})$) reaction. The purity of proton rich beam is usually low, because it often suffer from large amount of contaminant of isotones. However, this is not the case for ^{10}C . The purity of a ^{10}C beam is expected to be exceptionally high among proton rich beams, since neighboring isotones with $N = 4$ (^8Be , ^9B , ^{11}N , ^{12}O) are unbound as shown in Fig.3. Thus, a clean experiment will be possi-

ble.

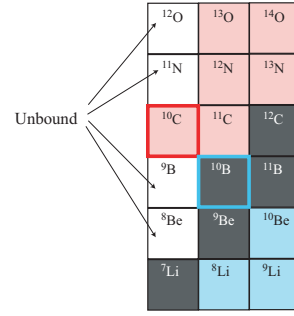


Figure 3. Nuclei around ^{10}C and ^{10}B .

4. Summary and Prospects

The super-allowed Fermi type charge exchange reaction with RI beams will have a new capability which we have not acquired using *stable-beam induced* reactions. Among them, ($^{10}\text{Be}, ^{10}\text{B}(\text{IAS})$) reaction has a good selectivity to the non-spin-flip transition and is the most suitable to IVMR studies. It should be also noted that both ($^{13}\text{C}, ^{13}\text{N}$) and ($^7\text{Li}, ^7\text{Be}$) reactions are of β^+ type and no attempt has been made to observe IVMR with a β^- type HICE reaction in the past. Once the method of the super-allowed Fermi type reaction is established, it will be the first attempt to excite IVMR with a β^- type HICE reaction. Subsequently, it can be also applied to β^+ side with the ($^{10}\text{Be}, ^{10}\text{B}(\text{IAS})$) reaction. With transition strengths for β^+ and β^- , the sum-rule value can be discussed in the model independent sum-rule for the non-spin flip excitation of

$$S_- - S_+ = N \langle r^4 \rangle_n - Z \langle r^4 \rangle_p,$$

where S_{\pm} is the total IVMR strength for the β^{\pm} type.

References

- [1] G. Colo and N. Van Giai, Phys. Rev. C **53** (1996) 2201.
- [2] A. Bohr and B. Mottelson, "Nuclear Structure".
- [3] A. Erell *et al.*, Phys. Rev. C **34** (1986) 1822.
- [4] I. Lhenry, Nucl. Phys. A **599** (1996) 245c.
- [5] T. Ichihara *et al.*, Phys. Rev. Lett. **89** (2002) 142501.
- [6] S. Nakayama *et al.*, Phys. Rev. Lett. **83** (1999) 690.
- [7] M. A. Franey *et al.*, Phys. Rev. C **31** (1985) 488.
- [8] B. K. Fujikawa *et al.*, Phys. Lett. B **449**, (1999) 6.
- [9] T. Suzuki *et al.*, Phys. Rev. C **67**, (2003) 044302.
- [10] H. Lenske *et al.*, Phys. Rev. Lett. **62**, (1989) 1457.

**Experimental Nuclear Physics:
PHENIX Experiment at BNL-RHIC and
ALICE Experiment at CERN-LHC**

Activities on the RHIC-PHENIX and LHC-ALICE experiments in the Year 2009

H. Hamagaki, T. Gunji, Y. Tsuchimoto, Y. Aramaki, Y.L. Yamaguchi, S. Sano, A. Takahara, R. Akimoto, Y. Hori, and T. Tsuji

Center for Nuclear Study, Graduate School of Science, University of Tokyo

1. Introduction

The physics goal of the studies with ultra-relativistic heavy-ion collisions is to realize a new form of matter, called quark-gluon plasma (QGP), and to study its properties.

The CNS group has been participating in the PHENIX experiment at the Relativistic Heavy Ion Collider (RHIC) of Brookhaven National Laboratory, USA, with the financial support from the Japan-US cooperation in the field of high energy physics sponsored by MEXT. The PHENIX experiment is one of the major experiments at RHIC, which consists of two central arms (East and West), two muon arms (North and South) and inner detectors for event trigger and event characterization. The PHENIX experiment was designed so as to address as many signatures as possible for QGP formation, by having a very unique capability to measure photons, electrons and muons as well as hadrons.

The group also has been actively participating to the ALICE experiment at the Large Hadron Collider (LHC) in CERN. The ALICE collaboration consists of more than 1000 members from 115 institutes in 33 countries. The ALICE experiment is designed to be optimized to the studies with heavy ion collisions at LHC.

In this report, major topics of the PHENIX and ALICE experiments and the activities of the CNS group in the Japanese fiscal year (JFY) 2009 are summarized.

2. Progress in the PHENIX Experiment

2.1. Physics runs; Run 9 and 10

In the JFY 2009, PHENIX has successfully performed data taking in Run 9, whose span was from the middle of March 2009 until the end of June 2009, and the first part of Run 10, whose span was from the beginning of January 2010 until the end of May.

Run 9 was totally devoted to polarized p-p collisions at two energies; $\sqrt{s} = 500$ GeV and 200 GeV. Recorded integrated luminosity was 10 pb^{-1} for $\sqrt{s} = 500$ GeV, and 16 pb^{-1} for $\sqrt{s} = 200$ GeV.

Run 10 is totally devoted to Au+Au collisions at several different energies. A new detector, named as HBD (Hadron Blind Detector), was fully installed for this run, and large deduction of background is expected in the low-mass region of e^+e^- invariant mass spectrum due to Dalitz decay of neutral mesons.

The CNS group has been responsible for maintenance, operation during the run, and calibration for data analysis of the RICH (Ring Imaging Cherenkov) subsystem, which is a gaseous Cherenkov counter using CO_2 gas as a Cherenkov radiator. RICH is a primary device for electron identification in the PHENIX experiment. RICH has worked without

serious problems in Run 9 and Run 10.

2.2. Physics output & group activities

Eleven physics papers were published in refereed journals in JFY 2009 by the PHENIX collaboration, as listed in the publication list of this annual report. Several others have been submitted for publication and are in different stages before final publication. Press release was made by BNL on February 15, 2010, on the recent results from PHENIX, which suggests initial temperature of the system created in the head-on collision of the two Au nuclei at RHIC would reach 4 trillion degrees.

The CNS group had several distinct data analysis activities in the JFY 2009. Brief introduction is intended in this article as an overview, and detailed descriptions will be provided in the following separate articles. Major efforts of the CNS group has been on the physics with photons and leptons.

One of the most important yet uncultivated subjects at RHIC is to find evidence of chiral symmetry restoration. Low-mass vector mesons are considered to be the sensitive probes. Huge combinatorial background has been preventing us from extracting clean signals. Systematic studies have been made by measuring low-mass vector mesons via lepton channel and hadron channel in p-p, Cu-Cu, and Au-Au collisions. Current status is presented in [1].

Path length dependence of energy loss is considered to provide crucial information to understand the mechanism of jet quenching effect and properties of hot and dense matter. Path length of a parton can be determined with less ambiguity by measuring azimuthal angle of a parton relative to the reaction plane in event by event, in addition to the centrality selection. Extensive analysis of π^0 for Au + Au collisions at $\sqrt{s_{NN}} = 200$ GeV has been performed, as described in [2].

Since direct photons mostly escape from the sources without scattering or absorption, they provide unique information from the interior of the hot and dense matter. Although direct photons are emitted at various stages of collision process, enhancement of photons from a particular stage is possible by setting appropriate energy window. Excess of the photon yield over background was clearly observed, using the virtual photon method, in central Au+Au collisions in the p_T region between 1 and 3 GeV/c, where thermal radiation from QGP phase is expected to have a large share. In order to quantify other possible nuclear effects, deduction of direct photon yield in d+Au collisions has been performed. Recent progress is described in [3].

In an ultra-peripheral collision (UPC) between ultra-relativistic nuclei, very strong Lorentz-contracted electromagnetic pulse enough to produce even massive particles is

generated. The J/ψ production via UPC has been considered to be utilized to determine the PDF (parton distribution function) of gluons at small x region, where gluon-PDF is not well determined and may suffer significant saturation due to gluon recombination, which is a non-linear effect inherent to QCD. Current status at RHIC is described in [4].

3. Progress in the ALICE Experiment

3.1. Physics runs in 2009 and 2010

Majority of the ALICE detector system has been ready for p+p collisions at LHC, and ALICE succeeded in detecting the first p+p collisions at $\sqrt{s} = 900$ GeV on 16:47, Nov. 23, 2009.

The first p+p collisions at $\sqrt{s} = 7$ TeV was realized in the last day of March 2010, and a long physics run is anticipated in the coming months. Heavy ion runs with Pb ions is planned in November 2010. Performance of the ALICE experiment in the first p+p collisions at LHC is described in [5].

3.2. Physics output & group activities

From the 284 events of data, which corresponds to ~ 3.7 authors per event, accumulated in the first p-p runs at $\sqrt{s} = 900$ GeV, the first physics paper was prepared and submitted to European Physics Journal in several days, and was accepted for publication in Dec. 1, 2009 [6].

Charged particle multiplicity is one of the very basic quantities which is measured in the beginning of collisions. Efforts to deduce charged particle multiplicity in $\sqrt{s} = 900$ GeV and 7 TeV p+p collisions using ALICE TPC has been performed [7]

4. R & D efforts

4.1. R & D efforts on Silicon-Tungsten Calorimeter

It is expected that saturation of gluon density is realized in the small x region. The effect would be more apparent in the smaller x . It is a matter of simple kinematics to show that forward corresponds to smaller x region.

Since the particle density is high and two photon separation capability is demanding in the forward rapidity region, a new type of electro-magnetic calorimeter which consists of silicon (Si) and Tungsten (W) layers, is drawing attention as a candidate for measuring photons and neutral mesons.

W is a material with the shortest radiation length, and expected good capability of particle separation will be favorable in the environment of high particle multiplicity. With Si layers with PAD readout, good gamma-hadron separation is expected by making reasonable longitudinal and transverse segmentations. Although π^0 and γ separation is possible up to a certain momentum which is already higher than that possible with conventional calorimeters, further capability could be realized by adding charged particle tracking capability, which may be realized by adding Si strip-type layers or Si pixel-type layers.

The CNS group has started R&D efforts with intension to realize a forward calorimeter system (FOCAL) at ALICE, as an ALICE upgrade in near future. The group has joined the R & D project carried by the PHENIX group, which has been constructing prototypes. Performance evaluation of

the forward calorimeter for PHENIX upgrade is described in [8]. In parallel, simulation study of the W+Si tracking calorimeter for ALICE upgrade has been performed [9, 10].

4.2. R & D efforts on GEM and its Applications

Development and application of GEM (gas electron multiplier) has been a central R & D effort of our group in the last several years. GEM, originally developed at CERN [11], has very simple structure with regularly arrayed holes pierced through a sheet made of polyimide (Kapton) or LCP (liquid crystal polymer) with typical thickness of $50 \sim 100\mu\text{m}$ with both sides coated by copper foils with thickness of $\sim 5\mu\text{m}$. The Cu plates serve as electrodes.

MPGD (micro-pattern gas detector), to which GEM is categorized, has a common weakness of fragility to sparks. An idea proposed to prevent large sparks is to use resistive material as electrodes. It was tried last year to use conductive polymer as electrodes for the Thick GEM, which has macroscopic thickness and holes, and reasonable gain was attained [12]. In this year, GEM with conductive Kapton as electrodes was developed. The conductive Kapton is made by doping carbon power to the Kapton. Performance study is in progress.

As an application of GEM, a TPC using GEM (GEM-TPC) was developed which is a prototype of tracker used to measure recoil nuclei in the scattering experiment of unstable nuclei at RIKEN RIBF facility [13].

5. Summary

In the year 2009, PHENIX had completed Run 9 and has executing Run 10. ALICE at LHC had the first p-p collisions in Nov. 2009, and physics runs for p-p collisions at $\sqrt{s} = 7$ TeV is on going. The major activities of the CNS groups are introduced, which includes data analysis efforts, and R & D efforts related to FOCAL and GEM.

References

- [1] Y. Tsuchimoto *et al.*, CNS Ann. Rep. 2009 (2011).
- [2] Y. Aramaki *et al.*, CNS Ann. Rep. 2009 (2011).
- [3] Y.L. Yamaguchi *et al.*, CNS Ann. Rep. 2009 (2011).
- [4] A. Takahara *et al.*, CNS Ann. Rep. 2009 (2011).
- [5] T. Gunji *et al.*, CNS Ann. Rep. 2009 (2011).
- [6] K. Aamodt, R. Akimoto, T. Gunji, H. Hamagaki, Y. Hori, S. Sano, A. Takahara *et al.* (ALICE Collaboration): Eur. Phys. J. **C65** (2010) 111–125.
- [7] S. Sano *et al.*, CNS Ann. Rep. 2009 (2011).
- [8] T. Tsuji *et al.*, CNS Ann. Rep. 2009 (2011).
- [9] Y. Hori *et al.*, CNS Ann. Rep. 2009 (2011).
- [10] T. Gunji *et al.*, CNS Ann. Rep. 2009 (2011).
- [11] F. Sauli, Nucl. Instrum. Meth. A **386** (1997) 531.
- [12] R. Akimoto *et al.*, CNS Ann. Rep. 2008, (2010), 59p.
- [13] R. Akimoto *et al.*, CNS Ann. Rep. 2009 (2011).

Performance Report of the ALICE for the first $p + p$ collisions at $\sqrt{s} = 0.9$ and 7 TeV

T. Gunji, H. Hamagaki, S. Sano Y. Hori, for the ALICE Collaboration

Center for Nuclear Study, Graduate School of Science, University of Tokyo, Japan

1. Introduction

The Large Hadron Collider (LHC) at CERN is the largest accelerator in the world and the LHC sheds lights on new era for the elementary particle physics and nuclear physics.

ALICE (A Large Ion Collider Experiment) is one of the experiments performed at LHC and is dedicated for the study of strongly interacting matter created in heavy ion collisions at the LHC. The ALICE experiment consists of a larger number of detectors [1]. Central barrel detectors measuring hadrons, electrons and photons at $|\eta| \leq 0.9$ are composed of an Inner Tracking System (ITS) of high-resolution silicon detectors, a cylindrical Time-Projection Chambers (TPC), a Transition Radiation Detectors and a Time-Of-Flight (TOF) detector. A single arm detectors of lead-scintillator ElectroMagnetic Calorimeter (EMCal), a lead-tungsten crystal calorimeter (PHOS), and a ring imaging Cherenkov hodoscope (HMPID) complement the central barrel of ALICE. The forward muon arm consists of a complex of absorbers, a dipole magnet, and tracking and triggering muon chambers. Several smaller detectors (T0, V0, ZDC, FMD, PMD) are also installed at forward rapidity in ALICE for the global event characterization and trigger. At present, the central barrel detectors ITS, TPC and TOF are completely installed. 7 out of 18 TRD super-modules have been installed and EMCal and PHOS are partially installed. Trigger detectors such as ZDC, V0 and T0 are fully installed. A High Level Trigger (HLT) is available to trigger the events on the basis of on-line reconstruction, select physics region of interest within event and reduce the data size without loss of physics information.

CNS has an activity for the commissioning of the TRD, especially taking a leading role for the development of the slow control system, surface testing of the super-module and installation in the experimental area [2, 3].

2. First $p + p$ collisions at LHC-ALICE

On 23rd Nov. in 2009, two counter-rotating proton bunches with the LHC injection energy of 450 GeV were circulated for the first time at the LHC. Although the intensity was low, with only one bunch per beam and no systematic attempt for optimization of the collisions optics, the ALICE measured a number of collisions candidates. Proton-proton collisions with $\sqrt{s} = 900$ GeV had been conducted until Dec. 14th and followed by the 2.36 TeV proton-proton collisions, which lasted on Dec. 16th. During this period, the ALICE measured roughly 0.4 M events, which correspond to $10 \mu\text{b}^{-1}$ as an integrated luminosity. Commissioning of 2010 proton-proton collisions started from January and physics data taking with $\sqrt{s} = 7$ TeV proton-proton collisions started from 30th March. Data tak-

ing is successfully continued and the ALICE has collected 50 M events in 7 TeV proton-proton collisions corresponding to 1 nb^{-1} by the end of April.

3. Detector Performance

In this section, the detector performance of ALICE in 0.9 and 7 TeV proton-proton collisions at LHC is described. Figure 1 shows dE/dx measured by TPC as a function of momentum. dE/dx for electrons, pions, Kaons and protons are clearly separated. The momentum resolution measured with TPC is 7% at 10 GeV/c from 2009 cosmic ray experiments. Figure 2 shows the correlation between transverse momentum and measured β by TOF. Signals from π/K /proton are clearly separated. Upper of Fig. 3 shows the mean pulse height of electrons and pions measured by TRD and right shows the signal spectrum for electrons and pions. The pion rejection factor with the TRD is studied by projecting dE/dx distribution measured with TPC as shown in Fig. 4, where TPC dE/dx signals relative to the electron Bethe-Bloch line with and without electron tagging in the TRD are shown. Pion rejection factor of 90 is achieved at the electron efficiency of 50%.

Figure 5 shows the resolution of transverse impact parameter measured with the ITS as a function of the transverse momentum, which is crucial for the measurement of displaced decay vertex of heavy quarks. The achieved resolution is less than $50 \mu\text{m}$ for $p_T \geq 3$ GeV/c and compatible to that obtained in the simulation.

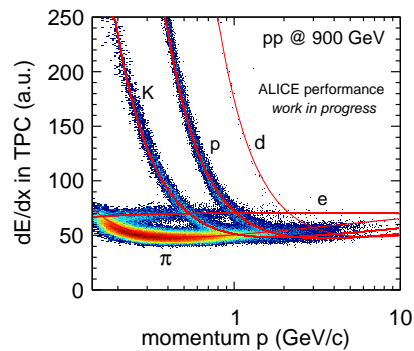


Figure 1. The measured dE/dx as a function of momentum in the TPC in $p + p$ collisions at $\sqrt{s} = 900$ GeV

4. Status and Prospects for Early Physics

The ALICE detectors are successfully commissioned during the first $p + p$ collisions at the LHC. Using the first $p + p$ collisions at \sqrt{s} of 900 GeV, ALICE measured charged particle multiplicities and published the results to

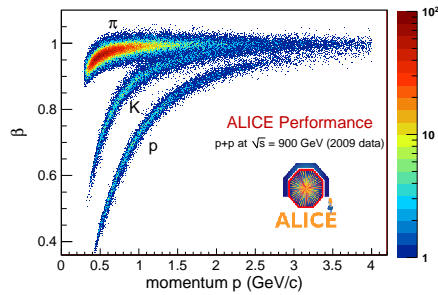


Figure 2. Particle velocity measured by TOF as a function of momentum in $p + p$ collisions at $\sqrt{s} = 900$ GeV

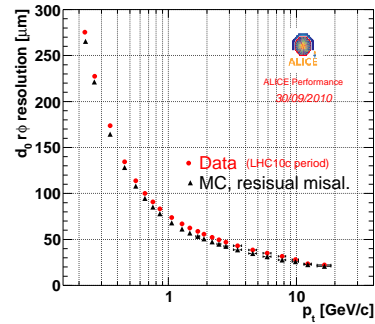


Figure 5. Transverse impact parameter resolution with respect to primary vertex as a function of the transverse momentum measured by ITS.

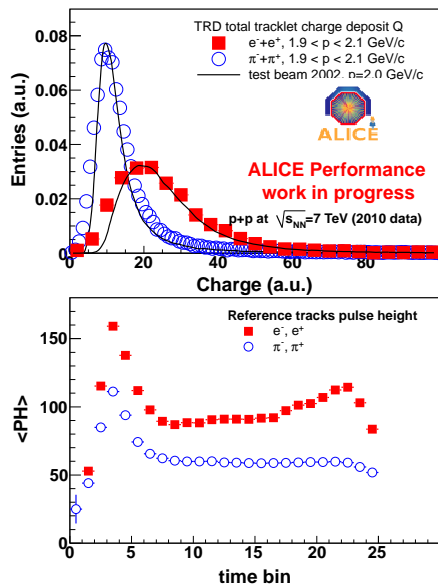


Figure 3. Response of the TRD to π from K_s^0 decays and to electrons from conversion. Upper shows the spectra of energy-deposit in the TRD and bottom shows pulse height as a function of drift time [100 nsec/bin].

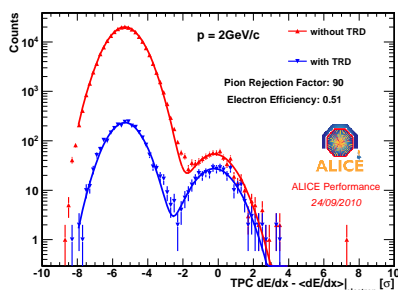


Figure 4. TPC dE/dx signal relative to the electron Bethe Bloch line for 2 GeV/c, with and without electron tagging in the TRD.

Ref. [4], where the results are in good agreement with the results from UA5 collaboration. The charged particle multiplicity at 7 TeV has been also measured and multiplicity dependence of particle production (p_T distribution, strangeness particles, resonances, ratio of particle yield, high p_T and jet production, heavy quark production) are under studying [5, 6]. Around the end of 2010, first Pb+Pb collisions will be performed with the center of energy per nucleon ($\sqrt{s_{NN}}$) of 2.76 TeV, which is 13 times larger than at RHIC. Due to the limited luminosity planed, the ALICE will measure the soft particle production such as multiplicities, integrated elliptic flow, and p_T distribution of charged particles in the first Pb+Pb collisions.

5. Summary and Outlook

The first proton+proton collisions at \sqrt{s} of 0.9, 2.36 and 7 TeV were conducted at the LHC-ALICE and the ALICE detectors are successfully commissioned. Analysis of the detector performances has been conducted and the ALICE demonstrated the excellent capability for the measurement of various particles with a wide kinematic range. The analysis in 7 TeV proton+proton is on going, especially multiplicity dependence of soft particle production and hard probes such as high p_T particles, jets and heavy quarks. The first Pb+Pb collisions with the center of mass energy per nucleon of 2.76 TeV will start around the end of October in 2010. The ALICE is ready for the first Pb+Pb collisions.

References

- [1] ALICE Collaboration, Physics Performance Report Vol. 1 J. Phys. **G 30** (2003) 1517.
- [2] T. Gunji *et al.*, CNS Ann. Rep. 2007 (2008).
- [3] T. Gunji *et al.*, CNS Ann. Rep. 2008 (2010).
- [4] ALICE Collaboration, Eur. Phys. J. **C65**, 111-125, 2010.
- [5] ALICE Collaboration, arXiv:1004.3514, arXiv:1007.0719, arXiv:1007.0516, arXiv:1006.5432.
- [6] S. Sano *et al.* CNS Ann. Rep. 2009 (2011).

Measurement for charged particle multiplicity in $\sqrt{s}=0.9, 2.36, \text{ and } 7 \text{ TeV p+p collisions at LHC-ALICE}$

S. Sano, H. Hamagaki, T. Gunji, for the ALICE collaboration

Center for Nuclear Study, Graduate School of Science, University of Tokyo

1. Introduction

Parton saturation is expected to be realized in high energy collisions at LHC energy. This is the state expected to be seen in smaller Bjorken x of hadrons, where gluon yield (distribution) is saturated due to the balance between $g \rightarrow gg$ and $gg \rightarrow g$ [1, 2]. It is suggested that parton saturation leads to suppression of particle production (about 5% suppression at 7 TeV p+p [3]) and therefore, this can be studied from the measurement of particle multiplicity in p+p and A+A collisions.

On the other hand the multiplicity measurement takes a significant role as preparation for the future physics analysis. In the LHC energy, there is possibility of the “heavy-ion-like” collective effects in p+p collisions [5], which would make further strangeness enhancement. One of the useful probes for the study of QGP-like behavior in p+p collisions is the particle abundance, especially, (multi-)strangeness particle production. Particle ratios including multi-strangeness particles have been measured at RHIC and the yields are found to be well described by the statistical models with fully chemical equilibration of strangeness [4]. Final destination of this study is to evaluate multiplicity dependence of strangeness particle production and its applicability of thermal statistical models in p+p collisions at LHC energy. As the start up of this analysis, charged particle multiplicities in p+p collisions at $\sqrt{s}=0.9, 2.36, \text{ and } 7 \text{ TeV}$ have been measured and the results are described in this report.

2. Multiplicity measurement and analysis

In the ALICE, tracks of charged particles are mainly measured with Inner tracking system (ITS) and Time Projection Chamber (TPC). Multiplicity is defined as the number of tracks of charged primary particles. The results of multiplicity distribution at $\sqrt{s}=0.9, 2.36, \text{ and } 7 \text{ TeV}$ was published [6, 7, 8]. They are analyzed with Silicon Pixel Detector (SPD, inner two layers of ITS, radii 3.9 and 7.6 cm) for tracking and VZERO counters (two scintillators located on either side of the interaction region at $z=3.3$ and -0.9 m and covering $2.8 < \eta < 5.1$ and $-3.7 < \eta < -1.7$) for the event trigger.

The ALICE trigger system is sensitive to two types of events, inelastic (INEL) and non-single-diffractive (NSD). INEL corresponds to non-diffractive (ND), single-diffractive (SD), and double-diffractive (DD), and NSD is subtraction of SD from INEL. For the INEL and NSD analysis, data triggered with OR between the signals from the SPD and VZERO detectors and with a coincidence between the two sides of VZERO detectors are used, respectively. The correction for the number of events used in normalization is obtained from cross sections in $p\bar{p}$ collisions of other

experiments.

SD and DD production cross section were obtained from UA5 [9] at 0.9 TeV and CDF [10, 11] at 1.8 TeV. The data of CDF at 1.8 TeV is used for the 2.36 TeV, because the relative fractions for SD and DD change very slowly with energy. For 7 TeV, there is only the data with INEL for at least one charged particle in $|\eta| < 1$ ($\text{INEL} > 0_{|\eta| < 1}$), because this is the new energy collision.

3. Result

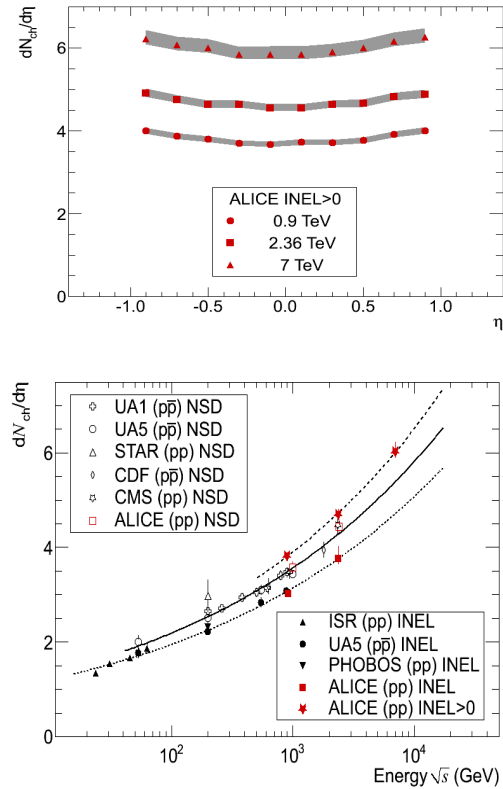


Figure 1. The tendency of \sqrt{s} dependence is well-described by the extrapolation from lower energy results with the form of $a * \ln(\sqrt{s}) + b$, which indicates there is no clear decrease of multiplicity due to the occurrence of gluon saturation.

The results of η distribution and \sqrt{s} dependence of $dN_{ch}/d\eta$ at $\sqrt{s}=0.9, 2.36, \text{ and } 7 \text{ TeV}$ are shown in the upper and lower panel of Fig. 1, respectively. 47000, 35000, 350000 events are analyzed after the event selection ($\text{INEL} > 0_{|\eta| < 1}$ and $|z| < 5.5$ cm for the reconstructed vertex z -position) for 0.9, 2.36, and 7 TeV, respectively. The fitting function used in the \sqrt{s} dependence is a power-law. There is no decrease of $dN/d\eta$ as suggested by parton saturation model [3].

Figure 2 shows the multiplicity distributions at $\sqrt{s}=0.9,$

2.36, and 7 TeV in $\text{INEL} > 0_{|\eta| < 1}$. The fitting function is the negative-binomial distribution (NBD). While NBD describes well 0.9 and 2.36 TeV, it slightly underestimates at low multiplicities ($N_{\text{ch}} < 5$) and slightly overestimates at high multiplicity ($N_{\text{ch}} > 55$).

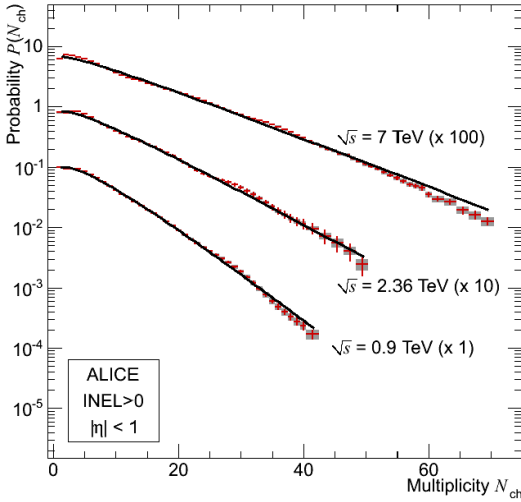


Figure 2. Multiplicity distributions at $\sqrt{s}=0.9, 2.36,$ and 7 TeV in $\text{INEL} > 0_{|\eta| < 1}$. The error bars and the shaded areas represent statistical and systematic uncertainties, respectively. Solid lines are the negative-binomial distribution (NBD).

Multiplicity distribution evaluated by global tracking with ITS and TPC is important in the event characterization for the next physics analysis. Global tracking with TPC can avoid uncorrect high-multiplicity events which have many tracks of combinatorial background. Figure 3 shows

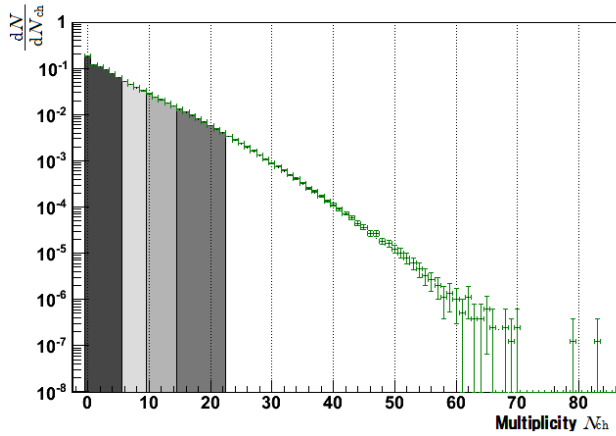


Figure 3. Multiplicity distribution for 7.9M events in $\sqrt{s}=7$ TeV p+p collisions. Each region with different color shows the binning as 0-5 (64%), 6-9 (17%), 10-14 (11%), 15-22 (6%), 23-(2%), which will be used in the analysis for the multiplicity dependence of the multi-strangeness production.

the multiplicity distribution in 7.9M events at $\sqrt{s}=7$ TeV p+p collisions with the global tracking in the region of $|\eta| < 0.8$ and $p_T > 0.15$. The cuts applied are as follows: $N_{\text{clst}} > 70$ for the number of clusters on TPC, $\chi^2/N_{\text{clst}} < 4$, no kink daughter, TPC and ITS refit, hit on SPD,

$\text{DCA}_{xy} < 0.0182 + 0.035/p_T^{1.01}$ cm, $\text{DCA}_z < 2$ cm. Tracking starts from the outer-wall of TPC with applying Kalman filter to the direction to the collision vertex. Applying Kalman filter is iterated as TPC→ITS, ITS→TPC(→TRD→TOF), and (TOF→TRD→)TPC→ITS. The TPC and ITS refit means the success in the last iteration of applying Kalman filter for TPC and ITS, respectively.

DCA is distance to closest approach, where DCA_{xy} or z means the minimum distance between the reconstructed primary vertex and the point on the track for x-y or z direction, respectively. The reason why the shape of distributions around $N_{\text{ch}} \sim 0$ are different between Fig 2 and Fig 3 is that the reconstruction of the primary vertex is not required in Fig 3. In the study of the multiplicity dependence of the multi-strangeness production, binning as 0-5 (64%), 6-9 (17%), 10-14 (11%), 15-22 (6%), 23-(2%) will be used.

4. Summary

The charged-particle multiplicity distributions at $\sqrt{s}=0.9, 2.36,$ and 7 TeV p+p collisions were obtained in the LHC-ALICE. No decrease in $dN/d\eta$ was seen in the \sqrt{s} dependence. Multiplicity distribution at $\sqrt{s}=7$ TeV p+p collisions with the tight quality cut for the track selection was evaluated with ITS and TPC. Multiplicity dependence of the multi-strangeness particle production will be investigated in the future.

References

- [1] L.V. Gribov, E.M. Levin, M.G. Ryskin, Phys. Rep.100 (1983) 1.
- [2] L. McLerran, R. Venugopalan, Phys. Rev. D49 (1994) 2233.
- [3] E. Levin, A.H. Rezaeian, Phys. Rev. D82 (2010) 014022.
- [4] B.I. Abelev et al, STAR Collaboration, Phys. Rev. C 77, 044908 (2008)
- [5] L. Cunqueiro, J. Dias de Deus, and C. Pajares, arXiv:0806.0523 [hep-ph] (2009)
- [6] K. Aamodt et al., for the ALICE Collaboration, Eur. Phys. J. C 65, 111 (2010)
- [7] K. Aamodt et al., for the ALICE Collaboration, Eur. Phys. J. C 68, 89 (2010)
- [8] K. Aamodt et al., for the ALICE Collaboration, Eur. Phys. J. C 68, 345 (2010)
- [9] R.E. Ansorge et al., UA5 Collaboration, Z. Phys. C 33, 175 (1986)
- [10] F. Abe et al., Phys. Rev. D 50, 5535 (1994)
- [11] T. Affolder et al., CDF Collaboration, Phys. Rev. Lett. 87, 141802 (2001)

Measurement of Low-Mass Vector Mesons in RHIC-PHENIX

Y. Tsuchimoto, D. Sharma^a, K. Kijima^b, Y. Nakamiya^b and K. Shigaki^b

Center for Nuclear Study, Graduate School of Science, University of Tokyo

^a Weizmann Institute of Science, Israel

^b Graduate School of Science, Hiroshima University

1. Introduction

QCD is a non-abelian quantum gauge theory which describes the strong interaction. The QCD predicts that a Quark Gluon Plasma (QGP) is created at hot and/or dense nuclear matter. Recently, there are many experimental results suggesting that the QGP has been created in heavy ion collisions at RHIC. Our task in the next stage is to study properties of QGP.

Within the framework of QCD, major part of the mass of ordinary hadrons is considered to be generated through the spontaneous breaking of chiral symmetry [7]. This effective mass depends on the vacuum energy density, and it will vanish in hot and/or dense matter. Some model calculations predict mass modification of low-mass vector mesons (LVM's), ρ , ω and ϕ mesons, in medium [3, 8, 4, 2]. The mass may be affected and become lighter and the width may become wider in a hot and dense medium.

LVM's have both leptonic and hadronic decay channels. The hadronic decay channels have an advantage of larger branching ratios. However, hadrons from deep within the hot matter are scattered by the strong force, thereby losing information of the original decay. On the other hand, as leptons are not subject to the strong interaction, leptonic probes can carry purer information of the vector mesons in medium. The most straight-forward and direct method to detect the mass modification is a line-shape analysis of invariant mass spectra of daughter leptons of the LVM's. KEK E325 collaboration has reported an excess on the lighter side of the LVM peaks in the e^+e^- invariant mass spectra [6]. However, this line-shape analysis needs high counting statistics, which is difficult to achieve in the collider experiments.

Another interesting probe is the decay branch of $\phi \rightarrow K^+K^-$ to $\phi \rightarrow e^+e^-$. Due to the small Q-value of $\phi \rightarrow K^+K^-/\bar{K}^0K^0$, the decay branch of ϕ may be sensitive to the in-medium mass modification. Some models predict that mass of ϕ can be modified to be lighter than the mass of a pair of kaons in a hot and/or dense medium [5]. In the extreme case, $\phi \rightarrow K^+K^-$ decay is suppressed, and the branching ratio would be changed.

2. Experiment

The LVM measurements presented in this contribution were obtained from the data samples accumulated by the PHENIX experiment during $p+p$, $d+Au$ and $Au+Au$ collisions at $\sqrt{s_{NN}} = 200$ GeV/c in 2003-2007 physics runs. LVM's are measured in both electronic and hadronic channels using the PHENIX central spectrometer, which measures fully identified hadrons, electrons and photons [1]. Charged particles were tracked by drift chambers and pad

chambers which provide momentum of the charged particles. Kaons were identified using the time of flight information measured by ToF counters in a limited momentum range. In order to extend momentum range of kaons, the ϕ was reconstructed by all charged particles without kaon identification (no-PID method). Electrons and positrons were identified by Čerenkov emissions in RICH detectors, which has been built and maintained by the CNS group mainly, and by the ratio of momentum to energy measured by electromagnetic calorimeters. $\phi \rightarrow e^+e^-$ are reconstructed by e^+e^- pairs.

3. Results

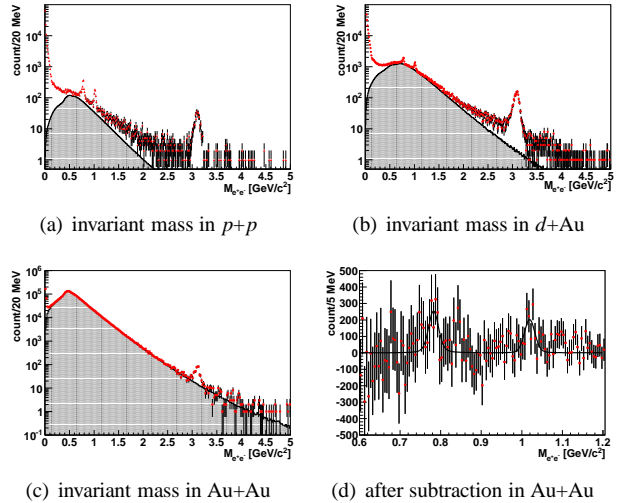


Figure 1. Invariant mass of e^+e^- pairs detected by the PHENIX central arm spectrometers in $p+p$ (a), $d+Au$ (b) and $Au+Au$ (c,d) collisions at $\sqrt{s_{NN}}=200$ GeV. Points are raw invariant mass spectra for each collision, and filled areas are combinatorial background estimated by event mixing for each collision. In each collision, the ϕ and ω resonances are visible. (d) shows background subtracted mass spectra corresponding to difference of points and background of (c), and solid line is a fit by component of ϕ , ω and ρ with fixed mass centroids and widths.

We obtained invariant mass spectra of e^+e^- in each collision as Fig. 1. The solid line in (d) is the best fits of sums of mesons' components as relativistic Breit-Wigner functions convoluted with Gaussian, corresponding to detector resolutions whose sigmas are estimated by full simulations. The ρ yield is assumed to be the same with the yield of ω .

While relatively large modification is predicted on ω , there is inseparable ρ contribution in this mass region of the e^+e^- invariant mass spectra. ϕ is a cleaner probe, de-

spite relatively small modification expected, because there is no overlapping contribution of other resonances. In case of $d+Au$ and $Au+Au$ collisions, while there is a huge background, the peaks of ϕ and ω are seen in e^+e^- at $d+Au$ (b) and $Au+Au$ after precise subtraction of the combinatorial background (d). It is difficult to apply line-shape analysis with the statistics.

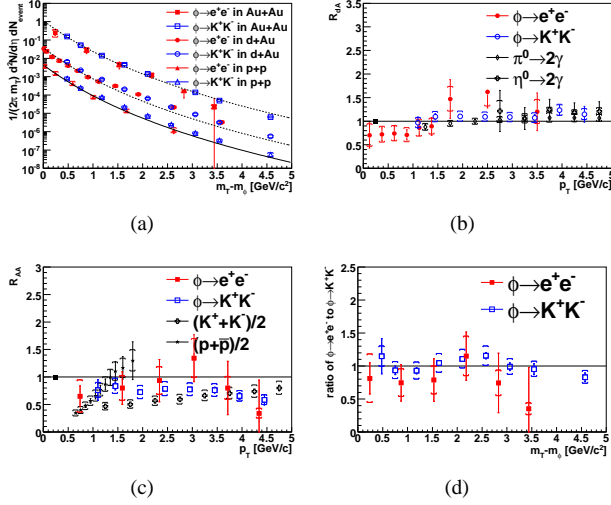


Figure 2. Corrected m_T spectra of $\phi \rightarrow e^+e^-$ in $p+p$, $d+Au$ and $Au+Au$ collisions shown in as closed points and $\phi \rightarrow K^+K^-$ as open points (a), Nucleon modification factor of $d+Au$ collisions (R_{dAu}) (b), Nucleon modification factor of $Au+Au$ collisions (R_{AA}) (c), and ratio of $\phi \rightarrow e^+e^-$ to $\phi \rightarrow K^+K^-$ (d).

The number of ϕ and ω are counted in the mass regions, and corrected for the acceptance and efficiency which are estimated by a full GEANT3 simulation. A special electron trigger called as 'ERT Electron Trigger' is used for $p+p$ and $d+Au$ collisions. Its trigger efficiency is also simulated in the full simulation using efficiency curves obtained by minimum bias data. Figure 2 shows the corrected m_T spectra of $\phi \rightarrow e^+e^-$ (closed) and $\phi \rightarrow K^+K^-$ (open) in $p+p$ and $d+Au$ and $Au+Au$ collisions (a), where the solid lines are global fits for $\phi \rightarrow K^+K^-$ and e^+e^- , and dashed lines show the yield in $p+p$ scaled by the number of binary nucleon-nucleon collisions (N_{coll}) for each collision centrality. The spectra of $\phi \rightarrow e^+e^-$ and $\phi \rightarrow K^+K^-$ are consistent with each other in all collisions.

In case of $d+Au$, the yield is slightly higher than the scaling line. This is a well-known nuclear effect called Cronin effect. In case of $Au+Au$, the yield is slightly suppressed at least in the K^+K^- channel. The ratio of $\phi \rightarrow e^+e^-$ to the fit by Levy function to K^+K^- at $Au+Au$ collisions is shown as Fig. 2(d). As mentioned in the introduction, the branching ratio of $\phi \rightarrow K^+K^-$ to e^+e^- is an important measurement. A change of the ratio may be seen as a difference in these spectra. The yields measured by both channels are consistent within the errors. More counting statistics and careful analysis are needed to discuss a possible difference in the central collisions.

4. Summary and Outlook

In-medium modification of low-mass vector mesons is considered as one of the best probes to study chiral symmetry restoration in hot and/or dense matter. We measured yield of ϕ mesons via electronic and hadronic decay channels in $p+p$, $d+Au$ and $Au+Au$ collisions at $\sqrt{s_{NN}} = 200$ GeV/c in PHENIX. The production is consistent with each other in the both decay channels.

A higher statistics run with an in full detector, which has a capability to reject the π^0 dalitz background, will enable measurements in central $Au+Au$ collisions in this year. The data should help increase the accuracy of the LVM measurement significantly.

References

- [1] K. Adcox *et al.*, *Nucl. Instrum. Meth. A* **499** (2003) 489–507.
- [2] Y. Aoki, Z. Fodor, S. D. Katz, and K. K. Szabo, *Phys. Lett. B* **643** (2006) 46–54.
- [3] G. E. Brown and Mannque Rho, *Phys. Rev. Lett.* **66** (1991) 2720–2723.
- [4] M. Cheng *et al.*, *Phys. Rev. D* **74** (2006) 054507.
- [5] Tetsuo Hatsuda and Su Hounng Lee, *Phys. Rev. C* **46** (1992) 34–38.
- [6] R. Muto *et al.*, *Phys. Rev. Lett.* **98** (2007) 042501.
- [7] Yoichiro Nambu and G. Jona-Lasinio, *Phys. Rev.* **122** (1961) 345–358.
- [8] R. Rapp and J. Wambach, *Adv. Nucl. Phys.* **25** (2000) 1.

Direct virtual photon measurement in $\sqrt{s_{NN}} = 200$ GeV $d+Au$ collisions at RHIC-PHENIX

Y.L. Yamaguchi, H. Hamagaki, Y. Akiba^a, and T. Gunji, for the PHENIX collaboration

Center for Nuclear Study, Graduate School of Science, University of Tokyo
^a RIKEN (The Institute of Physical and Chemical Research)

1. Introduction

Direct photons are one of the most important probes to investigate properties of the matter created by heavy ion collisions. They are emitted from every stage of the collisions and their p_T reflect the temperature of the sources. Especially, direct photons in $1.0 < p_T < 5.0$ GeV/c are of special interest since thermal photons from the Quark Gluon Plasma (QGP) are considered to be the primary contributor [1]. The observation of thermal photons can allow the determination of the initial temperature of the QGP.

The measurement of direct photons for such a low p_T region is notoriously difficult due to large background photons from hadron decays, particularly π^0 . The difficulty on the measurement can be solved by measuring e^+e^- pairs from direct virtual photon decays since any source of real photons can also emit virtual photons which convert to low-mass e^+e^- pairs. The direct virtual photon measurements for $p+p$ and Au+Au collisions have been made in the PHENIX experiment and the direct photon yields in the low p_T region for both collision systems have been successfully determined from the direct virtual photon measurement [2]. Figure 1 shows the direct photon spectra in

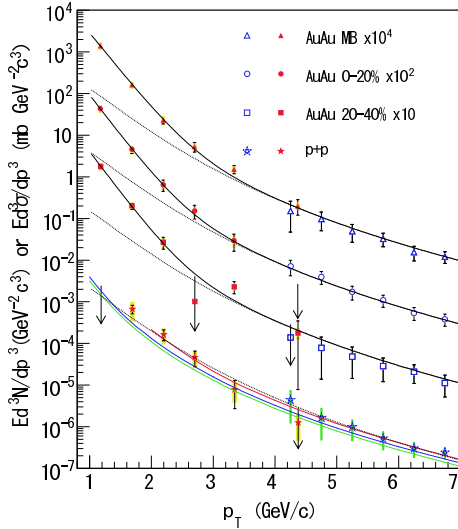


Figure 1. The direct photon spectra in $p+p$ and Au+Au collisions [2].

$p+p$ and Au+Au collisions. A significant excess over the binary-scaled $p+p$ result is clearly seen for Au+Au collisions in $p_T < 3.0$ GeV/c. However, the observed excess cannot be concluded as thermal origin at this moment because nuclear effects such as the Cronin effect, the nuclear shadowing and so on [3] may increase or decrease the low p_T direct photon yield. Efforts for measuring the low p_T direct photons in $d+Au$ collisions are being made in order

to evaluate the contribution of nuclear effects in the low p_T direct photon yield. The current status of the analysis for 200 GeV $d+Au$ collisions is presented in this report.

2. Direct Virtual Photon Measurement

A direct photon production process has an associated process in which γ^* instead of γ is emitted, i.e. $q + g \rightarrow q + \gamma^* \rightarrow q + e^+e^-$. The relation between the photon production and the associated e^+e^- production can be expressed as [4]

$$\frac{d^2n_{ee}}{dm_{ee}} = \frac{2\alpha}{3\pi} \frac{1}{m_{ee}} \sqrt{1 - \frac{4m_e^2}{m_{ee}^2}} \left(1 + \frac{2m_e^2}{m_{ee}^2}\right) S dn_\gamma, \quad (1)$$

where α is the fine structure constant, m_e and m_{ee} are the masses of the electron and the e^+e^- pair, respectively, and S is a process-dependent factor that goes to 1 as $m_{ee} \rightarrow 0$ or $m_{ee} \ll p_T$. The relation between the photons from hadron decays and the e^+e^- pairs from Dalitz decays are also described by Eq. (1). For π^0 and η , S is given as $S = |F(m_{ee}^2)|^2 \left(1 - \frac{m_{ee}^2}{m_h^2}\right)^3$ [5], where $F(m_{ee}^2)$ is the form factor and m_h is the hadron mass. The factor S is obviously zero for $m_{ee} > m_h$. This cutoff can help to separate the direct photon signal from the hadronic background. Since 80% of the hadronic photons are from π^0 decays, the signal to background ratio (S/B) for the direct photon signal improves dramatically for $m_{ee} > m_{\pi^0}$.

3. Analysis

In this analysis, minimum bias events from the data taken in RHIC-Year 8 are used. All combinations of electrons and positrons in a same event are considered. The obtained e^+e^- mass distribution contains several components from different sources, which are listed below.

- Direct virtual photon decays
- Hadron decays
- Photon conversions
- Combinatorial background
- Cross pairs from decays with 2 e^+e^- pairs in a final state (e.g., $\pi^0, \eta \rightarrow 2\gamma(\text{or } \gamma e^+e^-) \rightarrow e^+e^-e^+e^-$)
- Pairs from two independent decays in the same jet or back-to-back jets

The pairs from photon conversions are removed by a cut on the orientation of the pair in the magnetic field, and the combinatorial background is computed with a mixed-event

technique. The like-sign pair distributions consist of the combinatorial background pairs, cross pairs and pairs from two independent decays in the same jet or back-to-back jets. Thus, the contributions of these background pairs are evaluated using like-sign pair distributions and a Monte Carlo simulation. Then, these pairs are subtracted. Finally, the correlated e^+e^- mass distribution, which consists of pairs from known hadron decays and direct virtual photon decay, is obtained.

Since the factor S in Eq. (1) is considered to be almost unity in the region of $p_T > 1.0$ GeV/c and $m_{ee} < 350$ MeV/c², the direct virtual photon component can be extracted from the e^+e^- mass distribution by utilizing the different e^+e^- mass dependence of the factor S . The equation (2) is fitted to the data in order to determine the fraction of the direct virtual photon component in the e^+e^- mass distribution.

$$f(m_{ee}) = (1-r) \cdot f_{cock}(m_{ee}) + r \cdot f_{dir}(m_{ee}), \quad (2)$$

where f_{cock} is the mass distribution from the known hadron decays and f_{dir} is the expected distribution from the direct virtual photon decays, and r is the direct virtual photon fraction. The mass distribution from the known hadron decays is calculated by a Monte Carlo calculation which incorporates the measured yields of the hadrons at the PHENIX. Figure 2 shows the e^+e^- mass distribution in $d+Au$ collisions

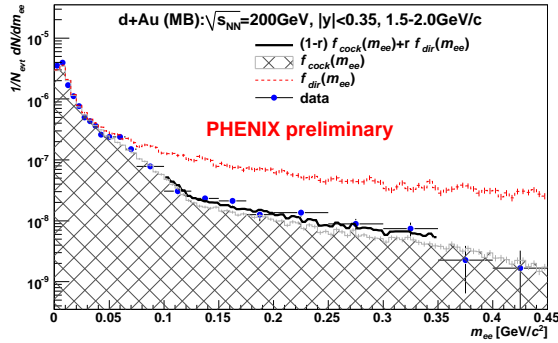


Figure 2. The e^+e^- mass distribution in $d+Au$ collisions for $1.5 < p_T < 2.0$ GeV/c together with the fit result by Eq. (2).

sions for $1.5 < p_T < 2.0$ GeV/c together with the fit result by Eq. (2) shown with a thick solid line.

4. Result

Figure 3 shows the obtained direct virtual photon fractions as a function of p_T in $d+Au$ collisions. The direct virtual photon fractions in $d+Au$ collisions seem to be very close to the ones in $p+p$ collisions shown in the left panel of Fig. 4. This fact implies that the contribution of nuclear effects in the low- p_T direct photon yield is small.

5. Summary and Outlook

The direct virtual photon measurement in $d+Au$ collisions has been going on at the PHENIX experiment in order to evaluate the contribution of nuclear effects in the observed excess yield in $1.0 < p_T < 3.0$ GeV/c for Au+Au collisions. The direct virtual photon fractions in $d+Au$ collisions have been determined successfully from the e^+e^-

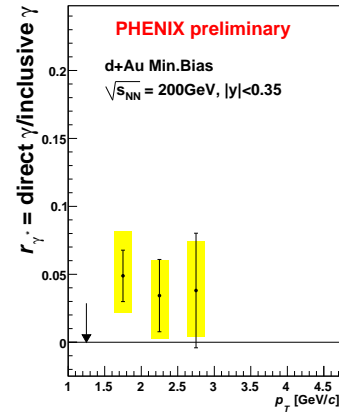


Figure 3. The obtained direct virtual photon fractions as a function of p_T in $d+Au$ collisions.

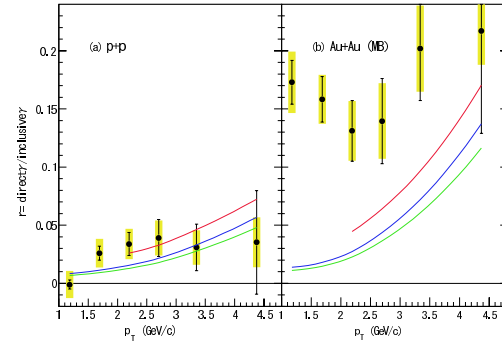


Figure 4. The direct virtual photon fractions as a function of p_T in $p+p$ (left) and Au+Au (right) collisions [2].

mass distribution. The contribution of nuclear effects seems to be small in the low- p_T direct photon yield according to the obtained direct virtual photon fractions in $d+Au$ collisions.

The triggered data samples for $d+Au$ collisions are also available and they can provide much more counting statistics in $p_T > 1.5$ GeV/c than the minimum bias data which is dedicated to determine the lowest p_T data point. The triggered data can extend the p_T reach up to 6 GeV/c and the existing data points in $1.5 < p_T < 3.0$ GeV/c will be improved in their accuracy. After the direct virtual photon fractions are obtained using the triggered data, the cross section of the direct photon in $d+Au$ collisions will be determined.

References

- [1] S. Turbide *et al.*, Phys. Rev. C **69**, 014903 (2004).
- [2] A. Adare *et al.*, for the PHENIX collaboration, Phys. Rev. Lett. **104**, 132301 (2010).
- [3] I. Vitev, B.W. Zhang, Phys. Lett. B **669**, 337 (2008).
- [4] A. Adare *et al.*, for the PHENIX collaboration, Phys. Rev. C **81**, 034911 (2010).
- [5] L.G. Landsberg, Phys. Rep. **128**, 301 (1985).

Azimuthal angular dependence of neutral pion production in $\sqrt{s_{NN}} = 200$ GeV Au+Au collisions at PHENIX

Y. Aramaki, T. Sakaguchi^a, G. David^a, H. Hamagaki, for the PHENIX Collaboration

Center for Nuclear Study, Graduate School of Science, The University of Tokyo

^aPhysics Department, Brookhaven National Laboratory

1. Introduction

It has been observed in central Au+Au collisions at Relativistic Heavy Ion Collider (RHIC) that the yield of neutral pion at high transverse momentum of $p_T > 5$ GeV/c is strongly suppressed compared to the expected yield extrapolated from the $p + p$ collisions assuming the scaling with the number of binary collisions. This suppression is regarded due to the energy loss of hard scattered partons in the hot dense matter created in heavy ion collisions, and it is called as jet quenching.

Path length dependence of energy loss should provide further insight into the energy loss mechanism. Several theoretical models suggest that Landau-Pomeranchuk-Migdal (LPM) effect in QCD plays an important role in radiative energy loss process [1]. These models predict that the magnitude of energy loss is proportional to square of the path length.

Path length can be determined by measuring the azimuthal angle of emitted particles with respect to the reaction plane in non-central collisions. In non-central collisions, the hot dense matter has a spacial anisotropy, and the reaction plane is defined by the two vectors representing beam direction and impact parameter.

For recent theoretical approach to the energy loss mechanism, the properties of the HT [2], AMY [3] and ASW [4] models have been studied [5]. The HT and ASW include only coherent radiative energy loss, while the AMY includes radiative and collisional energy loss. In this paper, they were implemented in a 3-D hydrodynamical simulation with the same initial Wood-Saxon nuclear geometry, space-time evolution of medium and fragmentation functions.

The nuclear modification factor, R_{AA} , is defined to quantify the suppression of yield in heavy-ion collisions. The R_{AA} is given as a function of p_T and the centrality ($cent$) as:

$$R_{AA}(p_T, cent) = \frac{dN/dy_{AA}}{dN/y_{pp}\langle N_{col}(cent) \rangle}, \quad (1)$$

where dN/dy_{AA} and dN/dy_{pp} correspond to the yields in Au+Au and $p + p$ collisions, respectively, and $\langle N_{col}(cent) \rangle$ is an average number of nucleon-nucleon collisions for a given impact parameter which is associated to the centrality. If R_{AA} is equal to one, the particle production in Au+Au collisions can be considered as a superposition of nucleon-nucleon collisions.

All the models have different energy loss schemes, while they can be reproduced the p_T and centrality dependence of R_{AA} . However, the extracted values for the transport coefficient of the HT, AMY and ASW have a large discrepancy as 2.3 GeV²/c, 4.1 GeV²/c and 10 GeV²/c, respectively. This

discrepancy appears on the azimuthal angular dependence of the R_{AA} . Therefore, the measurement of the R_{AA} for each azimuthal angle enables us to verify these models and to have the hint of the energy loss mechanism.

The $R_{AA}(p_T, cent, \Delta\phi)$ for a given azimuthal angle can be expressed by using the azimuthal integrated $R_{AA}^{ave}(p_T, cent)$.

$$R_{AA} = \frac{N(\Delta\phi)}{\int d\phi N(\Delta\phi)} \cdot R_{AA}^{ave}, \quad (2)$$

$$N(\Delta\phi) \propto 1 + 2 \sum_{n=1}^{\infty} (v_n \cos(n\Delta\phi)), \quad (3)$$

where $N(\Delta\phi)$ can be expressed in terms of a Fourier expansion with $\Delta\phi$, and v_n is the magnitude of the harmonics of n -th order. The second harmonics, v_2 , represents the strength of elliptic azimuthal anisotropy.

2. Azimuthal angular dependence of $\pi^0 R_{AA}$

The anisotropy v_2 at low p_T is created by the collective flow, which is an origin of the background in measuring the $R_{AA}(p_T, \Delta\phi)$ for investigating the energy loss. In order to reduce the effect of the collective flow, the measurement of yields at high p_T is needed.

The Muon piston calorimeter (MPC), which is made of lead tungstate (PbWO₄) crystal is used to determine the reaction plane at PHENIX. Even though MPC is similar rapidity coverage to the detector which is used in the previous measurement at PHENIX, the reaction plane determination is expected to be improved due to better energy resolution.

Figure 1 shows the R_{AA} of π^0 as a function of azimuthal angle at high p_T for different three centrality classes. The bars and solid lines represent the statistical and systematic uncertainties for the $R_{AA}(p_T, \Delta\phi)$, respectively. The central data point shows the azimuthal-angle integrated $R_{AA}(p_T)$, and the bar and the band on the point show the statistical error and the systematic uncertainty for the R_{AA} , respectively. As shown in Fig. 1, the angular dependence of the R_{AA} for each centrality class can be clearly seen.

3. Comparison of $\pi^0 R_{AA}(p_T, \Delta\phi)$ and models

The measured $R_{AA}(p_T, \Delta\phi)$ is compared to the predictions of the HT, AMY and ASW. Figure 2 and 3 show the in-plane and out-of-plane R_{AA} as a function of p_T , the each prediction of the HT, AMY and ASW for centrality 20-30 %, respectively. The Closed symbols show the measured $R_{AA}(p_T, \Delta\phi)$, the dash-dotted line is the expectation of the AMY, the dashed and solid lines show the expectation of the HT and ASW, respectively. The central big band on $R_{AA} = 0.5$ shows the p_T -correlated systematic uncertainty for the azimuthal angle integrated R_{AA} . The right small band on $R_{AA} = 0.5$ shows the combined uncertainty of

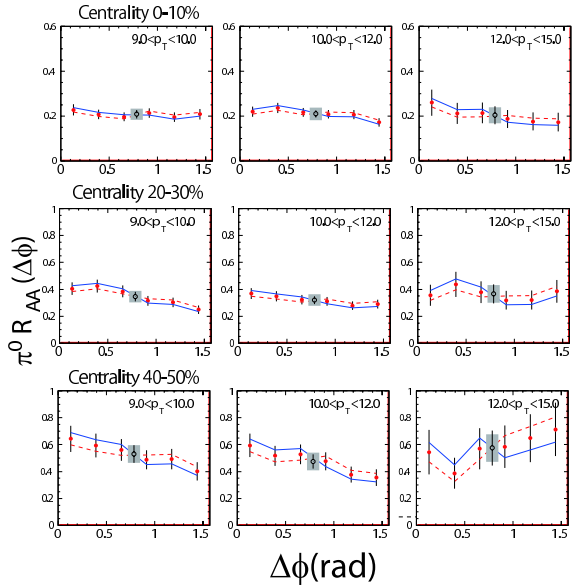


Figure 1. The R_{AA} of π^0 as a function of azimuthal angle for three p_T ranges and three centrality classes.

the number of collisions uncertainty from Glauber calculation and $p + p$ normalization uncertainty. The boxes around the measured points show the p_T -correlated systematic uncertainties from the azimuthal anisotropy v_2 .

As shown in Fig. 2 and 3, the in-plane R_{AA} seems to be independent of p_T , while the out-of-plane R_{AA} seems to be slowly rising as p_T is higher. Obviously, the measured $R_{AA}(p_T, \Delta\phi)$ has strong azimuthal-angular dependence. The AMY and ASW can reproduce the measured out-of-plane R_{AA} , on the other hand, they predict smaller values than the measured in-plane R_{AA} . The HT also can not reproduce both of in-plane and out-of-plane R_{AA} . Even though all the models fail to reproduce the in-plane and out-of-plane R_{AA} , the data favor a large value of the transport coefficient like the ASW rather than the HT and AMY.

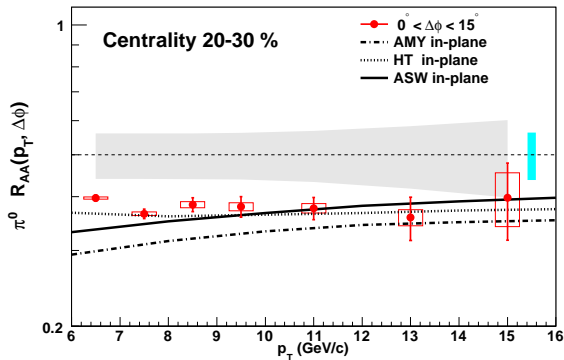


Figure 2. The in-plane R_{AA} of π^0 as a function of p_T , the HT (dashed line), the AMY (dashed and dotted line), and the ASW (solid line) for centrality 20-30 %.

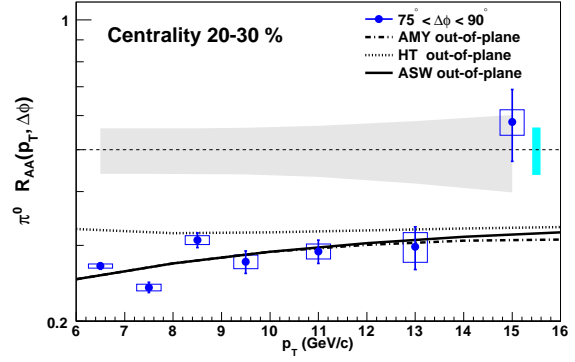


Figure 3. The out-of-plane R_{AA} of π^0 as a function of p_T , the HT (dashed line), the AMY (dash-dotted line), and the ASW (solid line) for centrality 20-30 %.

4. Summary

The study of dependence of R_{AA} on azimuthal angle has been started with the new reaction plane detector. Even though all models can be reproduced the p_T and centrality dependence of the R_{AA} of π^0 , the HT, AMY and ASW models have a large discrepancy for the extracted transport coefficients, Measuring the azimuthal anisotropy v_2 of π^0 with new detector, the R_{AA} of π^0 at $6 < p_T < 16$ GeV/c as a function of azimuthal angle and p_T are measured for each centrality class.

The $R_{AA}(p_T, \Delta\phi)$ for centrality 20-30 % is compared to the HT, AMY and ASW models. Even though the ASW has the strongest azimuthal angular dependence of R_{AA} in these models, it fails to reproduce the in-plane and out-of-plane R_{AA} . The measured R_{AA} requires an initial state of the collisions with the greater spacial anisotropy.

References

- [1] M. Gyulassy *et al.*, Nucl. Phys. B **571**, (2000) 197.
- [2] A. Majumder *et al.*, Phys. Rev. **C76**, 041902 (2007).
- [3] G-Y. Qin *et al.*, Phys. Rev. **C76**, 064907 (2007).
- [4] T. Renk *et al.*, Phys. Rev. **C75**, 031902 (2007).
- [5] S.A. Bass *et al.*, Phys. Rev. **C79**, 024901 (2009).

Measurement of J/ψ and high-mass e^+e^- pairs in Ultra-Peripheral $\sqrt{s_{NN}} = 200$ GeV Au+Au Collisions at RHIC-PHENIX

A. Takahara, H. Hamagaki, T. Gunji, Z. C. Valle^a, Y. Akiba^{b,f}, M. Chiu^c, J. Nystrand^d, S. White^e,
K. Skjerdal^d, E. T. Atomssa^a, for the PHENIX Collaboration

Center for Nuclear Study, Graduate School of Science, University of Tokyo

^aLaboratoire Leprince-Ringuet, Ecole Polytechnique

^bRIKEN BNL Research Center

^cColumbia University

^dDepartment of Physics, Lund University

^eBrookhaven National Laboratory

^fRIKEN Nishina Center for Accelerator-Based Science

1. Introduction

We present the measurements of the photoproduction of $J/\psi \rightarrow e^+e^-$ pairs in ultra-peripheral nucleus-nucleus interactions of Au nuclei at $\sqrt{s_{NN}} = 200$ GeV in RHIC 2007 Run. Ultra-peripheral collision (UPC) refers to a collision in which impact parameter is greater than the sum of the nuclear radii. UPC has attracted considerable interests to study photoproduction at hadron colliders in recent years [1, 2, 3]. UPC can be used for determining gluon density at low Bjorken $x = \frac{Q^2}{2MV}$. Same measurements performed in RHIC 2004 Run have been reported in Ref. [4].

2. Data analysis

The equation to calculate J/ψ production cross-section at mid-rapidity is:

$$\frac{d\sigma_{J/\psi}^{UPC}}{dy} \Big|_{|y|<0.5} = \frac{1}{BR} \cdot \frac{N_{J/\psi}}{(Acc \cdot \epsilon_{reco} \cdot \epsilon_{cuts}) \cdot \epsilon_{trigger} \cdot L_{int}} \cdot \frac{1}{\Delta y} \quad (1)$$

BR and Δy correspond to the branching ratio of $J/\psi \rightarrow e^+e^-$ and rapidity coverage of PHENIX, respectively. Integrated luminosity L_{int} is counted by Beam Beam counter trigger. Acc is PHENIX acceptance for measuring $J/\psi \rightarrow e^+e^-$. ϵ_{reco} is reconstruction efficiency of J/ψ . ϵ_{cuts} is efficiency of analysis cut. $N_{J/\psi}$ is Number of J/ψ . $\epsilon_{trigger}$ is efficiency of UPC trigger. UPC events are tagged by the emission of forward neutrons by the Coulomb excitation of one or both Au* nuclei. The event triggers have 3 following requirements; 1) There should be no coincident signals from the beam-beam counters; 2) a 2x2(PbSc 10.5 x 10.5 cm, PbGl 8 x 8cm) tile EMCal trigger with a energy threshold of 1.0 GeV is needed; 3) A minimum of 30 GeV energy deposition in (one or two) Zero degree calorimeters is required. Further, the offline requirements are $|Z \text{ vertex}| \leq 30$ cm, less than 20 charged tracks and only two electron and positron in the tracks. The measured e^+e^- pairs will contain not only the pairs from J/ψ but also the pairs from two photon fusion process [1]. The former pairs will contribute the exponential shape to the invariant mass spectrum. Efficiency of EMcal trigger, ϵ_{ERT2x2} , has momentum dependence. Fig. 1 shows typical sector's ϵ_{ERT2x2} momentum dependence. UPC events should have 2 electron or positron track. $\epsilon_{effective}$ that means trigger effi-

ciency for pairs should be $1 - (1 - \epsilon_{ERT2x2}^{track1})(1 - \epsilon_{ERT2x2}^{track2})$. It means $\epsilon_{trigger} = \epsilon_{BBCVETO} \epsilon_{ZDC} \epsilon_{effective}$ and we assume $\epsilon_{BBCVETO} = 1, \epsilon_{ZDC} = 1$. Then the UPC trigger efficiency is not constant in mass region 2 - 4 GeV. Then we generated 38M $\gamma\gamma \rightarrow e^+e^-$ events using STARLIGHT model, which corresponds to the coherent production followed by Au Coulomb breakup (Xn).

Only 290k events are accepted in the PHENIX acceptance and events are used to determine the trigger efficiency for the e^+e^- pairs. Fig. 2 shows the effective trigger efficiency as a function of pair mass. By using this effective efficiency, we fitted the mass distribution with $gaus(pairmass) + \epsilon_{effective}(pairmass) \times \exp(pairmass)$. The fitting result is shown in Fig. 3. There

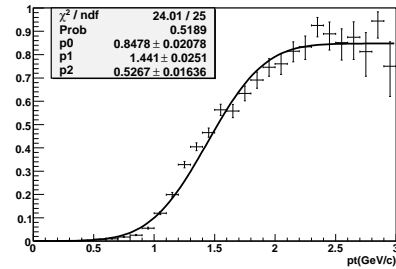


Figure 1. Typical ERT2x2 trigger turn on curve

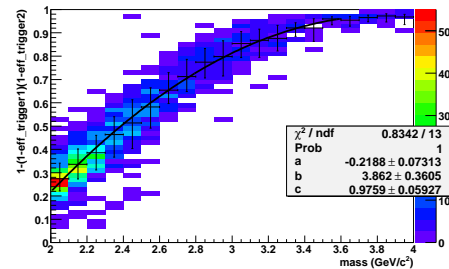


Figure 2. Scatter plot of $1 - (1 - \epsilon_{fortrack1})(1 - \epsilon_{fortrack2})$ and pair mass for continuum e^+e^- simulation..

are 17 e^+e^- pairs between 2.8 GeV and 3.2 GeV. From the fitting we have 18.5 J/ψ (in Run-4 9.9). Then we simulate 455000 $J/\psi \rightarrow e^+e^-$ events to get $(Acc \cdot \epsilon_{reco} \cdot \epsilon_{cuts})$ and $\epsilon_{trigger}$ for J/ψ using STARLIGHT model. Finally we calcu-

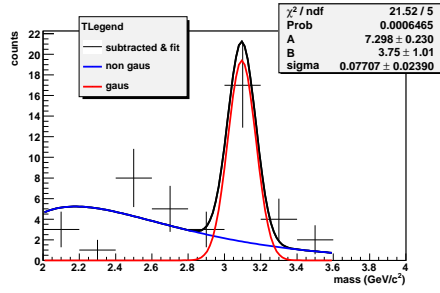


Figure 3. Invariant mass distribution of PHENIX 2007 run UPC J/ ψ cross section.

$$\left. \frac{d\sigma_{J/\psi}^{UPC}}{dy} \right|_{|y|<0.5} = 54.1 \pm 14.6 \text{ (stat)}^{+10.3}_{-9.76} \text{ (sys)} \mu\text{b}$$

Combining result of 2004 and 2007 runs, the UPC J/ψ cross section of $60.8 \pm 13.7 \text{ (stat)}^{+10.5}_{-10.1} \text{ (sys)} \mu\text{b}$ is obtained.

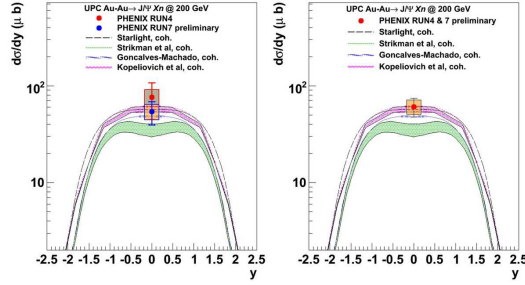


Figure 4. 2007, 2004 and combine cross-section compared to theoretical coherent part [7, 8, 9, 10, 11].

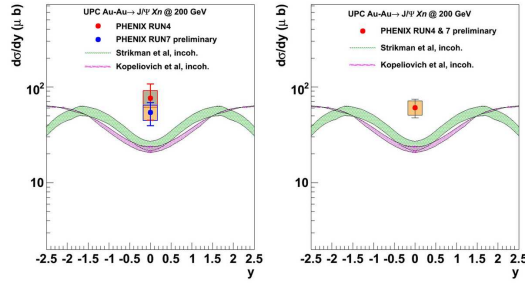


Figure 5. 2007, 2004 and combine cross-section compared to theoretical incoherent part [7, 9].

We calculate the probability to evaluate how the different theoretical coherent and incoherent curves agree with the combined Run-7 + Run-4 data point. Strikman's [7] upper line at central point is 0.471σ . Strikman's lower line at central point is 0.626σ . Kopeliovich's [9] upper line at 0 point is 1.78σ . Kopeliovich's upper line at 0 point is 1.05σ . Then, the Strikman's theoretical curves fit best.

3. Summary and Outlook

We got UPC J/ψ cross section from an analysis of the 2007 run Au-Au $\sqrt{s_{NN}} = 200$ GeV UPC data. J/ψ peak is clearly seen. The total number of J/ψ is 18.75 ± 5.05 . The run7 central UPC cross section is $\left. \frac{d\sigma_{J/\psi}^{UPC}}{dy} \right|_{|y|<0.5} = 54.1 \pm$

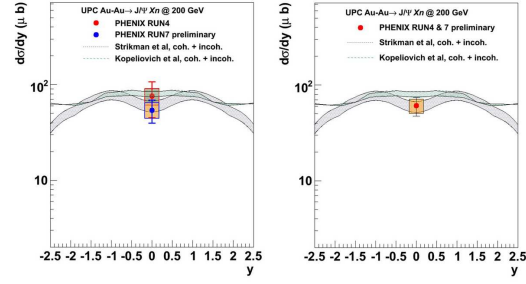


Figure 6. 2007, 2004 and combine cross-section compared to theoretical [7, 9].

$14.6 \text{ (stat)}^{+10.3}_{-9.76} \text{ (sys)} \mu\text{b}$. The combine result is $60.8 \pm 13.7 \text{ (stat)}^{+10.5}_{-10.1} \text{ (sys)} \mu\text{b}$.

Now, we have only point at mid-rapidity in our cross section plot and still we don't have enough statistics to separate incoherent and coherent central UPC. RHIC Au+Au running in 2010 has 1.5 and 1.5 times statistics for mid-rapidity and forward rapidity. These data will be analyzed in the future.

References

- [1] G. Baur, K. Hencken, D. Trautmann, S. Sadovsky, and Y. Kharlov, Phys. Rept. B, **359**, (2002).
- [2] C. A. Bertulani, S. R. Klein, and J. Nystrand, Ann. Rev. Nucl. Part. Sci. B, **271**, (2005).
- [3] A. Baltz *et al.*, Phys. Rept. B, **171** (2008).
- [4] S. Afanasiev for the PHENIX Collaboration, Phys. Lett. B, **321**, (2009).
- [5] K. T. R. Davies and J. R. Nix, Phys. Rev. B, **1977**, (1976).
- [6] J. Nystrand, Nucl. Phys. A **752**, (2005)470c; A.J. Baltz, S.R. Klein, and J. Nystrand, Phys. Rev. Lett. **89**, (2002), 012301; S.R. Klein, J. Nystrand, Phys. Rev. C **60**, (1999), 014903.
- [7] M. Strikman, M. Tverskoy, and M. Zhalov, Phys. Lett. B **626** **72** (2005)
- [8] V. P. Goncalves and M. V. T. Machado, arXiv:0706.2810 (2007).
- [9] Yu. P. Ivanov, B. Z. Kopeliovich, and I. Schmidt, arXiv:0706.1532 (2007).
- [10] L. Frankfurt, V. Guzey, M. Strikman, and M. Zhalov, JHEP **0308** 043 (2003)
- [11] V. P. Goncalves and M. V. T. Machado, Int. J. Mod. Phys. D **16** 533 (2007)

Accelerator and Instrumentation

SHARAQ Project – Progress in FY2009 –

T. Uesaka, S. Michimasa, K. Nakanishi, A. Saito^a, S. Ota, Y. Sasamoto, K. Miki^{a,b}, S. Noji^a, H. Miya, H. Tokieda, S. Kawase, M. Sasano^a, S. Itoh^a, H. Kurei, T. Kawabata, N. Yamazaki, A. Yoshino, S. Shimoura, H. Sakai^a, T. Kubo^b, Y. Yanagisawa^b, K. Itahashi^b, H. Baba^b, G. P. Berg^c, P. Roussel-Chomaz^d, D. Bazin^e, for the SHARAQ collaboration.

Center for Nuclear Study, Graduate School of Science, University of Tokyo

^a *Department of Physics, Graduate School of Science, University of Tokyo*

^b *RIKEN Nishina Center*

^c *Department of Physics, Notre Dame University*

^d *GANIL*

^e *National Superconducting Cyclotron Laboratory, Michigan State University*

In this article, we review the progress in the SHARAQ project in 2009.

In succession to the first commissioning run in March 2009, we conducted the second commissioning run of the SHARAQ spectrometer [1] and the high-resolution beam line [2] in May 2009. The first physics run with the spectrometer was performed in November 2009.

1. The second commissioning run

In the first commissioning run, a momentum resolution $\delta p/p$ of 1/2500 was achieved [3]. Detailed ion-optical studies of the SHARAQ spectrometer and the high-resolution beam line were made in the second commissioning run to improve the momentum resolution and to achieve a simultaneous fulfillment of lateral and angular dispersion matching conditions.

Primary ¹⁴N beams at 250 MeV/nucleon and secondary ¹²B, ⁹Li, ⁶He, and ³H beams produced by projectile fragmentation reactions of the primary beam off a ⁹Be target were used to tune the high-resolution beam-line and the SHARAQ spectrometer.

The beam line was designed to have five focal points in between the starting point F3 and the SHARAQ target. Performance of the whole ion-optical system depends on how precisely the beam line is tuned to have focus at the designed positions. In this respect it is important to tune the beam line to have a focus at the designed position. However, in the first commissioning run, a beam image broadening due to a large dispersion and a beam momentum spread prevented us from diagnosing the focus conditions. As described in Ref. [4], a new procedure was introduced in this year to solve this problem and was established. In addition, response of each quadrupole magnets, examined prior to the experiment by using a computer code COSY INFINITY, were applied to the tuning procedure. As a result of all this, we have succeeded in completing the beam tuning in a shorter period of time than in March.

Tuning of lateral and angular dispersion matching conditions and double focus conditions at the SHARAQ target position was performed by adjusting the excitation currents of the four quadrupole magnets; QH18, STQH19a, b, and c. During the tuning, the correlations between particle trajectories at the dispersive focal plane FH7 and at the fo-

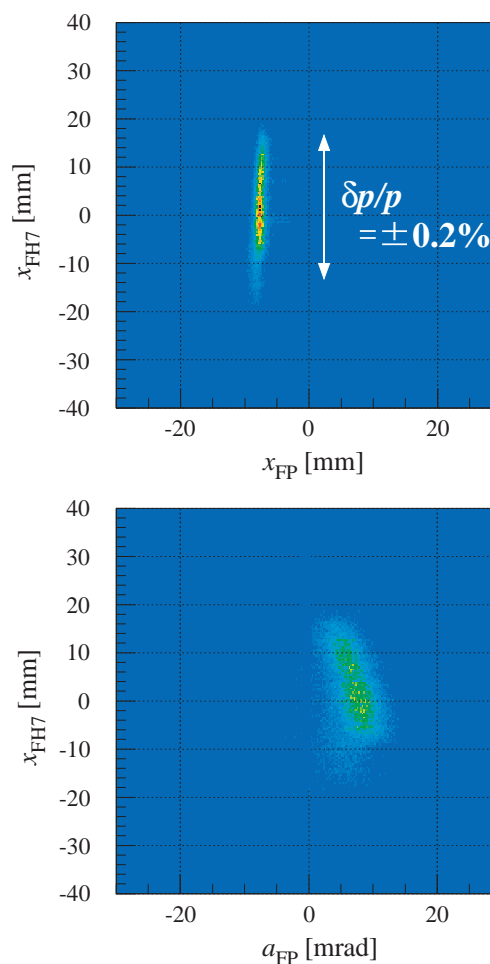


Figure 1. Horizontal beam images at the final focal plane in the achromatic (upper panel) and the dispersion matching transport (lower panel).

cal plane of the SHARAQ spectrometer were used for diagnostics. The beam position at FH7, x_{FH7} , corresponds to the beam momentum, and thus, the correlation between x_{FH7} and the position in the focal plane of the SHARAQ spectrometer, x_{FP} , provides a good measure of $(x|\delta)$ of the whole ion-optical system. The upper panel of Fig. 1 shows the correlation between x_{FH7} and x_{FP} . The upright correlation between x_{FH7} and x_{FP} in the figure clearly shows that the beam position at the focal plane of the SHARAQ spectrometer is independent of the beam momentum, which indicates the achievement of the lateral dispersion matching condition.

Similarly, the correlation between x_{FH7} and the horizontal angle at the focal plane of the SHARAQ spectrometer, a_{FP} , which is shown in the lower panel of Fig. 1 is a good measure of the angular dispersion matching. After tuning, we succeeded in obtaining the lateral and angular dispersion matching conditions simultaneously.

Figure 2 shows the horizontal image of a ^{14}N beam at the focal plane of the SHARAQ spectrometer. Its width corresponds to the momentum resolution of the ion-optical system. The upper panel presents the data obtained in the achromatic transport mode. In this mode, the resolution was limited by the momentum spread of the beam. After the dispersion matching condition was obtained by carrying out beam line tuning, the beam image was narrowed down considerably, as shown in the lower panel of Fig. 2.

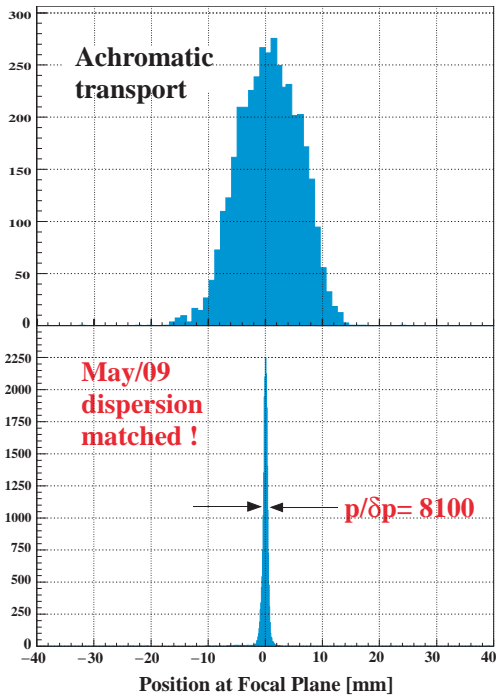


Figure 2. Horizontal beam images at the final focal plane in the achromatic transport mode (upper panel) and in the dispersion matched transport mode (lower panel).

The resulting momentum resolution $\delta p/p$ was found to be approximately $1/8100$. Further studies to improve the momentum resolution are in progress. From the ion-optical studies, it is clearly demonstrated that capability of the

beam tracking in the beam line facilitates beam line tuning that is required to obtain the dispersion matching conditions [5].

In the commissioning run, detector responses to light ions with $Z=1$ and 2 was investigated. Some of the beam line detectors were operated at a gas pressure of 50 kPa and their detection efficiencies for a triton beam were found to be as good as 90% [6]. Cathode read-out drift chamber at the focal plane of the SHARAQ spectrometer operated at 4 kPa also showed a satisfactory detection efficiency of better than 90% for tritons [7]. Thus, we have confirmed that the SHARAQ detector system can be used in experiments with light ion beams.

2. The ($t, ^3\text{He}$) Experiment

The first physics program with the SHARAQ spectrometer was performed in November 2009, where β^+ -type isovector spin monopole resonances in ^{90}Zr and ^{208}Pb were searched for. The ($t, ^3\text{He}$) reaction at 300 MeV/nucleon was used to extract β^+ strengths. An intense triton beam of 10^7 s^{-1} was produced by projectile fragmentation of a primary 320-MeV/nucleon ^4He beam, and the produced ^3He ions were momentum-analyzed by the SHARAQ spectrometer.

The details of the experiment are described in Ref. [8].

Acknowledgment

The authors thank Director T. Otsuka and all the members of CNS for continuous support for the SHARAQ project. They are also indebted to the RIKEN and CNS staffs for operation of accelerators during the runs.

References

- [1] T. Uesaka *et al.*, Nucl. Instrum. Methods B **266**, 4218 (2008).
- [2] T. Kawabata *et al.*, Nucl. Instrum. Methods B **266**, 4201 (2008).
- [3] T. Uesaka *et al.*, CNS Ann. Rep. 2008, 43 (2009).
- [4] Y. Sasamoto *et al.*, CNS Ann. Rep. 2009 (2011).
- [5] T. Uesaka *et al.*, AIP Conf. Proc. **1235**, 308 (2010).
- [6] H. Miya *et al.*, CNS Ann. Rep. 2009 (2011).
- [7] S. Michimasa *et al.*, CNS Ann. Rep. 2009 (2011).
- [8] K. Miki *et al.*, CNS Ann. Rep. 2009 (2011).

Focal-Plane Detector System of SHARAQ Spectrometer

S. Michimasa, H. Tokieda, S. Noji^a, S. Ota, S. Shimoura, T. Uesaka, H. Sakai^a,
P. Roussel-Chomaz^b, J-F. Libin^b, P. Gangnant^b, and C. Spitaels^b

Center for Nuclear Study, Graduate School of Science, University of Tokyo

^aDepartment of Physics, University of Tokyo

^bGANIL, France

The SHARAQ spectrometer [1] and the high-resolution beam line [2] have been constructed in the RI Beam Factory (RIBF) at RIKEN. In March and May, 2009, we performed the beam study to examine dispersion-matching ion optics and to evaluate performances of detectors installed in the beam line and the spectrometer. In November, the first experiment has been done to measure the ($t, {}^3\text{He}$) reaction induced by triton beam at 300 MeV/u. Through the beam studies and experiment, valuable information has been obtained to evaluate the basic performances of the high-resolution spectrometer system. This report describes basic performances of detector system installed at the dispersive focal plane of SHARAQ.

Figure 1 shows the detector setup at the final focal plane of the SHARAQ spectrometer used in the experiment. Two tracking detectors and three plastic scintillators were installed. The focal plane is located 3.04-m downstream from

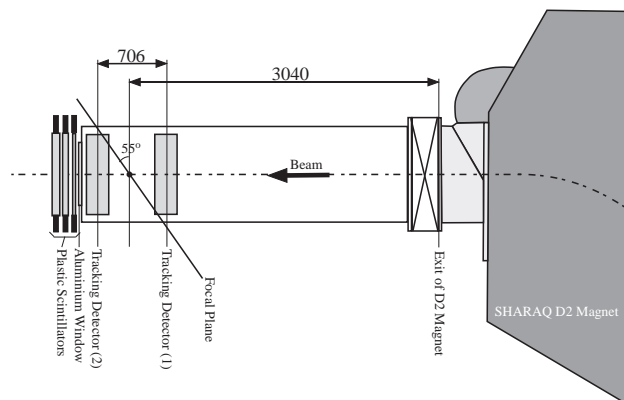


Figure 1. Detector setup for the dispersive focal plane of SHARAQ. Two tracking detectors and two plastic scintillators were installed for the experiment.

the exit of the SHARAQ D2 magnet and inclined at 35 degrees relative to the central orbit. Beam passed through the tracking detectors installed in vacuum, and went out to the air through a 10 mm-thick aluminum window. The plastic scintillators were placed downstream of the aluminum window.

The plastic scintillators were used to measure the timings passing through the focal plane, and to measure energy deposits in them. The three-layer configuration of scintillators is efficient for rejecting cosmic-ray events. Each scintillator is read out by two photomultiplier tubes attached on both sides. The effective area of the plastic scintillator is 650 (H) \times 400 (V) mm². Their thicknesses are 5 mm, 10 mm and 20 mm, respectively. Charge and timing data of the scintillators were obtained by utilizing the charge-to-

time conversion (QTC) technique and multi-hit TDC modules [3].

Tracks of beam particles were measured by the tracking detectors, which are cathode-readout drift chambers (CRDCs) [4]. The CRDCs have manufactured in the fiscal year of 2008 by collaboration with an experimental group of GANIL. Detailed structure of the CRDC is described in Ref. [5]. The CRDCs were operated with isobutane gas at 15 or 30 torr in this study and the experiment. The CRDC has 2 signals from the anode wires and 2 multiplexed signals from the cathode pads. The anode signals were utilized to deduce drift time and charge amount of secondary electrons in the CRDC. Preamplifiers for anode signals were charge sensitive type and were set to be gain of 0.9 V/pC and time constant of 20 μs . Since the anode signal is generated when avalanche occurs around anode wires, the drift time are determined by difference between an anode timing signal and a timing signal of the plastic scintillator. For a calibration of drift velocities of secondary electrons in CRDCs, a plastic scintillator with horizontal slit apertures was installed on the focal plane. Slits were located at every 10 mm and their width was 0.2 mm. By using the plastic scintillator, the drift velocities were estimated to be 5.9 cm/ μs with 83.3-V/cm drift field at 15 torr and 5.3 cm/ μs with 140-V/cm drift field at 30 torr, respectively. These values are consistent with those evaluated by using the GARFIELD code [6].

The horizontal hit position is determined by a charge distribution induced on the cathode pads. The charge signals from the cathode pads were read out by GASSIPLEX chips [7]. With its capability of high multiplexing, the charge signals from 256 cathode pads can be transmitted through a single signal line and read out with a CAEN sequencer with a CRAM module [8]. In this study and experiment, the track-and-hold signals for GASSIPLEX chips were generated by the timing of anode signal of the CRDC under the condition that plastic scintillators and the anode were coincident.

Figure 2 shows detection efficiencies of 250-MeV/u ${}^{14}\text{N}$ particles with 15- and 30-torr operations as a function of high voltage supplied to the anode wires. Compared with the 30-torr operation, the gas amplification at 15 torr was roughly 5 times smaller. However, in the tracking of heavier elements, the 15-torr operation of CRDC is considered to be sufficiently sensitive.

Detection efficiencies for light particles were shown in Fig. 3. The three panels show the data on ${}^9\text{Li}$, ${}^6\text{He}$ and triton. In each panel, a solid (dashed) line indicates detection efficiencies by anode (cathode) as a function of high

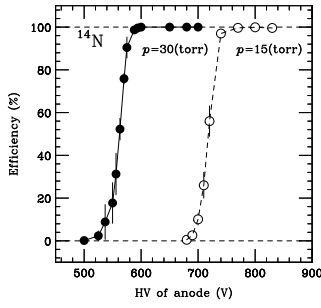


Figure 2. Detection efficiencies of the anode with the 15-torr and 30-torr operations for 250-MeV/u ^{14}N particles. The horizontal axis shows high voltage supplied to the anode wires.

voltages (HV) supplied to the anode wires. The detection efficiency is estimated by coincident ratio with two layers of anodes (cathode) outputs from one CRDC and plastic scintillators installed downstream. A difference of detec-

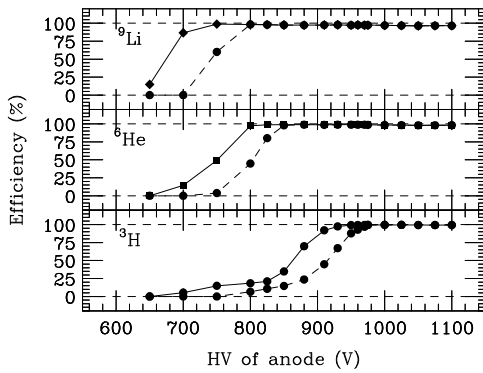


Figure 3. Detection efficiencies of the anode (solid lines) and the cathode (dashed lines) with the 30-torr operations for t , ^6He and ^9Li particles at around 200 MeV/u. The horizontal axis shows high voltage supplied to the anode wires.

tion efficiencies between anode and cathode is caused by small mismatching of their preamplifier gains. The CRDCs of SHARAQ achieved 100-% detection efficiency by low-pressure operation for light ions such as tritons. In the next step of the optimization, we are analyzing HV dependence of anode in horizontal position resolution.

The potential wires located between anode wires to form strong field around anode wires are equipped only in the upstream tracking chamber (CRDC1), and downstream one (CRDC2) has no potential wires. The difference of configurations causes a difference of avalanche gains as described in the last report [5]. Figure 4 (a) shows pulse height distributions of anode signals. The black histogram was obtained by CRDC1 at 950 V and the red one was done by CRDC2 at 970V. In spite of the difference of supplied voltages, the pulse height distributions were almost same. Therefore, potential wires were valid to achieve an avalanche gain by lower anode HV, but did not improve the energy resolution of CRDCs as the function of avalanche gain. Figure 4 (b) illustrates the pulse-height spectrum decomposed by passing particles, where each particle is identified by the plastic scintillator installed downstream. The energy resolution of CRDCs with 30-torr operation was estimated to be 50%

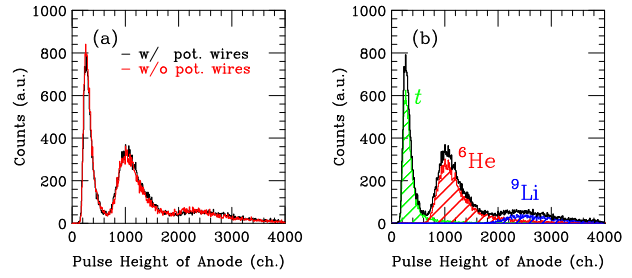


Figure 4. (a) Pulse height distributions of anode signals. The black (red) histogram was obtained by the upstream (downstream) tracking detector with 950-V (970-V) anode HV. (b) Anode pulse-height spectrum decomposed by passing particles, t , ^6He and ^9Li .

(FWHM). This resolution is capable for particle identifications of light particles, such as $Z = 1-3$, but identification of the beryllium and heavier is difficult.

Discussions about achieved position resolution of the tracking detectors are described in the report by Tokieda *et al* [9].

In the summary, we performed the beam study using light radioactive isotopes at 200A–250A MeV and examined the detector system installed in the final focal-plane of the SHARAQ spectrometer. All the detectors operated successfully even for light particles and we obtained basic data of their performance in order to optimize the detectors' parameters and to improve their data analysis algorithm. In November 2009, we have performed the first experiment using a ($t, ^3\text{He}$) reaction at 300 MeV/u. The details on the experiment is described in Ref. [10].

References

- [1] T. Uesaka *et al.*, Nucl. Instrum. Meth. B **266** (2008) 4218.
- [2] T. Kawabata *et al.*, Nucl. Instrum. Meth. B **266** (2008) 4201.
- [3] S. Ota *et al.*, CNS-REP-83, (2010) 57.
- [4] M.H. Tanaka *et al.*, Nucl. Instrum. Meth. A **362** (1995) 521.
- [5] S. Michimasa *et al.*, CNS-REP-80, (2009) 55; CNS-REP-83, (2010) 55.
- [6] R. Veenhof, GARFIELD, CERN Program Library W5050.
- [7] The GASSIPLEX is a re-designed chip of the AM-PLEX by J.C. -Santiard of CERN. The AM-PLEX is described in E. Beuville *et al.*, Nucl. Instrum. Meth. A **288** (1990) 157.
- [8] V551 C.A.E.N sequencer User Guide, V550 C.A.E.N CRAM User Guide.
- [9] H. Tokieda *et al.*, CNS Ann. Rep. 2009 (2011).
- [10] K. Miki *et al.*, CNS Ann. Rep. 2009 (2011).

Focus tuning method of the high-resolution beam line for the SHARAQ spectrometer

Y. Sasamoto, T. Uesaka, S. Shimoura, H. Sakai^a, T. Kubo^a, Y. Yanagisawa^a, H. Takeda^a, S. Michimasa, A. Saito, S. Ota, S. Noji^b, K. Miki^b, H. Tokieda, H. Miya, S. Kawase, T. Kawabata^c, G.P.A. Berg^d, and SHARAQ collaboration

Center for Nuclear Study, Graduate School of Science, University of Tokyo

^aRIKEN (The institute of Physical and Chemical Research)

^bDepartment of Physics, University of Tokyo

^cDepartment of Physics, Kyoto University

^dDepartment of Physics and Joint Institute for Nuclear Astrophysics, University of Notre Dame

New missing mass spectroscopy with an RI beams is planned at RIBF with the SHARAQ spectrometer [1]. The SHARAQ spectrometer is designed to achieve a resolving power of $p/\delta p = 1.5 \times 10^4$ and a high angular resolution of $\delta\theta \sim 1$ mrad for particles with a maximum magnetic rigidity of $B\rho = 6.8$ Tm. To avoid loss of energy resolution due to the momentum spread of RI beams, the dispersion matching (DM) technique is applied in high resolution measurements [2].

A high resolution beam line has been constructed [3] based on the ion optical design described in Ref. 2. Figure 1 shows the layout of the high resolution beam line. An RI beam emitted from the production target at F0 is achromatically focused at F3. F3 is an ion-optical starting point of the high resolution beam line. The beam line after F3 consists of 30 superconducting quadrupole magnets, 3 normal-conducting quadrupole magnets, and 5 dipoles. Although the initial settings of magnets were deduced from the ion optical calculation based on the precise magnetic field measurement [4], a fine tuning is still needed in actual experiment to achieve the required resolution. In this report, the tuning method which is applied in the commissioning of the high-resolution beam line for the SHARAQ spectrometer [5] is described.

The fine tuning requires measurements of the transfer matrix R , which connects the initial and final coordinate vectors X and X' as $X' = RX$. The elements of R are usually obtained from the correlation between quantities of the two focal planes. For example, to tune the focus condition, namely $(x|a)_{if} = 0$ where each digit in the subscript means the corresponding focal plane, we use the correlation between the position x_f at the final plane and the angle a_i at the initial plane. The slope of the correlation corresponds to the magnitude of $(x|a)_{if}$. Actually, for the beam tuning between F3 and F4 of the high-resolution beam line, the correlation of the positions at F4 with the angles at F3 can be used. In this report, we call this method to use the correlation between x_f and a_i directly as the *standard focus tuning method*.

Use of the $x - a$ correlation alone is not always effective in RI beam experiments. Figure 2 shows the correlation between the angle at F3 and the position at F6 with the primary ^{14}N beam at the commissioning. The position and angle are determined experimentally by using the multiwire drift

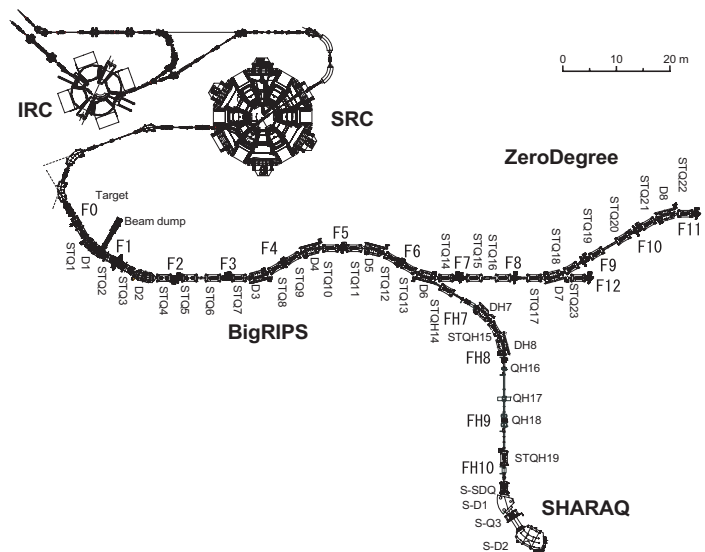


Figure 1. Layout of the high resolution beam line. It branches from BigRIPS after F6. F3 is an ion-optical starting point of the high resolution beam line.

chambers [6]. The magnetic field settings corresponding to the left and right panels of the figure are different (about 5%). And then, the slopes in the panels should be different. However, the difference is not obvious. The difficulty is caused by the spread of the image at the focal plane due to the large dispersion and beam energy spread.

The value of dispersion at the focal planes in the DM mode are summarized in Table 1. The standard tuning method could be applied between F3 and F4 as described above because the spread of the image caused by the dispersion is not so larger than other points. When the primary beam with the momentum spread of $\Delta p \sim \pm 0.1\%$ is used, the horizontal beam image, for example, at F6 spreads over ± 8 mm due to the dispersion. The beam spread smears information about $(x|a)$. Even if momentum slits are used, the resulting momentum spread is of almost the same order of the primary beam.

We propose a simple method which do not depend on the beam momentum. In this report, we call this the momentum independent tuning method. This method is efficient

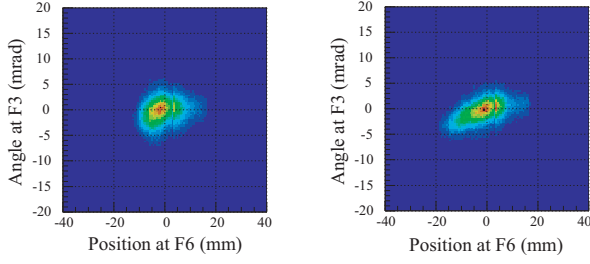


Figure 2. The correlation of the angles at F3 and the positions at F6 with the primary ^{14}N beam under the different field settings. The slope corresponds to the magnitude of $(x|a)_{36}$.

Focal plane	F4	F6	FH7	FH9	FH10
Design value	-19	76.7	-73.7	229	150
(mm/%)					

Table 1. Design dispersion $(x|\delta)$ for the DM mode.

for the tuning in the focal planes which have the large dispersion. Let us consider the focus tuning between FH7 and F4 to achieve $(x|a)_{74} = 0$: the beam momentum δ could be assumed to be $x_7/(x|\delta)_{37}$ using the position at the largely dispersive focal plane of FH7. Then, phase space variables are related in the first order optics as,

$$x_4 - \left((x|x)_{74} - \frac{(x|\delta)_{74}}{(x|\delta)_{37}} \right) x_7 = (x|a)_{74} a_7. \quad (1)$$

It is found that the left-side term in Eq.(1) is a quantity independent of the beam momentum by elimination of the effect due to the beam energy spread at FH7 using the data for F4 and FH7.

In the following, we will consider the simple case, for example, between F6 and FH7 since there is no dispersive element; i.e. dipole magnet. The quantity independent of the beam momentum can be described as,

$$x_6 - (x|x)_{76} x_7 = (x|a)_{76} a_7. \quad (2)$$

In Eq.(2), the particles are assumed to be emitted from FH7 to F6. To obtain the quantity described above, the magnification $(x|x)_{76}$ is needed to be deduced experimentally. Figures 3 and 4 show the correlation of positions and angles at F6 and FH7. Figure 3 is the correlation of x_6 with x_7 whose slope corresponds to the magnification. Figure 4 shows the correlation between the quantities in the left side of Eq.(2) and the angle at FH7, a_7 , under the different magnetic field settings where we use $(x|x)_{76}$ determined from Fig. 3 experimentally. In Fig. 4, it is clearly seen that the slope indicating the magnitude of $(x|a)_{76}$ is changed. If the standard tuning method is applied using the correlation of x_6 with a_7 , the spread of image caused by the x_7 due to the large dispersion smear information for $(x|a)_{76}$. The fine tuning is, thus, possible by introducing the momentum independent focus tuning.

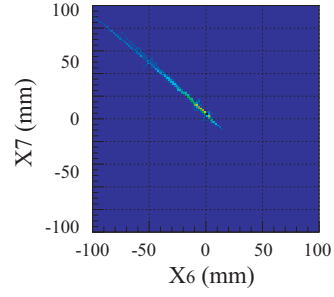


Figure 3. The correlation of positions at F6 and FH7, which are indicated as x_6 and x_7 , respectively. The slope corresponds to the magnification between F6 and FH7, namely $(x|x)_{67}$. $(x|x)_{76}$ is obtained as $\sim 1/(x|x)_{67}$ under the condition of $(x|a)_{67} \sim 0$.

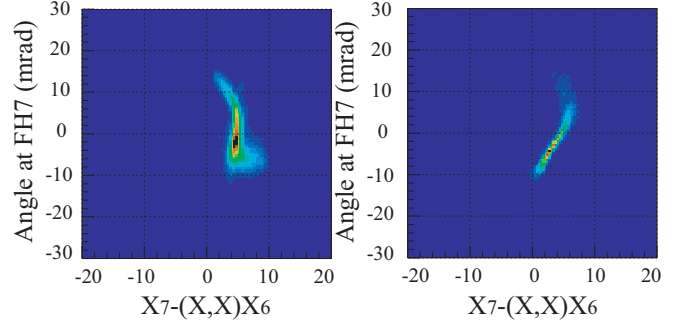


Figure 4. The correlation of the quantities in the left side in Eq.(2) and angle at FH7, a_7 , under the different magnetic field settings. It is clearly seen that the slope which corresponds to the magnitude of $(x|a)_{67}$ is changed.

This is the expeditious tuning method because it doesn't require the complicated procedure. This method enables us to quickly optimize the magnetic settings of the high-resolution beam line for the SHARAQ spectrometer. The quick beam tuning is important for the beam line with many focal planes.

References

- [1] T. Uesaka *et al.*, Nucl. Instrum. Meth. B **266**, 4218 (2008).
- [2] T. Kawabata *et al.*, Nucl. Instrum. Meth. B **266**, 4201 (2008).
- [3] Y. Yanagisawa *et al.*, Bull. Amer. Phys. Soc. **54**, 48 (2009).
- [4] H. Takeda *et al.*, Private communication.
- [5] T. Uesaka *et al.*, AIP Conf. Proc. **1224**, 573 (2010).
- [6] A. Saito *et al.*, RIKEN Accel. Prog. Rep. **43**, (2010).

Performance of Focal-Plane Tracking Detector CRDC in SHARAQ

H. Tokieda, S. Michimasa, S. Noji^a, S. Ota, S. Shimoura, T. Uesaka, H. Sakai^a,
P. Roussel-Chomaz^b, J-F. Libin^b, P. Gangnant^b and C. Spitaels^b

Center for Nuclear Study, Graduate School of Science, University of Tokyo

^aDepartment of Physics, University of Tokyo

^bGANIL, France

1. Introduction

High-resolution magnetic spectrometer [1] has been constructed at the RI Beam Factory (RIBF) at RIKEN. For tracking of charged particles at the dispersive focal plane of SHARAQ, we have developed 2-dimensional position-sensitive Cathode Readout Drift Chambers (CRDCs). Figure. 1 shows the schematic view of the CRDC. Detailed detector setup for the dispersive focal plane of SHARAQ are described in Ref. [2].

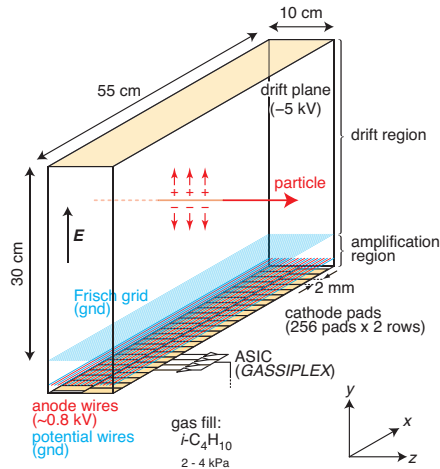


Figure 1. The schematic view of SHARAQ CRDC. There are 512 pads of cathode pads from two rows on the bottom. The cathode signals are readout by using GASSIPLEX chips.

The CRDC has a large effective area of 550 (H) x 300 (V) mm². Secondary electrons produced by energy loss of charged particles drift vertically along the electric field made by the drift plane and field cage, and finally cause avalanche around the anode wires. In the sensor part of the CRDC, 10 anode wires are placed between 11 potential wires. The potential wires and Frisch grid wires are arranged to make axially-symmetric electric fields in the vicinity of anode wires and to minimize position dependence in avalanche gains. The CRDC has 2 rows of the cathode pads perpendicular to the beam axis. Each row consists of 256 pads, 2.2-mm pitch. The cathode signals are read out by using GASSIPLEX chips [3]. The vertical and horizontal positions of charged particles are determined by measuring the drift time of electrons in the CRDC and by the center of the distribution of induced charges on the cathode pads, respectively.

We evaluated the performance of the CRDCs (CRDC1, 2)

in November 2009 [4]. In this article, the analysis algorithm of the position resolution and the results are reported.

2. Experiment

Table. 1 summarizes the experimental conditions in the (*t*, ³He) experiment. Figure. 2 shows the detection efficiency curve as a function of the applied anode HV for ⁶He and ³He at i-C₄H₁₀ gas pressure of 4 kPa. It was found out that efficiency has reached a plateau with anode HV at 940 V for ³He with the anode HV of 980 V (CRDC1) and 1000 V (CRDC2).

Table 1. The experimental conditions in the (*t*, ³He) experiment of SHARAQ.

Primary Beam	⁴ He, 300 MeV/u
Secondary Beam	<i>t</i> , ³ He, ~300 MeV/u
Operation Gas	i-C ₄ H ₁₀
Gas Pressure	4 kPa
Anode HV	940 – 1000 V
Drift HV	-4.2 kV

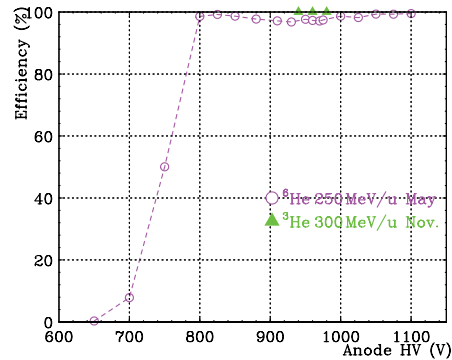


Figure 2. The detection efficiency curve as a function of the applied anode HV for ⁶He and ³He at 4 kPa.

3. Analysis and Results

3.1. Horizontal (*x*) and Vertical (*y*) Position

The horizontal position was determined from the distribution of induced charges on the cathode pads. The information of cathode signal which are readout by using GASSIPLEX chips includes gain variations and pedestals for each channel, so that they calibrated. Typical gain varia-

tions were about 5% for the typical cathode charge. Cluster search was done after the calibration. The cluster was the upper than noise levels. The fitting function is the SE-Cant Hyperbolic Squared (SECHS) function. The details of SECH function are described in Ref. [2].

The vertical position was deduced from the drift time of electrons. The slit-plastic scintillator to calibrate the drift time was located on the focal plane. The details are described in Ref. [2].

3.2. Position Resolution

The position resolution was deduced from the standard deviation of the residual distribution. See an example of how to derive the x residual distribution in Fig. 3. The example is how to derive the x residual distribution of CRDC1-2, the second-upstream row. Firstly, the positions of all rows are determined. Secondly, the incident particle-ray is tracked by using the rows except CRDC1-2. Finally, the residual distribution is derived by subtracted the position of CRDC1-2 from the incident particle-ray. The relation between the standard deviation of the residual distribution Δx_{res}^i ($i=1, 2$; $x^1 = x, x^2 = y$) and the position resolution of each row δx^i is the following:

$$\delta x^i \simeq \Delta x_{\text{res}}^i / \sqrt{2}.$$

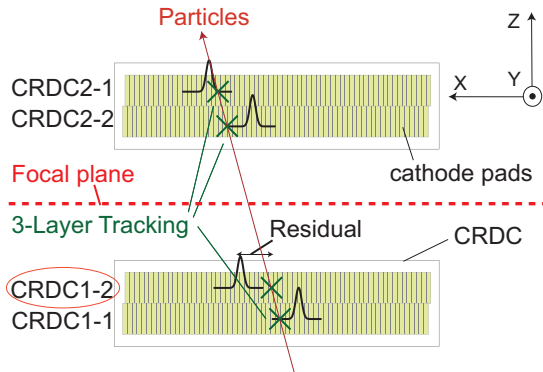


Figure 3. An example of how to derive the x residual distribution of CRDC1-2.

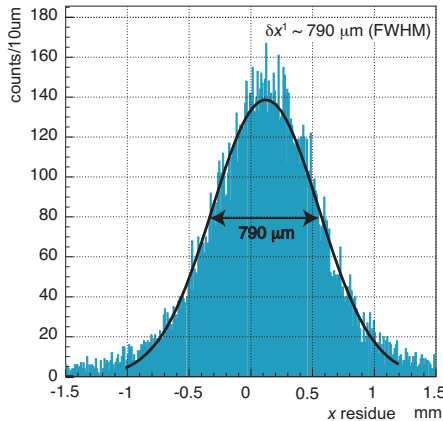


Figure 4. The residual distribution of CRDC1-1. The position resolution was $780 \mu\text{m}$ FWHM.

The geometric relation between the position resolution of each row δx^i and of the SHARQA focal plane δx_{fp}^i was the following:

$$\delta x_{\text{fp}}^i \simeq \delta x^i / 2.$$

The result of horizontal and vertical position resolution was $380(160) \mu\text{m}$ and $340(140) \mu\text{m}$ FWHM(rms), respectively.

4. Summary

We evaluated the performance of the CRDCs by using the secondary beam ^3He at 300 MeV/u. The CRDCs were operated with the anode of 980 V(CRDC1) and 1000 V(CRDC2) at $i\text{-C}_4\text{H}_{10}$ gas pressure of 4 kPa. The horizontal and vertical position resolution were $380 \mu\text{m}$ and $340 \mu\text{m}$ FWHM, respectively. Analysis to optimize the algorithm of multi-hit events progresses.

References

- [1] T. Uesaka *et al.*, Nucl. Instrum. Meth. A **266** (2008) 4218.
- [2] S. Michimasa *et al.*, CNS Ann. Rep. 2007 (2009); CNS Ann. Rep. 2008 (2010); CNS Ann. Rep. 2009 (2010).
- [3] The GASSIPLEX is a re-designed chip of the AMPLEX by J. C. Santiard of CERN. The AMPLEX id described in E. Beuville *et al.*, Nucl. Instrum. Meth. A **288** (1990) 157.
- [4] K. Miki *et al.*, CNS Ann. Rep. 2009 (2011).

PACIFIC data processing system for high-rate RI-beam experiments

S. Ota, S. Shimoura, H. Baba^a, E. Ideguchi, M. Kurokawa^a, A. Saito, H. Tokieda, and T. Otsuka

Center for Nuclear Study, Graduate School of Science, University of Tokyo

^a Nishina Center for Accelerator Based Research, RIKEN

The data-processing system called “Parallel Acquisition and Control Intelligent system for Femto-frontier Collaboration (PACIFIC)” has been developed under the collaboration between CNS and RIKEN. The system consists of three main devices:

- analog signal processing for fast signals (QTM),
- digital signal processing for slow signals (APU7110-P),
- asynchronous control and data collection (e-RT3) for monitoring the status of detectors and experimental conditions.

The basic features are written in Ref. [1].

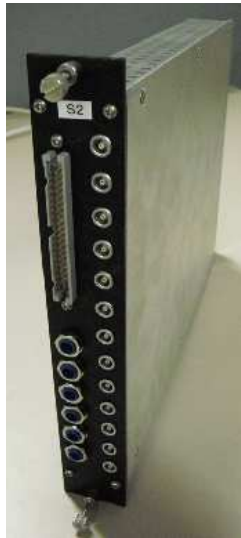


Figure 1. Photo of QTM. 6-inputs, 6-monitor and 1-veto with LEMO connector. The outputs are from 50-pin flat connector. The 6 potentiometer (left bottom) are for the optional input shapers.

The QTM modules are usually used with non-stop TDC which can digitize the timings of the leading and trailing edge of the logic pulse, such as V1190 VME TDC module produced by CAEN. Although the charge and time resolutions of this system are limited by the time resolution of V1190 modules, the time resolution of around 110 ps and the charge resolution of 3% are achieved. The QTM is used for the readout of the plastic scintillators at foci in SHARQA beamline and its performance is very well. Details are described in Ref. [2].

The algorithm of digital signal processing by using APU7110-P has been developed [3]. By this algorithm the

preamplifier output is pipeline processed and then the deduced information such as energy, timing and three dimensional position are buffered instead of the original pulse shape. This helps to reduce the data size significantly and make the load of the data transfer much smaller. Each APU7110-P has CPU and then can be a subsystem of the BABIRL system [4], which is an example of so-called ubiquitous DAQ system.

In 2009, we have added one more asynchronous control and monitoring system using e-RT3 CPU module for the SHARQA beamline. For now, we can control and monitor the parameters of power supplies and gas handling system for MWDCs at all the foci and the parameters of magnet system.

References

- [1] S. Ota *et al.*, CNS Ann. Rep. 2008 (2010).
- [2] S. Kawase *et al.*, CNS Ann. Rep. 2009 (2011).
- [3] S. Go *et al.*, CNS Ann. Rep. 2009 (2011).
- [4] H. Baba *et al.*, Nucl. Instrum. and Methods A, 616, 65 (2010)

Performance evaluation of Low-Pressure Multi-Wire Drift Chamber for RI Beam

H. Miya, S. Shimoura, A. Saito, K. Miki^{a,b}, T. Kawabata^c, K. Itahashi^b, S. Itoh^a, S. Ota, M. Sasano^b, Y. Shimizu, H. Baba^b, H. Kurei, S. Michimasa, S. Noji^a, K. Nakanishi, Y. Sasamoto, Y. Shimbara^d, H. Tokieda, T. Uesaka and H. Sakai^a

Center for Nuclear Study, Graduate School of Science, University of Tokyo

^aDepartment of Physics, University of Tokyo

^bRIKEN (The institute of Physical and Chemical Research)

^cDepartment of Physics, Kyoto University

^dDepartment of Physics, Niigata University

1. Introduction

We have developed low-pressure multi-wire drift chambers (LP-MWDCs) for light heavy ions at 100–300 MeV/nucleon. The LP-MWDCs are used in BigRIPS and High-Resolution Beamline (HRBL) [1] in RI Beam Factory.

The LP-MWDCs have 3 anode layers (x, u, and y). The u wires was tilted by 30° with respect to the x wires. The counter gas is pure isobutane at the pressure of around 10 kPa. The details of the structure of the LP-MWDCs are described [2].

The performance of the LP-MWDCs was evaluated with RI beams having an atomic number (z) from 1 to 7 in the commissioning of SHARAQ spectrometer and HRBL. We report the position resolutions and tracking efficiencies for the RI beams as a function of the applied voltage.

2. Experimental prodedures

Performance test was made on March, May, and November 2009. On March and May, a primary beam was ^{14}N at 250 MeV/nucleon. RI beams of ^3H , ^6He , ^9Li , ^{10}B , ^{12}Be , ^{11}C were produced by a projectile-fragmentation reaction of the ^{14}N with a primary target of ^9Be . On November, a primary beam was ^4He at 320 MeV/nucleon. RI beams of ^3H , ^3He were produced by the reaction of the ^4He with the target.

The LP-MWDCs and plastic scintillators were placed in the focal planes of BigRIPS and HRBL. The plastic scintillators were used to determine the start of the drift time for the LP-MWDCs and to identify the RI beams. The details of the experimental setup at focal planes are described in the ref [3].

Information of time and charge of the beams were obtained from the anode wires. The amount of the charge is converted to the pulse width using the amplifier and discriminators (REPIC RPA-131) and charge-to-time converter (QTC) [4, 5]. The timing signal was made using the leading-edge discriminator. The timing signal and pulse-width were recorded by using the multihit TDC (CAEN V1190).

3. Analysis and Results

The RI beams were identified with the ΔE -TOF method where ΔE is the energy loss in the plastic scintillator at F-H7 and TOF is the time-of-flight between the scintillators at

F-3 and F-H7. The performance of the LP-MWDC installed at F-H7 was evaluated for each RI beam with $z = 1-7$.

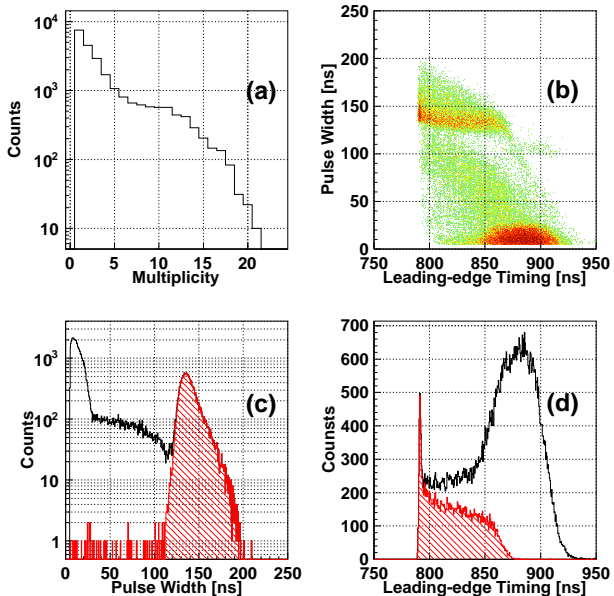


Figure 1. (a) Multiplicity distribution of on x layer (b) Relation between the pulse width and leading-edge timing acquired from the wires, (c) Spectra of the pulse width and (d) Spectra of the leading-edge timing by selecting the pulse width at 1100V and 10 kPa for the ^{14}N .

Figure 1(a) shows the multiplicity distribution on x layer for the ^{14}N at 1100 V. Here, the multiplicity is defined as the number of the hit wires on one layer. Only 32% of the events has one hits. This is due to by δ -rays generated along the beam trajectory. In order to obtain the high tracking efficiency, it is needed to discriminate the signals between the beam and δ -rays. Figure 1(b) shows the relation between the pulse width and leading-edge timing from the all wires on x layer. It is reasonable that the signals with the pulse width more than 130 ns are from the signals of the beam in Fig. 1(a). Figure 1(c) shows the spectra of the pulse width. The open and hatched spectra show the signals from the wires and the signals with the maximum pulse width selected for each trigger event, respectively. The hatched spectrum of the leading-edge timing is shown in Fig. 1(d). The hatched area which is for the signals with the maximum pulse width shows a reasonable drift time distribution.

From the obtained drift time, it is possible to calculate the distance of the hit from an anode wire in one cell. The hit positions of each plane were determined by calculating the minimum residual of $u_U - u_{xy}$. Here, u_U is a hit position on u layer and u_{xy} is a hit position in u axis which is calculated from the hit positions in x and y layers. The details on how to make track reconstruction was described in the ref [2].

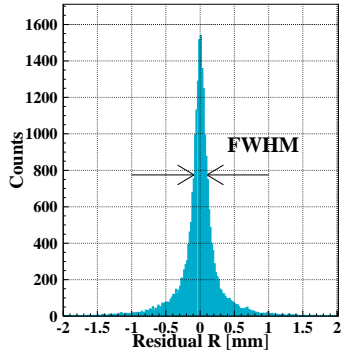


Figure 2. Residual distribution of $u_U - u_{xy}$ at 1100 V and 10 kPa for the ^{14}N .

The position resolution is obtained from the residual distribution of $(u_U - u_{xy})/\sqrt{2}$. Figure 3 shows the distribution of $u_U - u_{xy}$ at 1100 V and 10 kPa for the ^{14}N . From the distribution, the position resolution was obtained to be 171 μm in FWHM.

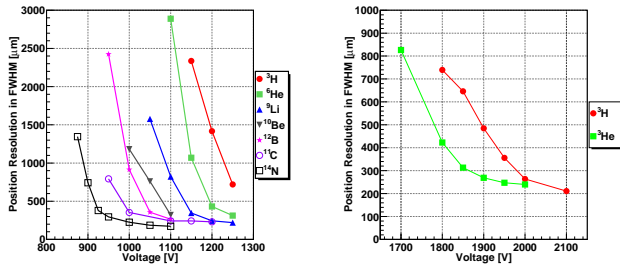


Figure 3. Position resolution as a function of the applied voltage at the pressure of 10 kPa (left) and 50 kPa (right).

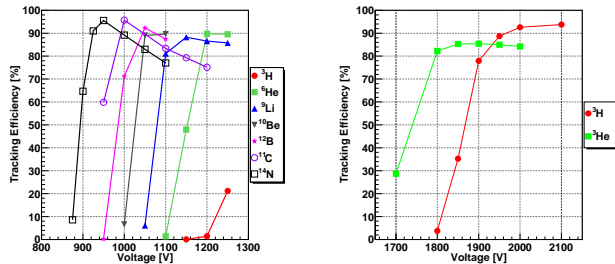


Figure 4. Tracking Efficiency(b) as a function of the applied voltage at the pressure of 10 kPa (left) and 50 kPa (right).

Figure 3 shows the position resolutions evaluated as a function of the applied voltage at the gas pressure of 10 kPa and 50 kPa. The position resolutions were around 200–300 μm for the beam with $z = 2-7$ at 10 kPa and around

200–300 μm for the beam with $z = 1-2$ at 50 kPa, respectively. At the applied voltage of 1100 V, the LP-MWDCs have the dynamic range of $z = 3-7$.

The tracking efficiency was defined as the ratio of the number of the events having the residual within 3σ to the counted number of the beams by using the scintillator at the downstream of the LP-MWDCs. Figure 4 shows the tracking efficiencies as a function of the applied voltage. The tracking efficiencies reached around 90% for the RI beams at 10 kPa and 50 kPa.

4. Summary

The position resolutions and tracking efficiencies of the LP-MWDCs were evaluated for the RI beam with $z = 1-7$ as a function of the applied voltage at 10 kPa and 50 kPa. The position resolutions were around 200–300 μm in FWHM for the beams with $z = 2-7$ at 10 kPa and around 200–300 μm in FWHM for the beams with $z = 1-2$ at 50 kPa, respectively. At 10 kPa and 1100 V, the LP-MWDCs have the dynamic range of $z = 3-7$. The tracking efficiencies reached around 90% for the beams at 10 kPa and 50 kPa.

References

- [1] T. Kawabata *et al.*: Nucl. Instrum. Meth. *B* **266** (2008), 4201.
- [2] H. Miya *et al.*: CNS Ann. Rep. 2008 (2010).
- [3] A. Saito *et al.*: RIKEN Prog. Rep. Vol.43 (2010).
- [4] S. Kawase *et al.*: CNS Ann. Rep. 2009 (2011).
- [5] H. Nishino *et al.*: Nucl. Instrum. Meth. *A* **610** (2009) 710.

Evaluation of basic performance of Charge-to-Time Converter Module (QTM)

S. Kawase, S. Ota, H. Baba^a, S. Shimoura and T. Uesaka

Center for Nuclear Study, Graduate School of Science, University of Tokyo

^aRIKEN (The Institute of Physical and Chemical Research)

Advanced accelerator technology has been giving us the high-intensity radioactive ion beams. We can now make various experiments with those beams. However, as the beam intensity increases, it becomes more and more difficult to take full data because of growing dead time of data acquisition system. It is mainly limited by relatively long conversion time of Analog-to-Digital Converter (ADC) or Charge-to-Digital Converter (QDC). To make it shorter, we developed general purpose Charge-to-Time Converter Module (QTM) [1, 2] which has much shorter dead time than ADC and QDC. The heart of QTM is the Charge-to-Time Converter (QTC) chip, which is developed originally in Kamioka Observatory [3] and produced by IWATSU Test Instruments Corporation. QTM converts the charge of signal into the width of rectangular output pulse as shown in Fig. 2 in ref. [2]. Therefore by using QTM, we can take information of time and charge at once.

QTM is a NIM module including two QTC chips and each chip has 3 channel inputs. A QTC chip accepts input charges up to about 50 pC. Input signals are equally divided into three identical ones and two of them are attenuated by factors of 7 (medium gain) and 49 (large gain). Thus dynamic range of input charge is expanded up to 2.5 nC. QTM has 6 inputs with 50 Ω termination and 18 (2x3x3) LVDS outputs. Internal parameters such as threshold or integration time can be reconfigured via USB connection.

To evaluate basic performance of QTM, we measured the time and the charge resolution of QTM in medium gain (50–350 pC) and compared them to those of the traditional setup using Time-to-Digital Converter (TDC) and QDC. The setup of this measurement is shown in Fig. 1. Input

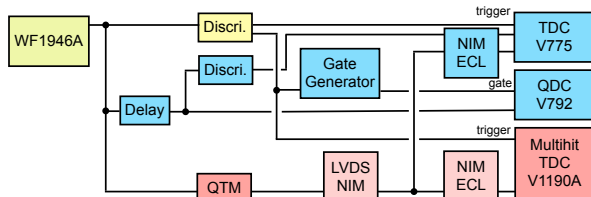


Figure 1. Electronic scheme of the measurement.

signal, which was generated by Multifunction Synthesizer WF1946A (NF corporation), had the trapezoidal shape with the lower-base width of 50 ns and the rise- and fall-time of 10 ns as shown in Fig. 2. Input charge was varied by adjusting the height of input pulse. QTM threshold was fixed to 15 mV. To digitize timing signals, TDC V775 (CAEN) and multi-event non-stop TDC V1190 (CAEN) were used, and for the traditional system, input charge was digitized by QDC V792 (CAEN).

Figure 3 and 4 show the results of measurements of time resolution and charge resolution, respectively. In Fig. 3, time resolution of the system including QTM plus V775 (indi-

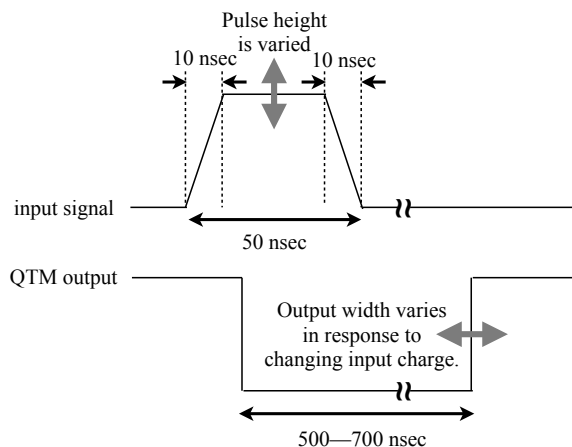


Figure 2. Input signal and QTM output signal. QTM converts the charge of input signal into the width of output pulse.

cated by the stars) is about 40 psec, while the resolution of the traditional one (i.e. Discr. plus V775, indicated by the circles) is about 30 psec. These results show the usability of QTM. However, time resolution of the new system (i.e. QTM plus V1190) is seemingly worse, but it seems to be due to the bad time resolution of V1190 (~ 100 psec LSB), because the system including QTM with V775 (typically ~ 30 psec LSB) has rather good resolution (this is even below the catalog value of QTM) closing up to the traditional system. The new system is enough usable for processing of data from plastic scintillators because the current time resolution of the new system is on par with that of plastic scintillators. To achieve better resolution and shorter dead time simultaneously, we still need a good multi-event non-stop TDC

On the other hand, the charge resolution of new system is about 1.4 pC, worse than that of traditional system being ~ 0.5 pC as in Fig. 4. But it is sufficiently good in some application e.g. γ -ray detection with $\text{LaBr}_3(\text{Ce})$ scintillator, which is expected to be a new-generation γ -ray detector, because it is still below 3% under the condition that input charge is greater than 50 pC and independent from the amount of input charge. In addition, if input charge is smaller than 50 pC, one should use the small gain. The analysis to deduce the charge resolution with small gain is in progress.

We also carried out spectral measurement with $\text{LaBr}_3(\text{Ce})$ scintillator. The spectrum of γ ray emitted from ^{60}Co and ^{137}Cs source was taken with a system including QTM and one including QDC. The result is shown in Fig. 5. Upper panel shows the result with QDC, lower with QTM. The result with QTM seems as good as that with QDC.

QTM was already used in an experiment using the SHARAQ Spectrometer [4] as a readout circuit of plastic

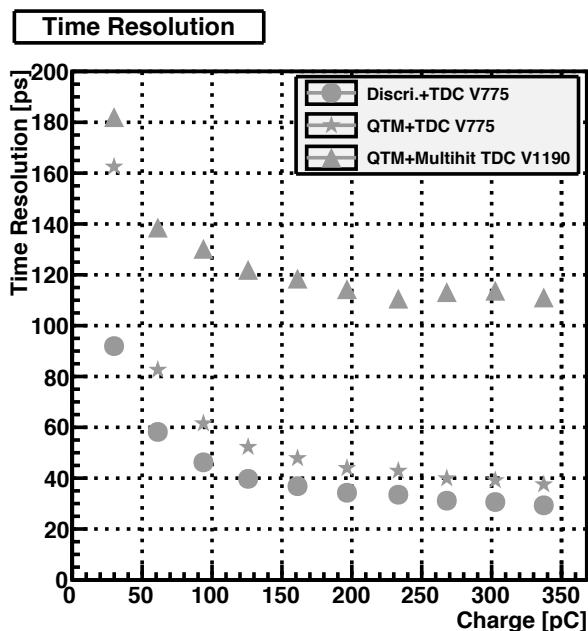


Figure 3. Measured time resolution. Circles show the results with Discriminator plus TDC V775, stars show those with QTM plus V775 and triangles show those with QTM plus Multihit TDC V1190.

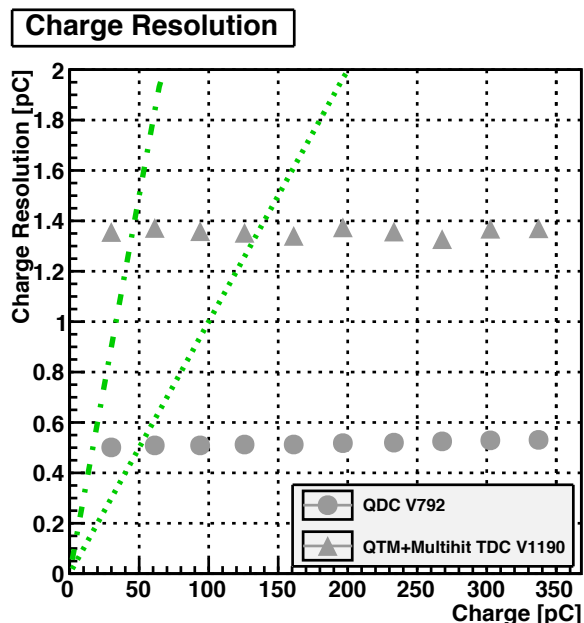


Figure 4. Measured charge resolution. Circles show the results with QDC V792 and triangles show those with QTM plus Multihit TDC V1190. Dashed-dotted-line shows the charge resolution of 3% and dotted-line shows that of 1%.

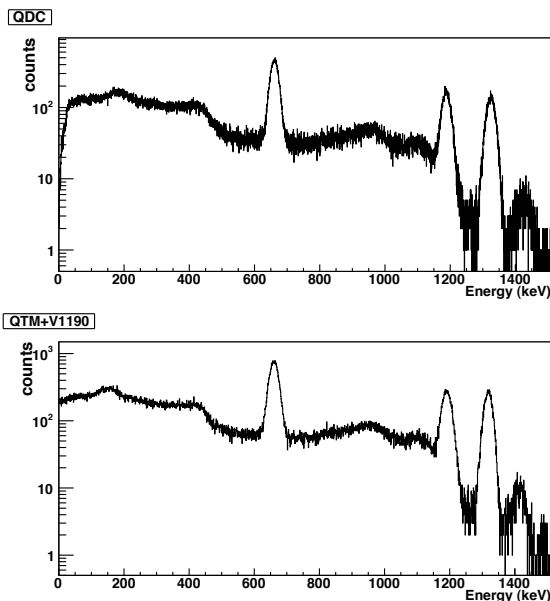


Figure 5. γ -ray spectra with $\text{LaBr}_3(\text{Ce})$. Upper panel shows the spectrum taken with QDC, lower with QTM.

scintillators and provided good performance.

In conclusion, QTM in medium gain is sufficiently usable in actual experiment as it is now and further analysis of its performance in both small and large gain is needed.

References

- [1] S. Ota *et al.*, CNS Ann. Rep. 2008 (2010).
- [2] S. Ota *et al.*, CNS Ann. Rep. 2009 (2011).
- [3] H. Nishino *et al.*, Nucl. Instrum. Meth. A **610** (2009) 710.
- [4] K. Miki *et al.*, CNS Ann. Rep. 2009 (2011).

New Intergroup Collaboration for Development of GEM-TPC Active Target

S. Ota, S. Michimasa, T. Gunji, H. Yamaguchi, R. Akimoro, T. Hashimoto, K. Devid, S. Hayakawa, H. Tokieda, S. Kawase, T. Tsuji, S. Kubono, H. Hamagaki, T Uesaka

Center for Nuclear Study, Graduate School of Science, University of Tokyo

We are developing two types of active targets using Gas Electron Multiplier (GEM) [1] for the experimental study with intense (10^{5-7} Hz) radioisotope beams in inverse kinematics. Active target has two functions of target and detector and enables us to measure the low-energy recoiled particle. In this report, the brief summary of collaborative development of two active targets and the details of common readout system for them are described.

One type being developed is “beam transparent type” one (Fig. 1) for the studies of nuclear structure and property of nuclear matter by measuring the giant resonances such as monopole, dipole, and Gamow-Teller excitation, via (α, α') , (d, d') or $(d, ^2\text{He})$ reactions. Missing mass spectroscopy is a powerful tool for these measurements, since such resonances locate at highly excited region and then the excited nuclei decay immediately by emitting the particles. Hence we need to measure the recoiled particles such as α , d and protons with low kinetic energy in the forward angle, which is essential to identify the transfer momentum in the reaction. The structure of this active target is optimised so as not to measure the beam particles for the high-rate up to 10^7 Hz at the high incident energy of 100–200 MeV/u. The detail of the structure is described in Ref. [2].

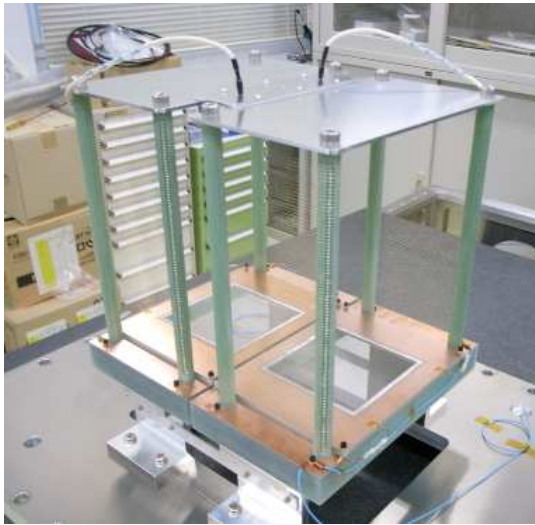


Figure 1. Picture of the field cage of the “beam transparent” type active target.

The other type is “beam measurement type” one (Fig. 2) for the studies of nuclear astrophysics, especially the rp -process in nucleosynthesis. So far, the (α, p) reaction has been studied by using the thick-target method at the CRIB facility of the University of Tokyo in RIKEN. Although a large excitation energy range can be studied by this method,

there still remain some uncertainties in identification of the reaction processes. To reduce these uncertainties, we need to measure the tracks of the beam particles as well as the ejectiles. The details are described in Ref. [3].



Figure 2. Picture of the field cage of the “beam measurement” type active target.

To develop these active target system efficiently, we made a collaboration among the three groups of SHARAQ, astrophysics and quark physics group. The thin GEMs have been studied by quark physics group and its basic property for the generally used gasses such as Ar+CH₄, Ar+CO₂ is studied and its operation is established. In this year we tried to operate thin GEMs with ⁴He+CO₂ and successfully evaluated its property. The structure of the field cage and readout pad was originally studied by astrophysics group and more precise simulation was performed to construct the “beam transparent type” active target.

The main data acquisition system (BABIRL) was imported from SHARAQ project, which had been developed by RIBF DAQ team which the authors (S.O and H.T) also join. BABIRL consists of the event builder (EB) and the event sender (ES). The ES is actual data taking system and has one CPU to collect the data from the VME (and/or other) modules and to send the data to the EB. The EB collect the data from each EB and reconstruct events. We first used SIS3301 flash ADCs produced by SIS to digitize the pulse shape of the preamp (REPIC RPA210) output. A typical event taken in the experiment at University of Tsukuba is shown in Fig. 3. COPPER II system, which was developed by KEK, was also combined to BABIRL as EBs. The COPPER II system consists of a mother board, CPU board and four daughter board of flash ADC. A sampling clock (50 MHz) and gate was common for 8 channel signal inputs in each ADC board. The normal LINUX was used as operating system and the driver software was developed to be

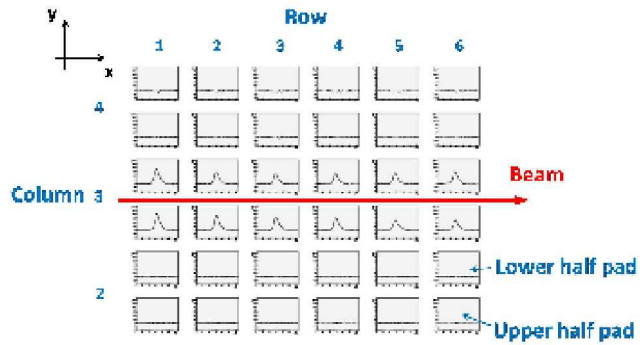


Figure 3. Typical event of “beam transparent type” active target taken by SIS3301 flash ADCs. A beam trajectory is clearly seen. Figure is taken from Ref. [4]

combined to BABIRL. A capability of the zero suppression to reduce the data size was realized in the software. This system successfully worked at the test experiment.

This intergroup collaboration just began in 2009 and the prototype of the active targets are completed within this year. We exchanged not only the human resource and devices but also the knowledge and technique in each research field. Such kind of collaboration among the people from the different field drive the project efficiently. We plan to have some physics and test experiment in 2010.

References

- [1] M. Inuzuka *et al.*, Nucl. Instrum. Meth. A **525**, 529(2004).
- [2] R. Akimoto *et al.*, CNS Ann. Rep. 2009 (2011).
- [3] T. Hashimoto *et al.*, CNS Ann. Rep. 2009 (2011).
- [4] R. Akimoto, Master Thesis (2009)

Development and performance evaluation of a GEM-TPC for the experiment of highly excited state of nuclei with high rate and high energy unstable nuclear beam

R. Akimoto, S. Ota, S. Michimasa, T. Gunji, H. Yamaguchi, T. Hashimoto, H. Tokieda, T. Tsuji, S. Kawase, H. Hamagaki, T. Uesaka, S. Kubono, T. Isobe^a, T. Kawabata^b, A. Ozawa^c, H. Suzuki^c, D. Nagae^c, T. Moriguchi^c, Y. Ito^c, Y. Ishibashi^c, H. Ooishi^c, and Y. Abe^c

Center for Nuclear Study, Graduate School of Science, University of Tokyo

^a*RIKEN (The Institute of Physical and Chemical Research)*

^b*Department of Physics, Kyoto University*

^c*Institute of Physics, University of Tsukuba*

1. Introduction

A study of the giant resonances, which appear in highly excited region characterized by varieties of nuclear collective motions, is one of the interesting subjects in the nuclear physics.

The giant resonances of stable nuclei were studied with missing mass spectroscopy at a small momentum transfer region such as (α, α') measurement for the isoscalar mode [1]. In order to extend our understanding to isospin asymmetric region, experiments in inverse kinematics using neutron-rich unstable nuclear beam are planned. Since the excited state of the beam decays with particle emission in flight, the ejectile has to be detected for minimum-bias measurement independent of the beam decay modes. However, it is difficult to measure the ejectile in forward scattering due to its very low energy. In the case of (α, α') using ^{68}Ni with 200 MeV/u as a beam, the energy of the scattered α is less than 1.5 MeV/u with both the scattering angle of less than 5° in center of mass frame and the excitation energy of 20 MeV. Therefore, an active target gas detector, which is a combined device of gas target and gas detector, can be a powerful tool to detect the ejecta with very low energy due to its small material budget.

A Time Projection Chamber using Gas Electron Multiplier (GEM-TPC) as an active target has been developed and a performance test was carried out. Requirements of the GEM-TPC for the above example are as follows:

- The GEM-TPC can be operated with a high intensity beam ($> 10^6$ pps) since the cross section is small, about 0.1 mb;
- The angular resolution of the track of the ejectile in the center of mass frame and the resolution for the excitation energy are required to be better than 3.5 mrad and 1 MeV, respectively. Thus, the angular and energy resolutions in the laboratory frame are required to be less than 7.5 mrad and 1 MeV, respectively.

2. Design of Active Target GEM-TPC

The rate of the ejecta by elastic scatterings is about 10^3 pps with a beam rate of 10^6 pps. Under the condition, GEMs [2], which are one of Micro-Pattern Gaseous Detectors (MPGDs), are suitable since they can suppress ion feedback and performance degradation of electron mul-

tiplication. The thickness, hole diameter, and hole pitch of the GEM used for the GEM-TPC are 100 μm , 70 μm , and 140 μm , respectively.

A gas mixture of He (95 %) + CO₂ (5 %) at about 760 Torr is used. The mixture proportion is optimized by taking account of the material budget and the gas gain of the GEM.

A field cage was designed using Garfield [3] by taking account of the field distortion from ground and the beam. The beam profile is 10×50 (the z direction ¹) mm² in RMS. The electric field is created by double-layered metallic wires (the distance between the layers is 15 mm) with a pitch of 2.5 mm. The length of the field cage for the z direction is 250 mm. The field distortion by electron-ion pairs created by the beam was evaluated with two configurations, with and without a 40 mm-gap at beam injection area. The right panel of Fig.1 shows the field cage with the gap. Figure 2 shows the position difference in the x direction during drift from the top to the bottom of the field cage as a function of the distance from the center of the field cage in the x direction where the beam was injected. The solid circles show the results with both beam and the gap, the solid squares show those with beam and without the gap, and the open circles show those without beam (a Ni beam with 200 MeV/u and an intensity of 10^7 pps). From the results, the gap is necessary for the track dispersion in the x direction to be less than 7.5 mrad. In the case with the gap, the dispersion for the track with a flight length of 100 mm is less than 5 mrad.

Readout pads with Backgammon geometry are used in order to reduce the number of the pads (right of Fig.3). Hit positions are determined from charge proportion of the neighboring pads. The pad size was optimized by a simulation [4] with consideration for the angular resolution in the xy-plane and the number of pads. In the simulation, the statistical fluctuation of the energy loss was assumed as the energy resolution. The pads with 16.45×16.45 mm² are used.

3. Performance Test

A performance test of the GEM-TPC was carried out using a $^4\text{He}^{2+}$ beam with 7.5 MeV/u accelerated by the 12UD Pelletron tandem accelerator at the University of Tsukuba Tandem Accelerator Complex (UTTAC) [5]. At the performance test, the position, angular, and energy resolutions

¹In this article, x, y, and z directions are defined as shown in Fig.1.

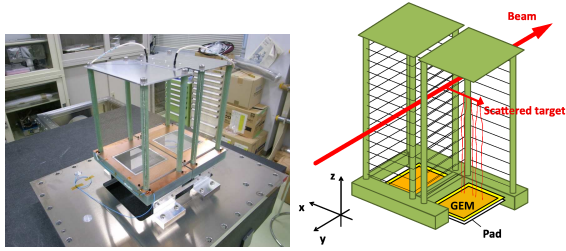


Figure 1. Left: A picture of the field cage. Right: A typical reaction with the field cage with the gap for beam injection. A beam scatters with the nucleus of the gas atom inside the TPC.

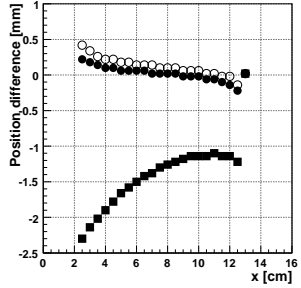


Figure 2. The simulation result of field distortion. The solid circles show the result with both beam and the gap, the solid squares show those with beam and without the gap, and the open circles show the result without beam. The beam passes at $x = 0$ and the active area of readout pad is $2.5 \text{ cm} < x < 12.5 \text{ cm}$.

were evaluated for several incident positions in the y direction. The beam passed along the x direction, shown in the left panel of Fig.3. The electric field in the field cage was 700 V/cm , where the drift velocity of electrons is $2 \text{ cm}/\mu\text{s}$ (according to the Magboltz simulation [6]). The voltage applied to the GEM was adjusted to achieve the gas gain of about 10^3 . A trigger was made by summed up signals from 4 upstream pads, shown in the right panel of Fig.3.

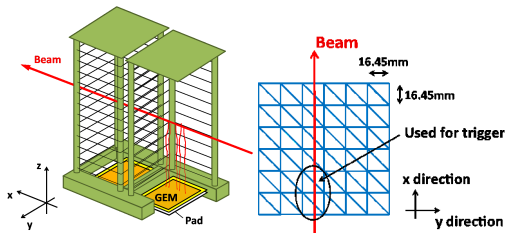


Figure 3. Left: A typical event at the performance test. Right: A schematic view of the readout pads.

4. Result

The results are shown in Fig.4. The top left and top right panels show the results of the position resolutions in the y and z directions as a function of the incident position, respectively. The bottom left figure shows the distribution of the induced charge summed for all pads. The geometry of the beam incident position is shown in the bottom right in Fig.4. The position resolutions in the y and z directions are less than $700 \mu\text{m}$ and about $80 \mu\text{m}$, which lead to the an-

gular resolution of less than 8.3 mrad and about 1.2 mrad , respectively, when effects due to straggling and the particles which stop inside the field cage are not considered. The energy resolution is 3.9% in RMS.

The position resolution in the z direction and the energy resolution satisfy our requirements though the position resolution in the y direction is slightly larger than the requirement since the energy resolution is larger than the statistical fluctuation of the energy loss.

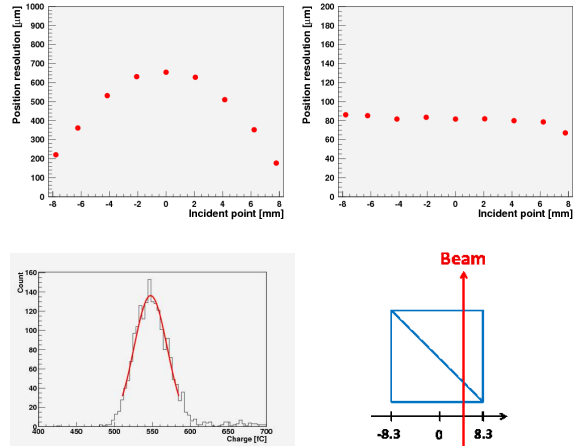


Figure 4. The top left and top right panels show the position resolutions in the y and z directions as a function of incident position, respectively. The bottom left panel shows the distribution of the induced charge summed for all pads. The bottom right panel shows the geometry of the beam incident position.

5. Conclusion and Outlook

A GEM-TPC for use as an active target has been developed for nuclear experiments using unstable nuclear beams. It is intended to measure the ejectile in forward scattering. A performance test was carried out using $^4\text{He}^{2+}$ with 7.5 MeV/u . From the test result, the position resolutions in the y and z directions are less than $700 \mu\text{m}$ and about $80 \mu\text{m}$, respectively. The energy resolution is 3.9% in RMS.

In the future, following items will be studied:

- Performances for incline incident particles;
- Effect of the field distortion and δ -ray from a high intensity and high energy beam.

References

- [1] M. Uchida *et al.*, Phys. Rev. C 69 (2004) 051301(R)
- [2] F. Sauli, Nucl. Instrum. Meth. A **386** (1997) 531.
- [3] <http://garfield.web.cern.ch/garfield/>
- [4] R. Akimoto, Master Thesis (2010)
- [5] S. Seki, *et al.*, Nucl. Instrum. Meth. **184** (1981) 113.
- [6] <http://consult.cern.ch/writeup/magboltz/>

Simulation Study for Forward Calorimeter in LHC-ALICE experiment

Y. Hori, H. Hamagaki, T. Gunji

Center for Nuclear Study, Graduate School of Science, University of Tokyo

1. Introduction

We propose the Forward Calorimeter (FOCAL) as an upgrade plan of ALICE detector. The physics goal of FOCAL is the understanding of the parton structure inside the proton and nuclei at small- x , especially, the gluon saturation effect like Color Glass Condensate (CGC). For this purpose, FOCAL measures prompt γ and neutral mesons at the forward rapidity region in p-p and p-Pb collisions. The FOCAL will also make a unique contribution for Quark Gluon Plasma (QGP) physics by measuring leading high p_T π^0 and jets in Pb-Pb collisions.

2. Small- x gluon PDF and its Saturation effect

Parton Distribution Functions (PDF) of the proton were precisely measured in HERA experiment and the rapid growth of the small- x gluon density was observed. The growth of the gluon density inside the hadron with decreasing x is ultimately expected to be balanced by the gluon-gluon fusion process. These nonlinear effects lead to the gluon saturation at the small- x region [1].

This phenomenon is expected to occur when the area occupied by the gluons becomes equal to the area of the hadron πR^2 . This situation is expressed by the saturation momentum Q_s as $\Lambda_{QCD}^2 \ll Q^2 < Q_s^2(x) \sim \alpha_s x G(x, Q^2) / \pi R^2 \propto A^{1/3} x^{-0.3}$. It is considered that Q_s^2 is ~ 10 GeV² at LHC. The situation $\Lambda_{QCD}^2 \ll Q_s^2$ will be realized in high energy collisions like LHC.

3. Prompt γ and π^0 measurements at the forward rapidity region

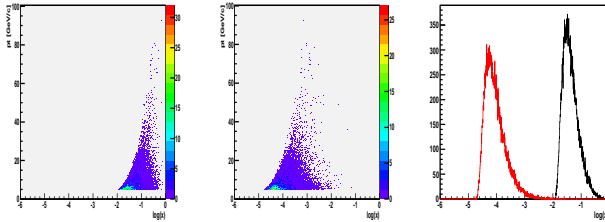


Figure 1. Left and Center: p_T and $x_1(x_2)$ range of relevant partons of γ production at $\eta = 3 - 3.5$, Right: Projection to the x -axis of the 2 left plots

Experimentally, saturation effects on small- x gluons are expected to be revealed in measurements of forward particle production. For a $2 \rightarrow 2$ parton scattering, the minimum x probed in a process with a particle momentum p_T and its pseudo-rapidity η is given as

$$x_2^{min} = \frac{x_T e^{-\eta}}{(2 - x_T e^{\eta})}, x_1^{min} = \frac{x_2 x_T e^{-\eta}}{(2x_2 - x_T e^{\eta})} \quad (1)$$

where $x_T = 2p_T / \sqrt{s}$. Thus, x_2^{min} decreases by a factor of \sim

10 every 2 units of rapidity.

The production of prompt γ at forward rapidity is sensitive to the small- x gluon distribution. The dominated production processes at leading order level are Compton scattering and annihilation process. Compton process is in particular interesting because small- x gluon and large- x (valence) quark are relevant if prompt γ is produced at the forward rapidity region. Figure 1 shows the accessible x range of the gluon by the prompt γ measurement at $\eta = 3 - 3.5$ in 8.8 TeV collisions calculated by Pythia simulation. The x range that can be probed by prompt γ is $10^{-3} - 10^{-5}$, which has hardly been probed even for the proton.

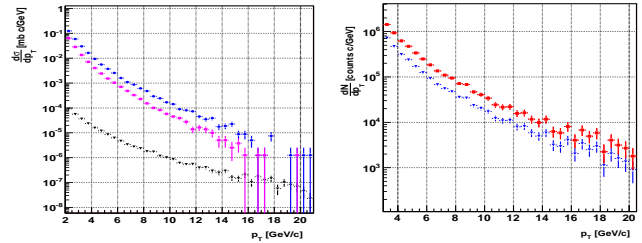


Figure 2. Left: p_T spectrum at $\eta = 3 - 4$ in 8.8 TeV p-p collisions (blue - π^0 , pink - γ from π^0 , black - prompt γ), Right: Annual yield of prompt γ at $\eta = 3 - 4$ in p-p (blue) and p-Pb (red) collisions for a standard year of running at LHC, which does not include any nuclear effects

Fig.2 shows the cross section and annual yield of prompt γ at $\eta = 3 - 4$ in 8.8 TeV p-p collisions. A width of p_T binning is 0.5 GeV/c and error bars are from simulation statistics.

4. Conceptual design of Forward Calorimeter and its Basic performance

Considering the physics requirements and the detector performance, the η coverage of FOCAL should be 3 - 4 and the distance from interaction point should be about 4.5 m, where is between ALICE L3 magnet wall and TPC. The layout of the FOCAL is summarized in Table 1.

Distance from IP	4.5 m	η coverage	3 - 4
Outer Radius	45 cm	ϕ coverage	2π
Inner Radius	15 cm	Area	~ 0.6 m ²

Table 1. Layout of the FOCAL

In order to measure γ and neutral mesons at the forward rapidity regions, FOCAL must have a large dynamic range (γ energy 1 - 200 GeV) and highly granularity (multiplicity ~ 1 particle/cm² at $\eta = 4$ according to the HIJING simulation). FOCAL also has to have good separation ability of 2 γ from high energy π^0 decays. A minimum distance of 2 γ from 100 (200) GeV π^0 is ~ 10 (6) mm.

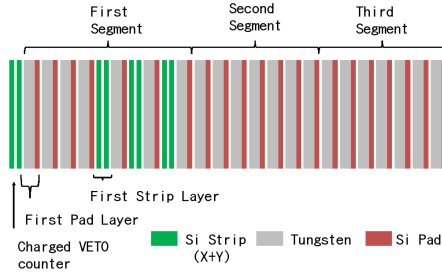


Figure 3. Conceptual design of the FOCAL module

These requirements can be fulfilled by a hybrid use of the Si Pad and W sandwich-type calorimeter and Si Strip layers as shown in Fig.3 [2]. The thickness of each Si Pad detector is 0.5 mm and that of W absorber is 3.5 mm. It has 21 radiation length depth and has 3 longitudinal segments. Each segment has 7 layers of Si Pad and W absorber. The Si Pad detector is laterally segmented by 1 cm x 1 cm. Fig.4 shows the longitudinal shower shapes calculated by GEANT 4 simulation and γ shower is effectively identified by a cut for χ^2 distribution. Other basic performances are listed in Table.2.

A few layers of the Si Strip detector is used to separate 2 γ from high energy π^0 . The thickness of Si Strip layer is 0.3 mm and the strip pitch is 0.5 - 1 mm.

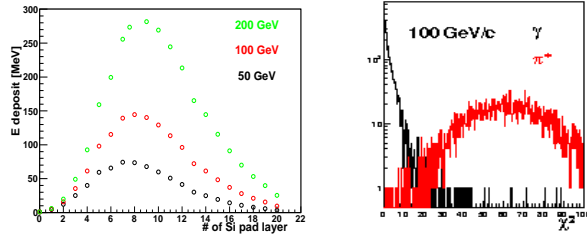


Figure 4. Left: Longitudinal shape of γ shower, Right: χ^2 distribution of the longitudinal deposited energy

Cell occupancy in p-Pb collisions	< 10%
Detection efficiency	> 95%
Linearity	< 1%
Sampling fraction	1.4%
Energy resolution	$18/\sqrt{E}$ %
Position resolution at 10 GeV γ	1.5 mm
Charged Hadron rejection factor	250 at γ eff.90%

Table 2. Basic performance of Si Pad Detector

5. π^0 reconstruction efficiency

π^0 with energy 7 - 70 GeV can be efficiently reconstructed by the invariant mass method using the Si Pad detector and its detection efficiency is > 60% as shown in Fig.5. To detect π^0 with energy 70 - 100 GeV, the lateral shower shape analysis of the Si Pad detector may be useful, but the further study is necessary.

By one layer of the Si Strip detector with 0.5 mm pitch strip, 100 - 200 GeV π^0 can be detected and its efficiency is

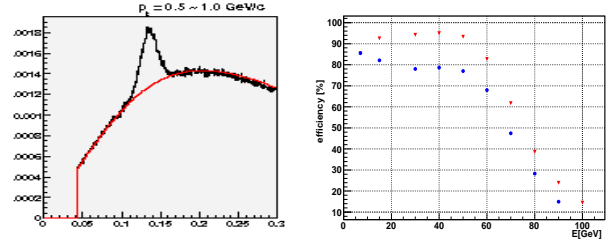


Figure 5. Left: $\gamma\gamma$ invariant mass spectrum in $\eta = 3.0 - 3.5$, Right: Reconstruction efficiency of π^0 with invariant mass method (red - without the energy asymmetry cut, blue - with the energy asymmetry cut < 0.8)

$\sim 50\%$ with misidentification probability < 1% as shown in Fig.6. The performance of the Si Strip detector with 1 mm pitch strip is not so different from that of 0.5 mm pitch strip. The position of the Si Strip detector should be the depth of 5 - 7 X_0 or deeper, which corresponds to the shower maximum depth. It is also found that the use of multi Si Strip layers does not change the π^0 reconstruction efficiency drastically.

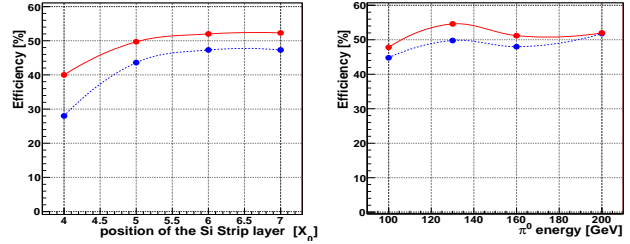


Figure 6. Left: Efficiency vs. the position of the Si Strip layer (solid line - 200 GeV π^0 , dot line - 100 GeV π^0), Right: Efficiency vs. π^0 energy (solid line - 0.5 mm pitch strip, dot - line 1 mm pitch strip)

The annual yield of π^0 with $19.5 < p_T < 20$ GeV/c at $\eta = 3 - 4$ is $\sim 5 \times 10^4$ according to Fig.2. The acceptance for π^0 with p_T 20 GeV/c is almost 100 % and the reconstruction efficiency by the Si Strip detector is ~ 50 %. Therefore, the annual count of π^0 with $19.5 < p_T < 20$ GeV/c at $\eta = 3 - 4$ is $\sim 2.5 \times 10^4$.

6. Summary and future plan

We performed a dedicated simulation study for the FOCAL in LHC-ALICE experiment. Next, we have to do full simulation and construct prototype of the FOCAL module including a readout electronics.

References

- [1] L.D.McLerran and R.Venugopalan, Phys.Rev.D **49** (1994) 2233
- [2] Technical Design Report for a Nosecone Calorimeter for the PHENIX experiment.

Simulation Study of the Forward Calorimeter for the upgrade of the LHC-ALICE experiment

T. Gunji, H. Hamagaki, Y. Hori

Center for Nuclear Study, Graduate School of Science, University of Tokyo, Japan

1. Introduction

Ultra-relativistic heavy-ion collisions is the unique tool in the laboratory to realize the hot and dense QCD medium, which are composed of deconfined quarks and gluons. One of the physics motivations at the Large Hadron Collider (LHC) at CERN is to study the properties of hot and dense QCD medium at the extremely high energy regime. High energy heavy ion collision experiments at RHIC reveals striking features of the created medium. The medium behaves like perfect liquid rather than the ideal gas and the medium is rapidly thermalized short after the collisions. The mechanism to manifest these features in heavy ion collisions are still under the discussion and studying the initial state of collisions is inevitably crucial for understanding the rapid thermalization of the system.

Studying the parton distribution functions in proton and its modification in heavy nuclei are specially important subjects for understanding the initial state of collisions. The gluon distribution inside proton is known to grow faster at small x than that of valence and sea quarks and the growth is expected to be saturated due to two competing processes between gluon splitting and gluon fusion, where this state is called as Color Glass Condensate. The saturation scale, Q_s , which corresponds to the typical momentum of gluons, is proportional to $Q_s^2 \sim A^{1/3}$. Due to its A dependence, CGC is easily realized in heavy nuclei.

At the LHC, where x coverage is $x \leq 10^{-4}$, modification of gluon PDF expects to have significant importance to understand the initial state of collisions.

2. Forward Calorimeter in ALICE

We propose the Forward Calorimeter (FOCAL) as the upgrade plan for the ALICE experiment [1]. The primary role of the FOCAL is to study the small- x gluons in proton and heavy nuclei by measuring the direct photons and π^0 -jet correlation at forward rapidity [2]. The detector is composed of 21 layers of tungsten (W) and silicon pads (Si), where the former and the latter serve as absorber and detector of the energy. The detail of the detector design and preliminary location of the FOCAL in the ALICE are summarized in Ref. [3]. The basic features of W+Si calorimeter have been studied with the GEANT4 simulation and are reported in Ref. [3]. The overall performances are well satisfied and fulfill the requirements.

To proceed the full simulation within the ALICE environment, the detector geometry and the composition of the detectors are fully implemented in the ALICE specific software packages called ALIROOT.

3. Single π^0 simulation and reconstruction in ALIROOT

Single π^0 simulation is performed to evaluate the reconstruction efficiency of π^0 . There are two ways for the reconstruct of π^0 utilized in this simulation. One way is the invariant mass method and this method is useful when two γ distance is larger than 2-3 cm and the energy showers of two γ are not merged into the one. The other is to use the correlation between two γ distance and the merged energy. This is useful to identify π^0 with high p_T and small two γ distance.

Figure 1 shows the π^0 reconstruction efficiency with invariant mass method as a function of the two γ distance, where the FOCAL is located at $z=450$ cm and generated π^0 p_T and rapidity are 5 GeV/c and 3, respectively. The efficiency is almost 0 for the two γ distance of 2 cm when the pad size is 1.5×1.5 cm². However, the efficiency is greatly improved when we utilize the pad size of 1×1 cm². Moreover, two γ s are perfectly separated with 1×1 cm² pad when two γ distance is larger than 3 cm.

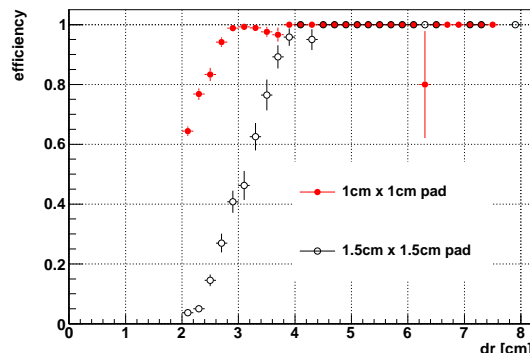


Figure 1. Reconstruction efficiency of π^0 with $p_T = 5$ GeV/c and $\eta=3$ as a function of two γ distance. Closed and open symbols correspond to the efficiency with the pad size of 1×1 cm² and 1.5×1.5 cm², respectively.

Figure 2 shows π^0 reconstruction efficiency as a function of p_T at the rapidity of 3.5. Open and closed symbols correspond to efficiencies with the invariant mass method and correlation method, respectively. The efficiency larger than 50% is achieved with FOCAL.

4. Full simulation of FOCAL and backgrounds

Full simulation has been conducted to evaluate the multiplicities and backgrounds on the FOCAL and to study the feasibility for the measurement of direct photons and π^0 with FOCAL. For the study of FOCAL performance in $p + p$ collisions, PYTHIA event generator is utilized with

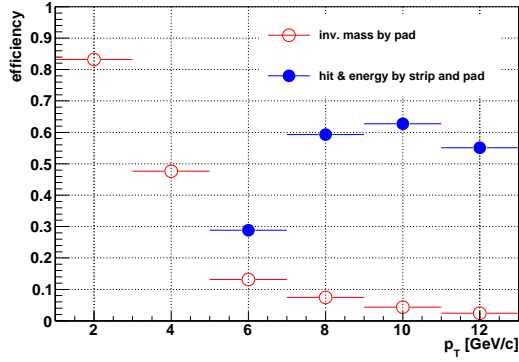


Figure 2. π^0 reconstruction efficiency as a function of p_T of π^0 at $\eta = 3.5$. Open and closed symbols correspond to the efficiency evaluated by invariant mass method and correlation method.

$\sqrt{s} = 7$ TeV [4]. The secondary backgrounds from the ALICE environments such as ALICE central detectors and forward detectors are carefully evaluated. Left of Fig. 3 shows the creation points of secondary particles, which contribute to the backgrounds on the FOCAL, where the FOCAL is located in $400 \leq z \leq 420$ cm and $r \leq 50$ cm. Right of Fig. 3 shows p_T distribution of the inclusive charged particles including primaries and secondaries with and without all the ALICE detectors. The background increases by a factor of 2 and is dominated at the p_T below 0.1 GeV/c. This doesn't affect to the FOCAL if we measure direct photon and π^0 with $p_T \geq 1$ GeV/c [3]. Further studies on feasibility for measuring direct photon and π^0 are on going.

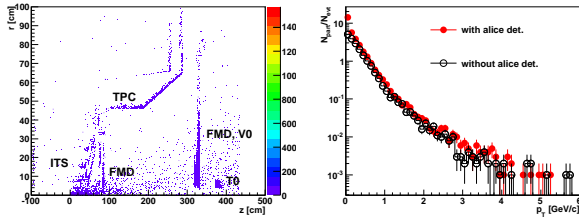


Figure 3. Left: (r, z) plot, which contributes the secondary backgrounds to FOCAL. Right: Inclusive charged particle spectrum with and without ALICE detectors. FOCAL is located in $400 \leq z \leq 420$ cm and $r \leq 50$ cm.

5. Hardware Preparation

Fabricate of the silicon pad sector by Hamamatsu co ltd has been started. Figure 4 shows the schematic view of the silicon pad. The size of the pad is 1.1 cm x 1.1 cm and 535 μm thickness. There 8 x 8 pads are implemented in one silicon wafer. The capacitance of the pad is ~ 30 pF and the dark current at the depletion voltage of 100 V is 2-10 nA.

The front end electronics for the amplification and shaping of the signal is still under the discussion. The ASIC preamplifier being developed by RIKEN, "RIK-ENDGCSP" is good candidate to cope with the high density channels and large dynamic range of 10^4 . The devel-

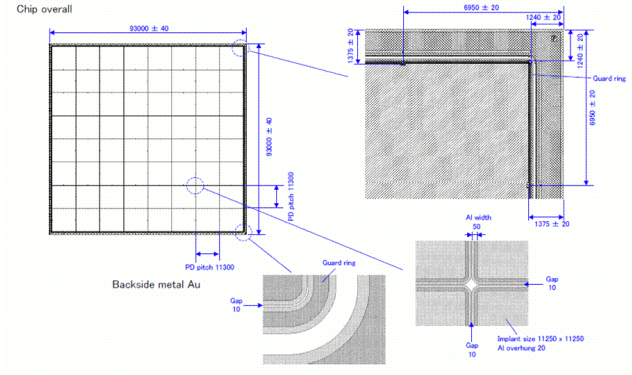


Figure 4. Design of Si pad.

opment of the dual gain preamplifier and shaper readout is on going. The mechanics to mount the silicon pad and connection to the front-end-electronics are also under investigation.

6. Summary and Outlook

The FOCAL has been proposed as one of the upgrade plans for the ALICE for the study of highly dense gluon field realized in proton and heavy nuclei at LHC energy. The detector is composed of W+Si sandwich calorimeters and is planned to be placed at the forward rapidity in the ALICE. The FOCAL is implemented in the ALIROOT for the study of detector performances under the realistic environment. Reconstruction efficiency for π^0 using pad and strips are evaluated and backgrounds to the FOCAL due to the detector services are studied for $p + p$ collisions. Feasibility study for the measurement of π^0 and prompt photon in $p + p$ and $p + A$ collisions will be studied in the future. The hardware development is also on going, especially the readout electronics to handle the large dynamic range and high density channels. First version of the ASIC preamplifier and shaper will be available in 2011.

References

- [1] ALICE Collaboration, Physics Performance Report Vol. 1 J. Phys. **G 30** (2003) 1517.
- [2] T. Gunji *et al.* CNS Ann. Rep. 2008 (2010).
- [3] Y. Hori *et al.* CNS Ann. Rep. 2009 (2011).
- [4] PYTHIA, T. Sjostrand *et al.* <http://home.thep.lu.se/~torbjorn/Pythia.html>

Performance evaluation of the Forward Calorimeter for PHENIX upgrade

T. Tsuji, H. Hamagaki, T. Gunji, Y. Hori, E. Kistenev^a, M. Chiu^a, A. Sukhanov^a, R. Seto^b,
for the PHENIX FOCAL group

Center for Nuclear Study, Graduate School of Science, University of Tokyo

^a*Physics Department, Brookhaven National Laboratory*

^b*Department of Physics and Astronomy, University of California, Riverside*

1. Introduction

The parton density inside the proton and a nucleus is described by the parton distribution function (PDF). According to results given by the HERA experiments, gluon PDF grows quickly with decreasing Bjorken's x (x_B) and gluon density becomes much larger than the valence and sea quark densities. According to Quantum chromodynamics (QCD), gluon density tends to saturate due to the balance between gluon splitting and gluon fusion at high density. Such state is called as gluon saturation [1].

At RHIC, the study of gluon distribution in heavy nuclei has been done with d+Au collision. In a heavy ion collision, the nucleus acts as an amplifier of the saturation effect because of the thickness of the nucleus. In the simple process $1 + 2 \rightarrow 3 + 4$, Bjorken's x_B of colliding partons are related to rapidity y of produced particles as,

$$x_{B1} = \frac{p_T}{\sqrt{s}}(e^{y_3} + e^{y_4}), \quad x_{B2} = \frac{p_T}{\sqrt{s}}(e^{-y_3} + e^{-y_4}), \quad (1)$$

where p_T is the transverse momentum of the scattered partons and \sqrt{s} is center-of-mass energy. These relations indicate that small x is accessible by measuring particles at forward rapidity. The BRAHMS experiment reported the suppression of charged particle yield in d+Au collisions at forward rapidity, which is consistent with the saturation of gluons at small- x [2].

The forward calorimeter (FOCAL) has been proposed to study more extensively the gluon distributions in proton and in nuclei at small x via measurements of inclusive direct photon production and of production of π^0 at forward rapidity [3, 4].

2. FOCAL for the PHENIX

The FOCAL is designed to cover the forward region. The layout of FOCAL is summarized in Table 1. Figure 1 shows

Distance from IP	44 cm
Outer Radius	31 cm
Inner Radius	18 cm
Pseudo-rapidity coverage	1 – 3
ϕ coverage	2π
Area coverage	0.65 m^2

Table 1. FOCAL layout of PHENIX

a longitudinal structure of a single FOCAL supertower. It is a silicon-tungsten sampling calorimeter, which is longitudinally composed of 3 calorimeter segments. The size of Si

readout pads is $1.5 \times 1.5 \text{ cm}^2$. The thickness of each Si pad detector is 0.5 mm and that of W absorber is 4.2 mm. Each segment has 8 radiation length. Since tungsten has a small Moliere radius (9.3 mm), two photons decayed from π^0 can be separate up to high p_T . Tungsten also has an excellent ratio of radiation and interaction lengths, which is important for electromagnetic energy measurements in the presence of heavy hadronic background. In addition, there are four sections of strip detectors with $500 \mu\text{m}$ pitch located in the first longitudinal segment to identify π^0 s to high energy even when there is an overlap of showers in the pads. This also allows discrimination of direct photons and high energy π^0 s.

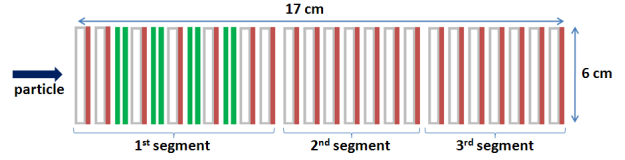


Figure 1. Longitudinal structure of a single calorimeter supertower showing the location of the three calorimetric segments. The opened boxes show Tungsten plates and Si pad detectors. The lines show Si strip detectors

3. FOCAL performance in simulation and beam test

The beam test of the FOCAL prototype was carried out with the electron and pion beam at the CERN PS (momentum range of 1–6 GeV/c) and the positron beam at the SPS (momentum range of 10–100 GeV). The energy resolution and linearity, and position resolution were studied. In order to study performance of FOCAL, we have done simulations by implementing realistic geometry and material into Geant4.

Figure 2(left) shows deposited energy from the simulation and it has good linearity. Figure 2(right) shows the ratio of the ADC value in the test beam and the deposited energy of the silicon pads from the simulation. For each electron beam energy, the value stays constant, which shows that good linearity is produced by the simulation.

Figure 3 shows the sampling fractions, which are defined as deposited energy in each segment divided by that of all segments. The filled symbols indicate simulated results and the opened symbols indicate test results. Circles show 1st segment, squares show 2nd segment and triangles show 3rd segment. According to Fig. 3, the simulated sampling fractions aren't consistent with those of the test results. At 1st segment, the simulated sampling fractions appear smaller

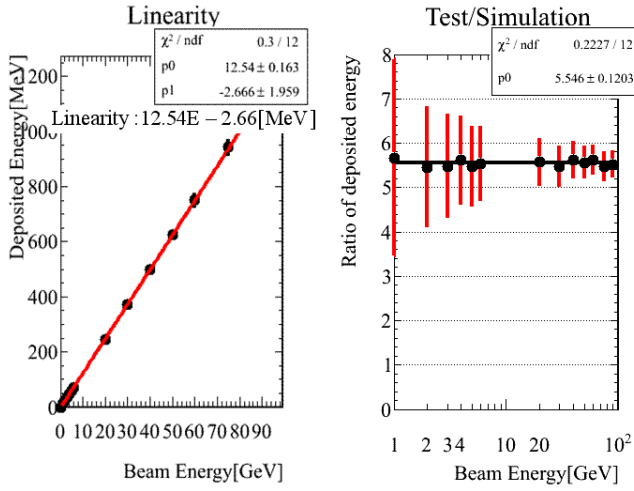


Figure 2. Left: Linearity from 1 GeV to 90 GeV in the electron beam. Right: Ratio which ADC value of test beam divided deposited energy of simulation.

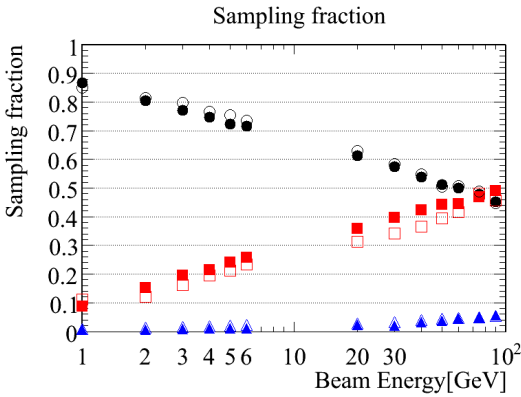


Figure 3. Sampling fraction, which is defined as deposited energy of each segment divided the total sum of the three segments. The filled ones indicate simulated results and the opened ones indicate test results. Circles show 1st segment, squares show 2nd segment and triangles show 3rd segment.

than those of test results. By contrast, simulated sampling fractions appear larger than those of test results at 2nd segment. At 3rd segment, the simulated values and values given by test results are in good agreement. These differences remain under investigation, which may be due to large cross talk signal between adjacent pads or electric noise, for example.

Figure 4 shows energy resolution. For comparison the results from simulation with that from test, constant term is sharply different. More studies need to be done with inclusion of electric noise and cross-talk.

Finally, there are some results from strip detector using π^- 50 GeV. Because strip sensors have low noise, peak of minimum ionizing particles (MIP) can be discerned from pedestal as shown Fig. 5(left). Figure 5(right) shows correlation between the hit positions; X-axis is a hit position of silicon strip detector in front of FOCAL and Y-axis is that of first silicon strip detector within FOCAL. Very clear

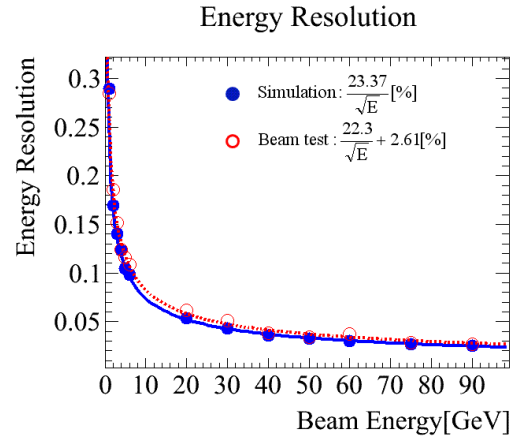


Figure 4. Energy resolution of FOCAL. The broken curve shows beam test experiment and its value is $22.3/\sqrt{E} + 2.61\%$. The solid curve shows simulation and its value is $23.37/\sqrt{E}$.

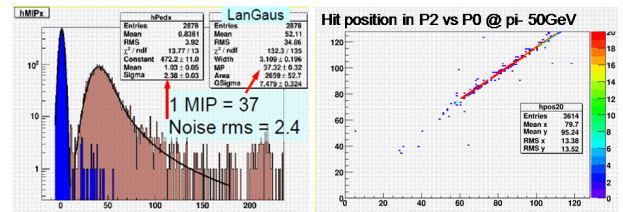


Figure 5. Left: ADC distribution of any strips. Right: Correlation of hit position between two planes of strip.

correlation is seen.

4. Summary and Outlook

FOCAL has been proposed as a PHENIX upgrade designed for the measurement of π^0 and direct γ at forward rapidity in order to study the gluon PDF in proton and nuclei at small- x . FOCAL is silicon and tungsten sampling calorimeter. We are studying basic properties of FOCAL via simulation and beam test. FOCAL has good linearity and energy resolution is $22.6\%/\sqrt{E}$. In the simulation, good linearity is reproduced and resolution is consistent except constant term. There is small difference in sampling fraction of each segment. More study will be done with inclusion of electric noise and cross-talk. In strip part analysis, MIP peak was observed and a strong correlation of the hit positions is seen between strip sensors.

References

- [1] E. Inauch, R. Venugopalan, hep-ph/0303204
- [2] I. Arsene *et al.*, for the BRAHMS collaboration, Phys. Rev. Lett **93** (2004) 242303.
- [3] E. Kistenev, Czech. J. Phys. **55** (2005) 1659.
- [4] PHENIX FOCAL
<https://www.phenix.bnl.gov/WWW/p/upgrades/focal/>.

Pulse structure dependence of the proton polarization rate

T. Kawahara, T. Uesaka^a, Y. Shimizu^b, S. Sakaguchi^b, A. Shibusawa and T. Wakui^c

Department of Physics, Toho University

^a*Center for Nuclear Study, Graduate School of Science, University of Tokyo*

^b*RIKEN (The Institute of Physical and Chemical Research)*

^c*Cyclotron and Radioisotope Center, Tohoku University*

1. Introduction

A polarized proton solid target for RI beam experiments has been developed at Center for Nuclear Study, University of Tokyo [1]. Protons are polarized through the transfer of the electron population difference in photo-excited triplet states of pentacene molecule. By this method, proton polarization of about 20% can be obtained at a low magnetic field of 0.1 T and at a relatively high temperature of 100 K. Although this target has been successfully applied to RI beam experiments [2, 3], further improvement in proton polarization is desirable for future applications.

At present, the photon number of the photo-excited light source is the bottleneck in achieving higher polarization because the photon number is fewer than the electron number of the pentacene. Simply, for increasing the photon number, the best laser light would be continuous wave. However, one problem arises that the lifetimes of the magnetic sub-levels in triplet states are different. A sublevel which has the largest population decays with the shortest lifetime. Therefore, by irradiating laser light for long time the electron polarization is decreased while the photon number is increased. Thus, the photo-excited light must be pulsed. In our system, the pulse structure is determined by the rotating speed and slit width of optical chopper.

When the duty factor, which is product of width and repetition frequency of the pulse, is increased, the polarization would be decreased by expanding the pulse width. Therefore, we examine that to what extent the proton polarization is enhanced when both the duty factor and the repetition frequency are changed.

2. Optical system

For the optical excitation of pentacene molecules, an Ar-ion laser (Coherent TSM25) with a wavelength ranging from 454.5 nm to 528.7 nm and a total maximum output power of 25 W is used. Since the output light of this laser is continuous wave (CW), the light is mechanically pulsed by using an optical chopper (Fig. 1). The frequency of laser pulse can be changed by varying rotating speed of the optical chopper. In addition the duty factor can be easily changed by shifting the overlap of two chopper blades. This optical system enables us to change the duty factor from 5 to 50%, and the repetition frequency from 0.75 to 10.5 kHz.

3. Measurement and result

As the material to be polarized, we used a single crystal naphthalene doped with pentacene (0.001mol%). The crystal size was 14 mm in diameter and 2.5 mm in thickness. Protons were polarized at a temperature of 100 K and in a

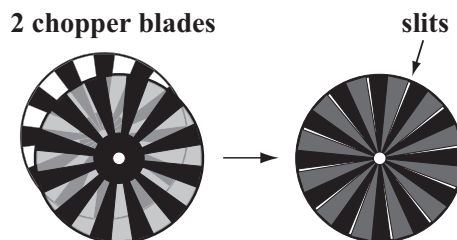


Figure 1. Optical chopper blades

magnetic field of about 80 mT.

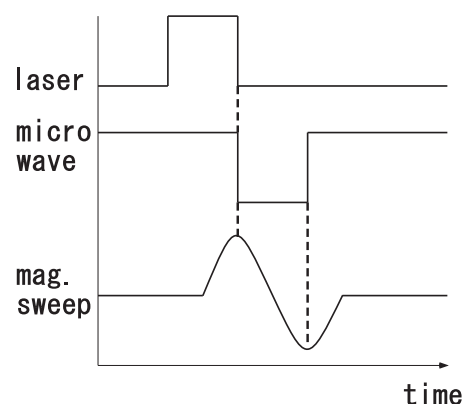


Figure 2. Time chart for polarization. When the laser irradiates the crystal, the electron polarization can be made. Just after the irradiation of laser light, the microwave irradiates and the magnetic field strength was swept in order to transfer the electron polarization to the protons.

Figure 2 shows a typical timing chart of polarization process. In the first step, the laser light irradiates the crystal. In the second step, just after the irradiation of laser light, we irradiate the microwave and sweep the magnetic field strength in order to transfer the electron polarization to the protons. These steps were repeated at a typical frequency of several kHz.

We measured polarization after 10-min build up with the pulse NMR method. This magnitude of polarization is defined as the proton polarization rate. The result is shown in Fig. 3 where the proton polarization rate is plotted as a function of the duty factor. In the previous work [1], the repetition frequency and the duty factor were 2.5 kHz and 5%, respectively. The measured data are normalized by the previous data. At the high frequency limit, the polarization rate is proportional to the duty factor. In the present works, we found that the proton polarization rate takes the maximum value when the repetition frequency and the duty factor were 10.5 kHz and 50%, respectively. The polariza-

tion rate was improved by a factor of 7.5 compared with the previous works. From this result, one can expect that the polarization is enhanced by increasing the duty factor and repetition frequency.

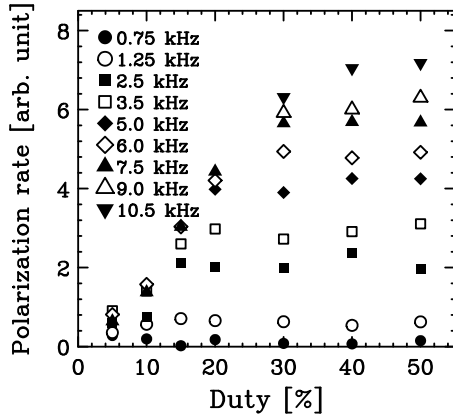


Figure 3. The polarization rate was measured by changing a duty factor and repetition frequency.

We measured the build up curve of polarization by changing the duty factor and the repetition frequency as summarized in Table 1. Measured data are shown in Fig. 4.

Table 1. The polarization conditions by changing the duty and the repetition frequency.

name	Duty	Repetition freq.
Set-5	5%	2.5 kHz
Set-15	15%	5.0 kHz
Set-30	30%	9.0 kHz
Set-50	50%	9.0 kHz

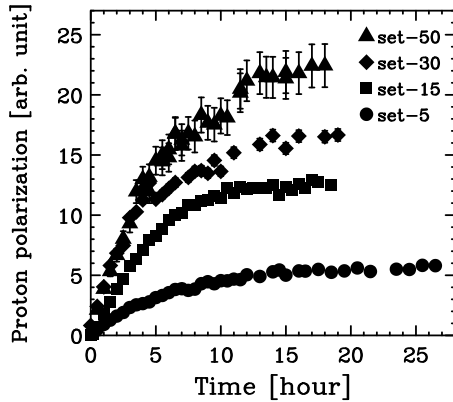


Figure 4. The build up curve of polarization measured by changing a duty factor.

The buildup curve of Fig. 4 is represented as

$$P(t) = \frac{A}{A + \Gamma} (1 - \exp(-\Gamma t)), \quad (1)$$

where A is proportional to polarization rate, and Γ is relaxation rate of polarization. The saturated polarization is described as

$$P(\infty) \propto \frac{A}{A + \Gamma}. \quad (2)$$

Therefore, the saturated polarization is determined by the balance between A and Γ . It is seen from the figure that the magnitude of saturated polarization with a duty factor of 50% (set-50) is improved by a factor of 4 compared with that of set-5.

4. Summary

We have studied the pulse structure dependence on the proton polarization rate. The proton polarization rate was measured by changing the duty factor from 5% to 50% and the repetition frequency from 0.75 kHz to 10.5 kHz. It was found that the proton polarization rate depends strongly on the pulse structure. The polarization rate was improved by a factor of 7.5 compared with the previous work by setting the duty factor to 50% and the repetition frequency to 10.5 kHz. In addition, the build up curve of polarization was measured at duty factors of 5%, 15%, 30%, and 50%. The magnitude of saturated polarization was improved by a factor of 4 compared with the previous work.

We expect that these results can be understood by considering lifetime difference among the electron photo-excited triplet states. A theoretical model which quantity deals with this polarization mechanism is now under construction.

References

- [1] T. Wakui *et al.*, Nucl. Instrum. Meth. A **550** (2005) 521.
- [2] M. Hatano *et al.*, Eur. Phys. J. A **25** (2005) 255.
- [3] S. Sakaguchi *et al.* Proceedings of ISPUN07, World Scientific (2009) 245.
- [4] M. Iinuma. Ph. D thesis, Kyoto University, (1997).

Method of pulse shape analysis for segmented Ge detectors

S. Go, S. Shimoura, E. Ideguchi, S. Ota, H. Miya, H. Baba^a.

Center for Nuclear Study, Graduate School of Science, University of Tokyo
^aRIKEN (The Institute of Physical and Chemical Research)

GRAPE consists of 18 detectors and each detector contains two planer-type Ge crystals with effective radius of 30 mm and thickness of 20 mm. Each detector is composed of a common anode between two crystals and two 3×3 cathodes. Fig.1 shows the definition of the coordinate. Carriers are generated when γ -ray interacts with Ge crystal, and move along the electric field in the crystal. Charge signal at cathode is induced by the movement of carriers and the pulse shape depend on the interaction point of γ ray. So the interaction point of γ ray can be deduced from pulse shape analysis. Our group developed the method of position extraction using the analog pulse shape technique^{1,3}.

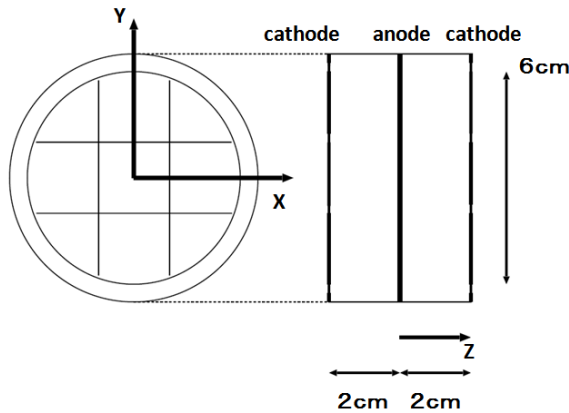


Figure 1. Schematic view of detector. Two Ge planer crystals with effective radius of 30 mm and thickness of 20 mm. Each detector has a common anode between two crystals and two 3×3 cathodes.

In 2008, we started to upgrade the system by adopting a digital signal processing (DSP) technology. The outputs from the preamplifier are digitized by 100-MHz flash ADC and are processed by digital filtering such as trapezoidal shaping, constant fraction time pick off, and so on (Fig.2). In order to add a position extraction capability to the DSP system, we are trying to find a simple algorithm. As a candidate of such algorithm, the moments of the digitized signals has been examined²). The n -th moment of the signal is expressed as:

$$\langle t \rangle_n = \frac{\sum_i t_i^n \times f(t_i)}{\sum_i f(t_i)}, \quad f(t_i) = \frac{dQ(t_i)}{dt}, \quad (1)$$

where $Q(t_i)$ denotes digitized charge from charge sensitive preamplifier, and t_i denotes digitized time. The first moment corresponds to the average of the pulse shape, the second one corresponds to RMS, and the third skewness.

In order to extract three-dimensional position, a detailed comparison between the real pulse shape and the simulated



Figure 2. DSP system consisting two 9-ch ADC and our daughter modules (TechnoAP, APU7110-A40) .

one important. The time evolution of induced charge signals can be simulated by calculating the three-dimensional electric potential and using the weighting potential proposed in the Schokley-Ramo theorem⁴). By using this theorem, the time evolution of induced charge $Q(t_i)$ is expressed as follows:

$$Q(t_i) = n_0 e \left(\phi_w(X_h(t_i), Y_h(t_i), Z_h(t_i)) - \phi_w(X_e(t_i), Y_e(t_i), Z_e(t_i)) \right), \quad (2)$$

The time at index i , which corresponds to the new time for a carrier after moving by dz from the previous position at time $i - 1$. t_i is calculated according the the following equation.

$$t_i = t_{i-1} + \frac{1 + \frac{\mu E(X(t_i), Y(t_i), Z(t_i))}{v_{sat}}}{\mu E(X(t_i), Y(t_i), Z(t_i))} dz, t_0 = 0. \quad (3)$$

n_0 is the number of carriers, e is elementary charge. The position of the carriers (electron and hole) at time t_i is denoted by $(X(t_i), Y(t_i), Z(t_i))$, which is determined by the static electric field $E(X(t_i), Y(t_i), Z(t_i))$, the mobilities μ , and saturation velocity v_{sat} , for each carrier. ϕ_w is the weighting potential. It is assumed in this simulation that the electron and the hole move along Z -direction. Pulse shapes at each segment were calculated with $dz = 1$ mm.

The extraction of the Z position was examined. From Fig 3, these pulse shapes have differnt shapes depending on the interaction points. In the case that Z is small (near from anode), the rising of pulse becomes slow because of the long elapsed time of holes. The average with time of pulse shape becomes bigger. On the other hand, when Z is

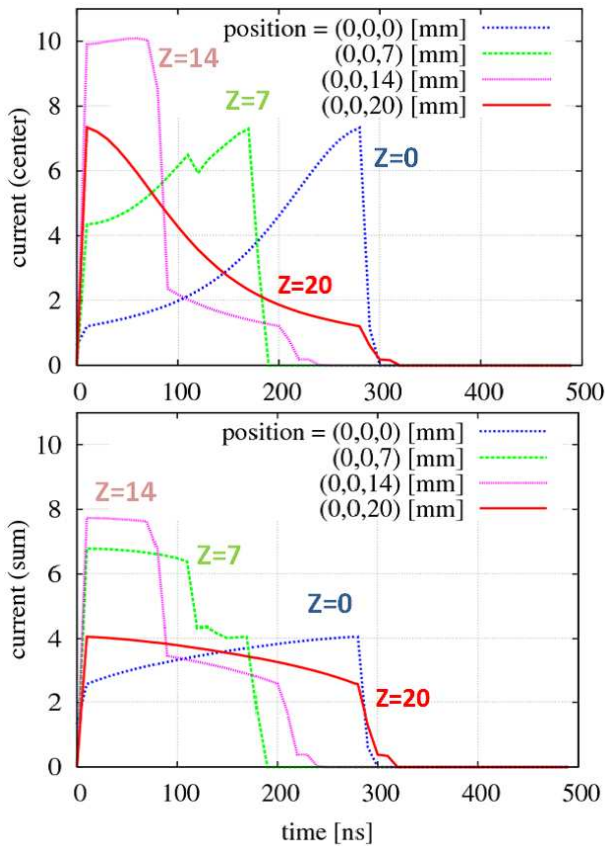


Figure 3. The example of simulated pulse shapes. In this case the γ -ray interacts at $(x, y, z) = (0, 0, Z)$. Virtual axis corresponds to time and horizontal axis to current. Pulse heights remain relatively constant. (Top Figure) Simulated pulse shapes at the center segment. (Below figure) Simulated pulse shape summed over signals from the all segments.

small (distant from anode), the rising of pulse is fast and the average with time of pulse shape becomes small. So the average of the pulse shape may have a good sensitivity to the Z position. Fig 4 shows the correlation between the mean time of the pulse at the center segment and that of the pulse summed over the all segment. From this Figure, the combination of first moment is useful to extract Z position.

The extraction of X and Y positions will also be examined with the simulated pulse shapes of non-hit segments, and also comparison between simulation and measurement is important. These approaches are now in progress.

Acknowledgment

This work is supported by the PACIFIC project, which aims at upgrading data acquisition system for high-rate RI-beam experiments.

References

- [1] S. Shimoura, Nucl. Instrum. Meth. A **525** (2004) 188.
- [2] S. Go, Am. Phys. Soc., **54**, No10 (2009) 119.
- [3] M. Kurokawa, IEEE **50** (2003) 1309.
- [4] Z. He, Nucl. Instrum. Meth. A **463** (2001) 250.

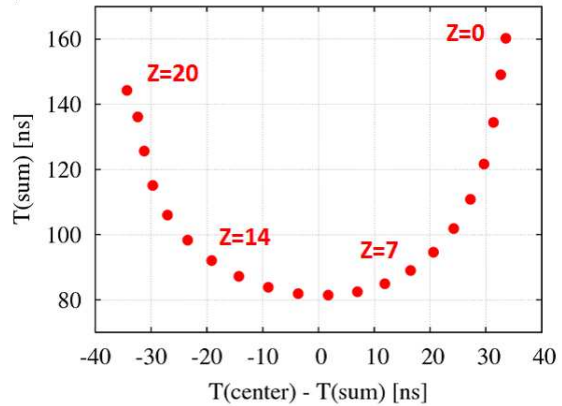


Figure 4. The simulated correlation of first moment. Each points corresponds to the interaction points $(x, y, z)=(0, 0, Z)$. The correlation between the first moment of sum and hit segment is useful to extract z-position.

Theoretical Nuclear Physics

Algebraic $N\alpha$ model (Applications for ^{12}C)

T. Yoshida^a, N. Itagaki^b and K. Katō^c

^aCenter for Nuclear Study, Graduate School of Science, University of Tokyo

^bDepartment of Physics, University of Tokyo

^cDivision of Physics, Graduate School of Science, Hokkaido University

In this report, we show that the algebraic approach can be effective method for $N\alpha$ cluster study by creating spatially extended Pauli allowed states. Here, we use $Sp(2, R)_z$ algebra to make large harmonic oscillation quanta in $SU(3)$ model space. By using this model space, we investigate the relation between monopole transition strength and symplectic structure in ^{12}C . Moreover, we apply this model space to study decay properties of excited states for ^{12}C . For this purpose, we combine $Sp(2, R)_z$ approach with complex scaling method for resonance states.

Recently, cluster structures of $N\alpha$ nuclei around α threshold region have been studied both for experimental and theoretical sides. Some of these excited states are assumed to have dilute states of relative α clusters. In ^{12}C , such kinds of 3α cluster structure appear around 3α threshold energy region as a resonance [1, 2]. In addition, dilute 4α cluster structures are also suggested in the excited states of ^{16}O near 4α threshold. Thus, the $N\alpha$ cluster studies have been focusing on larger N values. In order to see the physics around $N\alpha$ threshold, we need to use experimental α threshold energy correctly. For this purpose, we use orthogonal condition model (OCM) [3, 4, 5]. In the usual procedure of OCM, the pseudo-potential method is used where the projection operator to Pauli forbidden states is added to the original Hamiltonian. However, considering an applicability for more α clusters, we use only Pauli allowed states when we expand the wave function. Here, basis states which have large number of H.O. quanta are effectively prepared by using the $Sp(2, R)_z$ [6, 7] algebra on $SU(3)$ basis in the case of ^{12}C .

Experimentally, it is suggested that these α cluster structures appear with large monopole transition strength [8, 9, 10]. We expect that the $Sp(2, R)_z$ model is also suited to investigate the origin of the large monopole transition strength. Moreover, we need to check whether it can derive resonance states by correctly taking its boundary condition. There is a well known procedure called complex scaling method (CSM) [11] which describes resonance states. In CSM, the boundary condition of the resonance states around $N\alpha$ threshold is transformed to the regular wave functions which decay to zero as the relative α - α distances increase which is the same as that of bound states. Therefore, we can calculate resonance states by using finite number of basis set. We couple OCM generated by the $Sp(2, R)_z$ algebra and CSM. We focus on the two and three- α nuclei and convince basic properties.

Here, we mention how model space can be constructed for algebraic approach. We set harmonic oscillator quanta N_1 and N_2 for each α - α Jacobi coordinate. Basis states

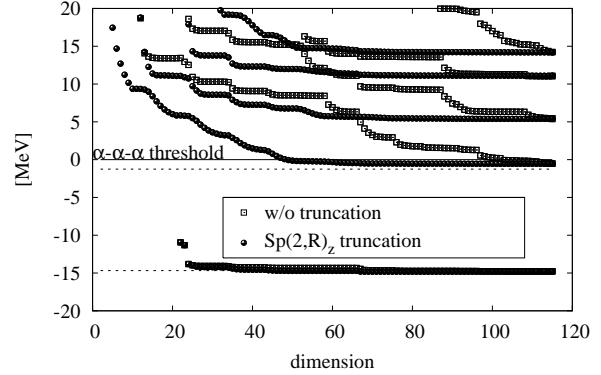


Figure 1. Energy convergence of the 3α system as a function of the number of basis states with (black dot) or without (white box) $Sp(2, R)_z$ truncation. The dotted lines are the energies obtained by using pseudo-potential method [3].

of 3α system can be specified by $SU(3)$ quanta, $N(\lambda, \mu)\rho$, where $\lambda = N_z - N_y$, $\mu = N_y$ and ρ shows the multiplicity of the states arose from the linear combination of N_1 and N_2 pairs. The 3α Pauli allowed wave functions are expanded as follows [7]:

$$U_i(r, R) = \sum_{N_1, N_2} A_{N_1, N_2}^{N(\lambda, \mu)\rho} V_{N_1, N_2}^{N(\lambda, \mu)\rho, J, K}(\vec{r}, \vec{R}), \quad (1)$$

where the index i denotes an abbreviation of the J, K and $N(\lambda, \mu)\rho$. The coefficients $A_{N_1, N_2}^{N(\lambda, \mu)\rho}$ are determined by orthogonal condition to Pauli forbidden states [4]. $V_{N_1, N_2}^{N(\lambda, \mu)\rho, J, K}(\vec{r}, \vec{R})$ is expressed by

$$\sum_{l_1, l_2} \langle N_1, l_1, N_2, l_2 | N(\lambda, \mu)\rho, J, K \rangle [u_{N_1, l_1}(\vec{r}) u_{N_2, l_2}(\vec{R})]_J. \quad (2)$$

However, simply using these basis is not convenient to describe the spatially extended states around 3α threshold. Because of the fact that the multiplicity increases as N increases, we need to use another index Λ which distinguishes the quanta of the $Sp(2, R)_z$ algebra by taking unitary transformation from ρ index. The z -index shows that this transformation acts only for z -direction. The quantum number Λ are obtained as a solution and eigenvalue of the Casimir operator of this algebra. We show the validity to use this $Sp(2, R)_z$ truncation method. As for the two-body nuclear interaction, we use α - α folding potential [12]. In the present stage, Coulomb and three-body potentials [13] are not taken into account for simplicity. In Fig. 1, we show the energy as a function of the number of basis states. When we apply the basis states sorted by $Sp(2, R)$ algebra (black dot), the energy convergence becomes much faster than the

case without it (white dot). We can see that the $Sp(2, R)_z$ algebra can be a powerful method to generate the basis sets around α threshold.

In order to investigate what causes the large monopole transition strength in ^{12}C , we see the relation between the monopole transition strength and symplectic structure. The Λ of the ground state is dominated by $\Lambda = 5/2$ configuration about 94%. This indicates that the Λ can be a good quantum number to characterize the ground state rather than $SU(3)$ quanta: $8(0, 4)$ configuration of $SU(3)$ occupies about 66% in the present calculation. The monopole operators can be also written by generators of $Sp(2, R)_z$ algebra. Therefore, it is natural to expect that the $Sp(2, R)_z$ quanta Λ has close relation to the strength of the monopole transition strength. We calculate monopole transition strength from the ground state to the excited 0^+ states. With this analysis, we confirm that the strong monopole transition is closely related to the Λ of the excited states.

As a next step, we combine this algebraic approach with CSM to treat the resonance states. Before calculating the resonance states of 3α , we check the reliability in 2α cases. Expansion of the basis states in 2α is done by the following procedure which is the same as for 3α calculation: Instead of using the pseudo-potential to project out the Pauli forbidden states, we solve the equation

$$(\hat{H} - E\hat{N})\hat{P}|\Phi\rangle = 0, \quad (3)$$

where \hat{P} is projection operator to Pauli allowed states. The complex scaling method is applied to the above equation, and we have

$$U_\theta \hat{P}(\hat{H} - E\hat{N})\hat{P}U_{-\theta}|\Phi_\theta\rangle = 0, \quad (4)$$

where U_θ is the complex scaling transformation. We compare it with the pseudo-potential method. Here, we use several parameter sets for CSM; the width parameter b of the wave function is set to be 1.4 fm and 1.8 fm. We obtained a good agreement with the pseudo potential method up to $\theta \sim 25^\circ$. However, we notice here that the overlap matrix element $\langle l, m; r, v | U_\theta | l, n; r, v_0 \rangle$ has large numerical oscillation as n increase under large θ conditions. Therefore, it is difficult to assure the numerical precision in our algebraic approach for large θ .

The similar calculation can be performed for the 3α cluster. In the present calculation, we check whether the ground state and some excited states are invariant under the rotation of complex scaling angle θ to find resonance states. In Fig. 2, the complex energy of 0^+ states are shown for different width parameters b and rotation angle θ . We can find complex energies around -7.3 MeV and 0.95 MeV are almost invariant under the deviation of these parameters. These states correspond to the ground and second 0^+ states. Due to the limitation of θ values which comes from the numerical reason (same as in the 2α case), the position of the third 0^+ state is not clearly specified. However, almost stable point around $\theta = 3^\circ$ has good correspondence with the energy (~ 5 MeV) given by bound state approximation. This state has linear chain configuration (The occupancy is about 45% in the present calculation).

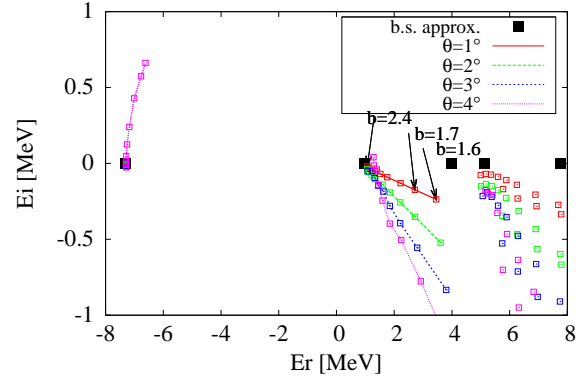


Figure 2. Complex energies of 0^+ states in ^{12}C . Here, b -trajectory for each complex rotation angle θ are shown around second 0^+ state.

In conclusion, we have constructed algebraic approach for $N\alpha$ nuclei which is applicable for $N = 3$ system. We have confirmed that the strong monopole transition strength in ^{12}C is related to the $Sp(2, R)_z$ quanta Λ . We have also suggested that the use of $Sp(2, R)_z$ algebra to make the Pauli allowed states is effective even if we treat resonance states by using CSM. To ensure it, we calculated two and three α systems. The result shows that we can use this procedure for 3α cluster, if we take care of the complex rotation angle θ and the oscillation quanta.

References

- [1] F. Hoyle, *Astrophys. J. Suppl.* **1**, 121 (1954).
- [2] A. Tohsaki *et al.*, *Phys. Rev. Lett.* **87**, 192501 (2001).
- [3] H. Horiuchi, *Prog. Theor. Phys.* **53**, 447 (1975).
- [4] H. Horiuchi, *Prog. Theo. Phys.* **58**, 204 (1989).
- [5] T. Yamada *et al.*, *Prog. Theor. Phys.* **120**, 6 (2008).
- [6] F. Arickx, *Nucl. Phys. A* **268**, 347 (1976).
- [7] K. Katō and H. Tanaka, *Prog. Theor. Phys.* **81**, 841 (1989).
- [8] B. F. Bayman and A. Bohr, *Nucl. Phys.* **9**, 596 (1959).
- [9] T. Kawabata *et al.*, *Phys. Lett. B*, **646**, 6 (2007).
Y. Sasamoto *et al.*, *Mod. Phys. Lett. A* **21**, 2393 (2006).
- [10] T. Yoshida, N. Itagaki and T. Otsuka, *Phys. Rev. C* **79**, 034308 (2009).
- [11] J. Aguilar and J. M. Combes, *Commun. Math. Phys.* **22**, 269 (1971). E. Balslev and J. M. Combes, *Commun. Math. Phys.* **22**, 280 (1971).
- [12] E. W. Schmidt and K. Wildrmuth, *Nucl. Phys.* **26**, 463 (1961).
- [13] C. Kurokawa and K. Katō, *Nucl. Phys. A* **738**, 455 (2004).

Activities of Nuclear Shell-Model Studies in CNS

N. Shimizu^a, T. Otsuka^{a,b,c}, and Y. Utsuno^d

^a*Department of Physics, Graduate School of Science, University of Tokyo*

^b*Center for Nuclear Study, Graduate School of Science, University of Tokyo*

^c*National Superconducting Cyclotron Laboratory, Michigan State University*

^d*Advanced Science Research Center, Japan Atomic Energy Agency*

1. Introduction

Our group has actively performed nuclear shell-model calculations to investigate nuclear structure and its underlying physics. These theoretical works have been supported by the CNS, RIKEN Nishina Center, and the Department of Physics, University of Tokyo [1]. As a part of these activities, we introduced a PC cluster consisting of 4 nodes and 8 Quad-core Xeon CPUs. We summarize major achievements of our activities in the following sections individually.

2. Code Development for the Monte Carlo Shell Model

The Monte Carlo shell model method (MCSM) has been developed since 1995 [2] in order to avoid the difficulty of diagonalizing the Hamiltonian matrix which has very large dimensions in the nuclear shell model. The MCSM has been successfully applied in the nuclear-structure study up to the medium-heavy nuclei, including exotic nuclei [3].

As its applicability is enlarged, the MCSM code has been extended accordingly. For instance, the MCSM was recently used to perform *ab initio* calculations. Nevertheless, the original MCSM code has some limitations that restrict its use in more up-to-date nuclear-structure calculations. In particular, it can handle only isospin-conserving interactions. In most *ab initio* calculations, the isospin symmetry is not assumed to be conserved.

In order to overcome these limitations and fully utilize modern computational technologies, we initiated a project to write a novel MCSM code from scratch. The new MCSM code is equipped with the following features:

1. The code is written in modern Fortran 95.
2. Hybrid parallel computing based on Message Passing Interface library (MPI) and OpenMP is used.
3. It can handle isospin-breaking interaction.
4. It can evaluate many physical quantities which are important in *ab initio* calculations (*e.g.* root-mean-square radius).
5. The code incorporates a new algorithm for the calculation of the Hamiltonian matrix elements.

At the fiscal year 2009, the new code has been partially completed and enabled us to calculate the Hamiltonian matrix elements using the angular-momentum and parity projection for any Slater determinant basis, and the eigenvalue of the Hamiltonian can be obtained with those matrix elements. Since calculating the Hamiltonian matrix element is the most time-consuming part in MCSM, it is worth examining its computing performance by comparing with the

original code. These benchmark results were reported in Ref. [4]. Afterward, this code played an essential role to develop a new framework of performing large-scale shell-model calculations [5].

3. Monopole Interaction and Shell Evolutions

We investigated novel simple properties of the monopole component of the effective nucleon-nucleon interaction and proposed the *monopole-based universal interaction*, V_{MU} [6]. The V_{MU} consists of two terms. The first term is the Gaussian central force, and should contain many complicated processes including multiple meson exchanges. The second one is the tensor force comprised of π and ρ meson exchanges [7].

Figure 1 shows applications of V_{MU} to the shell evolution assuming a filling configuration. Figure 1 (a) depicts neutron single-particle energies (SPEs) around $N=20$ for $Z=8\sim 20$. Starting from SPEs at $Z=8$, one sees the evolution of the $N=20$ gap, in a basically consistent manner with other shell-model studies [8, 9]. While the change is monotonic without the tensor force, the tensor force produces a sharp widening from $Z=8$ to 14, and then stabilizes the gap towards $Z=20$. It is worth mentioning that the normal SPEs arise at $Z=20$, whereas at $Z=8$ the inversion between $0f_{7/2}$ and $1p_{3/2}$ occurs and $0d_{3/2}$ is rather close to $1p_{3/2}$, leaving the major gap at $N=16$. The central force lowers the neutron $0d_{3/2}$ SPE more than the $0f_{7/2}$ SPE as protons occupy the *sd*-shell due to larger overlaps, yielding a wide $N=20$ gap at ^{40}Ca . The $N=20$ gap at $Z\sim 14$ is, however, largely due to the tensor force, and becomes smaller if protons are excited to $0d_{3/2}$.

Figure 1 (b) shows proton SPEs for the $Z=28$ core of $^{68-78}\text{Ni}$, by starting from empirical values at $N=40$. The SPE of $1p_{1/2}$ is not known empirically, and is placed above $1p_{3/2}$ by the energy difference predicted by the GXPFI1A interaction. The orbit $0f_{5/2}$ crosses $1p_{3/2}$ at $N=45$ consistently with a recent experiment, and the $0f_{7/2}$ - $0f_{5/2}$ splitting is reduced by 2 MeV from $N=40$ to 50. For both, the tensor force plays crucial roles. This lowering of $0f_{5/2}$ is seen in other shell model results, while the change is about a half of the present value.

Figure 1 (c) shows neutron SPEs relative to $0d_{5/2}$ on top of ^{90}Zr - ^{100}Sn , starting from empirical values at $Z=40$ obtained by averaging with spectroscopic factors. The lowering of $0g_{7/2}$ is remarkable. If there were no tensor-force effects, $0g_{7/2}$ and $0h_{11/2}$ do not repel, ending up with quite a different shell structure for ^{100}Sn , making this nucleus much softer. The closer spacing of $0g_{7/2}$ and $0d_{5/2}$ in ^{101}Sn seems to be seen experimentally.

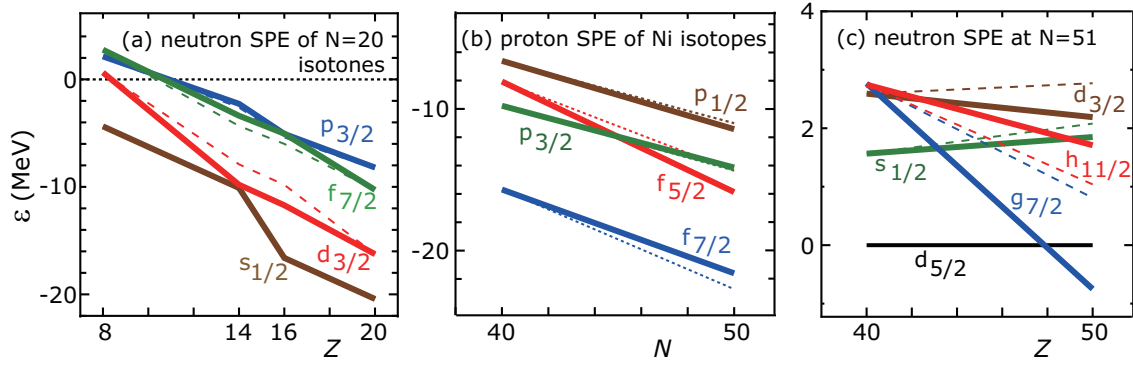


Figure 1. (color online) Single-particle energies calculated by V_{MU} interaction. The dashed lines are obtained by the central force only, while the solid lines include both the central force and the tensor force. Some states, *e.g.* $0f_{7/2}$ in (b), are hole states. Taken from [6].

The V_{MU} produces a variety of the shell evolution, connecting stable and exotic nuclei, *e.g.*, exotic Ne-Mg with ^{40}Ca , ^{68}Ni with exotic ^{78}Ni , and ^{90}Zr with exotic ^{100}Sn . The shell structure appears to vary considerably in exotic nuclei.

4. Beta-Decay of K Isotopes beyond $N = 28$

One-body potentials such as the Woods-Saxon potential have been successful in describing the shell structure of near-stable nuclei. The one-body picture always gives a smooth and monotonic change in the shell structure as the number of nucleons varies. On the other hand, the shell-model interaction V_{MU} , which was discussed in Sect.3, could cause a different behavior in very neutron-rich regions. It is thus of great interest to find such a manifestation of shell evolution.

The V_{MU} predicts the proton shell evolution to be quite different from that predicted by the potential picture. The $1s_{1/2}$ orbit moves above $0d_{3/2}$ at $N = 28$, and it goes down below $0d_{3/2}$ at $N = 32$, where $1p_{3/2}$ is fully filled. This is an example of nonmonotonic shell evolution, which is never given by the one-body picture. If non-monotonic shell evolution occurs, the ground state of ^{51}K must be $3/2^+$. Although there is no direct measurement of the spin/parity of ^{51}K , we have found that it is highly likely that the ground state is $3/2^+$. Our finding is supported by the good agreement between the β decay properties observed experimentally and those obtained theoretically [10, 11]. The experimental decay pattern cannot be explained from the $1/2^+$ state of ^{51}K .

References

- [1] Grant-in-Aid for Scientific Research (20244022) from the Ministry of Education, Science, Sport, Culture and Technology.
- [2] M. Honma, T. Mizusaki, and T. Otsuka, Phys. Rev. Lett. **75**, 1284 (1995).
- [3] T. Otsuka, M. Honma, T. Mizusaki, N. Shimizu, and Y. Utsuno, Prog. Part. Nucl. Phys. **46**, 319 (2001).

- [4] N. Shimizu, Y. Utsuno, T. Abe, and T. Otsuka, RIKEN Accel. Prog. Rep. **43**, 46, (2010).
- [5] N. Shimizu, Y. Utsuno, T. Mizusaki, T. Otsuka, T. Abe, and M. Honma, Phys. Rev. C **82**, 061305(R) (2010).
- [6] T. Otsuka, T. Suzuki, M. Honma, Y. Utsuno, N. Tsunoda, K. Tsukiyama, and M. H.-Jensen, Phys. Rev. Lett. **104**, 012501 (2010).
- [7] T. Otsuka, T. Suzuki, R. Fujimoto, H. Grawe and Y. Akaishi, Phys. Rev. Lett. **95**, 232502 (2005).
- [8] Y. Utsuno, T. Otsuka, T. Mizusaki and M. Honma, Phys. Rev. C **60**, 054315 (1999).
- [9] F. Nowacki and A. Poves, Phys. Rev. C **79**, 014310 (2009).
- [10] Y. Utsuno, T. Otsuka, B. A. Brown, M. Honma, and T. Mizusaki, RIKEN Accel. Prog. Rep. **43**, 44 (2010).
- [11] Y. Utsuno, T. Otsuka, B. A. Brown, M. Honma, and T. Mizusaki, AIP Conf. Proc. **1120**, 81 (2009).

Other Activities

The 8th CNS-EFES Summer School (CNS-EFES09)

H. Yamaguchi, H. Hamagaki, N. Itagaki^a, S. Kubono, T. Nakatsukasa^b, S. Ota, T. Otsuka^a,
H. Sakai^a, S. Shimoura, and T. Suzuki^c

Center for Nuclear Study, Graduate School of Science, University of Tokyo

^a*Department of Physics, Graduate School of Science, University of Tokyo*

^b*Nishina Center, RIKEN (The Institute of Physical and Chemical Research)*

^c*Department of Physics, Nihon University*

The 8th CNS-EFES International Summer School (CNS-EFES09) was organized jointly by the Center for Nuclear Study (CNS), the University of Tokyo, and the Japan Society for the Promotion of Science (JSPS) Core-to-Core Program “International Research Network for Exotic Femto Systems (EFES)”, in the period of Aug. 26 – Sep. 1, 2009. The summer school was held at the Nishina hall in the Wako campus of RIKEN and at the Koshiba hall in the Hongo campus, the University of Tokyo. This summer school was the eighth one in the series which aimed at providing graduate students and postdocs with basic knowledge and perspectives of nuclear physics. It consisted of lectures by leading scientists in the fields of both experimental and theoretical nuclear physics. Each lecture started with an introductory talk from the fundamental point of view and ended with up-to-date topics in the relevant field.

The lecturers and the lecture titles are listed below.

- M.H. Jensen (Oslo)** “Nuclear interactions and the shell model”
- C. Bertulani (Texas A & M Commerce)** “Coulomb excitation of exotic beams”
- P. van Duppen (Leuven)** “Nuclear structure studies along $Z=28$ and 82 closed proton shells using radioactive ion beams”
- S. Shimoura (CNS, Tokyo)** “Reactions of RI beams for studying exotic nuclei”
- H. Horiuchi (RCNP, Osaka)** “Coexistence of cluster states and mean-field states”
- N. Ishii (Tokyo)** “Hadronic interactions in lattice QCD”
- H. Sakurai (Nishina Center, RIKEN)** “RIBF project – present status and perspectives–”
- K. Makishima (Tokyo/RIKEN)** “Highlights from recent cosmic X-ray observations”
- T. Kawabata (Kyoto)** “Alpha inelastic scattering and cluster structures in light nuclei”
- T. Gunji (CNS, Tokyo)** “Experimental studies of hot and dense QCD medium in relativistic heavy ion collisions”

This year, 100 participants, including 10 lecturers from 10 countries, attended the school. Three lecturers and 27

participants were from foreign institutes, and 5 participants were foreign researchers belonging to domestic institutes.

Five lectures on Aug. 27 were held at the Koshiba hall in the Hongo campus and were broadcasted via the Internet. The student and postdoc sessions were also held in the school. 21 talks and 15 posters were presented by graduate students and postdocs. Attendances communicated each other in the free discussion time between the lectures and in the welcome and farewell parties with a relaxed atmosphere.

All information concerning the summer school is open for access at the following URL:

<http://www.cns.s.u-tokyo.ac.jp/index.php?Events/CNSEFES/2009>

This summer school was supported in part by the International Exchange Program of the Graduate School of Science, the University of Tokyo. The financial support was indispensable to organize this summer school successfully. The organizers deeply appreciate various accommodations provided by RIKEN Nishina center for the school. They are also grateful to administration staffs of the CNS and the Graduate School of Science for their helpful supports. They thank graduate students and postdocs in the CNS for their dedicated efforts. Finally, the organizers acknowledge all the lecturers and participants for their contributions to this summer school.

Laboratory Exercise for Undergraduate Students

S. Ota, K. Yako, H. Tokieda, K. Ozawa^a and S. Shimoura

Center for Nuclear Study, Graduate School of Science, University of Tokyo

^aDepartment of Physics, University of Tokyo

Nuclear scattering experiments were performed as a laboratory exercise for undergraduate students of the University of Tokyo. This program was aiming at providing undergraduate students with an opportunity to learn how to study subatomic physics by using an ion beam from an accelerator. In 2009, 31 students joined this program.

The four beam times were scheduled in the second semester for third-year students, and 8 (or 7) students participated in each beam time. The experiment was performed at the RIKEN accelerator research facility (RARF) using a 26-MeV alpha beam accelerated by the AVF cyclotron. The alpha beam extracted from the AVF cyclotron was transported to the CRIB beam line in the E7 experimental hall. In each beam time, the students were divided into two groups and took one of the following two subjects:

1. Size of a nucleus through the measurement of elastic scattering on ^{197}Au .
2. Deformation of nuclei through the measurement of gamma rays emitted in the cascade decay of highly excited ^{154}Gd and ^{184}Os .

Before the experiment, the students learned the basic handling of the semiconductor detectors and electronic circuits at the Hongo campus, and attended a radiation safety lecture at RIKEN. They also joined a tour to the RI beam factory at RIKEN.

In the $\alpha+^{197}\text{Au}$ measurement, α particles scattered from the Au target with a thickness of 1.42 mg/cm² were detected by a silicon PIN-diode located 11 cm away from the target. A collimator with a diameter of 6 mm was attached on the silicon detector. The energy spectrum of the scattered particles was recorded by a multi-channel analyzer (MCA) system. The beam was stopped by a Faraday cup in the scattering chamber. The cross section for the alpha elastic scattering was measured in the angular range of $\theta_{\text{lab}} = 25 - 160^\circ$.

The measured cross section was compared with the calculated cross section for the Rutherford scattering as shown in Fig. 1. The cross section was also analyzed by the potential model calculation, and the radius of the gold nucleus was discussed. Some students obtained the radius of 10 fm by using a classical model where the trajectory of the α particle in the nuclear potential is obtained by the Runge-Kutta method. Others tried to understand the scattering process by calculating the angular distribution by the distorted wave Born approximation with a Coulomb wave function and a realistic nuclear potential.

In the measurement of the rotational bands, excited states in ^{154}Gd and ^{184}Os nuclei were populated by the $^{152}\text{Sm}(\alpha,2n)$ and $^{182}\text{W}(\alpha,2n)$ reactions, respectively. The

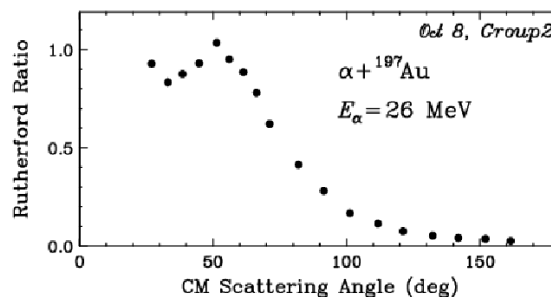


Figure 1. Ratio of the measured cross section for the $\alpha+^{197}\text{Au}$ elastic scattering to the Rutherford scattering cross sections.

gamma rays emitted from the cascade decay of the rotational bands were measured by a high purity germanium detector located 50 cm away from the target. The energies of the gamma rays were recorded by the MCA system. The gain and the efficiency of the detector system had been calibrated with standard gamma-ray sources of ^{22}Na , ^{60}Co , ^{133}Ba , and ^{137}Cs . The typical spectra of the gamma rays from the cascade decay of the rotational bands in ^{154}Gd and ^{184}Os are shown in Fig. 2. The gamma rays from the 12+ 10+ and 10+ 8+ decay in ^{154}Gd and ^{184}Os were successfully identified. Based on the energies of the gamma rays, the moment of inertia and the deformation parameters of the excited states were discussed by using a classical rigid rotor model and a irrotational fluid model. The students found that the reality lies between the two extreme models. The initial population among the levels in the rotational band was also discussed by taking the effect of the internal conversion into account.

We believe this program was very impressive for the students. It was the first time for most of the students to use large experimental equipments. They learned basic things about the experimental nuclear physics and how to extract physics from the data. The authors would like to thank Dr. Y. Uwamino, Prof. Y. Sakurai, Dr. H. Otsu, Dr. N. Aoi, the CNS accelerator group, and the RARF cyclotron crew for their helpful effort in the present program.

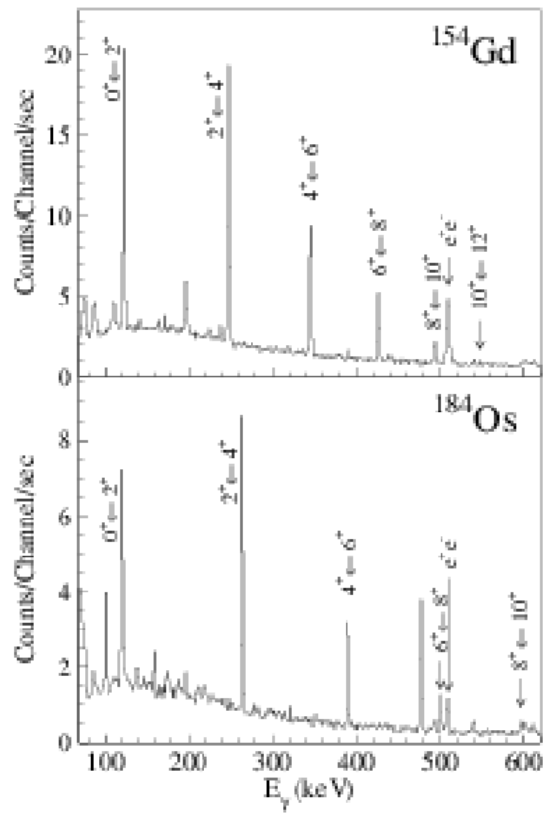


Figure 2. Typical spectra of the gamma rays from $\alpha+^{152}\text{Sm}$ and ^{182}W

Appendices

**Symposium, Workshop, Seminar, PAC and
External Review**

CNS Reports

Publication List

Talks and Presentations

Personnel

Symposium, Workshop, Seminar, Colloquium, and PAC

A. Symposium

1. The International Symposium on Origin of Matter and Evolution of Galaxies 2010 (OMEG2010)

March 8 – 10, 2010, Osaka, Japan

This is the 10th international symposium of nuclear astrophysics, which started in 1988 by INS (predecessor of CNS) together with RIKEN. It was hosted this time by seven institutions; Research Center for Nuclear Physics, Osaka University (RCNP), RIKEN Nishina Center (RNC), Center for Nuclear Study, University of Tokyo (CNS), Division of Theoretical Astrophysics, National Astronomical Observatory of Japan (NAO), High Energy Accelerator Research Organization (KEK), Japan Atomic Energy Agency (JAEA), Konan University.

The symposium was participated by 120 researchers, including 28 people from outside of Japan. Special emphasis was placed this time on the weak interaction as well as the electro-magnetic interaction for astrophysics. The symposium proceedings will be published in a book of AIP conference series.

Organizing committee was compromised of I. Tanihata (RCNP, chair), T. Kishimoto (RCNP, co-chair), T. Kajino (NAOJ, co-chair), S. Kubono (CNS, co-chair), W. Aoki (NAOJ), S. Chiba (JAEA), K. Kato (Hokkaido), Y. Fujita (Osaka), H. Miyatake (KEK), T. Motobayashi (RIKEN), S. Nishimura (RIKEN), K. Nomoto (IPMU), A. Tamii (RCNP), H. Toki (RCNP), and H. Utsunomiya (Konan), T. Hayakawa (JAEA, scientific secretary), H. J. Ong (RCNP, scientific secretary), and T. Shima (RCNP, scientific secretary)

B. Workshop

1. Arctic FIDIPRO-EFES workshop

April 20–24, 2009, Saariselka, Finland

Topics of the workshop covered nuclear structure theory and experiments with special focus on future developments. On the theoretical side, new developments in describing nuclei within the energy-density-functional and shell-model methods were discussed, with a particular emphasis on structure of exotic nuclei.

On the experimental side, the physics opportunities of the upgraded facilities at JYFL and emerging opportunities at other facilities like ISOLDE, SPIRAL2, RIKEN and FAIR were discussed. The upgrades at JYFL consists of the new recoil separator MARA in the present laboratory and the upgraded IGISOL facility to be located in the extension building of the experimental hall served also by the high-intensity proton beams from the new MC30 cyclotron. The symposium was hosted by University of Jyväskylä and TORIJIN

2. EFES workshop for “ab-initio calculations and nuclear forces”,

October 12, Hilton Waikoloa Village, Hawaii, USA

The workshop was hosted by JUSTIPEN and TORIJIN

3. JUSTIPEN-EFES workshop on unstable nuclei,

December 7–9, 2009, RIKEN, Japan

The workshop was hosted by JUSTIPEN and TORIJIN

C. CNS Seminar

1. “Low-lying Proton Intruder State in ^{13}B ”,

S. Ota (Center for Nuclear Study, the University of Tokyo) July. 21th, 2009.

2. “Measurement of Low-mass Vector Mesons in Hot-Medium created by Relativistic Heavy-Ion Collisions”

Y. Tsuchimoto (Center for Nuclear Study, the University of Tokyo) Sept. 8th, 2009.

3. “Recent results on the $^{10}\text{B}(p,\alpha)^7\text{Be}$ and $^{11}\text{B}(p,\alpha)^8\text{Be}$ reactions studied by means of the THM”

S. Romano (Univ. of Catania) Dec. 17th, 2009.

4. “Effects of distortion of the intercluster motion in light nuclei”
G. Pizzone (INFN - LAS) Dec. 17th, 2009.
5. “Nuclear Astrophysics at Catania”
S. Cherubini (Univ. of Catania) Dec. 17th, 2009.
6. “Presolar grains from meteorites: a new window to stars”
S. Amari (Washington University, St. Louis, USA) Mar. 12th, 2010.
7. “The measurement of $^{21}\text{Na}+\alpha$ in inverse kinematics and the $^{21}\text{Na}(\alpha,p)$ stellar reaction rate”
Dam Nguyen Binh (CNS, Univ. of Tokyo) Mar. 30th, 2010.

E. Program Advisory Committee for Nuclear-Physics Experiments at RI Beam Factory

1. The 5th Program Advisory Committee (NP-PAC) meeting for Nuclear Physics Experiments at RI Beam Factory
Date: June 18–19, 2009
Place: Conference room, 2F RIBF building
2. The 6th Program Advisory Committee (NP-PAC) meeting for Nuclear Physics Experiments at RI Beam Factory
Date: December 3–4, 2009
Place: Conference room, 2F RIBF building

CNS Reports

- #79** “Deuteron beam polarimeter in the Nuclotron ring and analyzing power for the $d-p$ elastic scattering at 88MeV”
T. Uesaka, K. Suda, P. K. Kurilkin, V. P. Ladygin, Yu. V. Gurchin, A. Yu. Isupov, K. Itoh, M. Janek, J. T. Karachuk,
T. Kawabata, A. N. Khrenov, A. S. Kiselev, V. A. Kizka, J. Kliman, V. A. Krasnov, A. N. Livanov, Y. Maeda,
A. I. Malakhov, V. Matousek, M. Morhach, S. M. Piyadin, S. G. Reznikov, S. Sakaguchi, H. Sakai, Y. Sasamoto,
K. Sekiguchi, I. Turzo, and T. A. Vasiliev, May. 2009.
- #80** “CNS Annual Report 2007”,
edited by E. Ideguchi, Aug. 2009.
- #82** “Computer modelling of Electromagnetic Fields for RIKEN AVY Cyclotron”,
A. S. Vorozhtsov, S. B. Vorozhtsov, S. Watanabe, S. Kubono
- #83** “CNS Annual Report 2008”,
edited by S. Michimasa, Feb. 2010.

Publication List

A. Original Papers

1. K. Aamodt, et al. for the ALICE Collaboration: “First proton+proton collisions at the LHC as observed with the ALICE detector-Measurement of the charged-particle pseudorapidity density at $\sqrt{s} = 900$ GeV”, *Eur. Phys. J.* **C65**, 111-125, 2010,
2. K. Aamodt, et al. for the ALICE Collaboration: “Alignment of the ALICE Inner Tracking System with cosmic-ray tracks”, *JINST*, **5**, PO3003, 2010
3. A. Adare, et al. for the PHENIX Collaboration: “Enhanced production of direct photons in Au+Au collisions at $\sqrt{s_{NN}} = 200$ GeV and implications for the initial temperature”, *Phys. Rev. Lett.* **104**, 132301, 2010
4. A. Adare, et al. for the PHENIX Collaboration: “Detailed measurement of the e^+e^- pair continuum in $p + p$ and Au+Au collisions at $\sqrt{s_{NN}} = 200$ -GeV and implications for direct photon production”, *Phys. Rev. C* **81**, 034911, 2010
5. A. Adare, et al. for the PHENIX Collaboration: “Double Helicity Dependence of Jet Properties from Dihadrons in Longitudinally Polarized $p + p$ Collisions at $\sqrt{s} = 200$ -GeV”, *Phys. Rev. D* **81**, 012002, 2010
6. S. Afanasiev, et al. for the PHENIX Collaboration: “Systematic Studies of Elliptic Flow Measurements in Au+Au Collisions at $\sqrt{s_{NN}} = 200$ -GeV”, *Phys. Rev. C* **80**, 024909, 2009
7. S. Adanasiev, et al. for the PHENIX Collaboration: “High- p_T π^0 Production with Respect to the Reaction Plane in Au + Au Collisions at $\sqrt{s_{NN}} = 200$ -GeV”, *Phys. Rev. C* **80**, 054907, 2009
8. S. Adanasiev, et al. for the PHENIX Collaboration: “Kaon interferometric probes of space-time evolution in Au+Au collisions at $\sqrt{s_{NN}} = 200$ -GeV”, *Phys. Rev. Lett.* **103**, 142301, 2009
9. A. Adare, et al. for the PHENIX Collaboration: “Measurement of Bottom versus Charm as a Function of Transverse Momentum with Electron-Hadron Correlations in $p + p$ Collisions at $\sqrt{s} = 200$ GeV”, *Phys. Rev. Lett.* **103**, 082002, 2009
10. A. Adare, et al. for the PHENIX Collaboration: “Photon-Hadron Jet Correlations in $p + p$ and Au+Au Collisions at $\sqrt{s} = 200$ -GeV”, *Phys. Rev. C* **80**, 024908, 2009
11. S. Afanasiev, et al. for the PHENIX Collaboration: “Photoproduction of J/ψ and of high mass e^+e^- in ultra-peripheral Au+Au collisions at $\sqrt{s_{NN}} = 200$ -GeV”, *Phys. Lett. B* **679**, 321-329, 2009
12. A. Adare et al. (for the PHENIX Collaboration): “The Polarized gluon contribution to the proton spin from the double helicity asymmetry in inclusive π^0 production in polarized $p + p$ collisions at $\sqrt{s} = 200$ -GeV”, *Phys. Rev. Lett.* **103**, 012003, 2009
13. T. Tamagawa, A. Hayato, F. Asami, K. Abe, S. Iwamoto, S. Nakamura, A. Harayama, T. Iwahashi, S. Konami, H. Hamagaki, Y.L. Yamaguchi, H. Tawara, and K. Makishima: “Development of Thick-foil and Fine-pitch GEMs with a Laser Etching Technique”, *Nucl. Instrum. Meth. in Physics Research A* **608** (2009) 390 – 396.
14. H. Yamaguchi, Y. Wakabayashi, S. Kubono, G. Amadio, H. Fujikawa, T. Teranishi, A. Saito, J.J. He, S. Nishimura, Y. Togano, Y.K. Kwon, M. Niikura, N. Iwasa, K. Inafuku and L.H. Khiem: “Low-Lying Non-Normal Parity States in ^8B measured by Proton Elastic Scattering on ^7Be ”, *Phys. Lett. B* **672** (2009) 230 - 234
15. J. J. He, S. Kubono, T. Teranishi, J. Hu, M. Notani, H. Baba, S. Nishimura, J. Y. Moon, M. Nishimura, H. Iwasaki, Y. Yanagisawa, N. Hokoiva, M. Kibe, J. H. Lee, S. Kato, Y. Gono, and C. S. Lee: “Investigation of excited states in ^{22}Mg via resonant elastic scattering of $^{21}\text{Na}+p$ and its astrophysical implications”, *Phys. Rev. C* **80** (2009) 015801-6
16. Y. Ichikawa, T.K. Onishi, D. Suzuki, H. Iwasaki, T. Kubo, V. Naik, A. Chakrabarti, N. Aoi, B.A. Brown, N. Fukuda, S. Kubono, T. Motobayashi, T. Nakabayashi, T. Nakamura, T. Nakao, T. Okumura, H.J. Ong, H. Suzuki, M.K. Suzuki, T. Teranishi, K.N. Yamada, H. Yamaguchi, and H. Sakurai: “ β decay of the proton-rich nucleus ^{24}Si and its mirror asymmetry”, *Phys. Rev. C* **80**, 044302 (2009)

17. P. Doornenbal, H. Scheit, N. Aoi, S. Takeuchi, K. Li, E. Takeshita, H. Wang, H. Baba, S. Deguchi, N. Fukuda, H. Geissel, R. Gernhauser, J. Gibelin, I. Hachiuma, Y. Hara, C. Hinke, N. Inabe, K. Itahashi, S. Itoh, D. Kameda, S. Kanno, Y. Kawada, N. Kobayashi, Y. Kondo, R. Krucken, T. Kubo, T. Kuboki, K. Kusaka, M. Lantz, S. Michimasa, T. Motobayashi, T. Nakamura, T. Nakao, K. Namihira, S. Nishimura, T. Ohnishi, M. Ohtake, N. A. Orr, H. Otsu, K. Ozeki, Y. Satou, S. Shimoura, T. Sumikama, M. Takechi, H. Takeda, K. N. Tanaka, K. Tanaka, Y. Togano, M. Winkler, Y. Yanagisawa, K. Yoneda, A. Yoshida, K. Yoshida, H. Sakurai: “Spectroscopy of ^{32}Ne and the Island of Inversion”, *Phys. Rev. Lett.* **103**, (2009) 032501 (4 pages).
18. K. Hagino, H. Sagawa, T. Nakamura, S. Shimoura: “Two-particle correlations in continuum dipole transitions in Borromean nuclei”, *Phys. Rev. C* **80**, (2009) 031301 (4 pages).
19. N. Imai, N. Aoi, H.J. Ong, H. Sakurai, K. Demichi, H. Kawasaki, H. Baba, Zs. Dombrádi, Z. Elekes, N. Fukuda, Zs. Fülöp, A. Gelberg, T. Gomi, H. Hasegawa, K. Ishikawa, M. Ishihara, H. Iwasaki, E. Kaneko, S. Kanno, T. Kishida, Y. Kondo, T. Kubo, K. Kurita, S. Michimasa, T. Minemura, M. Miura, T. Motobayashi, T. Nakamura, M. Notani, T. K. Ohnishi, A. Saito, S. Shimoura, T. Sugimoto, M. K. Suzuki, E. Takeshita, S. Takeuchi, M. Tamaki, H. Watanabe, K. Yoneda: “First lifetime measurement of 2_1^+ state in ^{12}Be ”, *Phys. Lett. B* **673**, (2009) 179 – 182.
20. Y. Kondo, T. Nakamura, Y. Satou, T. Matsumoto, N. Aoi, N. Endo, N. Fukuda, T. Gomi, Y. Hashimoto, M. Ishihara, S. Kawai, M. Kitayama, T. Kobayashi, Y. Matsuda, N. Matsui, T. Motobayashi, T. Nakabayashi, K. Ogata, T. Okumura, H.J. Ong, T.K. Onishi, H. Otsu, H. Sakurai, S. Shimoura, M. Shinohara, T. Sugimoto, S. Takeuchi, M. Tamaki, Y. Togano, Y. Yanagisawa: “One-neutron removal reactions of ^{18}C and ^{19}C on a proton target”, *Phys. Rev. C* **79**, (2009) 014602 (7 pages).
21. T. Nakamura, N. Kobayashi, Y. Kondo, Y. Satou, N. Aoi, H. Baba, S. Deguchi, N. Fukuda, J. Gibelin, N. Inabe, M. Ishihara, D. Kameda, Y. Kawada, T. Kubo, K. Kusaka, A. Mengoni, T. Motobayashi, T. Ohnishi, M. Ohtake, N.A. Orr, H. Otsu, T. Otsuka, A. Saito, H. Sakurai, S. Shimoura, T. Sumikama, H. Takeda, E. Takeshita, M. Takechi, S. Takeuchi, K. Tanaka, K.N. Tanaka, N. Tanaka, Y. Togano, Y. Utsuno, K. Yoneda, A. Yoshida, K. Yoshida: “Halo Structure of the Island of Inversion Nucleus ^{31}Ne ”, *Phys. Rev. Lett.* **103**, (2009) 262501(6 pages).
22. S. Takeuchi, N. Aoi, T. Motobayashi, S. Ota, E. Takeshita, H. Suzuki, H. Baba, T. Fukui, Y. Hashimoto, K. Ieki, N. Imai, H. Iwasaki, S. Kanno, Y. Kondo, T. Kubo, K. Kurita, T. Minemura, T. Nakabayashi, T. Nakamura, T. Okumura, T.K. Onishi, H. Sakurai, S. Shimoura, R. Sugou, D. Suzuki, M.K. Suzuki, M. Takashina, M. Tamaki, K. Tanaka, Y. Togano, K. Yamada: “Low-lying states in ^{32}Mg studied by proton inelastic scattering”, *Phys. Rev. C* **79**, (2009) 054319 (11 pages).
23. E. Ideguchi, B. Cederwall, E. Ganioglu, B. Hadinia, K. Lagergren, T. Bäck, A. Johnson, R. Wyss, S. Eeckhauudt, T. Grahn, P. Greenlees, R. Julin, S. Juutinen, H. Kettunen, M. Leino, A.-P. Leppanen, P. Nieminen, M. Nyman, J. Pakarinen, P. Rahkila, C. Scholey, J. Uusitalo, D.T. Joss, E.S. Paul, D.R. Wiseman, R. Wadsworth, A.V. Afanasjev, I. Ragnarsson: “High-spin intruder band in ^{107}In ”, *Phys. Rev. C* **81**, (2010) 034303 (12 pages).
24. C. Scholey, K. Andgren, L. Bianco, B. Cederwall, I.G. Darby, S. Eeckhauudt, S. Ertürk, M.B. Gomez Hornillos, T. Grahn, P.T. Greenlees, B. Hadinia, E. Ideguchi, P. Jones, D.T. Joss, R. Julin, S. Juutinen, S. Ketelhut, M. Leino, A.-P. Leppänen, P. Nieminen, M. Niikura, M. Nyman, D. O’Donnell, R.D. Page, J. Pakarinen, P. Rahkila, J. Sarén, M. Sandzelius, J. Simpson, J. Sorri, J. Thomson, J. Uusitalo, M. Venhart: “Isomeric and ground-state properties of ^{171}Pt , ^{167}Os , and ^{163}W ”, *Phys. Rev. C* **81**, (2010) 014306 (13 pages).
25. B. Hadinia, B. Cederwall, R.D. Page, M. Sandzelius, C. Scholey, K. Andgren, T. Bäck, E. Ganioglu, M.B. Gómez Hornillos, T. Grahn, P.T. Greenlees, E. Ideguchi, U. Jakobsson, A. Johnson, P.M. Jones, R. Julin, J. Juutinen, S. Ketelhut, A. Khaplanov, M. Leino, M. Niikura, M. Nyman, I. Özgür, E.S. Paul, P. Peura, P. Rahkila, J. Sarén, J. Sorri, J. Uusitalo, R. Wyss: “Identification of gamma rays from ^{172}Au and alpha decays of ^{172}Au , ^{168}Ir , and ^{164}Re ”, *Phys. Rev. C* **80**, (2009) 064310 (9 pages).
26. K. Morita, K. Morimoto, D. Kaji, H. Haba, K. Ozeki, Y. Kudou, N. Sato, T. Sumita, A. Yoneda, T. Ichikawa, Y. Fujimori, S. Goto, E. Ideguchi, Y. Kasamatsu, K. Katori, Y. Komori, H. Koura, H. Kudo, K. Ooe, A. Ozawa, F. Tokanai, K. Tsukada, T. Yamaguchi, A. Yoshida: “Decay Properties of ^{266}Bh and ^{262}Db Produced in the $^{248}\text{Cm} + ^{23}\text{Na}$ Reaction”, *J. Phys. Soc. Jpn.* **78**, (2009) 064201 (6 pages).
27. K. Tanaka, T. Yamaguchi, T. Suzuki, T. Ohtsubo, M. Fukuda, D. Nishimura, M. Takechi, K. Ogata, A. Ozawa, T. Izumikawa, T. Aiba, N. Aoi, H. Baba, Y. Hashizume, K. Inafuku, N. Iwasa, K. Kobayashi, M. Komuro, Y. Kondo, T. Kubo, M. Kurokawa, T. Matsuyama, S. Michimasa, T. Motobayashi, T. Nakabayashi, S. Nakajima, T. Nakamura,

- H. Sakurai, R. Shinoda, M. Shinohara, H. Suzuki, E. Takeshita, S. Takeuchi, Y. Togano, K. Yamada, T. Yasuno, M. Yoshitake: “Observation of a Large Reaction Cross Section in the Drip-Line Nucleus ^{22}C ”, *Phys. Rev. Lett.* **104**, (2010) 062701 (4 pages).
28. D. Suzuki, H. Iwasaki, D. Beaumel, L. Nalpas, E. Pollacco, M. Assié, H. Baba, Y. Blumenfeld, N. De Séréville, A. Drouart, S. Franchoo, A. Gillibert, J. Guillot, F. Hammache, N. Keeley, V. Lapoux, F. Maréchal, S. Michimasa, X. Mougeot, I. Mukha, H. Okamura, H. Otsu, A. Ramus, P. Roussel-Chomaz, H. Sakurai, J.-A. Scarpaci, O. Sorlin, I. Stefan, M. Takechi: “Breakdown of the $Z = 8$ Shell Closure in Unbound ^{12}O and its Mirror Symmetry”, *Phys. Rev. Lett.* **103**, (2009) 152503 (4 pages).
 29. E. Ideguchi, S. Ota, T. Morikawa, M. Oshima, M. Koizumi, Y. Toh, A. Kimura, H. Harada, K. Furutaka, S. Nakamura, F. Kitatani, Y. Hatsukawa, T. Shizuma, M. Sugawara, H. Miyatake, Y.X. Watanabe, Y. Hirayama, M. Oi: “Superdeformation in asymmetric $N > Z$ nucleus ^{40}Ar ”, *Phys. Lett. B* **686** (2010) 18–22.
 30. K. Sekiguchi, H. Sakai, H. Witala, W. Glockle, J. Golak, K. Itoh, H. Kamada, T. Kawabata, H. Kuboki, Y. Maeda, A. Nogga, H. Okamura, S. Sakaguchi, N. Sakamoto, Y. Sasamoto, M. Sasano, R. Skibiński, K. Suda, Y. Takahashi, T. Uesaka, T. Wakasa, and K. Yako, “Three-nucleon force effects in the $^1\text{H}(\bar{d}, \bar{p}p)n$ reaction at 135 MeV/nucleon”, *Phys. Rev. C* **79** (2009) 054008.
 31. K. Yako, M. Sasano, K. Miki, H. Sakai, M. Dozono, D. Frekers, M. B. Greenfield, K. Hatanaka, E. Ihara, M. Kato, T. Kawabata, H. Kuboki, Y. Maeda, H. Matsubara, K. Muto, S. Noji, H. Okamura, T. H. Okabe, S. Sakaguchi, Y. Sakemi, Y. Sasamoto, K. Sekiguchi, Y. Shimizu, K. Suda, Y. Tameshige, A. Tamii, T. Uesaka, T. Wakasa, and H. Zheng: “Gamow-Teller Strength Distributions in ^{48}Sc by the $^{48}\text{Ca}(p, n)$ and $^{48}\text{Ti}(n, p)$ Reactions and Two-Neutrino Double- β Decay Nuclear Matrix Elements”, *Physical Review Letters* **103** (2009) 012503.
 32. A. Tamii, Y. Fujita, H. Matsubara, T. Adachi, J. Carter, M. Dozono, H. Fujita, K. Fujita, H. Hashimoto, K. Hatanaka, T. Itahashi, M. Itoh, T. Kawabata, K. Nakanishi, S. Ninomiya, A.B. Perez-Cerdan, L. Popescu, B. Rubio, T. Saito, H. Sakaguchi, Y. Sakemi, Y. Sasamoto, Y. Shimbara, Y. Shimizu, F.D. Smit, Y. Tameshige, M. Yosoi, J. Zenihiro: “Measurement of high energy resolution inelastic proton scattering at and close to zero degrees”, *Nucl.Instrum.Methods Phys.Res. A* **605**, 326 (2009)
 33. T. Suzuki, M. Honma, K. Higashiyama, T. Yoshida, T. Kajino, T. Otsuka, H. Umeda and K. Nomoto: “Neutrino-induced reactions on ^{56}Fe and ^{56}Ni , and production of ^{55}Mn in population III stars”, *Phys. Rev. C* **79** (2009) 061603(R)/1-4.
 34. T. Otsuka, T. Suzuki, M. Honma, Y. Utsuno, N. Tsunoda, K. Tsukiyama and M. Hjorth-Jensen: “Novel features of nuclear forces and shell evolutions in exotic nuclei”, *Phys. Rev. Lett.* **104** (2010) 012501/1-4.
 35. T. Suzuki and T. Otsuka: “Exotic Electromagnetic Transitions in Neutron- rich Carbon Isotopes”, *Int.Journal of Modern Physics* **E18** (2009) 1992–1996.

B. Proceedings

1. T. Gunji: “Quarkonia production in high-energy heavy-ion collisions at the RHIC”. Proc. of the International Conference on Strangeness in Quark Matter 2008, Oct. 6-10, 2008, Tsinghua Univeristy, Beijing, China *J. Phys. G* **36**, -64015, 2009
2. Y. Tsuchimoto for the PHENIX Collaboration: “In-Medium Modifications of Low-Mass Vector Mesons in PHENIX at RHIC”, Proc. of the 21st International Conference on Ultra-Relativistic Nucleus-Nucleus Collisions (QM2009), Mar. 30–Apr. 4, 2009, Knoxville, USA, *Nucl. Phys. A* **830** (2009) 487c–490c.
3. Y.L. Yamaguchi for the PHENIX collaboration: “Measurements of Soft and Intermediate pT Photons from Hot and Dense Matter at RHIC-PHENIX”, Proc. of the 21st International Conference on Ultra-Relativistic Nucleus Nucleus Collisions (Quark Matter 2009), Mar. 30–Apr. 5, 2009, Knoxville, Tennessee, USA, *Nucl. Phys. A* **830** (2009) 575c–578c.
4. Y. Aramaki, for the PHENIX Collaboration: “Reaction plane dependence of neutral pion production in center-of-mass energy of 200 GeV Au+Au collisions at RHIC-PHENIX”, Proc. of the eighteenth Particles and Nuclei International Conference - PANIC08, November 9–14, 2008, Eilat, Israel, Conference record, (2009) pp. 570–572.

5. Y. Aramaki, for the PHENIX Collaboration: “Study of QGP with probes associated with photon at RHIC-PHENIX”, Proc. of the XLIVth Recontres de Moriond, March 14–21, 2009, La Thuile, Italy, Conference record, (2009) pp. 291–294.
6. R. Akimoto, H. Hamagaki, T. Gunji, Y.L.Yamaguchi and Y.Hori: “Measurement of the basic features of Thick-GEM and Resistive GEM”, Proc. of the 1st International conference on Micro Pattern Gaseous Detectors, Jun. 12–15, 2009, Crete, Greece, Journal of Instrumentation, **5** (2010)
7. C. Spitaleri, S. Romano, L. Lamia, S.M.R. Puglia, M.G. Del Szanto, N. Carlin, M.G. Munhoz, V.Kroha, S.Kubono, E.Somoryai, A. Szanto de Toledo, S. Cherubini, V. Crucill , M.Gulino, G.Kiss, M. La Cognata, Chengbo Li, R. Liguori Neto, M.M. De Moura, R.G. Pizzone, G.G.Rapisarda, M.L. Sergi, F.A. Souza, A.A.P. Suaide, E. Szanto, G.Tabacaru, S. Tudisco, A. Tumino, Y.Wakabayashi, Qungang Wen, and H.Yamaguchi: “New results on the Trojan Horse Method applied to the $^{10,11}\text{B}+p$ reactions”, Proceedings of the 6th Japan-Italy Symposium on Heavy-Ion Physics, AIP Conf. Proc. 1120 (2009) 171 - 176. (invited)
8. S. Cherubini, C. Spitaleri, V. Crucill , M. Gulino, M. La Cognata, L. Lamia, R.G. Pizzone, S. Romano, S. Kubono, H. Yamaguchi, Y. Wakabayashi, S. Hayakawa, N. Iwasa, S. Kato, H. Komatsubara, T. Teranishi, A. Coc, N. De Sereville, and F. Hammache: “The study of $^{18}\text{F}+p$ reaction at astrophysical energies”, Proceedings of the 6th Japan-Italy Symposium on Heavy-Ion Physics, AIP Conf. Proc. 1120 (2009) 294 - 297. (invited)
9. S. Kubono, Dam N. Binh, S. Hayakawa, H. Hashimoto, D. M. Kahl, Y. Wakabayashi, H. Yamaguchi, T. Teranishi, N. Iwasa, T. Komatsubara, S. Kato, Le H. Khiem: “Nuclear Clusters in Astrophysics”, Proc. of the 10th International Conference on Nucleus-Nucleus Collisions (NN2009), August 16-21, 2009, Beijing, China Nucl. Phys. A834 (2010) 647c – 650c. (invited)
10. S. Kubono, Dam N. Binh, S. Hayakawa, T. Hashimoto, D. M. Kahl, H. Yamaguchi, Y. Wakabayashi, T. Teranishi, N. Iwasa, T. Komatsubara, S. Kato, and L.H. Khiem: “Nuclear Astrophysics Programs with Low-Energy RI Beams at CRIB”, Proc. of the International Symposium on Exotic Nuclei (EXON), Sochi, Russia, October, 2009, AIP Conf. Proc. vol. 1224 (2010) 475 - 481 (2010). (invited)
11. S. Kubono: “Nuclear Cluster Aspects in Astrophysics”, Proc. of the 5th European Summer School on Nuclear Astrophysics, Sept. 20 - 27, 2009, Santa Tecla, Italy, AIP Conf. Proc. vol. 1213 (2010) 107 - 111. (invited)
12. H. Yamaguchi, Y. Wakabayashi, S. Hayakawa, D.N. Binh, D. Kahl, Y. Kurihara, S. Kubono, T. Teranishi, J.J. He, Y.K. Kwon, S. Nishimura, Y. Togano, N. Iwasa, M. Niikura and L.H. Khiem: “Nuclear Astrophysical Studies Using Low-Energy RI Beams at CRIB”, Perspective in Nuclear Physics, AIP conference proceeding **1120** (2009) 189–193.
13. J. Chen, A.A. Chen, H. Schatz, S. Kubono, A.B. Reyes, A. Smith, B. Wales, C. Ouellet, D. Kahl, D.G. Redondo, G. Lorusso, J. LeNestour, J.P. Conca, K. Smith, M. Amthor, M. Matos, H. Yamaguchi, N. Iwasa, S. Hayakawa, S. Michimasa, T. Teranishi, Y. Kurihara and Y. Wakabayashi: “Study of astrophysically important states in ^{26}Si with the $p(^{27}\text{Si},^{26}\text{Si}^*)d$ reaction and the $p(^{25}\text{Al},p)^{25}\text{Al}$ elastic scattering”, Nucl. Phys. A **834** (2010) 667c–669c.
14. M. Niikura, E. Ideguchi, N. Aoi, H. Baba, T. Fukuchi, Y. Ichikawa, H. Iwasaki, T. Kubo, M. Kurokawa, M. Liu, S. Michimasa, T. Ohnishi, T.K. Onishi, S. Ota, S. Shimoura, H. Suzuki, D. Suzuki, Y. Wakabayashi, K. Yoshida, Y. Zheng: “Yrast spectroscopy in $^{49-51}\text{Ti}$ via fusion-evaporation reaction induced by a radioactive beam”, Proceedings of the Fifth International Conference on Exotic Nuclei and Atomic Masses (ENAM’08), Sept. 7 – 13, 2008, Ryn, Poland, Eur. Phys. J. A **42** (2009) 471–475.
15. S. Shimoura: “High-resolution spectroscopy using RI-beams — SHARAQ project”, Proceedings of the Franco-Japanese symposium “New Paradigms in Nuclear Physics”, Sept. 29 – Oct. 2, 2008, Paris, France, Int. J. Mod. Phys. E **18**, (2009) 2011–2014.
16. S. Takeuchi, N. Aoi, H. Baba, T. Kubo, T. Motobayashi, K. Tanaka, K. Yamada, T. Fukui, S. Ota, Y. Hashimoto, Y. Kondo, T. Nakabayashi, T. Nakamura, T. Okumura, K. Ieki, S. Kanno, K. Kurita, R. Sugou, E. Takeshita, Y. Togano, N. Imai, T. Minemura, H. Iwasaki, T.K. Onishi, H. Sakurai, D. Suzuki, H. Suzuki, M.K. Suzuki, S. Shimoura, M. Tamaki: “Study of low-lying states in ^{32}Mg ”, Proceedings of the Franco-Japanese symposium “New Paradigms in Nuclear Physics”, Sept. 29 – Oct. 2, 2008, Paris, France, Int. J. Mod. Phys. E **18**, (2009) 2025–2029.

17. Y. Satou, T. Nakamura, N. Fukuda, T. Sugimoto, Y. Kondo, N. Matsui, Y. Hashimoto, T. Nakabayashi, Y. Okumura, M. Shinohara, T. Motobayashi, Y. Yanagisawa, N. Aoi, S. Takeuchi, T. Gomi, Y. Togano, S. Kawai, H. Sakurai, H.J. Ong, T.K. Onishi, S. Shimoura, M. Tamaki, T. Kobayashi, H. Otsu, N. Endo, M. Kitayama, M. Ishihara: “Invariant mass spectroscopy of $^{19,17}\text{C}$ and ^{14}B using proton inelastic and charge-exchange reactions”, Proc. the 10th International Conference on Nucleus-Nucleus Collisions (NN2009), Beijing, China, 16–21 August 2009, Nucl. Phys. A **834** (2010) 404c–407c.
18. P. Doornenbal, H. Scheit, N. Aoi, S. Takeuchi, K. Li, E. Takeshita, H. Wang, H. Baba, S. Deguchi, N. Fukuda, H. Geissel, R. Gernhäuser, J. Gibelin, I. Hachiuma, Y. Hara, C. Hinke, N. Inabe, K. Itahashi, S. Itoh, D. Kameda, S. Kanno, Y. Kawada, N. Kobayashi, Y. Kondo, R. Krücken, T. Kubo, T. Kuboki, K. Kusaka, M. Lantz, S. Michimasa, T. Motobayashi, T. Nakamura, T. Nakao, K. Namihira, S. Nishimura, T. Ohnishi, M. Ohtake, N.A. Orr, H. Otsu, K. Ozeki, Y. Satou, S. Shimoura, T. Sumikama, M. Takechi, H. Takeda, K.N. Tanaka, K. Tanaka, Y. Togano, M. Winkler, Y. Yanagisawa, K. Yoneda, A. Yoshida, K. Yoshida, H. Sakurai: “Exploring the Southern Boundaries of the “Island of Inversion” at the RIBF”, Proc. Int. Conf. on Nuclear Structure and Dynamics '09, Dubrovnik, Croatia, 4–8 May 2009, AIP Conf. Proc. **1165** (2009) 82–85.
19. S. Shimoura: “High-resolution spectroscopy using direct reactions of RI beams”, Proc. of the 6th Japan-Italy Symposium on Heavy-Ion Physics, Tokai, Japan, 11–15 November 2008, AIP Conf. Proc. **1120** (2009) 59–63.
20. N. Imai, N. Aoi, H.J. Ong, H. Sakurai, K. Demichi, H. Kawasaki, H. Baba, Zs. Dombrádi, Z. Elekes, N. Fukuda, Zs. Fülöp, A. Gelberg, T. Gomi, H. Hasegawa, K. Ishikawa, M. Ishihara, H. Iwasaki, E. Kaneko, S. Kanno, T. Kishida, Y. Kondo, T. Kubo, K. Kurita, S. Michimasa, T. Minemura, M. Miura, T. Motobayashi, T. Nakamura, M. Notani, T.K. Ohnishi, A. Saito, S. Shimoura, T. Sugimoto, M.K. Suzuki, E. Takeshita, S. Takeuchi, M. Tamaki, H. Watanabe, K. Yoneda: “Application of Doppler-shift attenuation method to the de-excitation γ rays from the in-flight ^{12}Be beam”, Proc. of the 6th Japan-Italy Symposium on Heavy-Ion Physics, Tokai, Japan, 11–15 November 2008, AIP Conf. Proc. **1120** (2009) 265–269.
21. P. von Neumann-Cosel, T. Adachi, C.A. Bertulani, J. Carter, M. Dozono, H. Fujita, K. Fujita, Y. Fujita, H. Hashimoto, K. Hatanaka, M. Itoh, Y. Kalmykov, K. Kato, T. Kawabata, H. Matsubara, K. Nakanishi, R. Neveling, H. Okamura, I. Poltoratska, V.Yu. Ponomarev, A. Richter, B. Rubio, H. Sakaguchi, Y. Sakemi, Y. Sasamoto, Y. Shimbara, Y. Shimizu, F.D. Smit, Y. Tameshige, A. Tamii, J. Wambach, M. Yosoi, J. Zenihiro, “Complete dipole response in ^{208}Pb from high-resolution polarized proton scattering at 0 degrees”, Proc. 13th Intern. Symposium on Capture Gamma-Ray Spectroscopy and Related Topics, Cologne, Germany, 25–29 Aug. 2008, J.Jolie, A.Zilges, N.Warr, A.Blazhev, Eds., p.404, AIP Conf. Proc. 1090 (2009)
22. T. Suzuki and T. Otsuka: “Structure of Light Neutron-rich Nuclei and Important Roles of Tensor Interaction”, Proc. of the International Conference on Nuclear Structure and Dynamics, May. 4-8, 2009, Dubrovnik, Croatia, AIP Conf. Proc. **1165** (2009) 54–56.

C. Theses

1. R. Akimoto: “Development of Time Projection Chamber using Gas Electron Multiplier, for Use as an Active Target”, Master Thesis, the University of Tokyo, March, 2010
2. Y. Hori: “Simulation Study for Forward Tracking Calorimeter in LHC-ALICE experiment”, Master Thesis, the University of Tokyo, March, 2010
3. H. Miya: “Development of Tracking Chamber for High-resolution Nuclear Spectroscopy with RI beam”, Master Thesis, University of Tokyo, March (2010).
4. H. Tokieda: “Cathode Readout Drift Chambers for the SHARAQ Spectrometer”, Master Thesis, University of Tokyo, March (2010).
5. Jun-young Moon: “Study of astrophysically important nuclear states of ^{27}P using radioactive ion beam”, Ph. D Thesis, Chung-Ang university (Seoul, Korea), August 2009

D. Other Publications

1. 浜垣 秀樹：「RHIC から LHC へ：高エネルギー重イオン衝突実験のこれから」、パリティ Vol. 25 No. 1 (2010) 47-49.
2. 浜垣 秀樹：「高エネルギー重イオン衝突における流体力学的振る舞いの発見」原子核研究 流体特集号「相対論的流体力学と高エネルギー重イオン反応：来し方行く末」 Vol. 54 Suppl. 3 (2010) 58 - 82.

Talks and Presentations

A. Conferences

1. H. Hamagaki: “A Critical Review of the Recent Results from Electro-Magnetic Measurements”, 12th Heavy Ion Cafe, at the University of Tokyo, Tokyo, May 9, 2009.
2. H. Hamagaki: “Discoveries of Hydro-Dynamical Behavior in High-Energy Heavy-Ion Collisions”, 13th Heavy Ion Cafe, at the University of Tokyo, Tokyo, Nov. 11, 2009.
3. T. Gunji, et al.: “Practice n GRID/CAF”, at the Workshop on ALICE Analysis Workshop for Asian Communities, Jan. 21–23, Hiroshima, Japan
4. T. Gunji, et al.: “Development of W+Si Tracking Calorimeter and readout for LHC-ALICE”, at the Detector workshop for RIBF experiments, Dec. 21–22, 2009, RIKEN, Wako, Japan.
5. T. Gunji, et al.: “東大 CNS における GEM 開発と Active Target GEM-TPC の開発”, at the 6th Workshop on Micor Pattern Gas Detector, Dec. 11–12, Kobe University, Japan
6. T. Gunji, et al.: “Forward Physics at LHC energy”, at the Workshop on ALICE upgrades in Asian countries, Nov. 11–15, Yonsei University, Korea
7. T. Gunji: “Heavy Quarkonia Production in High Energy Heavy Ion Collisions at RHIC and Perspectives for the LHC”, at the Workshop on the Expanding Future of High Energy Nuclear Physics at LHC and RHIC, Oct. 13, 2009, Waikoloa, Hawaii, USA.
8. T. Gunji: “Heavy Quarks and Quarkonia Production at RHIC as a Probe of hot and dense QCD medium”, at the International Symposium on Multiparticle Dynamics, Sept. 05-09, Gold Sands, Gomel, Belarus
9. T. Gunji: “Quarkonia Melting in expanding hot and dense medium at RHIC”, at the workshop on Heavy Quarkonium Production in Heavy Ion Collisions, May 25–29, ECT*, Trento, Italy
10. Y.L. Yamaguchi for the PHENIX collaboration (Oral): “Measurements of low pT direct photons in PHENIX”, at the Workshop on the Expanding Future of High Energy Nuclear Physics at LHC and RHIC, Oct. 13, 2009, Waikoloa, Hawaii, USA.
11. R. Akimoto, H. Hamagaki, T. Gunji, Y. Yamaguchi and Y. Hori (Oral): “Measurement of the basic features of Thick-GEM and Resistive GEM” at the 1st International conference on Micro Pattern Gaseous Detectors, Jun. 12–15, 2009, Orthodox Academy of Crete Conference Center, Crete, Greece.
12. R. Akimoto, S. Ota, S. Michimasa, T. Gunji, H. Yamaguchi, T. Hashimoto, H. Tokieda, T. Tsuji, S. Kawase, H. Hamagaki, T. Uesaka, S. Kubono, T. Isobe, T. Kawabata, A. Ozawa, H. Suzuki, D. Nagae, T. Moriguchi, Y. Ito, Y. Ishibashi, H. Ooishi, Y. Abe (Oral): “Design and performance of CNS active target TPC” at the Detector workshop for RIBF experiments, Dec. 21–22, 2009, RIKEN, Wako, Japan.
13. Y. Hori, et al.: “A simulation study for a Forward Calorimeter upgrade plan in ALICE at LHC”, at the Workshop on ALICE upgrades in Asian countries, Nov. 11–15, Yonsei University, Korea
14. A. Saito (oral): “The ${}^6\text{He}+{}^6\text{He}$ and $\alpha+{}^8\text{He}$ cluster states in ${}^{12}\text{Be}$ via inelastic scattering”, International Symposium on Frontiers of Researches in Exotic Nuclear Structures (Niigata2010), March 1–4, 2010, Tokamachi, Niigata, Japan.
15. S. Shimoura (invited): “Recent developments of radiation detector systems for RIBF experiments”, Workshop On Developments of new Scintillator Detectors for Gamma Spectroscopy and Imaging, November 16–17, 2009, Milano, Italy.
16. S. Ota, S. Shimoura, N. Aoi, E. Takeshita, S. Takeuchi, H. Suzuki, H. Baba, T. Fukuchi, T. Fukui, Y. Hashimoto, E. Ideguchi, K. Ieki, N. Iwasa, H. Iwasaki, S. Kanno, Y. Kondo, T. Nakabayashi, T. Nakamura, M. Niikura, T. Okumura, T.K. Onishi, H. Sakurai, M. Shinohara, D. Suzuki, M. K. Suzuki, M. Tamaki, K. Tanaka, Y. Togano, Y. Wakabayashi, K. Yamada: “High Resolution In-beam Spectroscopy of island-of-inversion nuclei via alpha induced reaction”, International Workshop on Direct Reactions with Exotic Beams (DREB2009), December 16–19, 2009, Tallahassee, Florida, USA.

17. S. Michimasa (invited): “SHARAQ Overview and Scientific Programs”, Sept. 9–10, 2009, JUSEIPEN Workshop.
18. T. Uesaka (Invited): “Polarized Solid Proton Target in Low Magnetic Field and at High Temperature”, 13th International Workshop on Polarized Sources, Targets and Polarimetry, Sept. 7–11, 2009, Ferrara, Italy.
19. T. Kawahara, T. Uesaka, Y. Shimizu, S. Sakaguchi, T. Wakui (Oral): “Pulse structure dependence of the proton spin polarization rate”, 13th International Workshop on Polarized Sources, Targets and Polarimetry Sep. 07–11, 2009, Camera di Commercio, Ferrara, Italy.
20. T. Uesaka (Invited): “SHARAQ Spectrometer —Current status and future experimental plans—”, International Symposium of Exotic Nuclei 2009, Sep. 28–Oct. 2, 2009, Sochi, Russia
21. T. Uesaka (Invited): “Current status and future experimental program of the SHARAQ Spectrometer”, 7th Japan-China Joint Nuclear Physics Symposium, Nov. 9–13, 2009, University of Tsukuba, Ibaraki, Japan
22. T. Uesaka (Oral): “The SHARAQ Spectrometer”, ICHOR-EFES International Symposium on New Facet of Spin-Isospin Responses 2010, Feb. 18–21, 2010, University of Tokyo, Tokyo, Japan
23. T. Uesaka, R. Akimoto, S. Ota, S. Michimasa, T. Gunji, H. Yamaguchi, T. Hashimoto, H. Tokieda, T. Tsuji, S. Kawase, H. Hamagaki, S. Kubono, T. Kawabata, T. Isobe, A. Ozawa, H. Suzuki, D. Nagae, T. Moriguchi, Y. Ito, Y. Ishibashi, H. Oishi, Y. Abe, N. Kamiguchi, SHARAQ collaboration (Oral): “CNS active targets for Missing Mass Spectroscopy with RI beams”, Detector Workshop for RIBF Experiments, Dec. 21–22, 2010, RIKEN, Saitama, Japan
24. Y. Shimizu (Oral): “Spin dependent momentum distribution of proton in ^3He studied via proton induced exclusive knockout reaction”, 19th International IUPAP Conference on Few-Body Problems in Physics, FB19, Aug. 31–Sep. 5, University of Bonn, Bonn, Germany.
25. Y. Sasamoto, T. Uesaka, H. Sakai, S. Shimoura, S. Noji, K. Yako, S. Michimasa, S. Ota, A. Saito, K. Miki, H. Tokieda, H. Miya, S. Kawase, T. Kubo, K. Yoshida, T. Ohnishi, Y. Yanagisawa, N. Fukuda, H. Takeda, D. Kameda, N. Aoi, S. Takeuchi, T. Ichihara, H. Baba, S. Sakaguchi, Y. Shimizu, H. Schiet, P. Doornembal, T. Kawabata, K. Itoh, T. Kawahara, Y. Maeda, T. Saitoh, M. Itoh, R.G.T. Zegers, M. Sasano, P. Roussel-Chomaz, G.P.A. Berg, “The super-allowed Fermi type charge exchange reaction for studies of isovector non-spin-flip monopole resonance”, ICHOR-EFES International Symposium on New Facet of Spin-Isospin Responses (SIR2010), Feb. 18–21, 2010, Koshiba Hall, University of Tokyo, Japan.
26. S. Ota (Oral): “High-resolution in-beam spectroscopy of island-of-inversion nuclei via alpha induced reactions”, Direct Reactions with Exotic Beams (DREB) 2009, Dec. 16–19, 2009, Florida State University, Tallahassee, Florida, USA.
27. S. Ota (Oral): “Active Target in CNS, UT”, Instrumentation discussion session, Direct Reactions with Exotic Beams (DREB) 2009, Dec. 16, 2009, Florida State University, Tallahassee, Florida, USA.
28. S. Ota (Oral): “Active Target Development in CNS”, GET-ACTAR General Meeting, Jan. 11–15, 2010, Ferme de la Rançonnière, Crepon, France.
29. S. Ota (Oral): “Study of giant resonances in unstable nuclei with CNS Active Target”, ICHOR-EFES International Symposium on New Facet of Spin-Isospin Responses (SIR2010), Feb. 18–21, 2010, Koshiba Hall, University of Tokyo, Japan.
30. K. Miki, H. Sakai, T. Uesaka, H. Baba, G.P.A. Berg, N. Fukuda, D. Kameda, T. Kawabata, S. Kawase, T. Kubo, K. Kusaka, S. Michimasa, H. Miya, S. Noji, T. Ohnishi, S. Ota, A. Saito, Y. Sasamoto, M. Sasano, S. Shimoura, H. Takeda, H. Tokieda, K. Yako, Y. Yanagisawa, A. Yoshida, K. Yoshida and R.G.T. Zegers (Oral): “Search for the Isovector Spin Monopole Resonance via the $^{208}\text{Pb}, ^{90}\text{Zr}(t, ^3\text{He})$ Reactions at 300 MeV/u”, The 4th LACM-EFES-JUSTIPEN Workshop, Mar. 15–17, 2010, Oak Ridge National Laboratory, Tennessee, USA
31. K. Miki, H. Sakai, T. Uesaka, H. Baba, G.P.A. Berg, N. Fukuda, D. Kameda, T. Kawabata, S. Kawase, T. Kubo, K. Kusaka, S. Michimasa, H. Miya, S. Noji, T. Ohnishi, S. Ota, A. Saito, Y. Sasamoto, M. Sasano, S. Shimoura, H. Takeda, H. Tokieda, K. Yako, Y. Yanagisawa, A. Yoshida, K. Yoshida and R.G.T. Zegers (Oral): “Measurement of the ^{208}Pb and $^{90}\text{Zr}(t, ^3\text{He})$ reactions at 300 MeV/u – the first physics measurement with SHARAQ –”, ICHOR-EFES International Symposium on New Facet of Spin-Isospin Responses (SIR2010), Feb. 18–21, 2010, University of Tokyo, Tokyo, Japan

32. H. Yamaguchi, T. Hashimoto, S. Hayakawa, D.N. Binh, D. Kahl, and S. Kubono (Oral): “Nuclear astrophysics and structure studies using low-energy RI beams at CRIB”, 7th Japan-China Joint Nuclear Physics Symposium, November 9–13, 2009, Tsukuba University, Ibaraki, Japan.
33. H. Yamaguchi, T. Hashimoto, S. Hayakawa, D.N. Binh, D. Kahl, and S. Kubono (Oral): “Status of the studies on nuclear reactions and structures at CRIB”, The 6th International Workshop on “Physics with Stopped and Slow Radioisotope Beams (SSRI), Mar 1–2, 2010, Tokyo Institute of Technology, Tokyo, Japan.
34. H. Yamaguchi, T. Hashimoto, S. Hayakawa, D.N. Binh, D. Kahl, and S. Kubono (Oral): “Studies for alpha-induced astrophysical reactions at CRIB”, The 10th. International Symposium on. Origin of Matter and Evolution of the Galaxies (OMEG10), March 8–10, 2010, RCNP, Osaka University, Osaka, Japan.
35. T. Suzuki and T. Otsuka (Oral): “Structure of Light Neutron- rich Nuclei and Important Roles of Tensor Interaction”, International Conference on Nuclear Structure and Dynamics, May 2009, Dubrovnik, Croatia
36. T. Suzuki (Invited): “Structure of Light Exotic Nuclei”, International Conference on Nuclear Structure and Related Topics, June 2009, Dubna, Russia
37. T. Suzuki (Invited): “Neutrino-induced Reactions on Nuclei and Nucleosynthesis in Stars”, Neutrinos and Dark Matter 2009, Sept. 2009, Wisconsin University, U.S.A.
38. T. Suzuki, M. Honma, K. Higashiyama, T. Yoshida, T. Kajino, T. Otsuka, H. Umeda and K. Nomoto (Oral): “Neutrino-induced Reactions on Ni and Fe Isotopes and Nucleo- synthesis in Stars”, 3rd Joint Meeting of the APS-DNP and Physical Society of Japan, Oct. 2009, Hawaii, U.S.A.
39. T. Suzuki (Invited): “Spin Responses in Nuclei, Neutrino-induced Reactions and Nucleo- synthesis in Stars”, 7th Japan-China Joint Nuclear Physics Symposium, Nov. 2009, Univ. of Tsukuba, Japan
40. T. Suzuki (Oral): “Gamow-Teller Transitions in Astrophysical Processes”, EFES- JUSTIPEN workshop, Dec. 2009, RIKEN, Wako, Japan
41. T. Suzuki (Oral): “Shell Model Study of Spin Modes in Ni and Ca Isotopes”, EFES-NSCLWorkshop on Perspectives on the Modern Shell Model and Related Experimental Topics, Feb. 2010, Michigan State University, U.S.A.
42. T. Suzuki (Invited): “Nuclear Weak Processes and Nucleosynthesis in Stars”, ICOR-EFES International Symposium on New Facet of Spin-isospin Responses (SIR2010), Feb. 2010, Koshiba Hall, Univ. of Tokyo, Japan
43. T. Suzuki, T. Yoshida and Y. Utsuno (Poster and Short Oral): “Half-lives of N=126 Isotones and the r-Process”, 10th International Symposium on Origin of Matter and Evolution of the Galaxies (OMEG10), Mar. 2010, RCNP, Osaka, Japan
44. T. Suzuki (Oral): “GT and FF Transitions in Astrophysical Processes”, The 4th LACM- EFES-JUSTIPEN Workshop, Mar. 2010, Oak Ridge, USA
45. T. Yoshida and K. Kato (Oral): “Algebraic N alpha model (applications for ^{12}C)”, Hadron and Nuclear Physics (HNP09), Nov. 16-19, 2009, RCNP, Osaka, Japan.

B. JPS Meetings

1. T. Gunji: “Quarkonia Melting in expanding hot and dense medium at RHIC”, at the 3rd Joint Meeting of the APS Division of Nuclear Physics and Physical Society of Japan, Oct. 14–17, 2009, Hilton Waikoloa Village, Hawaii, USA.
2. T. Gunji: “ J/ψ Production in High energy heavy ion collisions at RHIC”, at the JPS Spring meeting, Mar. 20–23, 2010, Okayama University, Okayama, Japan.
Y. Tsuchimoto, for the PHENIX Collaboration: “Measurement of Low-Mass Vector Mesons (LVM) in PHENIX at RHIC”, at the 3rd Joint Meeting of the APS Division of Nuclear Physics and Physical Society of Japan, Oct. 14–17, 2009, Hilton Waikoloa Village, Hawaii, USA.

3. Y. Aramaki, for the PHENIX Collaboration: “Neutral pion production with respect to the reaction plane in $\sqrt{s_{NN}} = 200$ GeV Au+Au collisions at PHENIX”, 3rd Joint Meeting of the Nuclear Physics Divisions of the APS and The Physical Society of Japan, October 13–17, 2009, Waikoloa, Hawaii, USA.
4. S. Sano, for the ALICE Collaboration: “LHC-ALICE 実験おける粒子多重度測定” at the JPS Spring meeting, Mar. 20–23, 2010, Okayama University, Okayama, Japan.
5. A. Takahara, for the PHENIX Collaboration: “Study of J/ψ photoproduction in ultra-peripheral Au+Au collisions at the PHENIX experiment”, at the JPS Spring meeting, Mar. 20–23, 2010, Okayama University, Okayama, Japan.
6. R. Akimoto, S. Ota, S. Michimasa, T. Gunji, H. Yamaguchi, T. Hashimoto, H. Tokieda, H. Hamagaki, T. Uesaka, S. Kubono (Oral): “Simulation study of performance of active target GEM TPC”, at the 3rd Joint Meeting of the APS Division of Nuclear Physics and Physical Society of Japan, Oct. 14–17, 2009, Hilton Waikoloa Village, Hawaii, USA.
7. R. Akimoto, S. Ota, S. Michimasa, T. Gunji, H. Yamaguchi, T. Hashimoto, H. Tokieda, T. Tsuji, S. Kawase, H. Hamagaki, T. Uesaka, S. Kubono, T. Isobe, T. Kawabata, A. Ozawa, H. Suzuki, D. Nagae, T. Moriguchi, Y. Ito, Y. Ishibashi, H. Ooishi, Y. Abe (Oral): “Performance evaluation of active target GEM-TPC” at the JPS Spring meeting, Mar. 20–23, 2010, Okayama University, Okayama, Japan.
8. T. Tsuji, H. Hamagaki, T. Gunji, Y. Hori, E. Kistenev, M. Chiu, A. Sukhanov, R. Seto, for the PHENIX FoCal group: “Study of basic properties of the Forward Calorimeter for PHENIX upgrade”, at the JPS Spring meeting, Mar. 20–23, 2010, Okayama University, Okayama, Japan.
9. E. Ideguchi (invited): “Lifetime measurements of RI beam and high-spin studies with degraded beams”, Workshop on Physics Opportunities with GRETINA, Third Joint Meeting of the Nuclear Physics Divisions of the APS and JPS, October 13, 2009, Hawaii, USA.
10. H. Miya, S. Shimoura, A. Saito, K. Miki, M. Sasano, S. Itoh, K. Itahashi, T. Kawabata, Y. Shimbara, K. Yako, Y. Shimizu, H. Baba, H. Kurei, S. Michimasa, K. Nakanishi, S. Noji, S. Ota, Y. Sasamoto, H. Tokieda, T. Uesaka H. Sakai (Oral): “Performance evaluation of Low Pressure Multi-Wire Drift Chamber for RI beam” Third Joint Meeting of the Nuclear Physics Divisions of the APS and JPS, October 13–17, 2009, Hawaii, USA.
11. S. Go, S. Shimoura, E. Ideguchi, S. Ota, H. Miya, H. Baba (Oral): “New method of digital pulse shape analysis of signals for segmented Ge detectors”, Third Joint Meeting of the Nuclear Physics Divisions of the APS and the JPS, October 13–17, 2009, Hawaii, USA.
12. E. Ideguchi, S. Ota, T. Morikawa, M. Oshima, M. Koizumi, Y. Toh, A. Kimura, H. Harada, K. Furutaka, S. Nakamura, F. Kitatani, Y. Hatsukawa, T. Shizuma, M. Sugawara, H. Miyatake, Y.X. Watanabe, Y. Hirayama, M. Oi (Oral): “Study of High-Spin States in ^{35}S ”, JPS Spring Meeting, March 20–23, 2010, Okayama University, Okayama, Japan.
13. S. Go, S. Shimoura, E. Ideguchi, S. Ota, H. Miya, H. Baba (Oral): “New method of digital pulse shape analysis of signals from segmented Ge detectors by using moments”, JPS Spring Meeting, March 20–23, 2010, Okayama University, Okayama, Japan.
14. S. Michimasa, H. Tokieda, S. Noji, S. Ota, S. Shimoura, T. Uesaka, H. Sakai, P. Roussel-Chomaz, J-F. Libin, P. Gangnant, C. Spitaels (Oral): “Performance of Detectors Installed at SHARQA Final Focal Plane”, JPS Spring Meeting, March 20–23, 2010, Okayama University, Okayama, Japan.
15. S. Kawase, S. Ota, H. Baba, S. Shimoura, T. Uesaka (Oral): “Performance Evaluation of Charge-to-Time-Converter (QTC)”, the 65th JPS Annual Meeting, Mar. 20–23, 2010, Okayama University, Okayama, Japan.
16. H. Tokieda, S. Michimasa, S. Ota, S. Shimoura, T. Uesaka, S. Noji, H. Sakai, P. Roussel-Chomaz, J-F. Libin, P. Gangnant, and C. Spitaels (Oral): “Performance of Focal-Plane Tracking Detector CRDC for SHARQA”, Third Joint Meeting of the Nuclear Physics Divisions of the APS and the JPS, Oct. 13–17, 2009, Hawaii, USA.
17. T. Uesaka, K. Nakanishi, H. Kurei, S. Ota, S. Michimasa, A. Saito, Y. Sasamoto, H. Miya, H. Tokieda, S. Shimoura, K. Miki, S. Noji, H. Sakai (Oral): “Field mapping measurement of SHARQA dipole magnets”, Third Joint Meeting of the Nuclear Physics Divisions of the APS and the JPS, Oct. 13–17, 2009, Hawaii, USA.

18. Y. Sasamoto, T. Uesaka, T. Kawabata, G.P.A. Berg, K. Nakanishi, S. Noji, H. Takeda, S. Shimoura, H. Sakai (Oral): “Ion optical studies in the high resolution beam line and the SHARQA spectrometer”, 3rd Joint Meeting of the Nuclear Physics Divisions of the APS and JPS, Oct. 13–17, 2009, Hilton Waikooa Village, Hawaii, USA.
19. S. Ota, S. Shimoura, N. Aoi, E. Takeshita, S. Takeuchi, H. Suzuki, H. Baba, T. Fukuchi, T. Fukui, Y. Hashimoto, E. Ideguchi, K. Ieki, N. Iwasa, H. Iwasaki, S. Kanno, Y. Kondo, T. Kubo, K. Kurita, T. Minemura, S. Michimasa, T. Motobayashi, T. Murakami, T. Nakabayashi, T. Nakamura, M. Niikura, T. Okumura, T.K. Onishi, H. Sakurai, M. Shinohara, D. Suzuki, M. Suzuki, M. Tamaki, K. Tanaka, Y. Togano, Y. Wakabayashi, K. Yamada (Oral): “High Resolution Gamma-ray Spectroscopy of N=20 Neutron-rich Nuclei via Direct Reactions”, the 65th JPS Annual Meeting, Mar. 20–23, 2010, Okayama University, Okayama, Japan.
20. K. Miki, H. Sakai, T. Uesaka, H. Baba, G.P.A. Berg, N. Fukuda, D. Kameda, T. Kawabata, S. Kawase, T. Kubo, K. Kusaka, S. Michimasa, H. Miya, S. Noji, T. Ohnishi, S. Ota, A. Saito, Y. Sasamoto, M. Sasano, S. Shimoura, H. Takeda, H. Tokieda, K. Yako, Y. Yanagisawa, A. Yoshida, K. Yoshida and R.G.T. Zegers (Oral): “Measurement of the the isovector spin monopole resonance via the $^{208}\text{Pb}, ^{90}\text{Zr}(t, ^3\text{He})$ reactions at 300 MeV/u”, at the JPS Spring meeting, Mar. 20–23, 2010, Okayama University, Okayama, Japan.
21. H. Yamaguchi, T. Hashimoto, S. Hayakawa, D.N. Binh, D. Kahl, and S. Kubono (Oral): “Study on astrophysical reactions using low-energy RI beams”, Workshop on Frontiers in Nuclear Astrophysics I, Third Joint Meeting of the Nuclear Physics Divisions of the APS and JPS, October 13–17, 2009, Hilton Waikoloa Village, Hawaii, USA.
22. Y. Wakabayashi, H. Yamaguchi, T. Hashimoto, S. Hayakawa, Y. Kurihara, D.N. Binh, D. Kahl, S. Kubono, S. Nishimura, Y. Gono, M. Suga, Y. Fujita (Oral): “Beta-decay measurement of ^{46}Cr ”, at third joint meeting of the APS and the JPS, Oct. 13–17, 2009, Waikoloa, Hawaii
23. S. Hayakawa, H. Yamaguchi, T. Hashimoto, Y. Wakabayashi, D.N. Binh, D.M. Kahl, S. Kubono, N. Iwasa, N. Kume, Y. Miura, T. Teranishi, J.J. He, Y.K. Kwon, T. Komatsubara, S. Kato and S. Wanajo (Oral): “Direct measurement of the $^{11}\text{C}(\alpha, p)^{14}\text{N}$ stellar reaction”, at 3rd Joint Meeting of the APS Division of Nuclear Physics and the Physical Society of Japan, Oct. 13–17, 2009, Hawaii, USA.
24. T. Suzuki (Oral): “Beta decay modes of nuclei in the third peak region of the r-process”, at the 65th JPS Annual meeting, Mar. 20–23, 2010, Okayama University, Okayama, Japan
25. T. Yoshida and K. Kato, (Oral): Study of ^{12}C structure based on Sp(2,R) algebra”, at the JPS meeting, Mar. 20-23, 2010, Okayama University, Okayama, Japan.
26. T. Yoshida and K. Kato, (Oral): “Algebraic N alpha model (applications for ^{12}C)”, at the APS and JPS meeting, Oct. 13–17, 2009, Waikoloa, Hawaii, US.

C. Lectures

1. Hideki Hamagaki: “Birth of our Universe – Early universe at one millionth of a second after the Big Bang – ” Public lecture in the Open Campus of the University of Tokyo, organized by the Center for Nuclear Study, Aug. 6 2009, University of Tokyo, Tokyo, Japan.
2. T. Gunji: “Experimental Studies of hot and dense QCD medium by Relativistic Heavy Ion Collisions” at the CNS-EFES Summer School 2009, 8/26-9/1, RIKEN, Saitama, Japan
3. S. Shimoura: “Reactions of RI beams for studying exotic nuclei”, The 8th CNS-EFES International Summer School (CNS-EFES09), Aug. 26 – Sep. 1, 2009, Wako, Japan
4. S. Kubono: “Special series of lectures on Nuclear Astrophysics”, Graduate school of science, Tsukuba University Jan. 6 – 8, 2010

D. Seminars

1. Y. Tsuchimoto: “Measurement of Low-mass Vector Mesons in Hot-Medium created by Relativistic Heavy-Ion Collisions”, at the CNS/RIBF Seminar, Aug. 29, 2009, RIKEN, Saitama, Japan.

2. S. Ota: “Low-lying Proton Intruder State in ^{13}B ”, at the CNS/RIBF Seminar, July 21st, 2009, RIKEN, Saitama, Japan.
3. D.N. Binh: “The measurement of $^{21}\text{Na}+\alpha$ in inverse kinematics and the $^{21}\text{Na}(\alpha,p)$ stellar reaction rate”, at the CNS/RIBF Seminar, March 30th, 2010, RIKEN, Saitama, Japan.

Personnel

Director

OTSUKA, Takaharu

*Professor, Department of Physics,
Graduate School of Science*

Scientific Staff

1. Heavy-Ion Collisions

SHIMOURA, Susumu

Professor

UESAKA, Tomohiro

Associate Professor

IDEGUCHI, Eiji

Lecturer

MICHIMASA, Shin'ichiro

Assistant Professor

OYA, Shinsuke

Assistant Professor

3. Nuclear Structure in Extreme States

KUBONO, Shigeru

Professor

HAMAGAKI, Hideki

Associate Professor

YAMAGUCHI, Hidetoshi

Assistant Professor

GUNJI, Taku

Assistant Professor

Guest Professors

SUZUKI, Toshio

Nihon University

MITSUMOTO, Toshinori

Sumitomo Heavy Industries, Ltd.

Technical Staff

OHSIRO, Yukimitsu

YAMAZAKI, Norio

Technical Assistants

WATANABE, Shin-ichi

YAMAKA, Shoichi

NINOMIYA, Hideaki

KUREI, Hiroshi

YOSHINO, Akira

Post Doctoral Associates

SHIMIZU, Yuhei (~ December 2010)

TSUCHIMOTO, Yuji

YOSHIDA, Toru

NIKURA, Megimi (~ April 2009)

HASHIMOTO, Takashi

SAITO, Akito

NAKANISHI, Kosuke (~ June 2009)

Graduate Students

SASAMOTO, Yoshiko

ARAMAKI, Yoki

SANO, Satoshi

KAHL, David. M

MIYA, Hiroyuki

HORI, Yasuto

TSUJI, Tomoya

KAWASE, Shoichiro

YAMAGUCHI, Yorito

DAM, Nguyen Binh

HAYAKAWA, Seiya

TAKAHARA, Akihisa

AKIMOTO, Ryoji

TOKIEDA, Hiroshi

GO, Shintaro

Administration Staff

HIRANO, Midori

YAMAMOTO, Ikuko

ENDO, Takako

KISHI, Yukino

ITAGAKI, Toshiko

SOMA, Yuko

Committees (not yet updated!!)

Council

YAMAGATA, Toshio (chair)	<i>Dean, Graduate School of Science</i>
AIHARA, Hiroaki	<i>Department of Physics, Graduate School of Science</i>
FUKUDA, Hiroo	<i>Department of Biological Science</i>
OTSUKA, Takaharu	<i>Department of Physics, Graduate School of Science</i>
HAYANO, Ryugo	<i>Department of Physics, Graduate School of Science</i>
KUBONO, Shigeru	<i>Center for Nuclear Study, Graduate School of Science</i>
SHIMOURA, Susumu	<i>Center for Nuclear Study, Graduate School of Science</i>
NAGAMIYA, Shoji	<i>J-PARC Project Office, High Energy Accelerator Research Organization</i>

Steering Committee

OTSUKA, Takaharu	<i>Department of Physics, Graduate School of Science</i>
SHIMOURA, Susumu	<i>Center for Nuclear Study, Graduate School of Science</i>
KUBONO, Shigeru	<i>Center for Nuclear Study, Graduate School of Science</i>
HAMAGAKI, Hideki	<i>Center for Nuclear Study, Graduate School of Science</i>
SAKAI, Hideyuki	<i>Department of Physics, Graduate School of Science</i>
AIHARA, Hiroaki	<i>Department of Physics, Graduate School of Science</i>
HAYANO, Ryugo	<i>Department of Physics, Graduate School of Science</i>
HAMAGUCHI, Hiroo	<i>Department of Chemistry, Graduate School of Science</i>
KOBAYASHI, Tomio	<i>International Center for Elementary Particle Physics</i>
YAMAZAKI, Yasunori	<i>Institute of Physics, Graduate School of Arts and Sciences</i>
MADARAME, Haruki	<i>Department of Nuclear Engineering and Management</i>

Program Advisory Committee

TRIBBLE, Robert	<i>Cyclotron Institute, Texas A&M University</i>
HASHIMOTO, Osamu	<i>Department of Physics, Tohoku University</i>
HIROSHI, Sakurai	<i>The Institute of Physical and Chemical Research, Nishina Center</i>
YABANA, Kazuhiro	<i>University of Tsukuba</i>
ODAHARA, Atsuko	<i>Osaka University</i>
HAMAMOTO, Ikuko	<i>University of Lund, Sweden</i>
CHIBA, Junsei	<i>Department of Physics, Tokyo University of Science</i>

